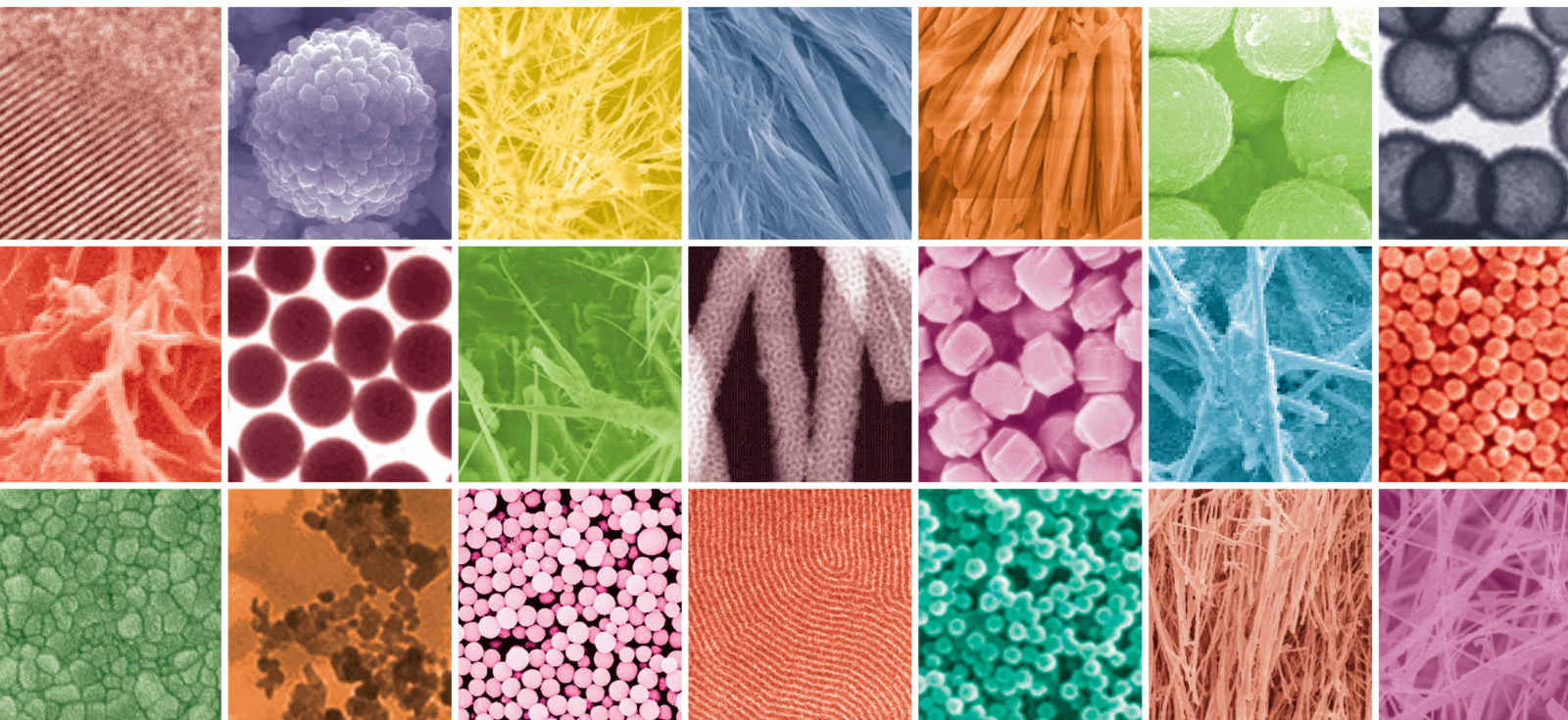


# Green Route Synthesis of Antimicrobial Nanoparticles

Lead Guest Editor: Shanmugam Rajeshkumar

Guest Editors: Venkat Kumar, Mahendran Vanaja, and Sheba David



---



# **Green Route Synthesis of Antimicrobial Nanoparticles**

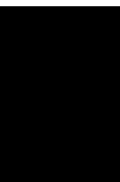
Journal of Nanomaterials

---

## **Green Route Synthesis of Antimicrobial Nanoparticles**

Lead Guest Editor: Shanmugam Rajeshkumar

Guest Editors: Venkat Kumar, Mahendran Vanaja,  
and Sheba David



---




Copyright © 2022 Hindawi Limited. All rights reserved.

This is a special issue published in "Journal of Nanomaterials." All articles are open access articles distributed under the Creative Commons Attribution License, which permits unrestricted use, distribution, and reproduction in any medium, provided the original work is properly cited.




# Chief Editor

Stefano Bellucci , Italy

















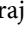
















## Associate Editors

Ilaria Armentano, Italy  
Stefano Bellucci , Italy  
Paulo Cesar Morais , Brazil  
William Yu , USA

## Academic Editors

Buzuayehu Abebe, Ethiopia  
Domenico Acierno , Italy  
Sergio-Miguel Acuña-Nelson , Chile  
Katerina Aifantis, USA  
Omer Alawi , Malaysia  
Nageh K. Allam , USA  
Muhammad Wahab Amjad , USA  
Martin Andersson, Sweden  
Hassan Azzazy , Egypt  
Ümit Ağbulut , Turkey  
Vincenzo Baglio , Italy  
Lavinia Balan , France  
Nasser Barakat , Egypt  
Thierry Baron , France  
Carlos Gregorio Barreras-Urbina, Mexico  
Andrew R. Barron , USA  
Enrico Bergamaschi , Italy  
Sergio Bietti , Italy  
Raghvendra A. Bohara, India  
Mohamed Bououdina , Saudi Arabia  
Victor M. Castaño , Mexico  
Albano Cavaleiro , Portugal  
Kondareddy Cherukula , USA  
Shafiul Chowdhury, USA  
Yu-Lun Chueh , Taiwan  
Elisabetta Comini , Italy  
David Cornu, France  
Miguel A. Correa-Duarte , Spain  
P. Davide Cozzoli , Italy  
Anuja Datta , India  
Loretta L. Del Mercato, Italy  
Yong Ding , USA  
Kaliannan Durairaj , Republic of Korea  
Ana Espinosa , France  
Claude Estournès , France  
Giuliana Faggio , Italy  
Andrea Falqui , Saudi Arabia





Matteo Ferroni , Italy  
Chong Leong Gan , Taiwan  
Siddhartha Ghosh, Singapore  
Filippo Giubileo , Italy  
Iaroslav Gnilitzkiy, Ukraine  
Hassanien Gomaa , Egypt  
Fabien Grasset , Japan  
Jean M. Greneche, France  
Kimberly Hamad-Schifferli, USA  
Simo-Pekka Hannula, Finland  
Michael Harris , USA  
Hadi Hashemi Gahruei , Iran  
Yasuhiko Hayashi , Japan  
Michael Z. Hu , USA  
Zhengwei Huang , China  
Zafar Iqbal, USA  
Balachandran Jeyadevan , Japan  
Xin Ju , China  
Antonios Kellarakis , United Kingdom  
Mohan Kumar Kesarla Kesarla , Mexico  
Ali Khorsand Zak , Iran  
Avvaru Praveen Kumar , Ethiopia  
Prashant Kumar , United Kingdom  
Jui-Yang Lai , Taiwan  
Saravanan Lakshmanan, India  
Meiyong Liao , Japan  
Shijun Liao , China  
Silvia Licocchia , Italy  
Zainovia Lockman, Malaysia  
Jim Low , Australia  
Rajesh Kumar Manavalan , Russia  
Yingji Mao , China  
Ivan Marri , Italy  
Laura Martinez Maestro , United Kingdom  
Sanjay R. Mathur, Germany  
Tony McNally, United Kingdom  
Pier Gianni Medaglia , Italy  
Paul Munroe, Australia  
Jae-Min Myoung, Republic of Korea  
Rajesh R. Naik, USA  
Albert Nasibulin , Russia  
Ngoc Thinh Nguyen , Vietnam  
Hai Nguyen Tran , Vietnam  
Hiromasa Nishikiori , Japan

Sherine Obare , USA  
Abdelwahab Omri , Canada  
Dillip K. Panda, USA  
Sakthivel Pandurengan , India  
Dr. Asisa Kumar Panigrahy, India  
Mazeyar Parvinzadeh Gashti , Canada  
Edward A. Payzant , USA  
Alessandro Pegoretti , Italy  
Oscar Perales-Pérez, Puerto Rico  
Anand Babu Perumal , China  
Suresh Perumal , India  
Thathan Premkumar , Republic of Korea  
Helena Prima-García, Spain  
Alexander Pyatenko, Japan  
Xiaoliang Qi , China  
Haisheng Qian , China  
Baskaran Rangasamy , Zambia  
Soumyendu Roy , India  
Fedlu Kedir Sabir , Ethiopia  
Lucien Saviot , France  
Shu Seki , Japan  
Senthil Kumaran Selvaraj , India  
Donglu Shi , USA  
Muhammad Hussnain Siddique , Pakistan  
Bhanu P. Singh , India  
Jagpreet Singh , India  
Jagpreet Singh, India  
Surinder Singh, USA  
Thangjam Ibomcha Singh , Republic of Korea  
Korea  
Vidya Nand Singh, India  
Vladimir Sivakov, Germany  
Tushar Sonar, Russia  
Pingan Song , Australia  
Adolfo Speghini , Italy  
Kishore Sridharan , India  
Marinella Striccoli , Italy  
Andreas Stylianou , Cyprus  
Fengqiang Sun , China  
Ashok K. Sundramoorthy , India  
Bo Tan, Canada  
Leander Tapfer , Italy  
Dr. T. Sathish Thanikodi , India  
Arun Thirumurugan , Chile  
Roshan Thotagamuge , Sri Lanka

Valeri P. Tolstoy , Russia  
Muhammet S. Toprak , Sweden  
Achim Trampert, Germany  
Tamer Uyar , USA  
Cristian Vacacela Gomez , Ecuador  
Luca Valentini, Italy  
Viet Van Pham , Vietnam  
Antonio Vassallo , Italy  
Ester Vazquez , Spain  
Ajayan Vinu, Australia  
Ruibing Wang , Macau  
Magnus Willander , Sweden  
Guosong Wu, China  
Ping Xiao, United Kingdom  
Zhi Li Xiao , USA  
Yingchao Yang , USA  
Hui Yao , China  
Dong Kee Yi , Republic of Korea  
Jianbo Yin , China  
Hesham MH Zakaly , Russia  
Michele Zappalorto , Italy  
Mauro Zarrelli , Italy  
Osman Ahmed Zeleke, Ethiopia  
Wenhui Zeng , USA  
Renyun Zhang , Sweden

## Contents


### **Synchronous and Futuristic Views on the Application of Silver Nanoparticles: A Journey towards Green Synthesis**

N. Nagaprasad , D. Chandralekha, Veera Venkata Satyanarayana Reddy Karri, R. Shanmugam , L. Priyanka Dwarampudi, Jule Leta Tesfaye , and R. Krishnaraj   
Research Article (9 pages), Article ID 7411352, Volume 2022 (2022)






### **Corrigendum to “A Pilot Study on Nanotherapy of *Momordica charantia* against Trimethyltin Chloride-Induced Neurotoxicity in *Danio rerio* (Zebrafish)”**

Bharathi Kumar, Siva Vijayakumar Tharumasivam, Vasuki Boominathan, Elumalai Perumal, Prabu Dhandapani, Kumaravel Kaliyaperumal, Suresh Arumugam, Kumaran Subramanian, Pugazhvendan Sampath Renuga, Vasanth Sakthivel, Bupesh Giridharan, Wilson Aruni, and Lokesh Kumar Boopathy  
Corrigendum (1 page), Article ID 9857195, Volume 2022 (2022)


### **Effect of Hafnium Coating on Osseointegration of Titanium Implants: A Split Mouth Animal Study**

Vaishnavi Rajaraman, Deepak Nallaswamy, Dhanraj Ganapathy, S. Rajeshkumar , Padma Ariga, and Karthik Ganesh  
Research Article (9 pages), Article ID 7512957, Volume 2021 (2021)




### **Antimicrobial Properties of Silver Nitrate Nanoparticle and Its Application in Endodontics and Dentistry: A Review of Literature**

Lakshmi Thangavelu , Abdul Habeeb Adil, Sohaib Arshad, Ezhilarasan Devaraj , Sreekanth Kumar Mallineni , Rishitha Sajja, Anil Chakradhar , and Mohmed Isaqali Karobari   
Review Article (12 pages), Article ID 9132714, Volume 2021 (2021)






### **A Pilot Study on Nanotherapy of *Momordica charantia* against Trimethyltin Chloride-Induced Neurotoxicity in *Danio rerio* (Zebrafish)**

Bharathi Kumar, Siva Vijayakumar Tharumasivam, Vasuki Boominathan, Elumalai Perumal, Prabu Dhandapani, Kumaravel Kaliyaperumal, Suresh Arumugam, Kumaran Subramanian, Pugazhvendan Sampath Renuga, Vasanth Shakhthivel, Bupesh Giridharan, Wilson Aruni, and Lokesh Kumar Boopathy   
Research Article (12 pages), Article ID 2180638, Volume 2021 (2021)



### **Novel Nano-Based Drug Delivery Systems Targeting Hepatic Stellate Cells in the Fibrotic Liver**

Devaraj Ezhilarasan , Thangavelu Lakshmi , and Biond Raut   
Review Article (9 pages), Article ID 4674046, Volume 2021 (2021)


### **Mycosynthesis and Physicochemical Characterization of Vanadium Oxide Nanoparticles Using the Cell-Free Filtrate of *Fusarium oxysporum* and Evaluation of Their Cytotoxic and Antifungal Activities**

Mohammadhassan Gholami-Shabani , Fattah Sotoodehnejadnematlahi , Masoomeh Shams-Ghahfarokhi , Ali Eslamifar , and Mehdi Razzaghi-Abyaneh   
Research Article (12 pages), Article ID 7532660, Volume 2021 (2021)

### **Applications of Nanomaterials in Agrifood and Pharmaceutical Industry**



Hiwa M. Ahmed , Arpita Roy , Muhammad Wahab, Mohammed Ahmed, Gashaw Othman-Qadir, Basem H. Elesawy, Mayeen Uddin Khandaker, Mohammad Nazmul Islam, and Talha Bin Emran  
Review Article (10 pages), Article ID 1472096, Volume 2021 (2021)

**Citrus Lemon Juice Mediated Preparation of AgNPs/Chitosan-Based Bionanocomposites and Its Antimicrobial and Antioxidant Activity**

S. Rajeshkumar 




Research Article (10 pages), Article ID 7527250, Volume 2021 (2021)

**Green versus Chemical Precipitation Methods of Preparing Zinc Oxide Nanoparticles and Investigation of Antimicrobial Properties**

Bulcha Bekele, Anatol Degefa, Fikadu Tesgera, Leta Tesfaye Jule, R. Shanmugam, L. Priyanka Dwarampudi, N. Nagaprasad , and Krishnaraj Ramasamy 

Research Article (10 pages), Article ID 9210817, Volume 2021 (2021)

**Ecofriendly/Rapid Synthesis of Silver Nanoparticles Using Extract of Waste Parts of Artichoke (*Cynara scolymus* L.) and Evaluation of their Cytotoxic and Antibacterial Activities**

Ayşe Baran, Mehmet Fırat Baran, Cumali Keskin , Sevgi Irtegun Kandemir, Mahbuba Valiyeva, Sevil Mehraliyeva, Rovshan Khalilov , and Aziz Eftekhari 



Research Article (10 pages), Article ID 2270472, Volume 2021 (2021)

**Green Synthesis, Characterization of Zinc Oxide Nanoparticles, and Examination of Properties for Dye-Sensitive Solar Cells Using Various Vegetable Extracts**

Anatol Degefa, Bulcha Bekele, Leta Tesfaye Jule, Boka Fikadu, Shanmugam Ramaswamy, Lalitha Priyanka Dwarampudi, N. Nagaprasad , and Krishnaraj Ramaswamy 

Research Article (9 pages), Article ID 3941923, Volume 2021 (2021)

**Green Synthesis and Characterizations of Zinc Oxide (ZnO) Nanoparticles Using Aqueous Leaf Extracts of Coffee (*Coffea arabica*) and Its Application in Environmental Toxicity Reduction**

Saka Abel, Jule Leta Tesfaye, R. Shanmugam, L. Priyanka Dwarampudi, Gudeta Lamessa, N. Nagaprasad , Mekonen Benti, and Ramaswamy Krishnaraj 

Research Article (6 pages), Article ID 3413350, Volume 2021 (2021)

**Anticariogenic Effect of Selenium Nanoparticles Synthesized Using *Brassica oleracea***

Ganapathy Dhanraj  and Shanmugam Rajeshkumar 

Research Article (9 pages), Article ID 8115585, Volume 2021 (2021)



## Research Article

# Synchronous and Futuristic Views on the Application of Silver Nanoparticles: A Journey towards Green Synthesis

**N. Nagaprasad**<sup>1</sup>, **D. Chandralekha**<sup>2</sup>, **Veera Venkata Satyanarayana Reddy Karri**<sup>3</sup>,  
**R. Shanmugam**<sup>4</sup>, **L. Priyanka Dwarampudi**<sup>5</sup>, **Jule Leta Tesfaye**<sup>6,7</sup> and **R. Krishnaraj**<sup>7,8</sup>

<sup>1</sup>Department of Mechanical Engineering, ULTRA College of Engineering and Technology, Madurai, 625104 Tamil Nadu, India

<sup>2</sup>Department of Pharmaceutical Analysis, Sree Vidyanikethan College of Pharmacy, Tirupati, Andhra Pradesh, India

<sup>3</sup>Department of Pharmaceutics, JSS College of Pharmacy, JSS Academy of Higher Education & Research, Ooty, Nilgiris, Tamil Nadu, India

<sup>4</sup>TIFAC, CORE-HD, JSS College of Pharmacy, JSS Academy of Higher Education & Research, Ooty, Nilgiris, Tamil Nadu, India

<sup>5</sup>Department of Pharmacognosy, JSS Academy of Higher Education and Research, JSS College of Pharmacy Ooty, Tamil Nadu, India

<sup>6</sup>Department of Physics, College of Natural and Computational Science, Dambi Dollo University, Ethiopia

<sup>7</sup>Centre for Excellence-Indigenous Knowledge, Innovative Technology Transfer and Entrepreneurship, Dambi Dollo University, Ethiopia

<sup>8</sup>Department of Mechanical Engineering, College of Engineering and Technology, Dambi Dollo University, Ethiopia

Correspondence should be addressed to R. Shanmugam; shanmugam\_55555@yahoo.co.in and R. Krishnaraj; prof.dr.krishnaraj@dadu.edu.et

Received 26 July 2021; Accepted 10 March 2022; Published 4 April 2022

Academic Editor: Shijun Liao

Copyright © 2022 N. Nagaprasad et al. This is an open access article distributed under the Creative Commons Attribution License, which permits unrestricted use, distribution, and reproduction in any medium, provided the original work is properly cited.

Historically, silver has been recognized as a powerful antibacterial agent with a broad spectrum of functions, and it has been employed safely in healthcare for several years. It seems that the incorporation of silver into embedded medical devices may be advantageous when particular genetic features, including such antibacterial behavior, are needed for the device to function. According to current and prior bacterial studies, it appears that the toxicity against bacteria was significantly more significant than the toxicity against human cells. Silver nanoparticles are nanoparticles with sizes ranging between one and one hundred nanometers (nm) in size. When it comes to molecular diagnostics, therapies, and equipment that are employed in a wide range of medical procedures, silver nanoparticles have a number of unique qualities that make them very useful. The physical and chemical approaches are the two majority ways for the creation of silver nanoparticles. The challenge with chemical and physical approaches is that the synthesis is complicated and can result in harmful compounds being absorbed onto the surfaces of the materials. In order to address this, the biological technique offers a viable alternative solution. Bacteria, fungus, and plant extracts are the three principal biological systems concerned in this process. A complete overview of the mechanism of action, manufacture, and uses in the medical area, as well as the healthcare and ecological concerns that are believed to be produced by these nanoparticles, is provided in this paper. The emphasis is on the proper and effective synthesis of silver nanoparticles even while exploring their numerous promising utility and attempting to assess the current status in the debates over the toxicity concerns that these nanoparticles pose, as well as attempting to reflect the needs in the debates over the toxicity concerns that these nanoparticles pose.

## 1. Introduction

When applied to science and technology, ecological nanotechnology has proven to be successful in providing answers for problems in a variety of fields, including healthcare and

catalysis, as well as industrial and farming applications. Nanostructures are the primary concern for all applications of nanotechnology, regardless of where they are found in nature, and the size of nanoparticles (NPs) determines their characteristic qualities. For thousands of years, silver and its

derivatives have been utilized as antibacterial and medicinal agents for various purposes. When storing water, food, and wine, the early Greeks and Romans utilized silverware in order to prevent decomposition. Historically, Hippocrates employed silver concoctions to cure ulcers and speed the healing of wounds. Silver nitrate was also utilized for pain management and instrument disinfecting [1–3]. Silver nanoparticles are well-known for their broad antibacterial spectrum and excellent antimicrobial activity; they are capable of killing a wide range of organisms even at extremely low concentrations. Silver, which is really a transition metal in the same group as copper and gold, is a smooth, white, glossy element with significant electrical and thermal conductivity [4–7]. Before it was recognized that bacteria are agents of infection, it was well-known for its medicinal and therapeutic effects, as well as its anti-inflammatory properties. Biotechnology, on the other hand, is concerned with the molecular, hereditary, and cellular processes that are involved in the development of medications for agricultural use [8]. It is possible that these latest updates in the farming sector will make a contribution to overcoming the challenges posed by climate change in terms of food security in their own right. Farming is the foundation of emerging countries; 60 percent of the population depends on their livelihood. Silver nanoparticles, in addition to their most well-studied antimicrobial and anticancer properties, have gained attention for their potential use in a variety of other cutting-edge clinical applications such as wound healing, tissue repair, tooth material filling, vaccine adjuvants (such as insulin), antidiabetic agents, and bioimaging [9–25]. In addition, we will provide a brief overview of these biomedical applications in this study [9–18]. On a regular basis, various illness organisms such as the Avian influenza virus, HIV/AIDS, the Middle East respiratory syndrome (MERS), the Ebola virus, and the zika virus are exposed to the environment, making it difficult to cure them [19]. Numerous studies are concentrating their efforts on employing silver nanoparticles as a method to combat these diseases because of their distinctive physical-chemical and biological features. This paper presents an objective evaluation of the usage of silver nanoparticles and their potential toxicity, as well as insights into the more profound significance of these findings for medical practice and research.

## 2. Applications of Silver Nanoparticles

### 2.1. Applications of Silver Nanoparticles in Pharmacy, Medicine, and Dentistry

- (a) Dermatitis treatment and HIV-1 propagation suppression [20]
- (b) Peptic ulcer and acne medication [21]
- (c) Antimicrobial agent used to treat contagious organisms [22]
- (d) Remotely controlled laser intensity induces microcapsule aperture [23]
- (e) Nanocomposite with a silver medal for cell labeling [20]
- (f) Cancerous cells imaging at the molecular level [24]
- (g) Spectrum analysis of improved Raman scattering (SERS) [25]
- (h) Identifying viral components (SERS and silver nanorods) [26]
- (i) Hospital fabric finishing (surgical nightgown and aspect mask) [27]
- (j) Bone cement additives [20]
- (k) Stockings for orthopedic use [28]
- (l) Wound treatment with hydrogel [29]
- (m) Polymerizable alveolar material additive silver-loaded SiO<sub>2</sub> nanoparticles [30]
- (n) Composite resin filler with a patent (dental resin composite) [28]

Polythene tubes bearing fibrin sponges were placed in Ag nanoparticles dispersion and allowed to dissolve. Using antibacterial agents, silver medal nanoparticles are employed for a variety of purposes, from cleaning medical devices and household appliances to water purification [1–6]. Furthermore, this gave the textile industry the confidence to use AgNPs in a variety of textile applications. The antibacterial effect of AgNPs in cotton fibers towards *Escherichia coli* was demonstrated by the researchers [7]. Silver nanoparticles were discovered to catalyze the chemiluminescent from the luminol–hydrogen peroxide system exhibiting catalytic activity superior to that of Au and Pt colloid, demonstrating superior catalytic activity [8]. Currently, the inkjet technique has been employed to fabricate flexible electronic circuits at the depression toll, and numerous research has been published in recent years to support this claim [9–11]. Due to the extreme homogeneity of the nanosized metal particles scattered throughout the inks and the electrical conductivity of its nanosized metallic particles, nanosized metal particles like Au or Ag are indispensable for the fabrication of electronic circuits. AgNP's with minute size can be used frequently, having a high electrical conductivity, making them suitable for use in the construction of electronic circuits. Nanoparticles should be sintered in order to achieve high electrical conductivity in electronic circuits throughout the manufacturing process.

2.2. *Bactericide*. The antibacterial activity of Ag nanoparticles toward bacteria from both Gram-positive and Gram-negative strains may be attributable to either (I) the establishment of a pore in the cell rampart that also consequently results in the escape of cellular substance or (II) the silver-grey ion perforate through ion channels that does not damage the cell tissue layers but moreover denatures the ribosome as well as inhibits the expression of enzymes containing silver-grey ions. AgNPs play an important role throughout the respiratory chain by interfering with the action of enzymes that are attached to the membranes [12].

2.3. *Fungicide*. Severe fungal infections have had a significant role in the rising frequency of a certain disease, as well as the

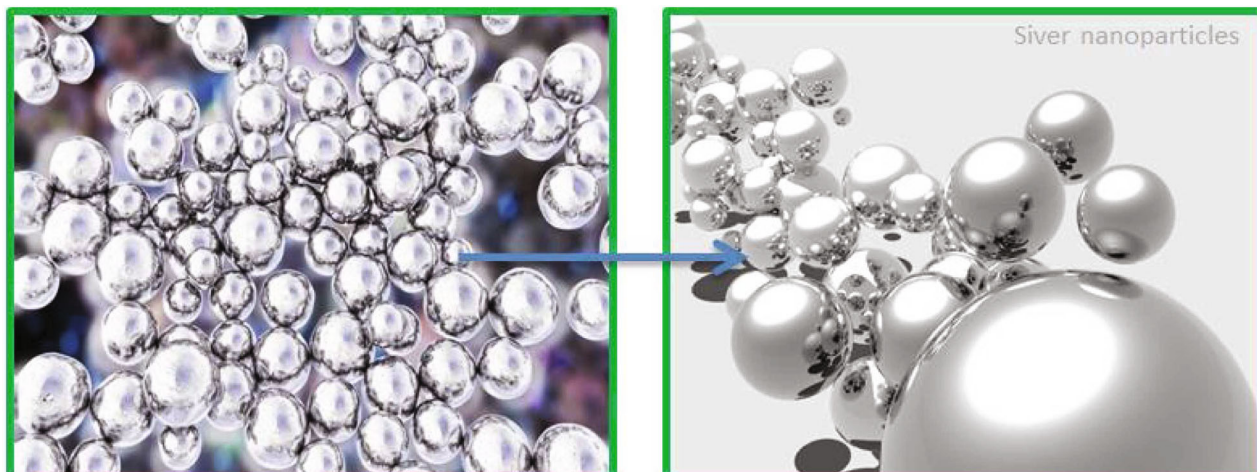


FIGURE 1: Silver nanoparticles.

increasing mortality of immunocompromised people in recent years [15]. *Candida* species, among the most common pathogens responsible for fungal infections, are among the most overlooked. It frequently causes nosocomial infection, which can result in a death rate of up to 40% in hospitalized patients [16]. A total of 44 antifungal strains of 6 fungal species were tested by Sun et al. to establish the antifungal effect of silver nanoformulation [17]. According to the literature, AgNPs are effective against *Candida glabrata*, *Candida albicans*, *Candida krusei*, *Candida parapsilosis*, and *T. mentagrophytes* in a potent manner. Several recent studies have demonstrated that AgNPs mediated by *Tulasi* (*Ocimum sanctum* L.) have antifungal efficacy against pathogenic fungal infections in humans [18]. As a result, AgNPs are believed to be a strong and rapid-acting antifungal against a broad spectrum of widespread fungus, including those belonging to the genera *Aspergillus*, *Candida*, and *Saccharomyces*.

**2.4. Antiviral Agent.** In particular, the cytoprotective qualities of silver are well-known, and it has been used to block the contact of the human immunodeficiency virus with host cells [19]. Agonist nanoparticles (AgNPs) can also be utilized to avoid infection following surgery [20]. Recent investigations have revealed that AgNPs contact HIV-1 by binding predominantly to the gp120 glycoprotein. The minimal contact of AgNPs with the virus concretely limits the virus's ability to attach to host cells [21]. The use of a luciferase-based pseudovirus entrance experiment demonstrated that AgNPs effectively blocked viral entry by interfering with the integrity of the virus. According to these findings, AgNPs are very effective microbicides towards SARS-CoV-2; nevertheless, they should be handled with care due to their cytotoxic actions as well as the possibility of destabilising natural ecosystems if they are not properly disposed of [31].

### 3. Medical Devices

**3.1. Wound Dressing.** When it comes to topical applications, such as wound care, burn treatment, and infection preven-

tion creams [22], AgNPs have a lot of potentials. AgNPs are widely used in medical equipment and implants, and their properties are well understood. In addition, they are being integrated into consumer goods like colloidal silver gel as well as silver-embedded fabrics, which are currently being used in athletic equipment, among other things. In the healing of wounds or burns, silver-coated biomedical equipment, implants, or textile fibers are used, as well as on glass windows and similar surfaces, to keep the environment clean and sanitary. Given that metallic AgNPs are highly effective microbicidal agents, they have garnered considerable attention in a variety of applications ranging between paints and textiles. Figure 1 illustrates the silver nanoparticles.

**3.2. Catheters.** The bioactive AgNPs are deposited on the inside of the plastic catheters. The scientists created an application approach that resulted in a thin (hundred nm) coating of silver nanoparticles on the outside of the catheters after applying the nanoparticles. They are biocompatible because they are nontoxic and have the ability to release categorical and prolonged relinquishment of silver at the insertion site [23–25]. In these catheters, the threat of infection is greatly reduced owing to the consequential *in vitro* antimicrobial action caused by the prohibition of biofilm shaping using *Escherichia coli*, *Enterococcus*, *Staphylococcus aureus*, coagulase-negative staphylococci, species *Pseudomonas aeruginosa*, and *Candida albicans*.

**3.3. Bone Cement.** Bone cement containing AgNPs and the additive polymethyl methacrylate (PMMA) has been developed. These bone cements are eager to also have efficacious antibacterial agents toward methicillin-resistant *S. epidermidis* and *S. aureus*. They also demonstrated cognitively challenged biofilm magnification in the presence of these bacteria [27]. Because of the inclusion of AgNPs in bone cement, it has antibacterial properties. Bone cement is a substance that is used by orthopedic surgeons for annexing prostheses such as hip and knee replacements. Infection rates associated with joint supersession surgery are significant, ranging from 1.0 to 4.0 percent on average [28]. As a

result of the spread of antibiotic resistance, the use of antibiotics is becoming increasingly restricted. This study indicated that nanosilver-PMMA bone cementum reduces the comparative incidence of resistance through a variety of mechanisms. It also received recognition because of its natural antibacterial activity and low cytotoxic potential.

**3.4. Tumor.** A build-up of reactive oxygen coinage may cause serious damage to biological molecules such as proteins, lipids, and DNA, which can ultimately result in the death of the cell in some cases. Cell death and oxidative stress have been shown to be induced by AgNPs in skin cancer cells and in humans' fibrosarcoma, according to recent findings. AgNPs have also been shown to activate the p53-mediated apoptotic pathway, which would be the pathway via which the vast majority of chemotherapeutic medicines cause apoptosis [29, 30]. Additional research has been conducted on the antiproliferative properties of piperidine derived from *Piper nigrum* towards cancer cell lines. Silver nanoparticles decreased by extracts of *Piper longum* could have a potent cytotoxic effect on the HEp-2 cell line when employed at a low dose. As a result, silver nanoparticles can be used in the creation of anticancerous drugs.

**3.5. Water Purification.** As a result of their improved antibacterial properties, AgNPs can be used for water treatment in water filtering systems. In accordance with the World Health Organization (WHO) guidelines, silver nanotechnology can be used in dihydrogen monoxide water treatment. Antimicrobial compounds are being considered for application in biomedical devices and healthcare and also in the victuals and hygiene sectors, in order to prevent the multiplication of harmful microorganisms on the surface of the equipment or on the surface of the product. Chemically resistant antimicrobial coatings should have high antibacterial efficacy while also being simple to manufacture and have low toxicity. Silver and silver-containing surfaces have long been used as antimicrobial coatings on a variety of surfaces [32, 33].

**3.6. Catalytic Function.** With the use of AgNPs produced from the plant *Guggulu tiktakam* Kashayam, the researchers were able to reduce methylene blue (MB) by fourfold [34], which they found to be highly effective in the reduction of MB. As previously reported, Waghmode et al. investigated the strengthened catalytic activity upon on decrease of benzyl cluster chloride through *Acacia nilotica* pod-mediated AgNP's altered glassy carbon electrode even though compared to the activity of glassy carbon as well as metallic silver electrodes in the presence of *Acacia nilotica* pod-mediated AgNP's altered glassy carbon electrode [35, 36]. The decomposition of methylene blue by AgNPs in the presence of *Gloriosa splendid* extract has been reported [37]. A study conducted by Kreibig and Vollmer used *Triticum aestivum* extract to synthesize AgNPs and found that AgNPs are an effective nanoaccelerator in the lowering of hydrogen peroxide. AgNPs mediated by plant extracts have also been found to be effective in the degradation of 4-nitrophenol (4-NP) onto 4-aminophenol (4-AP) [38].

**3.7. Biosensors.** It has been shown [38–41] that the size, shape, and dielectric mass medium surrounding AgNPs have a significant impact on their plasmonic capabilities. This dependence may, as a result, contribute to the usability of AgNPs in biosensor applications. This is because the refractive strength of biomolecules is greater than that of buffer storage solutions; as previously stated, surface plasmon reverberance (SPR) is used to measure the performance of biosensors that comprise plasmonic nanoparticles (local Earth surface plasmon resonance (LSPR)) and commercialized thin, plasmonic Dixie films [42]. They have a greater spatial resolution than SPR biosensors because they are less sensitive to changes in bulk refractive index, which reduces the amount of error introduced by the shift in bulk refractive index [43]. The variously shaped AgNPs are used in biosensors to detect different types of interactions between them. Biotin-streptavidin interactions were detected using the surface-coated nanobiosensor [44], which was developed to detect interactions among biomolecules. Silver nanoparticles with cubical or rhombohedral shapes were also employed to detect protein interactions in a variety of applications [45–48]. Recently, findings have been published on the use of AgNPs as predicted biosensors in cancer cells. Scientists have also established the use of nanosilver covered with silica as biosensors for the identification of bovine blood serum albumin (BSA), according to their findings.

**3.8. Bioimaging.** As a result of their plasmonic features, AgNPs may be identified using a wide range of optical microscopy methods, making them an excellent alternative to routinely employ fluorescent organic dyes that disintegrate throughout imaging (photobleaching). In addition to being photostable, AgNPs have the potential to be used as biological probes to monitor continuously dynamic events over an extended length of time. Authentic-time research of AgNPs was demonstrated by Raja et al. to track early embryonic development in terms [49]. Such minute metallic nanoparticles possess unique plasmonic features, which in turn inspire its application as a medicinal agent. Two approaches are used to use silver nanoparticle (AgNP) technology for bioimaging: incubating AgNPs with cells in order to assess physical contacts and uptake or functionalizing biomolecule on the surface of AgNPs in order to increase selectivity for the cell membrane. The former is more straightforward, but the latter necessitates the use of a categorical biofunctionalization molecule. The effects of AgNPs on neuroblastoma cells were investigated in the dark using a night-field illumination system. After being cultured with macrophages for a short period of time, AgNPs attached to iron oxide nanoparticles were imaged using two-photon imaging to determine whether they had been taken up by the cells [49–51].

**3.9. Agricultural Applications.** Nanosilver is the nanoparticle that has been investigated and used the most in biosystems. Significant inhibitory and bactericidal properties, as well as a wide range of antimicrobial activity, have been demonstrated in studies with this compound. Comparing silver nanoparticles to bulk silver, silver nanoparticles with a high

surface area and a considerable fraction of surface atoms exhibit a significant antibacterial effect. AgNPs have been investigated as a viable contender for increasing crop productivity by promoting seed germination as well as plant growth, and they have shown promise. It is possible that the amount of Ag nanoparticles (AgNPs) will have an impact on the growth rate of plants, either positively or negatively. Bacterial infections are another factor contributing to major crop yield losses around the world. AgNPs have been shown to be effective against bacteria that cause plant disease. When tested against the bacteria *Erwinia carotovora*, AgNPs show significantly more antimicrobial property over conventional antibiotics. Double capsulated nanosilver was created using a chemical process of silver ion with the assistance of a physical method, a reducing agent, and stabilisers, among other ingredients. It kills bacteria that are harmful to plants in planter soils as well as hydroponics systems. Furthermore, silver is a highly effective plant growth booster [52–66].

#### 4. Miscellaneous Applications of Silver Nanoparticles

*4.1. Water Treatment.* Using leaf infusion freshly at 80°C bud from the genus *Anacardium occidentale*, we were able to create stable AgNPs that were used in a unique inquiry for the detection of chromium ions in common water. Whenever the concentration of silver nanoparticles made using *Prosopis juliflora* leaf extract (10 mg) was combined with 100 ml of wastewater after six h and step-ups as the period of brooding growth approached, the number of bacteria decreased. Silver nanoparticles (Ag NPs) are incredibly poisonous to microorganisms. As a result, they exhibit potent antibacterial properties against a broad spectrum of pathogens, including viruses, bacteria, and fungi, among others. Silver nanoparticles, which are effective antibacterial agents, have been widely employed in the disinfection of drinking water [52–59].

#### 5. Scientific Applications

- (a) Silver nanomaterials can be used in a variety of scientific coatings due to their outstanding physical, chemical, and optical holding properties, among other things. Depending on the size, arrangement, and chemical nature of the nanomaterial, these qualities can be drastically different from one another
- (b) Metallic nanoparticles, especially nanosilver, display surface plasmon resonance (SPR) when exposed to light, resulting in SPR efflorescence in the ultraviolet half-dozen wavelength range, which can be used to detect the particles [54]
- (c) An outcome of the exchanges among incident light and an unbound electron throughout the conduction band of a nanomaterial, the SPR is produced by the nanomaterial

- (d) Surface plasmon resonance (SPR) peaks are characterized by their breadth and location, which are determined by the size, structure, and surface features of the nanomaterial [55]
- (e) Silver nanoparticles are commonly used for surface improved Raman scattering, and they are particularly effective (SERS). Whereas if analyte molecules were adsorbed on a hard metal surface, the Raman scattering by the analyte molecules might be amplified, resulting in an increase in the enhancement factor, which would allow for sufficient sensitivity to identify single molecules [67–73]
- (f) Consequently, silver nanomaterials have the potential to be used in sensing applications such as the identification of deoxyribonucleic acid chains [56, 57]
- (g) Colorimetric detector for histidine, real-time probing of membrane transport in living microbial cells, beam desorption mass spectrographic characterization of peptides, and a colorimetric detector for histidine [58, 59]
- (h) Colorimetric detector for assessing ammonia water content biosensors enabling identification of glucose sensors with medical diagnostics [60, 61]
- (i) Silver nanoparticles are also expected to be used in metal-improved fluorescence activities, according to recent reports. When metallic nanostructures are used in conjunction with fluorophores, their intrinsic spectral characteristics can be changed [74–78]
- (j) The closeness of metallic nanosilver resulted in an increase in the strength of low quantum proceed fluorophores due to the presence of metallic nanosilver. Fluorophore quenching over small periods, geographic change of the incident light theatre of operations, and vicissitudes in the radioactive decay rate are all factors contributing to the burden [62]
- (k) Using nano-Ag in purposes including such immunochemical assays and DNA/RNA detection is made possible by the device characteristics described above. Since it was previously stated, the airfoil features of the Earth have a significant impact on the features of the silver nanomaterial used in this research [64–66, 79–83]
- (l) Using an alkanethiol to modify the surface of a silver nano-optical prism, which may make them a suitable candidate for streptavidin as well as antibiotin sensing, as well as for the treatment of Alzheimer's illness is a promising approach [84–88]

#### 6. Conclusions

Silver nanoparticles have diverse physical properties that distinguish them from other biomaterials that are regularly used in dental care, and they have the potential to be used

in a variety of applications, including restorative dentistry, prosthetic dental services, endodontics, implantology, oral cancers, and periodontology. Because of their antibacterial, antiviral, and antifungal properties, silver nanoparticles have tremendous potential. Inclusion of AgNPs reduces biofilm development on nanocomposite, avoiding microleakage and supplementary caries. The precise mechanisms of connection with silver nanoparticles to bacterial cells must be clarified, as well as how the surface area of nanoparticles impacts its killing function. Animal models and clinical trials must also be conducted in order to gain a better knowledge of the antimicrobial performance of silver dressings and the toxicity of silver coatings, if any are used, among other things. As a result, care must be made to use this marvel wisely and in a decent, effective, and efficient manner while also comprehending its limitations and taking every precaution to ensure that it does not hurt people or the ecosystem. Overall, silver nanoparticles look to be potential in pharmaceutical, biomedical, and related disciplines owing to their unique silver and nanosized features, provided safety evidence is generated to verify their safety while similarly ruling out their toxicity.

## Data Availability

The data used to support the findings of this study are included within the article.

## Conflicts of Interest

The authors declare that there are no conflicts of interest.

## References

- [1] M. Bosetti, A. Masse, E. Tobin, and M. Cannas, "Silver coated materials for external fixation devices: in vitro biocompatibility and genotoxicity," *Biomaterials*, vol. 23, no. 3, pp. 887–892, 2002.
- [2] P. Jain and T. Pradeep, "Potential of silver nanoparticle-coated polyurethane foam as an antibacterial water filter," *Biotechnology and Bioengineering*, vol. 90, no. 1, pp. 59–63, 2005.
- [3] Q. Li, S. Mahendra, D. Y. Lyon et al., "Antimicrobial nanomaterials for water disinfection and microbial control: potential applications and implications," *Water Research*, vol. 42, no. 18, pp. 4591–4602, 2008.
- [4] M. Cho, H. Chung, W. Choi, and J. Yoon, "Different inactivation behaviors of MS-2 phage and *Escherichia coli* in TiO<sub>2</sub> photocatalytic disinfection," *Applied and Environmental Microbiology*, vol. 71, no. 1, pp. 270–275, 2005.
- [5] N. Durna, P. D. Marcato, G. I. De Souza, O. L. Alves, and E. Esposito, "Antibacterial effect of silver nanoparticles produced by fungal process on textile fabrics and their effluent treatment," *Journal of Biomedical Nanotechnology*, vol. 3, no. 2, pp. 203–208, 2007.
- [6] J. Z. Guo, H. Cui, W. Zhou, and W. Wang, "Ag nanoparticle-catalyzed chemiluminescent reaction between luminol and hydrogen peroxide," *Journal of Photochemistry and Photobiology A: Chemistry*, vol. 193, no. 2-3, pp. 89–96, 2008.
- [7] S. Cheng, H. Liu, H. Zhang, G. Chu, Y. Guo, and X. Sun, "Ultrasensitive electrochemiluminescence aptasensor for kanamycin detection based on silver nanoparticle-catalyzed chemiluminescent reaction between luminol and hydrogen peroxide," *Sensors and Actuators B: Chemical*, vol. 304, article 127367, 2020.
- [8] Y. Guo, F. Yang, Y. Yao et al., "Novel Au-tetrahedral aptamer nanostructure for the electrochemiluminescence detection of acetamidrid," *Journal of Hazardous Materials*, vol. 401, article 123794, 2021.
- [9] T. Jullabuth and P. Danwanichakul, "Silver nanoparticle synthesis using the serum obtained after rubber coagulation of skim natural rubber latex with chitosan solution," *Engineering and Applied Science Research*, vol. 48, no. 4, pp. 422–431, 2021.
- [10] P. K. Stoimenov, R. L. Klinger, G. L. Marchin, and K. J. Klambunde, "Metal oxide nanoparticles as bactericidal agents," *Langmuir*, vol. 18, no. 17, pp. 6679–6686, 2002.
- [11] I. Sondi and B. Salopek-Sondi, "Silver nanoparticles as antimicrobial agent: a case study on *E. coli* as a model for Gram-negative bacteria," *Journal of Colloid and Interface Science*, vol. 275, no. 1, pp. 177–182, 2004.
- [12] S. Pal, Y. K. Tak, and J. M. Song, "Does the antibacterial activity of silver nanoparticles depend on the shape of the nanoparticle? A study of the gram-negative bacterium *Escherichia coli*," *Applied and Environmental Microbiology*, vol. 73, no. 6, pp. 1712–1720, 2007.
- [13] G. S. Martin, D. M. Mannino, S. Eaton, and M. Moss, "The epidemiology of sepsis in the United States from 1979 through 2000," *New England Journal of Medicine*, vol. 348, no. 16, pp. 1546–1554, 2003.
- [14] A. Panacek, M. Kolar, R. Vecerova et al., "Antifungal activity of silver nanoparticles against *Candida* spp.," *Biomaterials*, vol. 30, no. 31, pp. 6333–6340, 2009.
- [15] J. S. Kim, E. Kuk, K. N. Yu et al., "Antimicrobial effects of silver nanoparticles," *Nanomedicine: Nanotechnology Biology and Medicine*, vol. 3, no. 1, pp. 95–101, 2007.
- [16] N. Khatoun, A. Mishra, H. Alam, N. Manzoor, and M. Sardar, "Biosynthesis, characterization, and antifungal activity of the silver nanoparticles against pathogenic *Candida* species," *Bio-NanoScience*, vol. 5, no. 2, pp. 65–74, 2015.
- [17] R. W. Y. Sun, R. Chen, N. P. Y. Chung, C. M. Ho, C. L. S. Lin, and C. M. Che, "Silver nanoparticles fabricated in Hepses buffer exhibit cytoprotective activities toward HIV-1 infected cells," *Chemical Communications*, vol. 40, pp. 5059–5061, 2005.
- [18] J. L. Elechiguerra, J. L. Burt, J. R. Morones et al., "Interaction of silver nanoparticles with HIV-1," *Journal of Nanobiotechnology*, vol. 3, no. 1, pp. 1–10, 2005.
- [19] H. H. Lara, N. V. Ayala-Nunez, L. Ixtepan-Turrent, and C. Rodriguez-Padilla, "Mode of antiviral action of silver nanoparticles against HIV-1," *Journal of Nanobiotechnology*, vol. 8, no. 1, pp. 1–10, 2010.
- [20] R. O. Becker, "Silver ions in the treatment of local infections," *Metal-Based Drugs*, vol. 6, no. 4-5, 314 pages, 1999.
- [21] M. E. Rupp, T. Fitzgerald, N. Marion et al., "Effect of silver-coated urinary catheters: efficacy, cost-effectiveness, and antimicrobial resistance," *American Journal of Infection Control*, vol. 32, no. 8, pp. 445–450, 2004.
- [22] F. Furno, K. S. Morley, B. Wong et al., "Silver nanoparticles and polymeric medical devices: a new approach to prevention of infection?," *Journal of Antimicrobial Chemotherapy*, vol. 54, no. 6, pp. 1019–1024, 2004.
- [23] D. Chandra Lekha, R. Shanmugam, K. Madhuri et al., "Review on Silver Nanoparticle Synthesis Method, Antibacterial

- Activity, Drug Delivery Vehicles, and Toxicity Pathways: Recent Advances and Future Aspects,” *Journal of Nanomaterials*, vol. 2021, Article ID 4401829, 11 pages, 2021.
- [24] D. Roe, B. Karandikar, N. Bonn-Savage, B. Gibbins, and J. B. Rouillet, “Antimicrobial surface functionalization of plastic catheters by silver nanoparticles,” *Journal of Antimicrobial Chemotherapy*, vol. 61, no. 4, pp. 869–876, 2008.
- [25] V. Alt, T. Bechert, P. Steinrücke et al., “An in vitro assessment of the antibacterial properties and cytotoxicity of nanoparticulate silver bone cement,” *Biomaterials*, vol. 25, no. 18, pp. 4383–4391, 2004.
- [26] C. E. Albers, W. Hofstetter, K. A. Siebenrock, R. Landmann, and F. M. Klenke, “In vitro cytotoxicity of silver nanoparticles on osteoblasts and osteoclasts at antibacterial concentrations,” *Nanotoxicology*, vol. 7, no. 1, pp. 30–36, 2013.
- [27] T. Premkumar, Y. Lee, and K. E. Geckeler, “Macrocycles as a tool: a facile and one-pot synthesis of silver nanoparticles using cucurbituril designed for cancer therapeutics,” *Chemistry—A European Journal*, vol. 16, no. 38, pp. 11563–11566, 2010.
- [28] S. K. Reshmi, E. Sathya, and P. S. Devi, “Isolation of piperidine from Piper nigrum and its antiproliferative activity,” *Journal of Medicinal Plants Research*, vol. 4, no. 15, pp. 1535–1546, 2010.
- [29] R. Pedahzur, O. Lev, B. Fattal, and H. I. Shuval, “The interaction of silver ions and hydrogen peroxide in the inactivation of E. coli: a preliminary evaluation of a new long acting residual drinking water disinfectant,” *Water Science and Technology*, vol. 31, no. 5–6, pp. 123–129, 1995.
- [30] V. S. Suvith and D. Philip, “Catalytic degradation of methylene blue using biosynthesized gold and silver nanoparticles,” *Spectrochimica Acta Part A: Molecular and Biomolecular Spectroscopy*, vol. 118, pp. 526–532, 2014.
- [31] S. S. Jeremiah, K. Miyakawa, T. Morita, Y. Yamaoka, and A. Ryo, “Potent antiviral effect of silver nanoparticles on SARS-CoV-2,” *Biochemical and Biophysical Research Communications*, vol. 533, no. 1, pp. 195–200, 2020.
- [32] T. N. Jebakumar Immanuel Edison and M. G. Sethuraman, “Electrocatalytic reduction of benzyl chloride by green synthesized silver nanoparticles using pod extract of Acacia nilotica,” *ACS Sustainable Chemistry & Engineering*, vol. 1, no. 10, pp. 1326–1332, 2013.
- [33] P. Kumar, M. Govindaraju, S. Senthamilselvi, and K. Premkumar, “Photocatalytic degradation of methyl orange dye using silver (Ag) nanoparticles synthesized from Ulva lactuca,” *Colloids and Surfaces B: Biointerfaces*, vol. 103, pp. 658–661, 2013.
- [34] S. Ashokkumar, S. Ravi, and S. Velmurugan, “Retracted: Green synthesis of silver nanoparticles from Gloriosa superba L. leaf extract and their catalytic activity,” *Spectrochimica Acta Part A: Molecular and Biomolecular Spectroscopy*, vol. 115, pp. 388–392, 2013.
- [35] S. Waghmode, P. Chavan, V. Kalyankar, and S. Dagade, “Synthesis of silver nanoparticles using Triticum aestivum and its effect on peroxide catalytic activity and toxicology,” *Journal of Chemistry*, vol. 2013, 5 pages, 2013.
- [36] A. Gangula, R. Podila, L. Karanam, C. Janardhana, and A. M. Rao, “Catalytic reduction of 4-nitrophenol using biogenic gold and silver nanoparticles derived from Breynia rhamnoides,” *Langmuir*, vol. 27, no. 24, pp. 15268–15274, 2011.
- [37] M. Walton, “Antimicrobial nanosilver coating for commercial applications,” *Advanced Coatings & Surface Technology*, vol. 23, no. 7, pp. 5–6, 2010.
- [38] U. Kreibig and M. Vollmer, *Optical properties of metal clusters*, Springer Science & Business Media, 2013.
- [39] J. Z. Zhang and C. Noguez, “Plasmonic optical properties and applications of metal nanostructures,” *Plasmonics*, vol. 3, no. 4, pp. 127–150, 2008.
- [40] J. N. Anker, W. P. Hall, O. Lyandres, N. C. Shah, J. Zhao, and R. P. Van Duyne, “Synthesis of silver nanoparticles, influence of capping agents, and dependence on size and shape: a review,” *Nanoscience and Technology: A Collection of Reviews from Nature Journals*, vol. 15, pp. 308–319, 2009.
- [41] A. J. Haes and R. P. Van Duyne, “A nanoscale optical biosensor: sensitivity and selectivity of an approach based on the localized surface plasmon resonance spectroscopy of triangular silver nanoparticles,” *Journal of the American Chemical Society*, vol. 124, no. 35, pp. 10596–10604, 2002.
- [42] A. J. Haes, W. P. Hall, L. Chang, W. L. Klein, and R. P. Van Duyne, “A localized surface plasmon resonance biosensor: first steps toward an assay for Alzheimer’s disease,” *Nano Letters*, vol. 4, no. 6, pp. 1029–1034, 2004.
- [43] W. J. Galush, S. A. Shelby, M. J. Mulvihill, A. Tao, P. Yang, and J. T. Groves, “A nanocube plasmonic sensor for molecular binding on membrane surfaces,” *Nano Letters*, vol. 9, no. 5, pp. 2077–2082, 2009.
- [44] S. Zhu, F. Li, C. Du, and Y. Fu, “A localized surface plasmon resonance nanosensor based on rhombic Ag nanoparticle array,” *Sensors and Actuators B: Chemical*, vol. 134, no. 1, pp. 193–198, 2008.
- [45] W. Zhou, Y. Ma, H. Yang, Y. Ding, and X. Luo, “A label-free biosensor based on silver nanoparticles array for clinical detection of serum p53 in head and neck squamous cell carcinoma,” *International Journal of Nanomedicine*, vol. 6, p. 381, 2011.
- [46] G. A. Sotiriou, T. Sannomiya, A. Teleki, F. Krumeich, J. Voros, and S. E. Pratsinis, “Non-toxic dry-coated nanosilver for plasmonic biosensors,” *Advanced Functional Materials*, vol. 20, no. 24, pp. 4250–4257, 2010.
- [47] K. J. Lee, P. D. Nallathambby, L. M. Browning, C. J. Osgood, and X. H. N. Xu, “In vivo imaging of transport and biocompatibility of single silver nanoparticles in early development of zebrafish embryos,” *ACS Nano*, vol. 1, no. 2, pp. 133–143, 2007.
- [48] A. M. Schrand, L. K. Braydich-Stolle, J. J. Schlager, L. Dai, and S. M. Hussain, “Can silver nanoparticles be useful as potential biological labels?,” *Nanotechnology*, vol. 19, no. 23, article 235104, 2008.
- [49] K. Raja, A. Saravanakumar, and R. Vijayakumar, “Efficient synthesis of silver nanoparticles from Prosopis juliflora leaf extract and its antimicrobial activity using sewage,” *Spectrochimica Acta A: Mole and Biomol Spectro*, vol. 97, pp. 490–494, 2012.
- [50] C. K. Balavigneswaran, T. S. J. Kumar, R. M. Packiaraj, and S. Prakash, “Rapid detection of Cr(VI) by AgNPs probe produced by Anacardium occidentale fresh leaf extracts,” *Applied Nanoscience*, vol. 4, no. 3, pp. 367–378, 2014.
- [51] S. N. Luoma, “Silver nanotechnologies and the environment: old problems or new challenges,” *Project on Emerging Nanotechnologies*, vol. 19, pp. 12–13, 2008.
- [52] Y. K. Mishra, S. Mohapatra, D. Kabiraj et al., “Synthesis and characterization of Ag nanoparticles in silica matrix by atom beam sputtering,” *Scripta Materialia*, vol. 56, no. 7, pp. 629–632, 2007.
- [53] C. A. Moyer, L. Brentano, D. L. Gravens, H. W. Margraf, and W. W. Monafo, “Treatment of large human burns with 0.5%

- silver nitrate solution," *Archives of Surgery*, vol. 90, no. 6, pp. 812–867, 1965.
- [54] I. Pastoriza-Santos and L. M. Liz-Marzan, "Colloidal silver nanoplates. State of the art and future challenges," *Journal of Materials Chemistry*, vol. 18, no. 15, pp. 1724–1737, 2008.
- [55] E. Roduner, "Size matters: why nanomaterials are different," *Chemical Society Reviews*, vol. 35, no. 7, pp. 583–592, 2006.
- [56] A. G. Skirtach, A. A. Antipov, D. G. Shchukin, and G. B. Sukhorukov, "Remote activation of capsules containing Ag nanoparticles and IR dye by laser light," *Langmuir*, vol. 20, no. 17, pp. 6988–6992, 2004.
- [57] S. W. Wijnhoven, W. J. Peijnenburg, C. A. Herberths et al., "Nano-silver—a review of available data and knowledge gaps in human and environmental risk assessment," *Nanotoxicology*, vol. 3, no. 2, pp. 109–138, 2009.
- [58] J. B. Wright, K. Lam, D. Hansen, and R. E. Burrell, "Efficacy of topical silver against fungal burn wound pathogens," *American Journal of Infection Control*, vol. 27, no. 4, pp. 344–350, 1999.
- [59] X. H. N. Xu, W. J. Brownlow, S. V. Kyriacou, Q. Wan, and J. J. Viola, "Real-time probing of membrane transport in living microbial cells using single nanoparticle optics and living cell imaging," *Biochemistry*, vol. 43, no. 32, pp. 10400–10413, 2004.
- [60] H. Q. Yin, R. Langford, and R. E. Burrell, "Comparative evaluation of the antimicrobial activity of ACTICOAT antimicrobial barrier dressing," *The Journal of Burn Care & Rehabilitation*, vol. 20, no. 3, pp. 195–200, 1999.
- [61] S. Abel, J. Leta Tesfaye, L. Gudata et al., "Synthesis, Characterization, and Antibacterial Activity of ZnO Nanoparticles from Fresh Leaf Extracts of Apocynaceae, *Carissa spinarum* L. (Hagamsa)," *Journal of Nanomaterials*, vol. 2022, Article ID 6230298, 6 pages, 2022.
- [62] H. H. Lara, E. N. Garza-Treviño, L. Ixtepan-Turrent, and D. K. Singh, "Silver nanoparticles are broad-spectrum bactericidal and virucidal compounds," *Journal of Nanobiotechnology*, vol. 9, no. 1, pp. 1–8, 2011.
- [63] S. S. D. Kumar, N. K. Rajendran, N. N. Houreld, and H. Abrahamse, "Recent advances on silver nanoparticle and biopolymer-based biomaterials for wound healing applications," *International Journal of Biological Macromolecules*, vol. 115, pp. 165–175, 2018.
- [64] J. Natsuki, T. Natsuki, and Y. Hashimoto, "A review of silver nanoparticles: synthesis methods, properties and applications," *International Journal of Materials Science and Applications*, vol. 4, no. 5, pp. 325–332, 2015.
- [65] A. K. Mandal, "Silver nanoparticles as drug delivery vehicle against infections," *Global Journal of Nanomedicine*, vol. 3, no. 2, article 555607, 2017.
- [66] M. J. Firdhouse and P. Lalitha, "Biosynthesis of silver nanoparticles and its applications," *Journal of Nanotechnology*, vol. 2015, 18 pages, 2015.
- [67] N. Abbasi, H. Ghaneialvar, R. Moradi, M. M. Zangeneh, and A. Zangeneh, "Formulation and characterization of a novel cutaneous wound healing ointment by silver nanoparticles containing Citrus lemon leaf: a chemobiological study," *Arabian Journal of Chemistry*, vol. 14, no. 7, article 103246, 2021.
- [68] J. Xiang, R. Zhu, S. Lang, H. Yan, G. Liu, and B. Peng, "Mussel-inspired immobilization of zwitterionic silver nanoparticles toward antibacterial cotton gauze for promoting wound healing," *Chemical Engineering Journal*, vol. 409, article 128291, 2021.
- [69] V. C. Vinay, D. M. Varma, M. R. Chandan et al., "Study of silver nanoparticle-loaded auxetic polyurethane foams for medical cushioning applications," *Polymer Bulletin*, pp. 1–18, 2021.
- [70] C. V. Restrepo and C. C. Villa, "Synthesis of silver nanoparticles, influence of capping agents, and dependence on size and shape," *Environmental Nanotechnology Monitoring & Management*, vol. 15, article 100428, 2021.
- [71] C. K. Venil, M. Malathi, P. Velmurugan, and P. Renuka Devi, "Green synthesis of silver nanoparticles using canthaxanthin from *Dietzia maris* AURCCBT01 and their cytotoxic properties against human keratinocyte cell line," *Journal of Applied Microbiology*, vol. 130, no. 5, pp. 1730–1744, 2021.
- [72] P. Kanniah, P. Chelliah, J. R. Thangapandi, G. Gnanadhas, V. Mahendran, and M. Robert, "Green synthesis of antibacterial and cytotoxic silver nanoparticles by *Piper nigrum* seed extract and development of antibacterial silver based chitosan nanocomposite," *International Journal of Biological Macromolecules*, vol. 189, pp. 18–33, 2021.
- [73] K. Jyoti, P. Pattnaik, and T. Singh, "Green synthesis of silver nanoparticles using sustainable resources and their use as antibacterial agents: a review," *Current Materials Science: Formerly: Recent Patents on Materials Science*, vol. 14, no. 1, pp. 40–52, 2021.
- [74] L. Yildirim, N. T. Thanh, M. Loizidou, and A. M. Seifalian, "Toxicology and clinical potential of nanoparticles," *Nano Today*, vol. 6, no. 6, pp. 585–607, 2011.
- [75] S. Vigneswari, T. S. M. Amelia, M. H. Hazwan et al., "Transformation of biowaste for medical applications: incorporation of biologically derived silver nanoparticles as antimicrobial coating," *Antibiotics*, vol. 10, no. 3, p. 229, 2021.
- [76] C. M. Crisan, T. Mocan, M. Manolea, L. I. Lasca, F. A. Tabaran, and L. Mocan, "Review on silver nanoparticles as a novel class of antibacterial solutions," *Applied Sciences*, vol. 11, no. 3, p. 1120, 2021.
- [77] B. Javed, M. Ikram, F. Farooq, T. Sultana, and N. I. Raja, "Biogenesis of silver nanoparticles to treat cancer, diabetes, and microbial infections: a mechanistic overview," *Applied Microbiology and Biotechnology*, vol. 105, no. 6, pp. 2261–2275, 2021.
- [78] A. S. Takamiya, D. R. Monteiro, L. F. Gorup et al., "Biocompatible silver nanoparticles incorporated in acrylic resin for dental application inhibit *Candida albicans* biofilm," *Materials Science and Engineering: C*, vol. 118, article 111341, 2021.
- [79] A. T. Le, T. T. Le, H. H. Tran, D. A. Dang, Q. H. Tran, and D. L. Vu, "Powerful colloidal silver nanoparticles for the prevention of gastrointestinal bacterial infections," *Advances in Natural Sciences: Nanoscience and Nanotechnology*, vol. 3, no. 4, article 045007, 2012.
- [80] K. Chamakura, R. Perez-Ballester, Z. Luo, S. Bashir, and J. Liu, "Comparison of bactericidal activities of silver nanoparticles with common chemical disinfectants," *Colloids and Surfaces B: Biointerfaces*, vol. 84, no. 1, pp. 88–96, 2011.
- [81] G. A. Kurian, A. Vivek Vishnu, N. Subhash, and A. Shakilabanu, "Characterization and biological evaluation of silver nanoparticles synthesized by aqueous root extract of *Desmodium gangeticum* for its antioxidant, antimicrobial and cytotoxicity," *International Journal of Pharmacy and Pharmaceutical Sciences*, vol. 7, no. 1, pp. 182–186, 2014.
- [82] T. Ninjbadgar, G. Garnweitner, A. Borger, L. M. Goldenberg, O. V. Sakhno, and J. Stumpe, "Synthesis of luminescent ZrO<sub>2</sub>: Eu<sup>3+</sup> nanoparticles and their holographic sub-



- micrometer patterning in polymer composites,” *Advanced Functional Materials*, vol. 19, no. 11, pp. 1819–1825, 2009.
- [83] Z. Khatti, S. M. Hashemianzadeh, and S. A. Shafei, “A molecular study on drug delivery system based on carbon nanotube compared to silicon carbide nanotube for encapsulation of platinum-based anticancer drug,” *Advanced pharmaceutical bulletin*, vol. 8, no. 1, pp. 163–167, 2018.
- [84] S. Jadoun, R. Arif, N. K. Jangid, and R. K. Meena, “Green synthesis of nanoparticles using plant extracts: a review,” *Environmental Chemistry Letters*, vol. 19, no. 1, pp. 355–374, 2021.
- [85] J. Al-Haddad, F. Alzaabi, P. Pal, K. Rambabu, and F. Banat, “Green synthesis of bimetallic copper–silver nanoparticles and their application in catalytic and antibacterial activities,” *Clean Technologies and Environmental Policy*, vol. 22, no. 1, pp. 269–277, 2020.
- [86] P. A. Luque, M. J. Chinchillas-Chinchillas, O. Nava et al., “Green synthesis of tin dioxide nanoparticles using *Camellia sinensis* and its application in photocatalytic degradation of textile dyes,” *Optik*, vol. 229, article 166259, 2021.
- [87] P. K. Dikshit, J. Kumar, A. K. Das et al., “Green synthesis of metallic nanoparticles: applications and limitations,” *Catalysts*, vol. 11, no. 8, p. 902, 2021.
- [88] R. Fanciullino, J. Ciccolini, and G. Milano, “Challenges, expectations and limits for nanoparticles-based therapeutics in cancer: a focus on nano-albumin-bound drugs,” *Critical Reviews in Oncology/Hematology*, vol. 88, no. 3, pp. 504–513, 2013.

## Corrigendum

# Corrigendum to “A Pilot Study on Nanotherapy of *Momordica charantia* against Trimethyltin Chloride-Induced Neurotoxicity in *Danio rerio* (Zebrafish)”

**Bharathi Kumar,<sup>1</sup> Siva Vijayakumar Tharumasivam,<sup>1</sup> Vasuki Boominathan,<sup>1,2</sup> Elumalai Perumal,<sup>3</sup> Prabu Dhandapani,<sup>4</sup> Kumaravel Kaliyaperumal,<sup>5</sup> Suresh Arumugam,<sup>6</sup> Kumaran Subramanian,<sup>7</sup> Pugazhvendan Sampath Renuga,<sup>8,9</sup> Vasanth Sakthivel,<sup>10</sup> Bupesh Giridharan,<sup>11</sup> Wilson Aruni,<sup>12,13</sup> and Lokesh Kumar Boopathy<sup>14</sup>**

<sup>1</sup>PG & Research Department of Biotechnology, Srimad Andavan Arts & Science College, Srirangam, Tiruchirappalli 620005, India

<sup>2</sup>Department of Biotechnology, Bharathidasan University, Tiruchirappalli 620024, India

<sup>3</sup>Departments of Pharmacology, Saveetha Dental College and Hospital, Chennai, Tamil Nadu, India

<sup>4</sup>Department of Microbiology, Dr. ALM PG IBMS, University of Madras, Chennai, Tamil Nadu, India

<sup>5</sup>National Navel Orange Engineering Research Centre, School of Life Sciences, Gannan Normal University, Ganzhou, Jiangxi, China

<sup>6</sup>Central Research Laboratory, Meenakshi Medical College Hospital & Research Institute, Kanchipuram, Tamil Nadu, India

<sup>7</sup>Centre for Drug Discovery and Development, Sathyabama Institute of Science and Technology, Chennai, Tamil Nadu, India

<sup>8</sup>Department of Zoology, Annamalai University, Annamalai Nagar, Cuddalore, 608002 Tamil Nadu, India

<sup>9</sup>Department of Zoology, Arignar Anna Government Arts College, Cheyyar, 604407 Tamil Nadu, India

<sup>10</sup>Research & Development Wing, Sree Balaji Medical College & Hospital (SBMCH), Bharath University, BIHER, Chrompet, Chennai, 600044 Tamil Nadu, India

<sup>11</sup>Department of Forest Science, Nagaland University, Nagaland 798627, India

<sup>12</sup>Department of Biotechnology, School of Bio and Chemical Engineering, Sathyabama Institute of Science and Technology, Chennai, Tamil Nadu, India

<sup>13</sup>School of Medicine, Loma Linda University, CA 92354, USA

<sup>14</sup>College of Health Sciences, Mizan Tepi University, Mizan Teferi, Ethiopia

Correspondence should be addressed to Lokesh Kumar Boopathy; [lokeshkumarunom@gmail.com](mailto:lokeshkumarunom@gmail.com)

Received 10 January 2022; Accepted 10 January 2022; Published 24 March 2022

Copyright © 2022 Bharathi Kumar et al. This is an open access article distributed under the Creative Commons Attribution License, which permits unrestricted use, distribution, and reproduction in any medium, provided the original work is properly cited.

In the article titled “A Pilot Study on Nanotherapy of *Momordica charantia* against Trimethyltin Chloride-Induced Neurotoxicity in *Danio rerio* (Zebrafish)” [1], the author names and their affiliations have been corrected. The corrected author names and affiliations are as above.


rafish),” *Journal of Nanomaterials*, vol. 2021, Article ID 2180638, 12 pages, 2021.

## References

- [1] B. Kumar, S. V. Tharumasivam, V. Boominathan et al., “A pilot study on nanotherapy of *Momordica charantia* against trimethyltin chloride-induced neurotoxicity in *Danio rerio* (zeb-

## Research Article

# Effect of Hafnium Coating on Osseointegration of Titanium Implants: A Split Mouth Animal Study

Vaishnavi Rajaraman,<sup>1</sup> Deepak Nallaswamy,<sup>1</sup> Dhanraj Ganapathy,<sup>1</sup> S. Rajeshkumar ,<sup>2</sup> Padma Ariga,<sup>1</sup> and Karthik Ganesh<sup>3</sup>

<sup>1</sup>Department of Prosthodontics and Implantology, Saveetha Dental College and Hospital, Saveetha Institute of Medical and Technical Sciences, Chennai 600077, India

<sup>2</sup>Nanobiomedicine Lab, Department of Pharmacology, Saveetha Dental College and Hospital, Saveetha Institute of Medical and Technical Sciences, Chennai 600077, India

<sup>3</sup>Department of Anatomy, BRULAC, Saveetha Dental College and Hospital, Saveetha Institute of Medical and Technical Sciences, Chennai 600077, India

Correspondence should be addressed to S. Rajeshkumar; [ssrajeshkumar@hotmail.com](mailto:ssrajeshkumar@hotmail.com)

Received 1 July 2021; Accepted 1 November 2021; Published 15 December 2021

Academic Editor: Domenico Acierno

Copyright © 2021 Vaishnavi Rajaraman et al. This is an open access article distributed under the Creative Commons Attribution License, which permits unrestricted use, distribution, and reproduction in any medium, provided the original work is properly cited.

The behaviour of hafnium as surface coating in biological environments has not been studied. Little is known about osseointegration of hafnium-coated titanium implants. Thus, further studies of hafnium coating under biological conditions are required in order to determine the suitability of this material, as a surface coating for biomedical application. The aim of the study is to analyse the difference between hafnium-coated titanium and uncoated titanium by evaluating the osseointegration ability of hafnium metal and mechanism of which promotes better bone integration. The study was conducted with a split mouth design on 16 Wistar Albino rats of both sexes, at the age of 6-7 months, weighing  $2526.5 \pm 74.4$  g. Self-tapping titanium osteosynthesis screws (4 mm × 2 mm) (LeFort System Bone Screw®) were implanted in the mandible of rats: Group A (pure titanium screws,  $n = 12$ ) and Group B (hafnium-coated screws,  $n = 12$ ). The implanted screws' stability was checked and noted with a specially customised torque apparatus during insertion and removal of implant. The tissue sections were then processed for hematoxylin and eosin and Masson's trichrome for bone and connective tissue examination, after 4 and 8 weeks of placement. Hafnium coating appears to have offered similar biocompatibility (aspartate transaminase (AST), alanine aminotransferase (ALT), and creatine kinase (CK) enzyme assay), statistically significant improvement (independent Student's  $t$ -test,  $p < 0.05$ ) in insertion torque ( $25.42 \pm 3.965$ ) and removal torque ( $29.17 \pm 2.887$ ) than commercially pure titanium with insertion torque ( $22.08 \pm .575$ ) and removal torque ( $25.42 \pm 2.575$ ). Hafnium coating in the rat mandible showed promising osseointegration with good tissue biocompatibility. Further human trials of hafnium-coated implants are needed to understand the biological behaviour better to enhance clinical performance.

## 1. Introduction

Tissue engineering is a novel and well-proven approach for repair and reconstruction of bone defects. An ideal implant material should have properties that include biocompatibility, corrosion resistance, elastic modulus, and favour bone anchorage [1–14]. One of the most commonly used materials for this purpose is titanium and its alloys. In various studies conducted till date, tantalum has revealed superior properties

fulfilling criteria required for an implant which include excellent chemical stability, body fluid resistance, biological inertia, and remarkable osteoconductivity. Although tantalum is shown to be promising in bone defect repair, its elastic modulus is much higher than that of human bone tissue and prone to stress shielding effect [15–25].

We wanted to evaluate alternative elements that may have the potential to offer equivalent or superior osseointegration. One such element of interest is hafnium. In the



FIGURE 1: Photograph showing commercially pure self-tapping micro titanium osteosynthesis implant screws (4 mm × 2 mm).

periodic table by IUPAC, tantalum belongs to period 6 (d block) of the periodic table. Hafnium belongs to the same period and block as tantalum, in the periodic table [26–32].

Hafnium is always found in association with zirconium in mineral ores with zircon Hf/Zr of about 2.5%. In 1984, Marcel Pourbaix proposed hafnium as a metal to be considered for surgical implants due to the passive state of the metal with properties like high ductility, strength, resistance to corrosion, and mechanical damage. Various in vitro studies were conducted on hafnium metal [33–42].

To date, the behaviour of hafnium as surface coating in biological environments has not been studied. Little is known about osseointegration of hafnium-coated titanium implants. Thus, further studies of hafnium coating under biological conditions are required in order to determine the suitability of this material, as a surface coating for biomedical applications.

This study is aimed at evaluating osseointegration of hafnium-coated titanium as compared to uncoated titanium implants. This study has two main purposes. One is to find the osseointegration ability of hafnium metal, and the second purpose is to study the mechanism of which promotes better bone integration.

## 2. Materials and Methods

The experimental study was conducted in accordance with the approval from the “Institutional Animal Ethical Committee,” approval no. BRULAC/SDCH/SIMATS/IAEC/09-2018/015. The study was conducted on 16 Wistar Albino rats of both sexes, at the age of 6–7 months, weighing  $2526.5 \pm 74.4$  g. Commercially pure self-tapping titanium osteosynthesis screws with a length of 4 mm and outer head diameter of 2 mm and thread diameter of 1.2 mm (LeForte System Bone Screw, Jeil Medical Corporation, Seoul®) were used for this experiment.

Two groups were utilized in these studies:

- (a) Commercially pure titanium implant (control group)
- (b) Commercially pure titanium implant coated with hafnium metal (test group)

**2.1. Coating Procedure.** Commercially pure self-tapping micro titanium osteosynthesis implant screws 4 mm long were used with 2 mm head and 1.2 mm outer thread diameter, respectively (LeForte System Bone Screw, Jeil Medical Corporation, Seoul®) (Figure 1).

The implant screws were coated with hafnium metal of 600 nm thickness using a magnetron stirrer. They were prepared by dipping the titanium screws in hafnium metal solution commercially available for industrial purposes and kept in a magnetic stirrer at 1000 rpm followed by heat exposure in a hot air oven at 70-degree Celsius for 4 days, 6 hours daily. The uncoated (Figure 2) and coated (Figure 3) implants were observed under a light microscope at 100x magnification, and the procedure was carried out till an even coating thickness was obtained.

**2.2. Surgical Procedure.** Surgical procedures were performed under sterile conditions in a sterile animal laboratory surgical room. Rats were anesthetized with ketamine hydrochloride intraperitoneally and xylazine intramuscularly at the dosage of 70 mg/kg body weight and 10 mg/kg body weight, respectively. The ventral part of the neck was shaved and aseptically prepared with a solution of Betadine. A 2 cm length single median vertical skin incision was made on the anterior part of the neck, exposing the fascia and muscles underneath (Figure 4).

These tissues were retracted, and the mandibular bone was exposed. A standardized, round, through-and-through osseous defect of 3 mm in diameter was created with

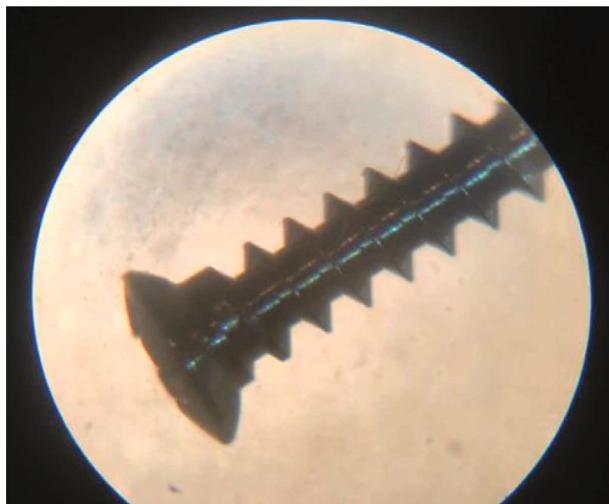


FIGURE 2: Photograph showing uncoated titanium screws under light microscope at 100x magnification.

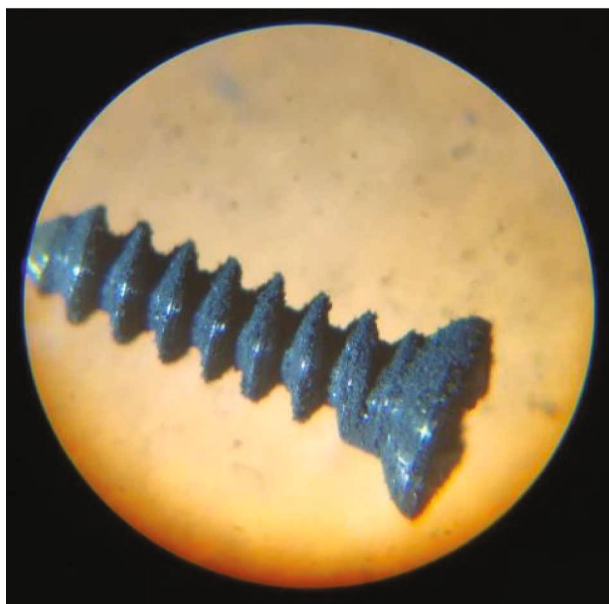


FIGURE 3: Photograph showing the hafnium-coated titanium implant screws under light microscope at 100x magnification.

simultaneous driving of implant inside, similarly on the single side of the jaw, with a self-tapping screw mounted on a straight hand-piece driller controlled by the motor regulator. During the drilling process, the tissues were periodically irrigated with saline water. Care was taken during the surgery not to damage the vessels. Titanium screws were then implanted in the drilled site, in such a way that the implant should penetrate the bone slowly by the clockwise self-tapping procedure.

The implanted screws' stability was checked and noted with a torque apparatus during insertion of implant. The torque apparatus consisted of a torque wrench and an implant hex drive; the head of which was specially customised according to the head of the implant screw (Figure 5).



FIGURE 4: Photograph showing a 2 cm length single median vertical skin incision was made on the anterior part of the neck.

The same procedure was carried in both the groups. Both the titanium and hafnium-coated screws were implanted in respective groups (Figure 6).

Then, the tissue flaps were sutured with resorbable suture threads (Vicryl 5/0, Ethicon®, Somerville, NJ, USA) and Betadine ointment was applied upon the sutured area, and then, the rats were isolated in separate cages.

**2.3. Postoperative Care for the Animal.** Analgesics like Fevastin 10 mg/kg body weight (intramuscularly) and diclofenac 10 mg/kg body weight (orally) were administered. The rats were examined daily for any change in body weight or signs of inflammation or infection in the surgical site.

Tissue samples were collected at the end of 4 weeks and 8 weeks by euthanizing the animals in a CO<sub>2</sub> chamber, and the mandibular bone alone containing the implant was dissected, photographed, and processed for histopathological examination. The excess fascial and muscular tissues adherents to the bones were removed. The mandibular bony part with the implant was fixed in 10% neutral buffered formalin. The removal torque was measured and noted in the same manner as mentioned earlier for stability using the torque apparatus, while the tissue samples were collected.

**2.4. Histological Preparation.** The fixed tissues were taken out and later decalcified in 20% formic acid for 7 days. Afterwards, the samples were embedded in paraffin and serial sections were cut at a thickness of 5 μm. The sections were then processed for hematoxylin and eosin staining and mounted permanently in DPX. For bone and connective tissue examination, the Masson's trichrome staining was done. The stained samples were photographed and analysed for histopathology.

### 3. Results

**3.1. Primary Stability (Insertion Torque) and Removal Torque.** The primary stability measured using removal torque was measured for both groups studied. The mean



FIGURE 5: Photograph showing torque wrench (range 0-70 N) and an implant hex drive with head specially customised according to the head of the implant screw.

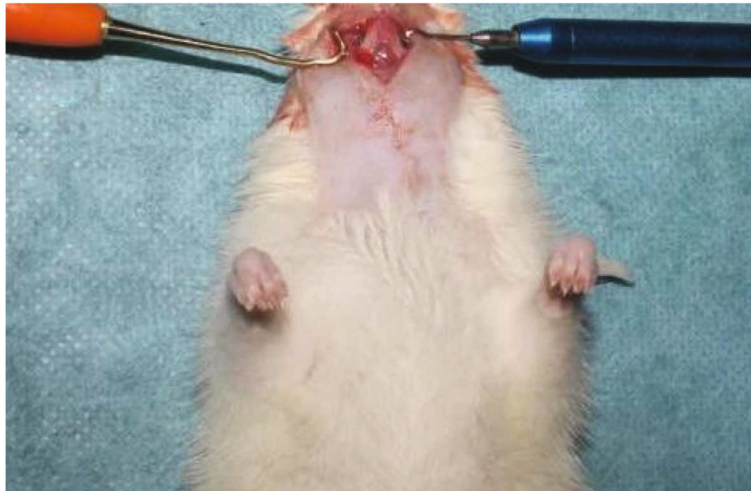


FIGURE 6: Photograph showing titanium and hafnium-coated screws implanted in respective sites.

TABLE 1: Table showing values (mean  $\pm$  SD) of independent *t*-test for insertion torque (primary stability) and removal torque for both the groups ( $p < 0.05$ ).

Torque values	Group A (pure titanium screws) <i>n</i> = 12	Group B (hafnium-coated screws) <i>n</i> = 12	Significance (* <i>p</i> value)
Insertion torque or primary stability (N/cm <sup>2</sup> )	22.08 $\pm$ 2.57	25.42 $\pm$ 3.96	$p < 0.05$ (0.003)
Removal torque (N/cm <sup>2</sup> )	25.42 $\pm$ 2.57	29.17 $\pm$ 2.88	$p < 0.05$ (0.023)

\*Independent sample *t*-test.

insertion torque/primary stability in the control group (pure titanium screws) was  $22.08 \pm .57$  N/cm<sup>2</sup> and that in the test group (hafnium-coated screws) was  $25.42 \pm 3.96$  N/cm<sup>2</sup>. The mean removal torque of the control group was  $25.42 \pm 2.57$  N/cm<sup>2</sup> and that of the test group was  $29.17 \pm 2.88$  N/cm<sup>2</sup>. The results were statistically significant ( $p < 0.05$ ) when the independent Student *t*-test was performed (IBM

SPSS Statistics 20) (Table 1). The corresponding bar graph for the primary stability and removal torque is depicted (Figures 7 and 8).

3.2. *Histomorphometric Analysis.* The histopathological evaluation was performed at 2 intervals, viz., 4 weeks (Figure 9) and 8 weeks (Figure 10), with two stains, namely,

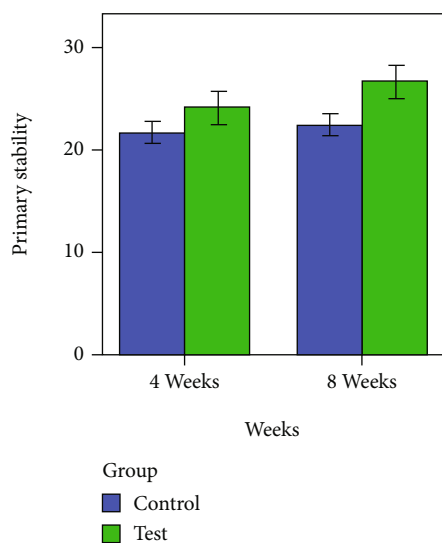


FIGURE 7: Bar graph shows mean primary stability torque values  $\pm$  1 SE of titanium and hafnium-coated implant screws.

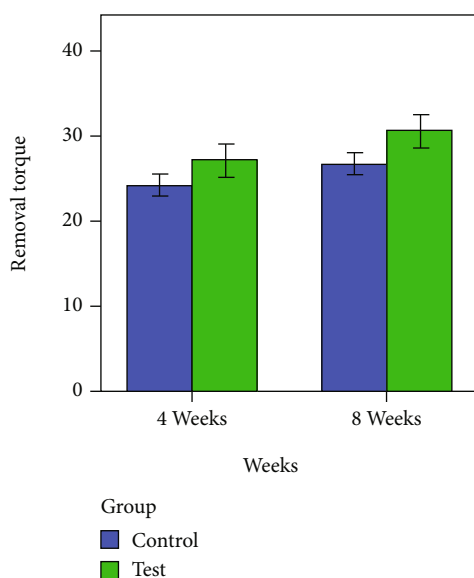


FIGURE 8: Bar graph shows mean removal torque values  $\pm$  1 SE of titanium and hafnium-coated implant screws.

hematoxylin and eosin stain and Masson's trichrome stain under magnifications 4x, 20x, 40x, and 40x, respectively.

At the end of 4 weeks, histopathological evaluation demonstrated the formation and accumulation of connective tissue fibres adjacent to the implant region in the control and test groups. The presence of collagen-rich connective tissue fibres in the test group indicates the course of transformation and maturation of the endochondral ossification. The screw threads were tightly lodged in the adjacent cortical bone tissues.

At the end of 8 weeks, histopathological evaluation demonstrated the accumulation of connective tissue fibres along with the presence of thin layers of newly transformed bone (asterisk marked) which are also in connection with trabec-

ular bone in some regions. The difference between the control and test groups is the site of formation of newly formed bone. In the control group, it is formed mostly at the inner core region of the bone away from the bone-implant contact site (\*). But in the test group, the bone is formed at the implant contact site influencing the implant surfaces for better osseointegration (\*). The trabecular bone tissue formation at the bone-implant contact site depicts contact osteogenesis confirmed by Masson's trichrome stain (40x) visible as green-coloured structures.

**3.3. Toxicology.** The animals were sacrificed after 4 weeks and 8 weeks and sent for enzyme toxicity, viz., AST, ALT, and CK using an ELISA kit (Elabscience®) with 96 wells and an Automatic ELISA Plate Analyser (Readwell Touch, ROBONIK®). The data for the enzyme toxicity is listed (Table 2). It was found that the results are statistically insignificant ( $p > 0.05$ ) (independent Student's  $t$ -test, IBM Statistics 20).

**3.4. Body Weight of Animal.** The body weight of rats was measured before the surgery and after each week, and any signs of inflammation or infection were carefully monitored. The data for body weight of animals sacrificed after 8 weeks (Table 3) have been listed. The body weight of the rats studied for 4 weeks decreased from before surgery till the end of the 2nd week, after which there was an increase in the body weight. The body weight of the rats studied for 8 weeks decreased from before surgery till the end of the 4<sup>th</sup> week, after which there was an increase in the body weight.

## 4. Discussion

In the current study, hafnium coating appears to have offered similar biocompatibility (aspartate transaminase (AST), alanine aminotransferase (ALT), and creatine kinase (CK) enzyme assay), statistically significant improvement (independent Student's  $t$ -test,  $p < 0.05$ ) in insertion torque ( $25.42 \pm 3.96$ ) and removal torque ( $29.17 \pm 2.88$ ) than commercially pure titanium with insertion torque ( $22.08 \pm .57$ ) and removal torque ( $25.42 \pm 2.57$ ). Hafnium has proved to have good tissue response and osseointegration, along with required mechanical properties [39–48]. Though these results seem to favour hafnium, it is necessary to analyse the factors that could have confounded our study.

Animal studies must have a proper protocol to be followed for care of animals used in the study as laid down by the Institutional Animal Ethical Committee (IAEC). The health of the animal was monitored throughout the study. The body weight of the animal was recorded at the start of the surgery and at the end of each week (Table 3). Signs of infection or inflammation were also checked. Proper and timely feeding of the animal was carried out every day to ensure good health of the animal. The results showed that there is an increase in the body weight towards the end of 4 weeks as well as 8 weeks, suggestive of a positive growth phase (Figures 5 and 6). Since it was a split mouth study, the health of the animal could not have affected the outcome or caused variation between the test and control groups.

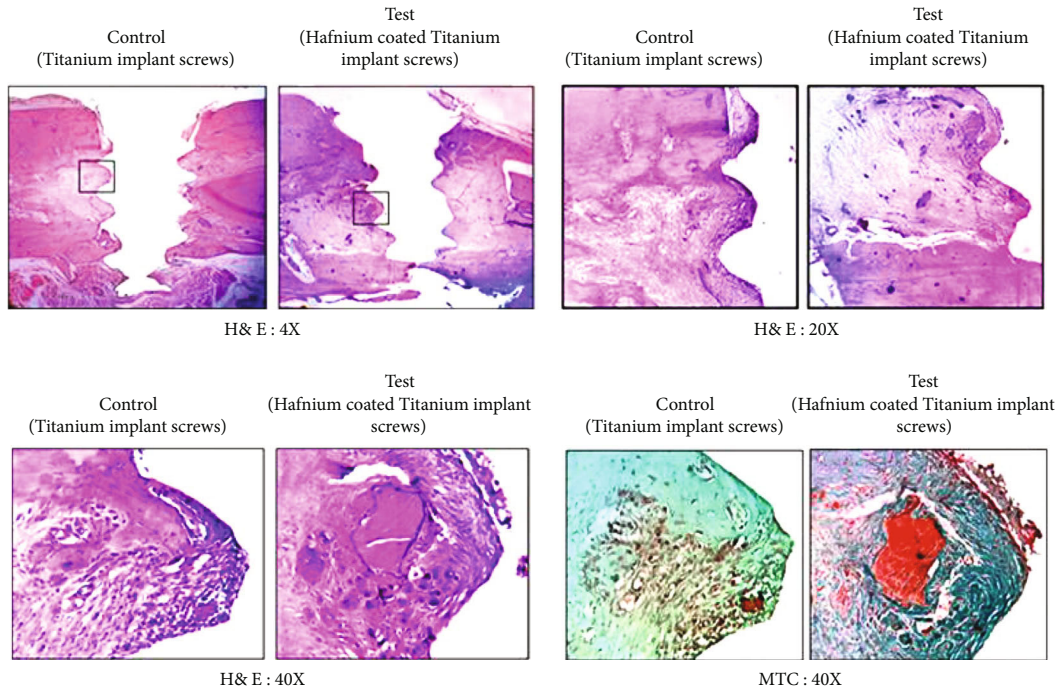


FIGURE 9: Photomicrographs showing the histopathology of the control (titanium implant screws) and the test group (hafnium-coated titanium implant screws) in 4 weeks.

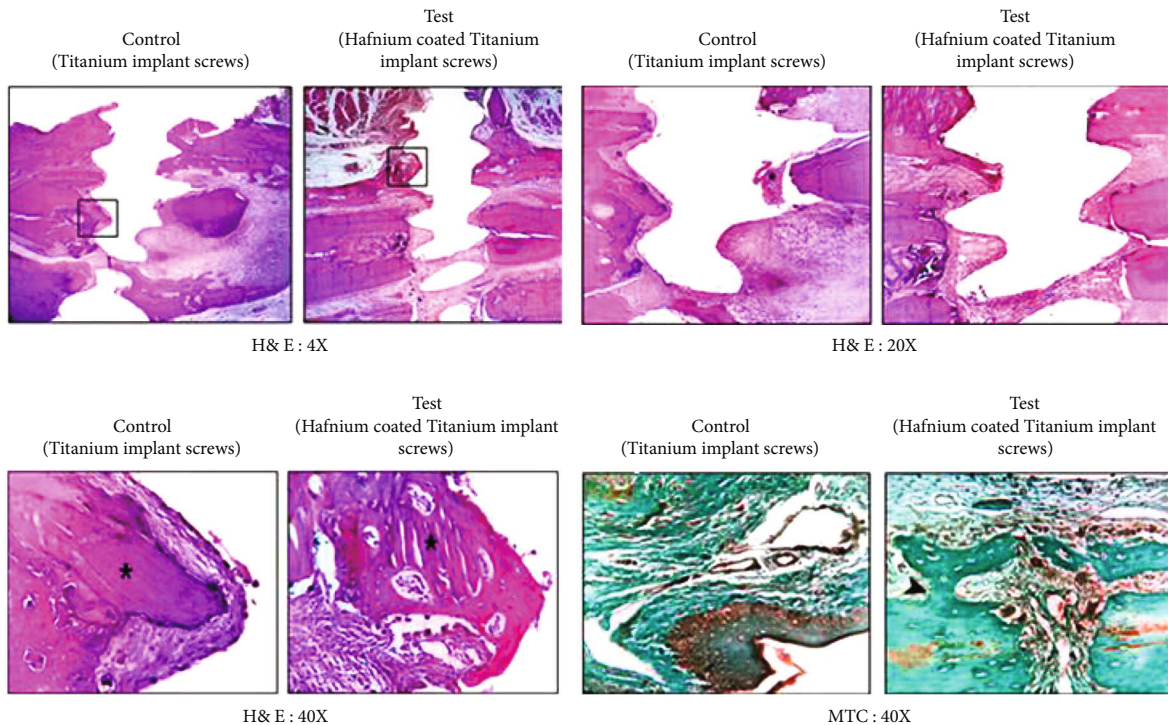


FIGURE 10: Photomicrographs showing the histopathology of the control (titanium implant screws) and the test group (hafnium-coated titanium implant screws) in 8 weeks.

The dexterity of the operator could be a confounding variable in the current study. However, the implant screws selected were a self-threading type with drill driver provided by the manufacturer of the implant screws. Hence, primary

stability could not have been affected by the dexterity of the implant placement [49–52].

The implant screws of both groups were placed in the mandible of the animal. As both groups were in the same



TABLE 2: Table showing data for enzyme toxicity (AST, ALT, and CK) for both the groups ( $p < 0.05$ ).

Enzyme toxicity	Group A (pure titanium screws) $n = 12$	Group B (hafnium-coated screws) $n = 12$	Significance ( $*p$ value)
AST	$80.43 \pm 1.35$	$79.94 \pm 1.78$	$p > 0.05$ (NS)
ALT	$47.85 \pm 2.75$	$49.27 \pm 3.52$	$p > 0.05$ (NS)
CK	$0.79 \pm 0.04$	$0.78 \pm 0.08$	$p > 0.05$ (NS)

\*Independent sample  $t$ -test; NS: not significant.

TABLE 3: Table showing data for body weight of rats before surgery till the 8th week after surgery for both the groups.

Body weight	Group A (pure titanium screws) $n = 12$	Group B (hafnium-coated screws) $n = 12$	Significance ( $*p$ value)
Before surgery	$232.66 \pm 4.84$	$232.66 \pm 4.84$	$p > 0.05$ (0.515)
After surgery	$230.83 \pm 13.54$	$230.83 \pm 13.54$	$p > 0.05$ (0.515)

\*Independent sample  $t$ -test.

anatomic location in the animal, this parameter could not have affected the outcome of the results. Similar studies conducted in animals also mention east variations in density of bone in the anatomically same region [53]. Magnetic stirring method was used for coating the implant screws with hafnium which ensures the same thickness of coating for all samples. Previous studies have shown the use of similar coating methods [54, 55], although the coating thickness or delamination of coating was not tested for in this study.

The accuracy of histopathology may be affected by the handling and processing of tissue samples [56, 57]. However, in this study, histopathology was carried out by an experienced senior pathologist, expert in animal tissue handling for over 15 years. Utmost care was taken to maintain consistent protocol. Effects of this would not have affected one group selectively. The limitations of the current study include the inability to measure the thickness of the coating prior to placement of the implant screws. Another limitation of this study is that the delamination of coating was not tested before the implant screws were placed in the animal model.

Future scope of the study involves studies on delamination of the coating, the scratch resistance of the coating in intraoral scenario, biofilm formation on the surface of the coating, and the side effects of leaching of the metal in the body. Researchers have emphasized that hafnium is a potential surface coating solution for titanium implants that can improve osseointegration. If research could be expanded to include hafnium as a metal for coating over dental implants or as a dental implant material to improve osseointegration, it could be used to investigate the potential of this metal in the rehabilitation of both intra- and extraoral defects, as well as in medically vulnerable patients with compromised bone quality [58]. Research could also be expanded on the possibility of newer metal alloys with hafnium for use as dental implants. Meticulous and extensive phase III and phase IV multicentre randomized control trials are required for breakthrough in this implant biomaterial.

## 5. Conclusion

Hafnium coating of endosseous implants in the current study on rat mandibles showed equivalent osseointegration and faster healing when compared to the gold standard, titanium. Hafnium is also similar to titanium in its biocompatibility with osseous tissues. Further human trials of hafnium-coated implants are needed to understand the biological behaviour better to enhance clinical performance.

## Data Availability

The authors confirm that the data supporting the findings of this study are available within the article.

## Conflicts of Interest

The authors declare no conflicts of interest.

## Authors' Contributions

This work was carried out in collaboration among all authors. Author 1 designed the study, performed the research and the statistical analysis, wrote the protocol, and wrote the first draft of the manuscript. Authors 2, 3, and 4 managed the analyses and revision of the study. Authors 5 and 6 managed the literature searches and manuscript revision. All authors read and approved the final manuscript.

## Acknowledgments

The team extends our sincere gratitude to the Saveetha Dental College and Hospitals for their constant support and successful completion of this work.

## References






- [1] B. A. Fishero, N. Kohli, A. Das, J. J. Christophel, and Q. Cui, "Current concepts of bone tissue engineering for craniofacial bone defect repair," *Craniofacial Trauma & Reconstruction*, vol. 8, no. 1, pp. 23–30, 2015.

- [2] M. A. K. Liebschner, "Biomechanical considerations of animal models used in tissue engineering of bone," *Biomaterials*, vol. 25, no. 9, pp. 1697–1714, 2004.
- [3] Y. Zhang, L. Hu, M. Lin, S. Cao, Y. Feng, and S. Sun, "RhBMP-2-loaded PLGA/titanium nanotube delivery system synergistically enhances osseointegration," *ACS Omega*, vol. 6, no. 25, pp. 16364–16372, 2021.
- [4] M. F. Kunrath, R. P. Dos Santos, S. D. de Oliveira, R. Hubler, P. Sesterheim, and E. R. Teixeira, "Osteoblastic cell behavior and early bacterial adhesion on macro-, micro-, and nanostructured titanium surfaces for biomedical implant applications," *The International Journal of Oral & Maxillofacial Implants*, vol. 35, no. 4, pp. 773–781, 2020.
- [5] B. Möller, H. Terheyden, Y. Açil et al., "A comparison of biocompatibility and osseointegration of ceramic and titanium implants: an *in vivo* and *in vitro* study," *International Journal of Oral and Maxillofacial Surgery*, vol. 41, no. 5, pp. 638–645, 2012.
- [6] A. M. Ektessabi, J. Mouhyi, P. Louvette, and L. Sennerby, "Investigation of corrosion and ion release from titanium dental implant," *International Journal of PIXE*, vol. 7, no. 3n04, pp. 179–199, 1997.
- [7] R. S. Bedi, D. E. Beving, L. P. Zanello, and Y. Yan, "Biocompatibility of corrosion-resistant zeolite coatings for titanium alloy biomedical implants," *Acta Biomaterialia*, vol. 5, no. 8, pp. 3265–3271, 2009.
- [8] R. Shah, R. Thomas, T. M. Gowda, T. K. A. Baron, G. G. Vemarnadhya, and S. Bhagat, "In vitro evaluation of osteoblast response to the effect of injectable platelet-rich fibrin coating on titanium disks," *The Journal of Contemporary Dental Practice*, vol. 22, no. 2, pp. 107–110, 2021.
- [9] Z. Badran, X. Struillou, N. Strube et al., "Clinical performance of narrow-diameter titanium-zirconium implants: a systematic review," *Implant Dentistry*, vol. 26, no. 2, pp. 316–323, 2017.
- [10] J. Li, J. A. Jansen, X. F. Walboomers, and J. J. van den Beucken, "Mechanical aspects of dental implants and osseointegration: a narrative review," *Journal of the Mechanical Behavior of Biomedical Materials*, vol. 103, article 103574, 2020.
- [11] A. Robau-Porrua, Y. Pérez-Rodríguez, L. M. Soris-Rodríguez, O. Pérez-Acosta, and J. E. González, "The effect of diameter, length and elastic modulus of a dental implant on stress and strain levels in peri-implant bone: a 3D finite element analysis," *Bio-medical Materials and Engineering*, vol. 30, no. 5–6, pp. 541–558, 2020.
- [12] A. Brizuela, M. Herrero-Climent, E. Rios-Carrasco et al., "Influence of the elastic modulus on the osseointegration of dental implants," *Materials*, vol. 12, no. 6, p. 980, 2019.
- [13] R. N. Salaie, A. Besinis, H. Le, C. Tredwin, and R. D. Handy, "The biocompatibility of silver and nanohydroxyapatite coatings on titanium dental implants with human primary osteoblast cells," *Materials Science & Engineering. C, Materials for Biological Applications*, vol. 107, article 110210, 2020.
- [14] J. Knaus, D. Schaffarczyk, and H. Cölfen, "On the future design of bio-inspired polyetheretherketone dental implants," *Macromolecular Bioscience*, vol. 20, no. 1, article e1900239, 2020.
- [15] T. P. Chaturvedi, "An overview of the corrosion aspect of dental implants (titanium and its alloys)," *Indian Journal of Dental Research*, vol. 20, no. 1, pp. 91–98, 2009.
- [16] N. Adya, M. Alam, T. Ravindranath, A. Mubeen, and B. Saluja, "Corrosion in titanium dental implants: literature review," *The Journal of Indian Prosthodontic Society*, vol. 5, no. 3, p. 126, 2005.
- [17] V. K. Balla, S. Bodhak, S. Bose, and A. Bandyopadhyay, "Porous tantalum structures for bone implants: fabrication, mechanical and *in vitro* biological properties," *Acta Biomaterialia*, vol. 6, no. 8, pp. 3349–3359, 2010.
- [18] R. Cohen, "A porous tantalum trabecular metal: basic science," *The American Journal of Orthopedics*, vol. 31, no. 4, pp. 216–217, 2002.
- [19] Q. Wang, H. Zhang, H. Gan, H. Wang, Q. Li, and Z. Wang, "Application of combined porous tantalum scaffolds loaded with bone morphogenetic protein 7 to repair of osteochondral defect in rabbits," *International Orthopaedics*, vol. 42, no. 7, pp. 1437–1448, 2018.
- [20] E. H. Mrosek, H.-W. Chung, J. S. Fitzsimmons, S. W. O'Driscoll, G. G. Reinholz, and J. C. Schagemann, "Porous tantalum biocomposites for osteochondral defect repair," *Bone & joint research*, vol. 5, no. 9, pp. 403–411, 2016.
- [21] Z. Tang, Y. Xie, F. Yang et al., "Porous tantalum coatings prepared by vacuum plasma spraying enhance bmscs osteogenic differentiation and bone regeneration *in vitro* and *in vivo*," *PLoS One*, vol. 8, no. 6, article e66263, 2013.
- [22] M. Arciniegas, C. Aparicio, J. M. Manero, and F. J. Gil, "Low elastic modulus metals for joint prosthesis: tantalum and nickel-titanium foams," *Journal of the European Ceramic Society*, vol. 27, no. 11, pp. 3391–3398, 2007.
- [23] T. Lu, J. Wen, S. Qian et al., "Enhanced osteointegration on tantalum-implanted polyetheretherketone surface with bone-like elastic modulus," *Biomaterials*, vol. 51, pp. 173–183, 2015.
- [24] R. Korabi, K. Shemtov-Yona, and D. Rittel, "On stress/strain shielding and the material stiffness paradigm for dental implants," *Clinical Implant Dentistry and Related Research*, vol. 19, no. 5, pp. 935–943, 2017.
- [25] R. Saha, R. B. Inturi, and J. A. Barnard, "Effect of thickness and annealing on stress in tantalum and tantalum nitride thin film hard Coatings," *MRS Online Proceedings Library*, vol. 436, 1996.
- [26] J. Rituerto Sin, A. Neville, and N. Emami, "Corrosion and tribocorrosion of hafnium in simulated body fluids," *Journal of Biomedical Materials Research. Part B, Applied Biomaterials*, vol. 102, no. 6, pp. 1157–1164, 2014.
- [27] S. Mohammadi, M. Esposito, M. Cucu, L. E. Ericson, and P. Thomsen, "Tissue response to hafnium," *Journal of Materials Science. Materials in Medicine*, vol. 12, no. 7, pp. 603–611, 2001.
- [28] H. Matsuno, A. Yokoyama, F. Watari, M. Uo, and T. Kawasaki, "Biocompatibility and osteogenesis of refractory metal implants, titanium, hafnium, niobium, tantalum and rhenium," *Biomaterials*, vol. 22, no. 11, pp. 1253–1262, 2001.
- [29] H. Lee, D.-H. Choe, S. Jo et al., "Unveiling the origin of robust ferroelectricity in Sub-2 nm hafnium zirconium oxide films," *ACS Applied Materials & Interfaces*, vol. 13, no. 30, pp. 36499–36506, 2021.
- [30] P. Ghana, S. Schrader, T. Rajeshkumar et al., "Reduced arene complexes of hafnium supported by a triamidoamine ligand," *Angewandte Chemie, International Edition*, vol. 60, no. 25, pp. 14179–14187, 2021.
- [31] E. C. Constable, "Evolution and understanding of the d-block elements in the periodic table," *Dalton Transactions*, vol. 48, no. 26, pp. 9408–9421, 2019.

- [32] P. Parsons, "The periodic table: a visual guide to the elements," *Teaching Science*, vol. 60, 2014.
- [33] K. Edalati, Z. Horita, and Y. Mine, "High-pressure torsion of hafnium," *Materials Science and Engineering: A*, vol. 527, no. 7, pp. 2136–2141, 2010.
- [34] X.-W. Gu, J. Pei, K. Shao, H.-M. Wen, B. Li, and G. Qian, "Chemically stable hafnium-based metal-organic framework for highly efficient C<sub>2</sub>H<sub>6</sub>/C<sub>2</sub>H<sub>4</sub> separation under humid conditions," *ACS Applied Materials & Interfaces*, vol. 13, no. 16, pp. 18792–18799, 2021.
- [35] H. Sato, M. Kikuchi, M. Komatsu, O. Okuno, and T. Okabe, "Mechanical properties of cast Ti-Hf alloys," *Journal of Biomedical Materials Research. Part B, Applied Biomaterials*, vol. 72B, no. 2, pp. 362–367, 2005.
- [36] M. A. Jenkins, K. E. K. Holden, S. W. Smith et al., "Determination of hafnium zirconium oxide interfacial band alignments using internal photoemission spectroscopy and X-ray photoelectron spectroscopy," *ACS Applied Materials & Interfaces*, vol. 13, no. 12, pp. 14634–14643, 2021.
- [37] S.-Y. Chun, "Low resistivity hafnium nitride thin films deposited by inductively coupled plasma assisted magnetron sputtering in microelectronics," *Journal of Nanoscience and Nanotechnology*, vol. 21, no. 7, pp. 4129–4132, 2021.
- [38] Z. Hu, Y. Wang, and D. Zhao, "The chemistry and applications of hafnium and cerium(iv) metal-organic frameworks," *Chemical Society Reviews*, vol. 50, no. 7, pp. 4629–4683, 2021.
- [39] B. R. Levine, S. Sporer, R. A. Poggie, C. J. Della Valle, and J. J. Jacobs, "Experimental and clinical performance of porous tantalum in orthopedic surgery," *Biomaterials*, vol. 27, no. 27, pp. 4671–4681, 2006.
- [40] A. Yousef, I. Akhtyamov, F. Shakirova, L. Zubairova, E. Gatina, and C. I. C. Aliev, "Effect of hafnium and titanium coated implants on several blood biochemical markers after osteosynthesis in rabbits," *International Journal of Clinical and Experimental Medicine*, vol. 7, no. 10, pp. 3473–3477, 2014.
- [41] J.-Y. Choi, S. Kim, S. B. Jo et al., "A laminin-211-derived bioactive peptide promotes the osseointegration of a sandblasted, large-grit, acid-etched titanium implant," *Journal of Biomedical Materials Research. Part A*, vol. 108, no. 5, pp. 1214–1222, 2020.
- [42] X. Liu, D. Li, Y. Liang et al., "Establishment of anti-oxidation platform based on few-layer molybdenum disulfide nanosheet-coated titanium dioxide nanobelt nanocomposite," *Journal of Colloid and Interface Science*, vol. 601, pp. 167–176, 2021.
- [43] A. Yousef, I. Akhtyamov, F. Shakirova, L. Zubairova, E. Gatina, and E. Aliev, "Changes of blood composition in rabbits before and after osteosynthesis utilizing coated and non-coated metal implants," *International Journal of Biomedical and Healthcare Science*, vol. 4, no. 1, pp. 21–27, 2014.
- [44] T. L. McGinnity, V. Sokolova, O. Prymak, P. D. Nallathamby, M. Epple, and R. K. Roeder, "Colloidal stability, cytotoxicity, and cellular uptake of HfO<sub>2</sub> nanoparticles," *Journal of Biomedical Materials Research Part B: Applied Biomaterials*, vol. 109, no. 10, pp. 1407–1417, 2021.
- [45] C. Herranz-Diez, C. Mas-Moruno, S. Neubauer et al., "Tuning mesenchymal stem cell response onto titanium–niobium–hafnium alloy by recombinant fibronectin fragments," *ACS Applied Materials & Interfaces*, vol. 8, no. 4, pp. 2517–2525, 2016.
- [46] L. Gällentoft, L. M. E. Pettersson, N. Danielsen, J. Schouenborg, C. N. Prinz, and C. E. Linsmeier, "Size-dependent long-term tissue response to biostable nanowires in the brain," *Biomaterials*, vol. 42, pp. 172–183, 2015.
- [47] S. Pereira, P. Veeraraghavan, S. Ghosh, and M. Gandhi, "Animal experimentation and ethics in India: the CPCSEA makes a difference," *Alternatives to Laboratory Animals*, vol. 32, 1<sub>suppl</sub>, pp. 411–415, 2004.
- [48] S. Farnaud, "The Dr Hadwen Trust for Humane Research: 39 years of replacement science," *Alternatives to Laboratory Animals*, vol. 37, Suppl 2, pp. 39–43, 2009.
- [49] B. Wilmes and D. Drescher, "Impact of bone quality, implant type, and implantation site preparation on insertion torques of mini-implants used for orthodontic anchorage," *International Journal of Oral and Maxillofacial Surgery*, vol. 40, no. 7, pp. 697–703, 2011.
- [50] A. Pozzi, G. Tabanella, A. Guida et al., "A novel parallel-walled dental implant with a self-tapping apex, conical connection, and platform shifting: short-term results from a retrospective multicenter clinical study," *The International Journal of Periodontics & Restorative Dentistry*, vol. 41, no. 4, pp. 521–529, 2021.
- [51] A. Moroi, Y. Saito, A. Takayama, and K. Ueki, "Comparison of nonself-tapping tapered implant and self-tapping hybrid implant in terms of implant stability at initial and second fixation: a prospective randomized clinical trial," *Clinical Implant Dentistry and Related Research*, vol. 22, no. 6, pp. 679–688, 2020.
- [52] G. Widmark, B. Friberg, B. Johansson, S. Sindet-Pedersen, and Å. Taylor, "Mk III: a third generation of the self-tapping Brånemark System® implant, including the new Stargrip internal grip design. A 1-year prospective four-center study," *Clinical Implant Dentistry and Related Research*, vol. 5, no. 4, pp. 273–279, 2003.
- [53] A. I. Pearce, R. G. Richards, S. Milz, E. Schneider, and S. G. Pearce, "Animal models for implant biomaterial research in bone: a review," *European Cells & Materials*, vol. 13, pp. 1–10, 2007.
- [54] W. Fu, H. Yang, M. Li, M. Li, N. Yang, and G. Zou, "Anatase TiO<sub>2</sub> nanolayer coating on cobalt ferrite nanoparticles for magnetic photocatalyst," *Materials Letters*, vol. 59, no. 27, pp. 3530–3534, 2005.
- [55] D. Djozan, B. Ebrahimi, M. Mahkam, and M. A. Farajzadeh, "Evaluation of a new method for chemical coating of aluminum wire with molecularly imprinted polymer layer. Application for the fabrication of triazines selective solid-phase microextraction fiber," *Analytica Chimica Acta*, vol. 674, no. 1, pp. 40–48, 2010.
- [56] J. W. Crissman, D. G. Goodman, P. K. Hildebrandt et al., "Best practices guideline: toxicologic histopathology," *Toxicologic Pathology*, vol. 32, no. 1, pp. 126–131, 2004.
- [57] L. Tomlinson, L. I. Boone, L. Ramaiah et al., "Best practices for veterinary toxicologic clinical pathology, with emphasis on the pharmaceutical and biotechnology industries," *Veterinary Clinical Pathology*, vol. 42, no. 3, pp. 252–269, 2013.
- [58] V. Rajaraman, D. Nallaswamy, D. M. Ganapathy, and S. Kachhara, "Osseointegration of hafnium when compared to titanium—a structured review," *The Open Dentistry Journal*, vol. 15, no. 1, pp. 137–144, 2021.

## Review Article

# Antimicrobial Properties of Silver Nitrate Nanoparticle and Its Application in Endodontics and Dentistry: A Review of Literature

Lakshmi Thangavelu <sup>1</sup>, Abdul Habeeb Adil,<sup>2</sup> Sohaib Arshad,<sup>3</sup> Ezhilarasan Devaraj <sup>1</sup>,  
Sreekanth Kumar Mallineni <sup>4,5</sup>, Rishitha Sajja,<sup>6</sup> Anil Chakradhar <sup>7</sup>,  
and Mohmed Isaqali Karobari <sup>8,9</sup>

<sup>1</sup>Department of Pharmacology, Saveetha Dental College and Hospital, Saveetha Institute of Medical and Technical Sciences, Saveetha University, Chennai, India

<sup>2</sup>Department of Community Dentistry, School of Dental Sciences, Health Campus, Universiti Sains Malaysia, Kubang Kerian, 16150 Kota Bharu, Kelantan, Malaysia

<sup>3</sup>Periodontics Unit, School of Dental Sciences, Health Campus, Universiti Sains Malaysia, Kubang Kerian, 16150 Kota Bharu, Kelantan, Malaysia

<sup>4</sup>Department of Preventive Dental Science, College of Dentistry, Majmaah University, Al-Majmaah, Saudi Arabia

<sup>5</sup>Department of Pediatric Dentistry, Saveetha Dental College and Hospital, Saveetha Institute of Medical and Technical Sciences, Saveetha University, Chennai, India

<sup>6</sup>Department of Research and Development, Bristol Myers Squibb, New Jersey, USA

<sup>7</sup>Department of Conservative Dentistry, Kathmandu University, Dhulikhel, Kavre, Nepal

<sup>8</sup>Conservative Dentistry Unit, School of Dental Sciences, Universiti Sains Malaysia, Health Campus, Kubang Kerian, Kota Bharu 16150, Kelantan, Malaysia

<sup>9</sup>Department of Conservative Dentistry & Endodontics, Saveetha Dental College & Hospitals, Saveetha Institute of Medical and Technical Sciences University, Chennai, 600077 Tamil Nadu, India

Correspondence should be addressed to Anil Chakradhar; [anil254413@gmail.com](mailto:anil254413@gmail.com) and Mohmed Isaqali Karobari; [dr.isaq@gmail.com](mailto:dr.isaq@gmail.com)

Received 18 August 2021; Accepted 17 September 2021; Published 9 November 2021

Academic Editor: Jianbo Yin

Copyright © 2021 Lakshmi Thangavelu et al. This is an open access article distributed under the Creative Commons Attribution License, which permits unrestricted use, distribution, and reproduction in any medium, provided the original work is properly cited.

**Background.** The silver nanoparticles (Ag NPs) are the most acceptable and excellent nanotechnology-based product among all metallic nanoparticles (noble metals). They are novel in terms of good conductivity, catalytic, chemical stability, and most significant anti-inflammatory and antiviral activities. **Aim.** This review is aimed at understanding the synthesis, mechanism, and applications of Ag NPs in dentistry and their qualities to aid clinicians and researchers. **Materials and Methods.** A electronic search for literature was performed on the Google Scholar, PubMed, EMBASE, and Web of Science databases for related articles using multiple keywords. The keywords used were antimicrobial properties, mechanism of action, and current uses of Ag NPs in dentistry. The search was limited to articles published in the English language; no deadline was set for publications. **Results.** About 185 articles were considered relevant to the reported research out of 6420 electronic search results. Only the publications that were required were received after all abstracts were assessed for relevance. After a final electronic and manual search, roughly 47 research publications were found to be helpful in this study. **Conclusion.** The Ag NPs, unlike other biomaterials used in dentistry, have unique biological features and could be used in endodontics, restorative dentistry, periodontology, prosthetic dentistry, implantology, and oral malignancies, because of their antimicrobial, antifungal, and antiviral effects.

## 1. Introduction

It is important to investigate and assess antimicrobial substances with minimum toxicity to periapical tissues [1]. After careful shaping and cleaning of roots, the hermetic sealing of the root canal system is critical in endodontics. Through mechanical and chemical debridement, root canal therapy is aimed at eradicating microbes from the root canal system completely. Chemical debridement is linked with high success rates in bacterial elimination from the root canal system, whereas mechanical cleaning can minimize microorganisms in the root canal [2]. However, because it is impossible to eradicate all microorganisms from the root canal system throughout the treatment, endodontic materials must contain specific components that release antibacterial substances [3]. The most likely cause for this is the complex anatomy of the root canal system, which allows bacteria to colonize in inaccessible places to antimicrobial agents [4]. Despite cleaning, shaping, and administration of highly effective antimicrobial agents, clinical trials have shown that bacteria remain within the root canal system because bacteria can form biofilms, infiltrate dentinal tubules, and cause monoinfection [5, 6].

The prefix “nano” has been increasingly applied to various domains of knowledge throughout the previous decade. Nanotechnology is the science of the very small. It involves the use and manipulation of materials on a very small scale. The molecules and atoms behave differently at this dimension, allowing for several unexpected and fascinating applications [7]. The Ag NPs are highly acceptable and excellent nanotechnology-founded products among all metallic nanoparticles (noble metals). They are novel in terms of good conductivity, catalytic, chemical stability, and most significant anti-inflammatory and antiviral activities [8]. The Ag NPs and silver-incorporated compounds are proven very poisonous to microbes, with substantial biocidal properties upon as many as 16 bacteria species, comprising bacteria, fungi, and viruses [9]. The discharge of silver ions, which increases absorbency and causes injury to the bacterial DNA and cytoplasm, is responsible for the antibacterial activity. By interfering with the bacterial metabolism, the development of complexes between silver nanoparticles and proteins may result in bacterial mortality. The bacteriostatic effect may come from particle interaction with bacterial DNA, inhibiting cell multiplication [10]. Ag NPs with a 1–10 nm particle size bind to the cell surface with bacterial breakdowns, such as absorbency and oxygenation [11]. Nanoparticles are characterized as either naturally occurring or synthesized based on their composition. In nature, they are classified as organic or inorganic. They are categorized as particles, spheres, tubes, rods, plates, and so on based on their shape, as shown in Figure 1.

Although the antibacterial process of Ag NPs is yet unknown, several characteristics of their antimicrobial activity have been identified. Silver ions have the aptitude for interacting with the cell structures of many bacteria [12]. These silver ions appear to attach to the cytoplasmic membrane and cell wall primarily by electrostatic affinity and attractiveness for sulphur proteins, therefore increasing the

absorbency of membrane and preceding the distraction of these structures. DNA, proteins, and lipids are among the bacterial components that Ag NPs can destroy. Silver nanoparticles also cause bacterial cell death by inducing an oxidative stress response. Bacteria in the mouth prefer to form biofilms, which provide excellent conditions for development, immune elusion, and antibiotic confrontation. The efficacy of nanoparticles in biofilm has an inverse connection with their size; nanoparticles larger than 50 nm cannot enter the biofilm because of their relative self-dispersal coefficients, which drop exponentially with the square of the nanoparticle diameter [13]. Furthermore, charged NPs do not readily disperse across the biofilm, owing to carboxyl groups and phosphoryl on the bacteria’s surface, which provides the cell surface an electronegative character [14].

Since their debut, the use of nanoparticles in many disciplines of dentistry has increased dramatically because of the abovementioned characteristics, mode of action, and advantages above other traditional materials. Nanotechnology has progressed, and the antibacterial capabilities of nanostructured silver-based formulations have been proven against fungi, bacteria, and viruses [15–18]. The Ag NPs were shown to have efficient antimicrobial constituents in adhesives [19], prosthetics materials [20], and in implants to enhance the arrest of caries, induce osteogenic induction, and inhibit biofilm development [21]. Nanomaterials have proven efficacy in biofilm development, enhancing tooth structure remineralization by preventing the removal of minerals and combating endodontic microorganisms. In endodontics, these NPs can be included in an intracanal medicament, obturating substance, irrigating solutions, and sealer [22]. As a result, it is realistic to expect Ag NPs to perform a significant role soon, especially in dentistry. With each passing year, the impact of nanoparticles in dentistry, for the treatment of various oral disorders grows exponentially.

Nanoparticles have been used in the development of new irrigation materials because of the drawbacks of conventional irrigants. The chitosan NPs were shown to have improved antibiofilm effectiveness and inhibit bacterial endotoxins [23]. Afkhami et al. compared 2.5% sodium hypochlorite with the irrigation qualities of 100 ppm Ag NPs in previous research and found that Ag NPs had more significant antibacterial activity. Furthermore, when related to sodium hypochlorite, polyvinyl-coated Ag NPs were shown to have lower cytotoxicity [24, 25]. Due to their size, which lets infiltration into the canalculus of the tooth, Ag NPs are viable for disinfection methods [26]. Therefore, these NPs-incorporated materials have immense ability to be employed as an intracanal medication and/or irrigating solution during endodontic treatment. Antimicrobial action was also observed against *Streptococcus mutans*, *E. coli*, *E. faecalis*, *Actinomyces*, and *Candida albicans* when mineral trioxide aggregate (MTA) and calcium-based cement were combined with Ag NP. Silver particles can help endodontic sealers to have better antibacterial qualities by reducing the adhesion of microorganism to the tooth surface [27, 28].

In the last three years, several significant studies on the uses of nanomaterials in dentistry were published, each with a distinct focus. However, the features of Ag NP

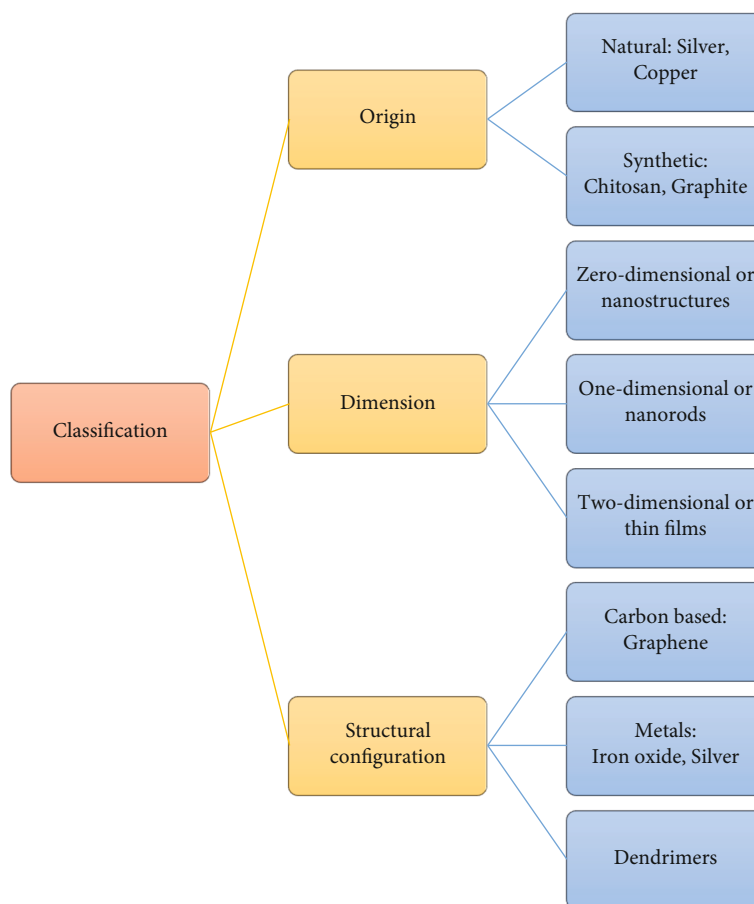


FIGURE 1: Classification of nanoparticles.

nanobiotechnological uses and its production were only examined broadly, not concerning dentistry. As a result, this article is aimed at presenting a literature review on the potential therapeutic application and antimicrobial properties of silver nanoparticles in dentistry, particularly in endodontics.

## 2. Materials and Methods

The relevant MESH terms like antimicrobial, endodontics, silver nanoparticles, and root canal were used to perform an electronic search for literature on the Google Scholar, PubMed, EMBASE, and Web of Science databases. The electronic literature search was conducted on July 5<sup>th</sup>, 2021. The keywords used were antimicrobial properties, mechanism of action, and current applications of silver nanoparticles in dentistry. The search was limited to articles that were published in the English language. There were no deadlines set for publication. In adjunct, supplementary documents on the concerns that had been neglected were identified by scanning the reference lists of each paper presenting data.

The data extracted depends on the antibacterial properties of Ag NPs. The current review focuses on silver NPs employed as antimicrobials in root canal infections and their uses in different fields of dentistry. The following inclusion criteria were used to refine further the search: root canal infections, general antibacterial mechanisms of Ag NPs, the

uses of Ag NPs in dentistry, and the antimicrobial effect of Ag NPs in endodontics.

## 3. Results and Discussion

Two researchers (A.H.A. and M.I.K.) performed the search and extraction of required data from the papers included in the current analysis after reading the entire texts. About 185 articles were thought relevant to the reported investigations out of 6420 electronic search results. Only the publications that were required were received after all abstracts were assessed for relevance. After a final electronic and manual search, roughly 47 research publications were helpful in this study.

**3.1. Synthesis of Ag NPs.** The synthesis of Ag NPs is of enormous concern to investigators because of their wide range of uses. The Ag NPs were first produced by reducing Ag NO<sub>3</sub> (silver nitrate) 0.500 mol/L with maltose 1.000 mol/L and then stabilizing them with 1.0 g gelatin [29]. Physical, chemical, and biological approaches are used to make Ag NPs [30]. There are two types of methods to produce Ag NPs: (1) bottom-up method and (2) top-down method as shown in Figure 2. In the bottom-up method, the production of Ag NPs is done by self-gathering of atoms to fresh nuclei that evolves into a particle, which can be formed by biological and chemical processes [31]. For the synthesis of NPs, the 'bottom-up' method

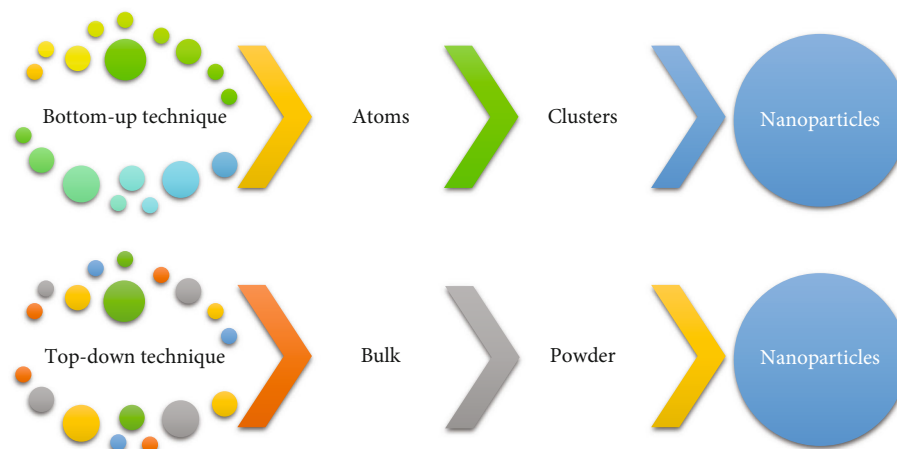


FIGURE 2: Schematic diagram for the bottom-up and top-down approach.

is preferable. It contains a uniform system in which catalysts (enzymes and reducing agents) generate nanomaterials tracked by reaction media, catalytic character, and conditions (such as temperature, solvents, and stabilizers). The chemical reduction approach, for example, is the most widely utilized synthetic route for Ag NPs [7]. In the top-down method, specified ablations, such as thermal decomposition, lithography, mechanical milling, thermal/laser ablation, sputtering, and etching, are used to break down a suitable bulk substance into nanoparticles [31, 32]. The Ag NPs are generally created in the top-down technique by evaporation/condensation in a tube heater at air compression. The foundation item, held centrally at the furnace within a boat, is boiled away into a carrier gas during this operation. The manufacturing of Ag NPs in a tube furnace has various drawbacks, including the fact that it takes up many places and consumes much power while increasing the ambient heat near the source substance, as well as the fact that it takes several minutes to achieve thermal stability [33, 34]. The synthesis of Ag NPs is explained in Table 1.

The use of plant extracts for Ag NP synthesis has piqued attention because of its environmental friendliness, speed, nonpathogenic, and cost-effectiveness. The application of biomolecules such as alkaloids, proteins, amino acids, enzymes, saponins, carbohydrates, tannins, vitamins, phenolics, enzymes, and terpenoids in the production of Ag NPs has earlier been founded in medicinal plants extracts. It is environmentally friendly, but it includes chemically complex structural elements [35–39].

**3.2. Antimicrobial Properties of Ag NPs.** The Ag NPs were reported to have a broad antibiotic action on Gram-positive and Gram-negative microorganisms and drug-resistant pathogens. The release of silver ions mainly causes the Ag NPs' antibacterial effect. When the fine Ag NPs (<10 nm particle size) are used for antibacterial action, the release of silver is superior to when bigger Ag NPs are employed [40]. The silver ions attach to electron donor assemblies in organic components comprising nitrogen, causing holes in the bacterial membrane, the release of cell contents, and bacterial death [10]. Presently, the silver-based compounds are known to be hazardous to microorganisms. As a result, numerous medici-

nal systems that discharge silver ions to achieve antibacterial activity have been developed. Boosting the relative contact area by reducing the size of silver particles, i.e., NPs, is an efficient technique of increasing their efficacy [41, 42].

The peptidoglycan bacterial cell wall is destroyed, and the cell membrane is lysed by silver ions. They adhere to DNA bases, causing DNA condensation. As a result, the bacterial cell loses its capacity to divide, stopping the binary fission of bacterial growth. They also solubilize ribosomes, preventing protein synthesis and causing plasma membrane breakdown [30]. The Ag NPs have germicidal properties against Gram-negative bacteria, causing depths to form in their cell walls [43]. Silver interacts with protein DNA of sulfhydryl groups, changing hydrogen bonding, cell growth, respiratory activities, DNA undoing, and cell wall formation [44]. Another way is that when silver NPs come into contact with bacteria, they produce free radicals, which break the cell membrane and render it porous, finally preceding cell mortality [45]. The process of antimicrobial action of Ag NPs is shown in Figure 3 and Table 2.

**3.3. Ag NP Uses in Restorative Dentistry.** Restoration failure is thought to be caused by restorative materials and mouth microorganisms in dentistry. Antibacterial agents should be used to achieve long-lasting restorations. The nanocomposites and inorganic nanoparticles are applied as effective antimicrobial agents [46]. Secondary caries is the significant cause of dental restorative failure. Several efforts have been undertaken to extend the lifespan of dental restorations by integrating antimicrobial bioactive substances. The gradual discharge of several depleted molecular weight antibacterial agents such as zinc ions, silver ions, chlorhexidine, antibiotics, and iodine was studied [47]. Evidence suggests that microleakage on restoration edges allows oral bacteria to colonize, leading to secondary decay. This results in the failure of restoration and the requirement for replacement or restoration. Antimicrobial agents, such as Ag NPs, can solve the problem by including them into adhesive systems and composite resins [40]. The antibacterial activities of restorative materials containing Ag NPs can minimize the incidence of recurrent decay beneath composite resins due to microleakage. Because of the high preventive action of

TABLE 1: Demonstration of the different approaches in Ag NP synthesis.

Physical	Chemical	Biological	Top-down	Bottom-up
Bal milling Thermal evaporation Lithography Vapor phase	Sol-gel processing Solution-based synthesis	Bacteria Fungi Yeast Plant extract ( <i>Salvadora persica</i> )	Mechanical milling Chemical etching Laser ablation Sputtering lithography Thermal decomposition	Electrochemical precipitation Vapor deposition Molecular condensation Sol-gel process Spray pyrolysis Laser pyrolysis Aerosol pyrolysis Green synthesis: bacteria plants (gymnosperms to angiosperms) <i>Fungus algae</i> <i>Yeasts</i> <i>Actinomycetes</i>

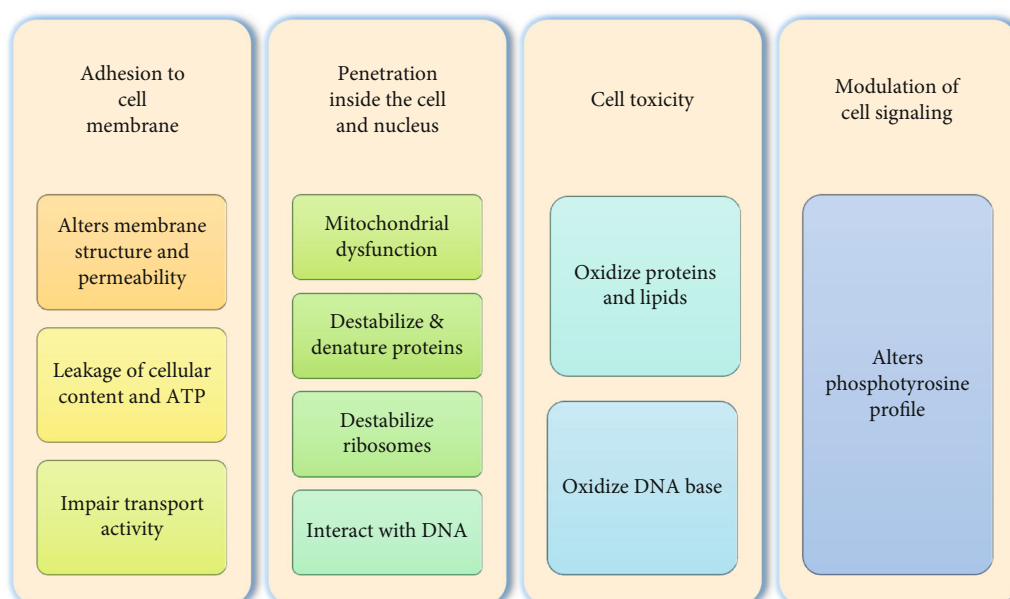


FIGURE 3: The process of antimicrobial activity of Ag NPs.

TABLE 2: The antimicrobial action of Ag NPs.

Antibacterial action	Antiviral action	Antifungal action
(i) Effective against Gram-positive and Gram-negative bacteria (ii) Minimum inhibitory concentration (MIC) of Ag NPs is in approximately 0.003 mg/mL for <i>Fusobacterium nucleatum</i> (iii) 0.04 mg/mL for <i>Streptococcus mutans</i> and 0.5 mg/mL for <i>Actinomyces oris</i> (iv) Concentration of 50–60 $\mu\text{g cm}^{-3}$ of Ag NPs causes 100% prevention of bacterial growth <i>Escherichia coli</i> (v) Ag NPs in the range of 1-10 nm with direct contact with cell membrane surface change the permeability and causes cell damage	(i) Effective against <i>Candida albicans</i> , <i>Fusarium oxysporum</i> (ii) Attach with the superficial proteins of viruses inhibiting their binding and replication	(i) Effective against arenavirus, HIV, <i>murine norovirus</i> , <i>hepatitis B virus</i> (ii) Ag NP action against <i>Candida albicans</i> could be destruction of cell membrane preventing the growth of cell (iii) Concentration of 1 $\mu\text{g/mL}$ of Ag NPs included in resins have shown strong antifungal action without any cytotoxicity



TABLE 3: Description of the incorporation of Ag NPs into different restorative materials used in dentistry.

Type of restorative material	Characteristics	References
Composites	(i) As filler particles, Ag NPs have been integrated into composite resins and adhesive systems (ii) To boost Ag salt solubility in resin solutions, the most frequent way is to add a monomer, commonly 2-(tertbutylamino) ethyl methacrylate (iii) Improves the antimicrobial properties of composite material (iv) The mechanical properties of many adhesive systems utilized with such composites are likewise influenced by Ag+	[30, 41]
Glass ionomer	(i) The antibacterial action of the newly designed nano-Ag-GIC was demonstrated by diffusion (ii) The oxidative breakdown of silver ions from the cement matrix is effective in avoiding caries and the development of biofilms on their exterior (iii) Ag NPs in GIC give a fast boost of silver and fluoride ions to be exchanged with carious dentin, demonstrating to be a useful material in the treatment of cavities in patients at high risk	[30, 41]

TABLE 4: Description of different materials with Ag NPs used in endodontics.

Type of material used in endodontics	Characteristics	References
Root canal irrigant	(i) An Ag NP-based solution for irrigation proved equally effective as sodium hypochlorite in the removal of <i>Staphylococcus aureus</i> and <i>Enterococcus faecalis</i> (ii) In comparison to sodium hypochlorite, a low concentration of Ag NPs demonstrated higher biocompatibility (iii) In comparison to sodium hypochlorite and chlorhexidine solutions, silver-based root canal irrigant successfully continued their antibacterial activity	[48, 70, 71]
Intracanal medicament	(i) Calcium hydroxide in comparison to the 0.01 percent Ag NP gel and calcium hydroxide groups, biofilms treated with 0.02 percent Ag NP gel as a medicament for 7 days considerably eliminated the formation with the least amount of residual functional <i>E. faecalis</i> cells (ii) Mineral trioxide when compared to unmodified MTA, the MTA containing 1% ag NPs have a stronger antibacterial activity against bacteria and fungi. Mineral trioxide aggregate with Ag NPs is biocompatible and does not cause inflammation	[72, 73]
Gutta-percha	(i) Gutta-percha coated with Ag NPs have antibacterial and antifungal characteristic which made them as effective as in preventing bacterial leakage (ii) Given the antibacterial properties of Ag NPs coated gutta-percha, it is possible that using this form of gutta-percha in endodontic treatments might be more effective (iii) Substantial antimicrobial effect against <i>Staphylococcus aureus</i> , <i>Candida albicans</i> , <i>E faecalis</i> , and <i>E coli</i>	[74–76]
Root canal sealer	(i) A new endodontic sealer with Ag NPs has potent antibiofilm abilities (ii) Do not cooperate the sealing and physical assets of a sealer	[77]

bacteria causing caries, restorative adhesives containing Ag NPs may interfere with biofilm growth [48]. Cheng et al. [49] investigated the mechanical characteristics and biofilm formation of Ag NPs inserted into composite resin in a study published in 2013. According to this study, the mechanical characteristics of composites were not affected when Ag NPs were added at concentrations of 0.028 and 0.042. When the Ag NP concentration was 0.042, however, *Streptococcus mutans* colony-forming units were reduced by 75%. The types of material used in restorative dentistry with incorporation Ag NPs were explained in Table 3.

**3.4. Ag NPs Used in Endodontics.** Antibiotic resistance and recurrent infections, which can lead to treatment failure, are critical issues in the field of endodontics [6]. For a successful root canal therapy, complete inhibition and eradication of

microorganisms from the root canal system is critical. Subsequently, after rigorous root canal disinfection, instrumentation, and obturation, microorganisms can still be found in the root canal [50]. According to research on unsuccessful endodontic therapy, apical periodontitis in root canal-treated teeth is frequently composed of several types of microbial infections. Many samples have been found to contain *Enterococcus faecalis* [51, 52]. While *E. faecalis* infects the dentinal tubules and cementum, it is resistant to most root canal disinfectants and can persist for extended periods inside the dentinal tubules, even in diminished nutrient environments [53]. When compared to 2% chlorhexidine, Ag NPs had the maximum zone of inhibition (19.55 mm) and the lowest zone of inhibition (10.32 mm) against *E. Faecalis*, indicating that it might be employed as an alternate antibacterial for endodontic disinfection [54]. The discharge of Ag+ ions, which provide an

TABLE 5: Demonstration of material combinations with Ag NPs used in dentistry.

Department of dentistry	Biomaterials	References
Prosthodontics	(i) Acrylic resin—the Ag NPs can be mixed into acrylic resin to stop the development of microorganisms like <i>Streptococcus aureus</i> , <i>E. coli</i> , and <i>Staphylococcus mutans</i> (ii) Porcelain—the latent compressive stress induced by a differential thermal expansion and ion exchange reaction of silver nanoparticles in porcelain is responsible for its reinforced mechanical qualities, including as hardness and fracture toughness	[78, 79]
Periodontics	(i) Guided tissue regeneration (GTR)—the GTR membrane with Ag NPs decreased the bacterial adhesion and permeation, treating intrabony defects and increase clinical outcomes (ii) Periodontal dressings—periodontal dressings A (25 percent v/v) and B (50 percent v/v) of Ag NP concentration were utilized to determine the optimal Ag NP dosages for postsurgery healing of periodontal wounds (iii) Capping agent—sodium alginate capped Ag NPs encourage the suppression of Gram-negative bacteria, which are the most common cause of periodontal diseases	[40, 48]
Orthodontics	(i) Adhesives—when compared to conventional adhesives, Ag NPs significantly reduced adhesion of streptococci to orthodontic adhesives while maintaining shear bond strength (ii) Cements—cements with Ag NPs could be used to avoid white spot lesions in orthodontic treatments	[40]
Dental implants	(i) Modification of implant surfaces with Ag NPs utilizing numerous doping approaches is presently a hot topic, related to the safety and effective bactericidal capabilities of Ag NPs (ii) Dental implants made of titanium infused with Ag NPs can improve bone mineral thickness, bone growth, and trabecular shape while causing no damage to the tissues surrounding the implants	[80]
Pedodontics	(i) Cements—the antibacterial activity is mediated by the discharge of Ag ions, who induces oxidative breakdown in the cement substance, preventing the formation of oral biofilms and suppressing tooth caries (ii) Resins—Ag NPs was added into a resin matrix, which is employed in chitosan polymer-based restorations of deciduous and permanent dentitions	[57]
Preventive dentistry	(i) Silver ions can precipitate and penetrate in carious lesions, causing enamel hardness (ii) Dental surgeons employ varnish like silver nanofluoride and silver diamine fluoride in the clinical practice to remineralize incipient lesions	[81]
Oral and maxillofacial surgery	(i) Anticancer effect—early detection of malignancies and the use of a drug delivery method to a cancer-affected spot can be advantageous because it reduces the patient's anxiety (ii) The green route method for Ag NPs was discovered to have an immediate suppressive anticancer effects	[40]

electrodynamic affinity to sulphur proteins, causes adhesion to bacterial cell membrane and rupture. Silver ions taken in the cell can cause malfunction of respiratory enzymes, causing responsive oxygen groups to form and adenosine triphosphate production to be disrupted. Direct denaturation of DNA and ribosomes can also be caused by silver ions [55]. Since it successfully dissolved *E. faecalis* biofilm and removed the bacteria from infected dentinal tubules, the Ag NP solution is an effective root canal irrigant [30]. The different uses of Ag NPs used in endodontics are explained in Table 4.

**3.5. Ag NPs Used as Biomaterials in Dentistry.** The application of Ag in dentistry dates back to the 19th century and exhibits various uses, owing to silver ions' antibacterial properties. [56]. Meanwhile, the emergence of nanotechnology in the twenty-first century gave rise to a new viewpoint on using silver in dentistry in the type of Ag NPs, which exhibit antibacterial properties owing to the slow discharge of silver ions [57]. The Ag NP research has risen in popularity in the modern era. The primary factor is that Ag NPs may modify the growth processes and nucleation with various synthetic chemicals.

Secondly, molecular covering agents like chemical groups and proteins can be used to precisely form Ag NPs. Thirdly, Ag NPs have a powerful antimicrobial impact that enhances clinical treatment results [58]. The primary goal of incorporating Ag NPs into dental products is to prevent or reduce the development of biofilms and the proliferation of microbes [59]. Therefore, the discovery of broad-spectrum antimicrobials that can be successfully included in dental biomaterials is critical. As a result, uniform silver nanoparticles with regulated size, shape, and action can be considered multipurpose parts in various dental biomaterials [48]. They have a superior antibacterial effect without altering the material's mechanical qualities due to their higher volume to surface area ratio and lesser particle dimension. The Ag NPs have unique features that make them ideal fillers for various biomaterials, where they play a critical role in improving qualities [40]. The uses of Ag NPs in different biomaterials are explained in Table 5.

**3.6. Toxicity of Silver Nanoparticles.** The biosafety and biocompatibility aspect of using Ag NPs in managing the individual illness, healing intervention, and directed medicine distribution

is the most significant and critical challenge. The growing popularity of Ag NP-based antimicrobials raises concerns about the clinical risks and biosafety they pose to humans [31]. The Ag NPs have a constant set of flexible features that make them suitable for various biomedical and associated applications. The Ag NPs were subjected to several *in vivo* and *in vitro* investigations over the years in order to learn more about their harmful effects on live tissues and organisms. Because of their antibacterial properties, Ag NPs remain the most extensively used nanocompound on the market. As the use of Ag NP products grows, so does the risk of negative effects on the environment and human health. The Ag NPs have distinct physiochemical qualities (surface area, size, capacity to aggregate, chemical composition of surface chemistry, and solubility) and biological activities than pure silver. These physiochemical traits result in a greater surface area, which increases toxicity [60]. Recent research has linked Ag NPs of various sizes and shapes to inflammatory, pulmonary inflammation, hepatotoxic, cytotoxic, neurotoxic, and genotoxic effects [61]. The dose limit for the usage of Ag NP in dentistry is considered to be less than 18 mg/kg of body weight, whereas greater than 20 mg/kg body weight is toxic [62]. The toxic effects of Ag NPs were shown to be precisely connected to the interaction of free Ag ions discharged in the medium [58]. Orally administered silver has been found in the range of 0.4–18 mg particles/kg of body weight/day and 18 percent in animals and humans, respectively. Silver appears to be distributed throughout all the organs examined, with the highest concentrations seen in the intestine and stomach. Silver causes argyria, a blue-grey staining of the skin [63]. The Ag NPs can easily disrupt human organ's biological molecules and cells due to their nanosize. According to some laboratory research, Ag NPs can cause oxidative emphasis in human cells and disrupt the function of mitochondria [64]. When silver and Ag NPs were given orally, the nanoparticles were shown to be less absorbed, with increased fecal excretion and lower amounts in organs [65]. Nanoparticles have a more complicated absorption mechanism than smaller molecules. Orally administered nanoparticles are absorbed primarily by macrophages and lymphatic uptake, while subcutaneous, intramuscular, and inhaled nanoparticles are absorbed primarily through paracellular transport, transcytosis, and M cell uptake in the GI tract [66]. Ag NPs were shown to pass the blood-brain barrier in rats, causing neural necrosis and deterioration due to long-term buildup in the brain [67]. Following a 28-day repeated oral exposure to 14 nm PVP-coated Ag NPs or silver acetate in rats, researchers found low silver excretion in urine (0.1% of 24 h intake for both groups) but high excretion of silver in feces (63 and 49% of daily dose for Ag NPs and silver acetate groups, respectively), and high excretion of silver in feces (63 and 49% of daily dose for Ag NPs and silver acetate [66]. The biological half-life of silver in humans (liver) ranges from several to 50 days [68]. The toxic effects of Ag NPs on the human body are explained in Figure 4.

**3.7. Future Implications and Recommendations.** Because laboratory conditions do not wholly replicate oral situations, one of the most crucial experiments to conduct is applying bench data to *in vivo* research. Another element to be exam-

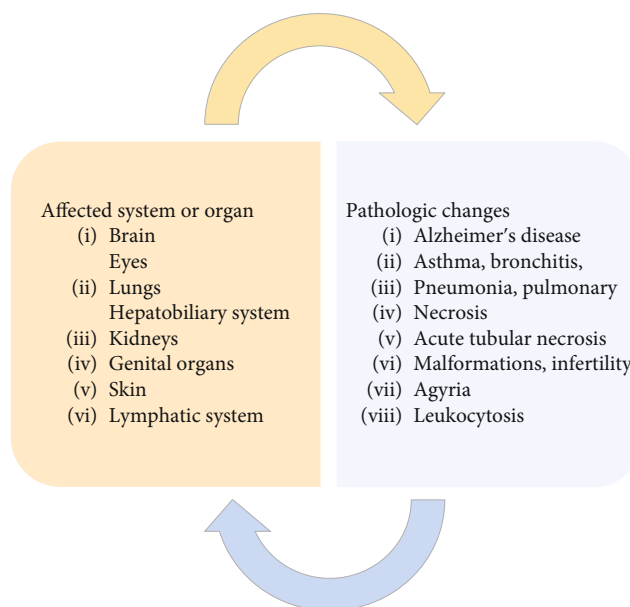


FIGURE 4: The toxic effects of Ag NPs.

ined is the long-standing efficiency of Ag NPs related to dental materials, as they should have a long-lasting antibacterial activity [59]. However, there has been a global rise in publications and technical progress on Ag NP in the health field, indicating a rise in investigations on this expertise, which has presently demonstrated the antimicrobial property of Ag NPs in nanocomposites or when combined with biomaterials. For restorative, prosthetic, periodontal, endodontic, orthodontic, and implant treatment, a rising variety of dental materials, including Ag NPs, are being manufactured and are shown in Figure 5. Human cells were found to be cytotoxic by silver nanoparticles in several laboratory investigations. However, the statistical significance of silver nanoparticles' possible toxicity is uncertain. Because clinical data is currently minimal, more research is needed [48]. When used at concentrations low in cytotoxicity to the patient's cells, the Ag NPs appear as antimicrobial means for preventing pathogens, inflammation of tissue, caries' activity, and bone loss [57]. Since Ag NPs are frequently related to dental biomaterials, the breadth of technological areas is still more apparent, such as the discovery of the Ag-PMMA nanocomposite film established on Aristo lochia bracteolate with preventive action on *E. coli*, growth of *Bacillus cereus* and *E. coli* in aqueous liquids [69]. There are numerous viable products and therapeutic applications like wound coverings, which have already been established for Ag NPs, while many other potential applications are being thoroughly researched. Because of the anti-inflammatory, antiviral, antibacterial, and antifungal capabilities, the Ag NPs have much potential, and recent research has discovered new osteoinductive assets as well. Though, the processes and biological relations that underpin these characteristics are still unknown [67]. Another innovation is putting Ag NPs on the surface of a tooth implant to provide it antibacterial qualities. This is an example of surfacing and coated technology as well as the pharmaceutical technological arena. Some patents also cover preventative dentistry, such as antibacterial, antifungal, and local

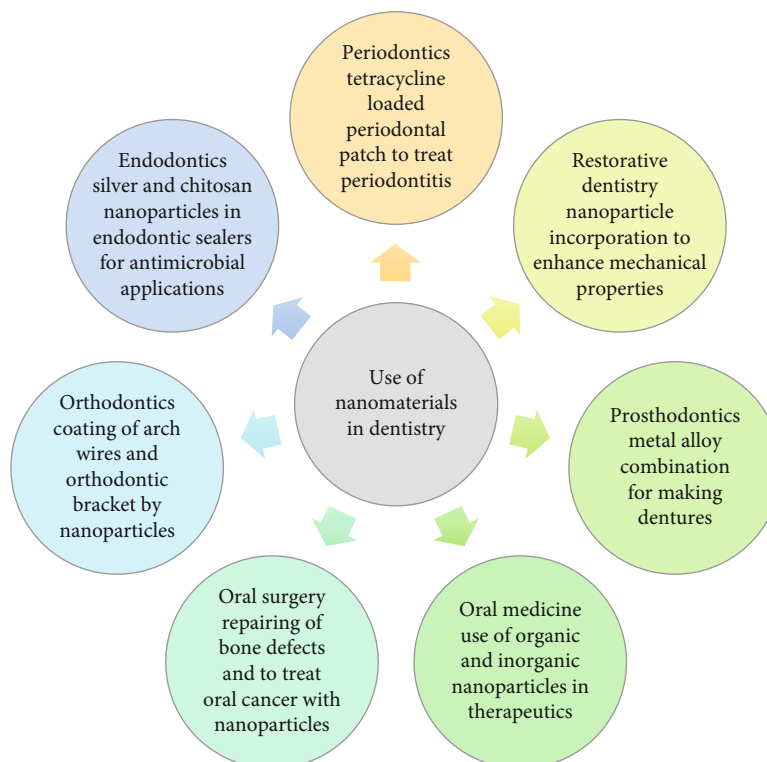


FIGURE 5: Uses of nanomaterials in dentistry.

anesthetic oral and throat care medicines that can be administered daily. They also have organoleptic qualities essential for dental treatments such as gum strengthening and gingival bleeding reduction [57]. Clinical trials are required before Ag NPs or Ag NP-based formulations can treat human therapeutic interventions or disease management. There are, nevertheless, some significant impediments. In this regard, we believe that further research should occur in three steps before Ag NPs can be used in therapeutic interferences, clinical trials, or drug release therapies. However, there are issues and controversies about the safe application of Ag NPs in the treatment of diseases and healthcare, and there are some benefits to using them. According to research so far, the Ag NPs can be modified to boost their antibacterial stability, usefulness, biosafety, specificity, and biocompatibility for larger therapeutic assistance and condensed possible toxicity.

#### 4. Conclusion

The Ag NPs, unlike other biomaterials used in dentistry, have unique biological features and could be used in endodontics, restorative dentistry, periodontology, prosthetic dentistry, implantology, and oral malignancies, because of their antiviral, antibacterial, and antifungal properties. The Ag NPs are among the most outstanding nanomaterials used in industrial and commercial applications. Antimicrobial, technological, and biomedical products have all made substantial use of it. This narrative review provides a broad summary of Ag NPs, including synthesis, antimicrobial properties, use in restorative dentistry, use in endodontics, Ag NPs in dental biomaterials, and potential toxicity concerns.

#### Data Availability

All types of data used to support these review findings have been included in this article.

#### Conflicts of Interest

The authors declare that they have no conflicts of interest.

#### References

- [1] S. Gurunathan, J. W. Han, D. N. Kwon, and J. H. Kim, "Enhanced antibacterial and anti-biofilm activities of silver nanoparticles against Gram-negative and Gram-positive bacteria," *Nanoscale Research Letters*, vol. 9, no. 1, pp. 1–17, 2014.
- [2] A. Byström, R. Claesson, and G. Sundqvist, "The antibacterial effect of camphorated paramonochlorophenol, camphorated phenol and calcium hydroxide in the treatment of infected root canals," *Dental Traumatology*, vol. 1, no. 5, pp. 170–175, 1985.
- [3] C. Rocha, M. A. Rossi, M. R. Leonardo, L. B. Rocha, P. Nelson-Filho, and L. A. B. Silva, "Biofilm on the apical region of roots in primary teeth with vital and necrotic pulps with or without radiographically evident apical pathosis," *International Endodontic Journal*, vol. 41, no. 8, pp. 664–669, 2008.
- [4] D. Ricucci, S. Loghin, and J. F. Siqueira Jr., "Exuberant biofilm infection in a lateral canal as the cause of short-term endodontic treatment failure: report of a case," *Journal of Endodontics*, vol. 39, no. 5, pp. 712–718, 2013.
- [5] R. A. Fernandes, D. R. Monteiro, L. S. Arias, G. L. Fernandes, A. C. B. Delbem, and D. B. Barbosa, "Biofilm formation by *Candida albicans* and *Streptococcus mutans* in the presence

- of farnesol: a quantitative evaluation," *Biofouling*, vol. 32, no. 3, pp. 329–338, 2016.
- [6] P. Nair, S. Henry, V. Cano, and J. Vera, "Microbial status of apical root canal system of human mandibular first molars with primary apical periodontitis after "one-visit" endodontic treatment," *Oral Surgery, Oral Medicine, Oral Pathology, Oral Radiology, and Endodontology*, vol. 99, no. 2, pp. 231–252, 2005.
- [7] S. L. Pal, U. Jana, P. K. Manna, G. P. Mohanta, and R. Manavalan, "Nanoparticle: an overview of preparation and characterization," *Journal of Applied Pharmaceutical Science*, vol. 1, no. 6, pp. 228–234, 2011.
- [8] S. Ahmed, M. Ahmad, B. L. Swami, and S. Ikram, "A review on plants extract mediated synthesis of silver nanoparticles for antimicrobial applications: a green expertise," *Journal of Advanced Research*, vol. 7, no. 1, pp. 17–28, 2016.
- [9] J. Spadaro, T. J. Berger, S. D. Barranco, S. E. Chapin, and R. O. Becker, "Antibacterial effects of silver electrodes with weak direct current," *Antimicrobial Agents and Chemotherapy*, vol. 6, no. 5, pp. 637–642, 1974.
- [10] C. Damm, H. Münstedt, and A. Rösch, "The antimicrobial efficacy of polyamide 6/silver-nano- and microcomposites," *Materials Chemistry and Physics*, vol. 108, no. 1, pp. 61–66, 2008.
- [11] A. Shrestha and A. Kishen, "Antibacterial nanoparticles in endodontics: a review," *Journal of Endodontics*, vol. 42, no. 10, pp. 1417–1426, 2016.
- [12] N. Takahashi, "Oral microbiome metabolism: from "who are they?" to "what are they doing?,"" *Journal of Dental Research*, vol. 94, no. 12, pp. 1628–1637, 2015.
- [13] T.-O. Peulen and K. J. Wilkinson, "Diffusion of nanoparticles in a biofilm," *Environmental Science & Technology*, vol. 45, no. 8, pp. 3367–3373, 2011.
- [14] N. I. Abu-Lail and T. A. Camesano, "Role of lipopolysaccharides in the adhesion, retention, and transport of *Escherichia coli* JM109," *Environmental Science & Technology*, vol. 37, no. 10, pp. 2173–2183, 2003.
- [15] M. Rai, A. P. Ingle, A. K. Gade, M. C. T. Duarte, and N. Duran, "Three *Phoma* spp. synthesised novel silver nanoparticles that possess excellent antimicrobial efficacy," *IET Nanobiotechnology*, vol. 9, no. 5, pp. 280–287, 2015.
- [16] M. Rai, K. Kon, A. Ingle, N. Duran, S. Galdiero, and M. Galdiero, "Broad-spectrum bioactivities of silver nanoparticles: the emerging trends and future prospects," *Applied Microbiology and Biotechnology*, vol. 98, no. 5, pp. 1951–1961, 2014.
- [17] M. Rai, S. Birla, A. P. Ingle et al., "Nanosilver: an inorganic nanoparticle with myriad potential applications," *Nanotechnology Reviews*, vol. 3, no. 3, pp. 281–309, 2014.
- [18] M. Rai, A. P. Ingle, A. Gade, and N. Duran, "Synthesis of silver nanoparticles by *Phoma gardeniae* and in vitro evaluation of their efficacy against human disease-causing bacteria and fungi," *IET Nanobiotechnology*, vol. 9, no. 2, pp. 71–75, 2015.
- [19] Y. Liu, Z. Zheng, J. N. Zara et al., "The antimicrobial and osteoinductive properties of silver nanoparticle/poly (dl-lactic-co-glycolic acid)-coated stainless steel," *Biomaterials*, vol. 33, no. 34, pp. 8745–8756, 2012.
- [20] R. E. Nuñez-Anita, L. S. Acosta-Torres, J. Vilar-Pineda, J. C. Martínez-Espinosa, J. de la Fuente-Hernández, and V. M. Castaño, "Toxicology of antimicrobial nanoparticles for prosthetic devices," *International Journal of Nanomedicine*, vol. 9, p. 3999, 2014.
- [21] B. Tian, W. Chen, Y. Dong et al., "Silver nanoparticle-loaded hydroxyapatite coating: structure, antibacterial properties, and capacity for osteogenic induction In Vitro," *RSC Advances*, vol. 6, no. 11, pp. 8549–8562, 2016.
- [22] American Association of Endodontists, *Glossary of endodontic terms*, American Association of Endodontists, 2003.
- [23] A. Shrestha and A. Kishen, "Antibiofilm efficacy of photosensitizer-functionalized bioactive nanoparticles on multispecies biofilm," *Journal of Endodontics*, vol. 40, no. 10, pp. 1604–1610, 2014.
- [24] T. V. Slenters, I. Hauser-Gerspach, A. U. Daniels, and K. M. Fromm, "Silver coordination compounds as light-stable, nano-structured and anti-bacterial coatings for dental implant and restorative materials," *Journal of Materials Chemistry*, vol. 18, no. 44, pp. 5359–5362, 2008.
- [25] S. L. Percival, P. Bowler, and D. Russell, "Bacterial resistance to silver in wound care," *Journal of Hospital Infection*, vol. 60, no. 1, pp. 1–7, 2005.
- [26] J. F. B. Bruniera, Y. T. C. Silva-Sousa, M. G. Lara, A. Pitondo-Silva, A. M. Marcaccini, and C. E. S. Miranda, "Development of intracanal formulation containing silver nanoparticles," *Brazilian Dental Journal*, vol. 25, no. 4, pp. 302–306, 2014.
- [27] N. Jonaidi-Jafari, M. Izadi, and P. Javidi, "The effects of silver nanoparticles on antimicrobial activity of ProRoot mineral trioxide aggregate (MTA) and calcium enriched mixture (CEM)," *Journal of Clinical and Experimental Dentistry*, vol. 8, no. 1, article e22, 2015.
- [28] M. S. Mendes, L. D. Resende, C. A. Pinto, D. P. Raldi, F. G. Cardoso, and S. M. Habitante, "Radiopacity of mineral trioxide aggregate with and without inclusion of silver nanoparticles," *The Journal of Contemporary Dental Practice*, vol. 18, no. 6, pp. 448–451, 2017.
- [29] J. F. B. Bruniera, L. Gabriel-Silva, R. S. Goulart et al., "Green synthesis, characterization and antimicrobial evaluation of silver nanoparticles for an intracanal dressing," *Brazilian Dental Journal*, vol. 31, no. 5, pp. 485–492, 2020.
- [30] S. Mitthra, L. Saatwika, B. Anuradha, and A. Subbiya, "Application of silver nanoparticles in conservative and endodontics," *Indian Journal of Public Health*, vol. 10, no. 8, p. 1634, 2019.
- [31] M. A. Barkat, Harshita, S. Beg et al., "Current progress in synthesis, characterization and applications of silver nanoparticles: precepts and prospects," *Recent Patents on Anti-Infective Drug Discovery*, vol. 13, no. 1, pp. 53–69, 2018.
- [32] M. Gomathi, A. Prakasam, R. Chandrasekaran, G. Gurusubramaniam, K. Revathi, and S. Rajeshkumar, "Assessment of silver nanoparticle from *Cocos nucifera* (coconut) shell on dengue vector toxicity, detoxifying enzymatic activity and predatory response of aquatic organism," *Journal of Cluster Science*, vol. 30, no. 6, pp. 1525–1532, 2019.
- [33] M. E. Samberg, S. J. Oldenburg, and N. A. Monteiro-Riviere, "Evaluation of silver nanoparticle toxicity in skin in vivo and keratinocytes in vitro," *Environmental Health Perspectives*, vol. 118, no. 3, pp. 407–413, 2010.
- [34] M.-C. Daniel and D. Astruc, "Gold nanoparticles: assembly, supramolecular chemistry, quantum-size-related properties, and applications toward biology, catalysis, and nanotechnology," *Chemical Reviews*, vol. 104, no. 1, pp. 293–346, 2004.
- [35] N. Kulkarni and U. Muddapur, "Biosynthesis of metal nanoparticles: a review," *Journal of Nanotechnology*, vol. 2014, Article ID 510246, 8 pages, 2014.
- [36] H. Agarwal, S. Menon, S. Rajeshkumar, and S. V. Kumar, "Green synthesis of silver nanoparticle using *Kalanchoe*

- pinnata leaf extract and its antibacterial effect against gram-positive and gram-negative species,” *Research Journal of Pharmacy and Technology*, vol. 11, no. 9, pp. 3964–3968, 2018.
- [37] P. Karthiga, S. Rajeshkumar, and G. Annadurai, “Mechanism of larvicidal activity of antimicrobial silver nanoparticles synthesized using *Garcinia mangostana* bark extract,” *Journal of Cluster Science*, vol. 29, no. 6, pp. 1233–1241, 2018.
- [38] S. Rajeshkumar, “Synthesis of silver nanoparticles using fresh bark of *Pongamia pinnata* and characterization of its antibacterial activity against gram positive and gram negative pathogens,” *Resource-Efficient Technologies*, vol. 2, no. 1, pp. 30–35, 2016.
- [39] S. Rajeshkumar, C. Malarkodi, M. Vanaja, and G. Annadurai, “Anticancer and enhanced antimicrobial activity of biosynthesized silver nanoparticles against clinical pathogens,” *Journal of Molecular Structure*, vol. 1116, pp. 165–173, 2016.
- [40] R. A. Bapat, T. V. Chaubal, C. P. Joshi et al., “An overview of application of silver nanoparticles for biomaterials in dentistry,” *Materials Science and Engineering: C*, vol. 91, pp. 881–898, 2018.
- [41] P. Kaur and R. Luthra, “Silver nanoparticles in dentistry: an emerging trend,” *SRM Journal of Research in Dental Sciences*, vol. 7, no. 3, p. 162, 2016.
- [42] S. Rajeshkumar, “Phytochemical constituents of fucoidan (*Padina tetrastromatica*) and its assisted AgNPs for enhanced antibacterial activity,” *IET Nanobiotechnology*, vol. 11, no. 3, pp. 292–299, 2017.
- [43] I. Sondi and B. Salopek-Sondi, “Silver nanoparticles as antimicrobial agent: a case study on *E. coli* as a model for Gram-negative bacteria,” *Journal of Colloid and Interface Science*, vol. 275, no. 1, pp. 177–182, 2004.
- [44] A. B. Lansdown, “Silver in health care: antimicrobial effects and safety in use,” *Biofunctional Textiles and the Skin*, vol. 33, pp. 17–34, 2006.
- [45] M. Danilczuk, A. Lund, J. Sadlo, H. Yamada, and J. Michalik, “Conduction electron spin resonance of small silver particles,” *Spectrochimica Acta Part A: Molecular and Biomolecular Spectroscopy*, vol. 63, no. 1, pp. 189–191, 2006.
- [46] K. Fatemeh, M. Mohammad Javad, and K. Samaneh, “The effect of silver nanoparticles on composite shear bond strength to dentin with different adhesion protocols,” *Journal of Applied Oral Science*, vol. 25, no. 4, pp. 367–373, 2017.
- [47] D. Xie, Y. Weng, X. Guo, J. Zhao, R. L. Gregory, and C. Zheng, “Preparation and evaluation of a novel glass-ionomer cement with antibacterial functions,” *Dental Materials*, vol. 27, no. 5, pp. 487–496, 2011.
- [48] I. X. Yin, J. Zhang, I. S. Zhao, M. L. Mei, Q. Li, and C. H. Chu, “The antibacterial mechanism of silver nanoparticles and its application in dentistry,” *International Journal of Nanomedicine*, vol. 15, pp. 2555–2562, 2020.
- [49] L. Cheng, M. D. Weir, H. H. K. Xu et al., “Effect of amorphous calcium phosphate and silver nanocomposites on dental plaque microcosm biofilms,” *Journal of Biomedical Materials Research Part B: Applied Biomaterials*, vol. 100B, no. 5, pp. 1378–1386, 2012.
- [50] J. F. Siqueira, I. N. Rôças, and D. Ricucci, “Biofilms in endodontic infection,” *Endodontic Topics*, vol. 22, no. 1, pp. 33–49, 2010.
- [51] A. Molander, C. Reit, G. Dahlén, and T. Kvist, “Microbiological status of root-filled teeth with apical periodontitis,” *International Endodontic Journal*, vol. 31, no. 1, pp. 1–7, 1998.
- [52] H. Hancock III, A. Sigurdsson, M. Trope, and J. Moiseiwitsch, “Bacteria isolated after unsuccessful endodontic treatment in a North American population,” *Oral Surgery, Oral Medicine, Oral Pathology, Oral Radiology, and Endodontology*, vol. 91, no. 5, pp. 579–586, 2001.
- [53] R. S. Halkai, M. N. Hegde, and K. R. Halkai, “Evaluation of Enterococcus faecalis adhesion, penetration, and method to prevent the penetration of Enterococcus faecalis into root cementum: confocal laser scanning microscope and scanning electron microscope analysis,” *Journal of Conservative Dentistry*, vol. 19, no. 6, p. 541, 2016.
- [54] K. R. Halkai, J. A. Mudda, V. Shivanna, V. Rathod, and R. Halkai, “Evaluation of antibacterial efficacy of fungal-derived silver nanoparticles against *Enterococcus faecalis*,” *Contemporary Clinical Dentistry*, vol. 9, no. 1, pp. 45–48, 2018.
- [55] S. Bhandi, D. Mehta, M. Mashyakhly et al., “Antimicrobial efficacy of silver nanoparticles as root canal Irrigant’s: a systematic review,” *Journal of Clinical Medicine*, vol. 10, p. 1152, 2021.
- [56] J.-Y. Peng, M. Botelho, and J. Matinlinna, “Silver compounds used in dentistry for caries management: a review,” *Journal of Dentistry*, vol. 40, no. 7, pp. 531–541, 2012.
- [57] C. C. Fernandez, A. R. Sokolonski, M. S. Fonseca et al., “Applications of silver nanoparticles in dentistry: advances and technological innovation,” *International Journal of Molecular Sciences*, vol. 22, no. 5, p. 2485, 2021.
- [58] V. T. Noronha, A. J. Paula, G. Durán et al., “Silver nanoparticles in dentistry,” *Dental Materials*, vol. 33, no. 10, pp. 1110–1126, 2017.
- [59] J. M. Corrêa, M. Mori, H. L. Sanches, A. D. Cruz, E. Poiate, and I. A. V. P. Poiate, “Silver nanoparticles in dental biomaterials,” *International Journal of Biomaterials*, vol. 2015, 9 pages, 2015.
- [60] S. P. Singh, C. S. Bhargava, V. Dubey, A. Mishra, and Y. Singh, “Silver nanoparticles: biomedical applications, toxicity, and safety issues,” *International Journal of Research in Pharmacy and Pharmaceutical Sciences*, vol. 4, no. 2, pp. 1–10, 2017.
- [61] L. Z. Flores-López, H. Espinoza-Gómez, and R. Somanathan, “Silver nanoparticles: electron transfer, reactive oxygen species, oxidative stress, beneficial and toxicological effects. Mini review,” *Journal of Applied Toxicology*, vol. 39, no. 1, pp. 16–26, 2019.
- [62] Z. Ferdous and A. Nemmar, “Health impact of silver nanoparticles: a review of the biodistribution and toxicity following various routes of exposure,” *International Journal of Molecular Sciences*, vol. 21, no. 7, p. 2375, 2020.
- [63] N. Hadrup and H. R. Lam, “Oral toxicity of silver ions, silver nanoparticles and colloidal silver - a review,” *Regulatory Toxicology and Pharmacology*, vol. 68, no. 1, pp. 1–7, 2014.
- [64] R. Y. Chou, “Volatility persistence and stock valuations: some empirical evidence using GARCH,” *Journal of Applied Econometrics*, vol. 3, no. 4, pp. 279–294, 1988.
- [65] M. van der Zande, R. J. Vandebriel, E. van Doren et al., “Distribution, elimination, and toxicity of silver nanoparticles and silver ions in rats after 28-day oral exposure,” *ACS Nano*, vol. 6, no. 8, pp. 7427–7442, 2012.
- [66] Z. Lin, N. A. Monteiro-Riviere, and J. E. Riviere, “Pharmacokinetics of metallic nanoparticles,” *Wiley Interdisciplinary Reviews: Nanomedicine and Nanobiotechnology*, vol. 7, no. 2, pp. 189–217, 2015.
- [67] M. Murphy, K. Ting, X. Zhang, C. Soo, and Z. Zheng, “Current development of silver nanoparticle preparation, investigation,

- and application in the field of medicine," *Journal of Nanomaterials*, vol. 2015, Article ID 696918, 12 pages, 2015.
- [68] H. G. Seiler, H. Sigel, and A. Sigel, *Handbook on Toxicity of Inorganic Compounds*, Marcel Dekker, New York, NY (USA), 1988.
- [69] M. A. Awad, A. A. Hendi, K. M. O. Ortashi, A. B. Alanazi, B. A. ALZahrani, and D. A. Soliman, "Greener synthesis, characterization, and antimicrobial effects of helba silver nanoparticle-PMMA nanocomposite," *International Journal of Polymer Science*, vol. 2019, Article ID 4379507, 7 pages, 2019.
- [70] L. Moghadas, T. Narimani, and M. Shahmoradi, "Antimicrobial activity of a new nanobased endodontic irrigation solution: in vitro study," *Dental Hypotheses*, vol. 3, no. 4, p. 142, 2012.
- [71] M. Samiei, S. Davaran, F. Valipour, A. Davari, T. Ghiasian, and F. Lotfipour, "Antibacterial efficacy of silver-crosslinked hydrogel nanocomposite versus sodium hypochlorite and chlorhexidine on *Enterococcus faecalis* for use in root canal infection," *International Journal of Biology, Pharmacy and Allied Sciences*, vol. 3, no. 11, pp. 2316–2332, 2014.
- [72] D. Wu, W. Fan, A. Kishen, J. L. Gutmann, and B. Fan, "Evaluation of the antibacterial efficacy of silver nanoparticles against *Enterococcus faecalis* biofilm," *Journal of Endodontics*, vol. 40, no. 2, pp. 285–290, 2014.
- [73] M. Samiei, M. Aghazadeh, M. Lotfi, S. Shakoei, Z. Aghazadeh, and S. M. Vahid Pakdel, "Antimicrobial efficacy of mineral trioxide aggregate with and without silver nanoparticles," *Iranian endodontic Journal*, vol. 8, no. 4, pp. 166–170, 2013.
- [74] P. Mishra and S. Tyagi, "Surface analysis of gutta percha after disinfecting with sodium hypochlorite and silver nanoparticles by atomic force microscopy: an *in vitro* study," *Dental research journal*, vol. 15, no. 4, pp. 242–247, 2018.
- [75] Y. Shantiaee, F. Maziar, O. Dianat, and F. Mahjour, "Comparing microleakage in root canals obturated with nanosilver coated gutta-percha to standard gutta-percha by two different methods," *Iranian endodontic journal*, vol. 6, no. 4, pp. 140–145, 2011.
- [76] V. Vishwanath and H. M. Rao, "Gutta-percha in endodontics—a comprehensive review of material science," *Journal of conservative dentistry: JCD*, vol. 22, no. 3, pp. 216–222, 2019.
- [77] B. H. Baras, M. A. S. Melo, J. Sun et al., "Novel endodontic sealer with dual strategies of dimethylaminohexadecyl methacrylate and nanoparticles of silver to inhibit root canal biofilms," *Dental Materials*, vol. 35, no. 8, pp. 1117–1129, 2019.
- [78] D. T. de Castro, C. do Nascimento, O. L. Alves, E. de Souza Santos, J. A. M. Agnelli, and A. C. dos Reis, "Analysis of the oral microbiome on the surface of modified dental polymers," *Archives of Oral Biology*, vol. 93, pp. 107–114, 2018.
- [79] R. Pokrowiecki, T. Zareba, B. Szaraniec et al., "In vitro studies of nanosilver-doped titanium implants for oral and maxillofacial surgery," *International Journal of Nanomedicine*, vol. 12, pp. 4285–4297, 2017.
- [80] W. Zhou, Z. Jia, P. Xiong et al., "Bioinspired and biomimetic AgNPs/gentamicin-embedded silk fibroin coatings for robust antibacterial and osteogenetic applications," *ACS Applied Materials & Interfaces*, vol. 9, no. 31, pp. 25830–25846, 2017.
- [81] A. Nozari, S. Ajami, A. Rafiei, and E. Niazi, "Impact of nano hydroxyapatite, nano silver fluoride and sodium fluoride varnish on primary teeth enamel remineralization: an in vitro study," *Journal of Clinical and Diagnostic Research: JCDR*, vol. 11, no. 9, pp. ZC97–ZC100, 2017.

## Research Article

# A Pilot Study on Nanotherapy of *Momordica charantia* against Trimethyltin Chloride-Induced Neurotoxicity in *Danio rerio* (Zebrafish)

**Bharathi Kumar,<sup>1</sup> Siva Vijayakumar Tharumasivam,<sup>1</sup> Vasuki Boominathan,<sup>1,2</sup> Elumalai Perumal,<sup>3</sup> Prabu Dhandapani,<sup>4</sup> Kumaravel Kaliyaperumal,<sup>5</sup> Suresh Arumugam,<sup>6</sup> Kumaran Subramanian,<sup>7</sup> Pugazhvendan Sampath Renuga,<sup>8,9</sup> Vasanth Shakthivel,<sup>10</sup> Bupesh Giridharan,<sup>10</sup> Wilson Aruni,<sup>11,12</sup> and Lokesh Kumar Boopathy<sup>13</sup>**

<sup>1</sup>PG & Research Department of Biotechnology, Srimad Andavan Arts & Science College, Srirangam, Tiruchirappalli 620005, India

<sup>2</sup>Department of Biotechnology Bharathidasan University, Tiruchirappalli 620024, India

<sup>3</sup>Departments of Pharmacology, Saveetha Dental College and Hospital, Chennai, Tamil Nadu, India

<sup>4</sup>Department of Microbiology, Dr. ALM PG IBMS, University of Madras, Chennai, Tamil Nadu, India

<sup>5</sup>National Navel Orange Engineering Research Centre, School of Life Sciences, Gannan Normal University, Ganzhou, Jiangxi, China

<sup>6</sup>Central Research Laboratory, Meenakshi Medical College Hospital & Research Institute, Kanchipuram, Tamil Nadu, India

<sup>7</sup>Centre for Drug Discovery and Development, Sathyabama Institute of Science and Technology, Chennai, Tamil Nadu, India

<sup>8</sup>Department of Zoology, Annamalai University, Annamalai Nagar, Cuddalore, 608002 Tamil Nadu, India

<sup>9</sup>Department of Zoology, Arignar Anna Government Arts College, Cheyyar, 604407 Tamil Nadu, India

<sup>10</sup>Department of Forest Science, Nagaland University, Nagaland 798627, India

<sup>11</sup>Department of Biotechnology, School of Bio and Chemical Engineering, Sathyabama Institute of Science and Technology, Chennai, Tamil Nadu, India

<sup>12</sup>School of Medicine, Loma Linda University, CA 92354, USA

<sup>13</sup>College of Health Sciences, Mizan Tepi University, Mizan Teferi, Ethiopia

Correspondence should be addressed to Lokesh Kumar Boopathy; [lokeshkumarunom@gmail.com](mailto:lokeshkumarunom@gmail.com)

Received 27 August 2021; Accepted 4 October 2021; Published 9 November 2021

Academic Editor: Mahendran Vanaja

Copyright © 2021 Bharathi Kumar et al. This is an open access article distributed under the Creative Commons Attribution License, which permits unrestricted use, distribution, and reproduction in any medium, provided the original work is properly cited.

**Background.** The direct or indirect effect of chemicals on the nervous system of humans or animals is referred to as neurotoxicity. Trimethyltin chloride (TMT) intoxication causes behavioral and cognitive deficiencies in humans and experimental animals. TMT has long been used as a model toxicant in the study of central nervous system (CNS) toxicity. *Momordica charantia*, which is used in traditional herbal medicine, has a variety of pharmacological functions. Mesoporous silica nanoparticles have a higher loading capacity, are less dense, and have a larger specific area. **Objectives.** To investigate a possible nanotherapy for Alzheimer's disease caused by trimethyltin chloride in freshwater zebrafish. **Methods.** An aqueous extract of *M.charantia* was used to perform the primary and secondary screening. The DPPH (2,2-diphenyl-1-picrylhydrazyl) radical scavenging assay was used to determine the antioxidant capacity of crude aqueous extracts of *M. charantia*. Mesoporous silica nanoparticles are made using a CTAB surfactant chemical process and tetraethyl orthosilicate. UV-Vis spectroscopy, Fourier transform infrared spectroscopy, scanning electron microscope, and EDAX were used to characterize it. *Danio rerio* was used to test the trimethyltin chloride for Alzheimer's disease. The *M. charantia* and mesoporous silica nanoparticles were then tested in the same method. **Results.** The extract has no adverse effects on zebrafish, indicating that *M. charantia* is safe for human consumption. The histopathological findings indicate that the tissues of the fish infected with the extract had no pathological modifications. **Conclusion.** The *M. charantia* showed higher antioxidant activity and anticholinesterase activity, and upon further characterization and assessment, this could be a safe and potential drug candidate for Neurotoxicity.



## 1. Introduction

Trimethyltin chloride (TMT) has been found in drinking water sources, household water systems, marine environments, and aquatic specimens [1]. Between 1978 and 2008, TMT poisoned 1849 people in 67 deaths around the world. The most frequent acute TMT exposures tend to be environmental, occurring during plastic manufacturing or other industrial processes involving plastic heating. Ingestion of organotin-contaminated food or water in places where plastics manufacture is prevalent is also expected to become a growing concern [2]. TMT intoxication causes severe behavioral and neurological problems in humans and laboratory animals. A limbic-cerebellar syndrome is the most common neurotoxic presentation in human cases, with symptoms such as memory loss, confusion, epilepsy, tinnitus, insomnia, and depression [3]. TMT has long been used as a model toxicant in the study of CNS toxicity. Experiments in the marine fish *Sebastes marmoratus* have led to suggestions that the glutamatergic receptor NMDAR and its signaling pathway components are essential for TMT neurotoxicity [4]. Neurotoxicity is a dynamic condition that is difficult to be successfully treated with a single treatment or other intervention. Current strategies are aimed at assisting patients in maintaining brain function, managing behavioral effects, and slowing the progression of disease symptoms. Cholinesterase inhibitors are not widely used in allopathic medicine, and existing therapies may not result in enough acetylcholine activity to assist with neurotoxicity control. The study of natural compounds with antioxidative and antiaging properties that may also be beneficial for neurodegenerative diseases has evolved into the area of phytochemicals. Donepezil is a cholinesterase agent that inhibits the degradation of acetylcholine in the brain. It is used to relieve effects in mild, moderate, and extreme cases. Various plants have been used as medicine all over the world since ancient times. For thousands of years, *Momordica charantia* (*Momordica* species) has been popular as a medicine and a vegetable. *M. charantia* is a Cucurbitaceae plant that is widely known as bitter melon, balsam pear, or bitter melon. The fruit of *M. charantia* is a thin cucumber-like spindle with pimples on the surface; the young fruit is emerald green and becomes orange when ripe, while the flesh becomes scarlet from white when it matures. The fruit can be eaten at any point of its growth, and it is widely consumed as a vegetable in various regions of the globe [5]. The whole plant, especially the seeds and fruit, has considerable pharmacological effects, for example, it has been used in the treatment of diabetes since ancient times and continues to play an important role in diabetes prevention and treatment in many developing countries. This plant is used in conventional herbal medicine and has several pharmacological properties, including antidiabetic, abortifacient, anthelmintic, contraceptive, antimalarial, and laxative properties. Dysmenorrhea, eczema, gout, jaundice, leprosy, piles, measles, psoriasis, rheumatism, and scabies are all treated by it [5]. The future applications of mesoporous silica nanoparticles (MSNs) have piqued the interest of many scientists over the last decade. Because of their higher loading volume, lower density, and the larger specific area, hollow mesoporous silica nanoparticles (HMSNs) with a deep central hole and an external mesoporous silica shell provide additional benefits.

TABLE 1: Phytochemical analysis of *M. charantia*.

S. No.	Phytochemical tests	Results
1	Test for steroid	Present
2	Test for alkane	Present
3	Test for flavonoids	Present
4	Test for saponins	Present
5	Test for terpenoids	Present
6	Test for phenols	Absent
7	Test for coumarins	Present
8	Test for emodols	Absent
9	Test for phlobatannis	Absent
10	Test for phlobatannis	Present
11	Test for phlobatannis	Absent
12	Test for phytosterol	Present
13	Test for reducing compound	Present
14	Test for cardiac glycosides	Absent

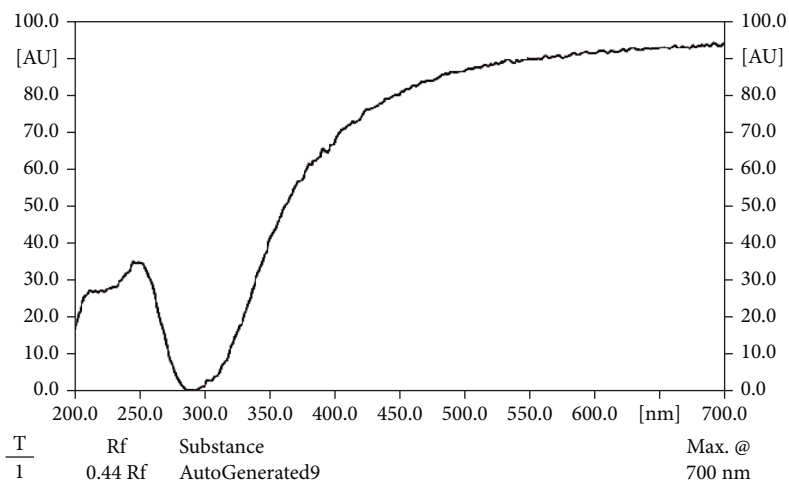
Mesoporous silica nanoparticles due to their low toxicity and high drug loading capacity so are used in controlled and target drug delivery systems. Silica is widely present in the environment in comparison to other metal oxides like titanium and iron oxides, and it has comparatively better biocompatibility [6]. The mesoporous form of silica has unique properties, particularly in the loading of therapeutic agents at high quantities, and in the subsequent releases. Due to the strong Si-O bond, silica-based mesoporous nanoparticles are more stable to external responses such as degradation and mechanical stress as compared to niosomes, liposomes, and dendrimers which inhibit the need for any external stabilization in the synthesis of MSNs [4, 7]. The mesoporous structure such as pore size and porosity can be tuned to the size and type of drugs.

Furthermore, MSN is very effective in a variety of applications, including enzyme encapsulation, drug transport and delivery, reactive material packaging, and light emitting. However, they have received little attention as corrosion inhibitor nanocarriers, with just a few studies conducted on them [8]. The zebrafish (*Danio rerio*) belongs to the minnow family of freshwater fish. Cypriniformes (Cyprinidae) is a family of fish in the class Cypriniformes. The zebrafish (*Danio rerio*) is an important model organism for vertebrate evolution, genetics, and human biology and disease, as well as a common tropical fish pet. *Danio rerio* has many characteristics, including large family size, external growth, and low maintenance and production expense [9].

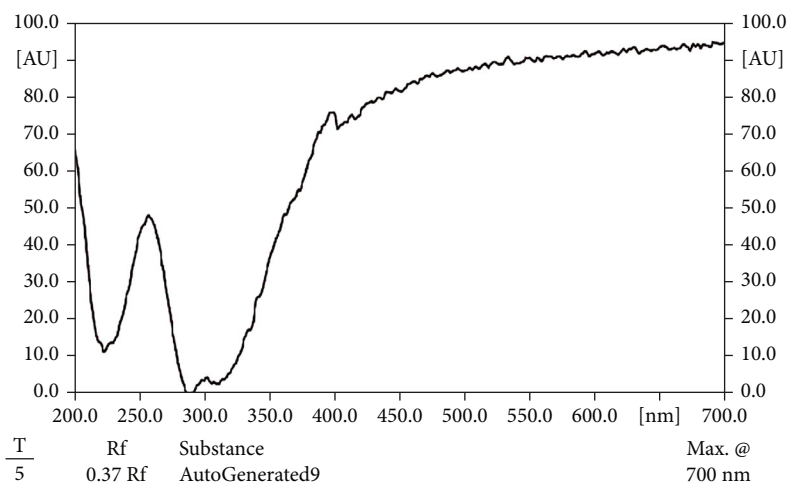
This research is aimed at investigating a possible nanotherapy for neurotoxicity induced by trimethyltin chloride in freshwater *Danio rerio* (zebrafish).

## 2. Materials and Methods

**2.1. Chemicals.** Tetraethyl orthosilicate (100 ml) was purchased from the Sigma Industry, and trimethyltin chloride was purchased in TCI Chemicals 1 g (India) Pvt. Ltd.



(a)



(b)

FIGURE 1: (a) Graph of stigmasterol. (b) Graph of lupeol.

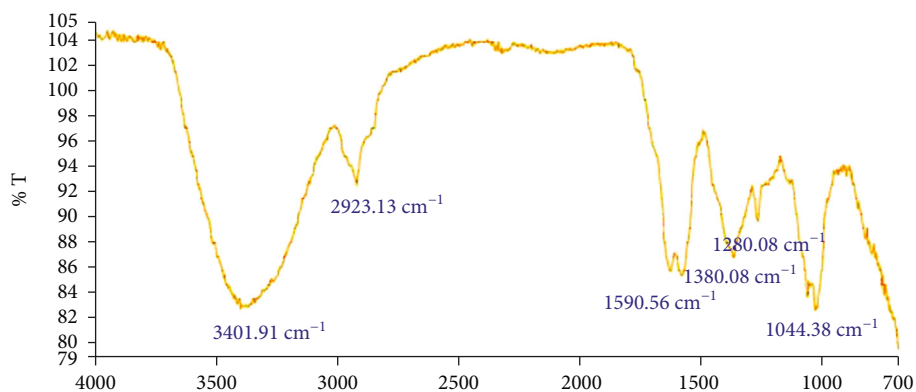


FIGURE 2: Fourier transform-infrared (FT-IR) spectrum of *M. charantia* extract.

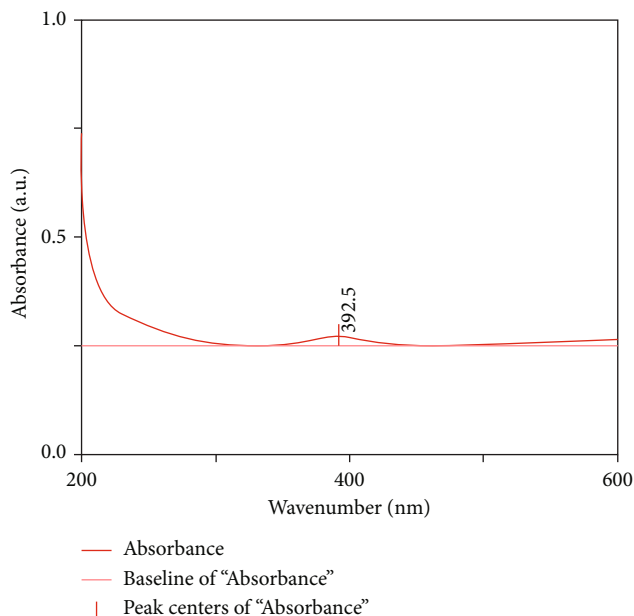


FIGURE 3: UV-visible spectrophotometer analysis of mesoporous silica nanoparticle.

**2.2. Collection and Authentication of the Sample (*Momordica charantia*).** *M. charantia* fruit samples were collected from a local farming field at Ayyarmalai village near Karur, Tamil Nadu. The *M. charantia* was air-dried and pulverized, sieved to get a coarse powder, and stored in airproof containers until their experimental use. The collected fruit was authenticated from the department of Botany, St. Joseph's College, Trichy, with a voucher specimen submitted and got the reference number of K.B.001.

**2.3. Extraction of *M. charantia* (Cold Extraction).** *M. charantia* powder was mixed with a suitable amount of ethanol (95%), extracted in an orbital shaker for 72 h, and then filtered through muslin cloth and dry extraction by using a vacuum.

**2.4. Preliminary Screening of Phytochemical Analysis.** The ethanol extract was assessed for the existence of the phytochemical analysis by using the following standard method [9].

**2.5. High-Performance Thin Layer (HPTLC) Identification.** The solution was packed with 95% ethanol. The stationary phase was a silica gel-coated sheet, and the mobile phase was ethyl acetate: methanol: distilled water 75:15:10 ratios. The R<sub>f</sub> was observed as a violet spot [6].

**2.6. Fourier Transform-Infrared (FT-IR) Spectrum Analysis of *M. charantia* Extract.** FT-IR was used to record the infrared spectrum (Shimadzu). To make the pellet samples, the *M. charantia* sample and KBr were mixed in a 1:10 ratio in a KBr press. The spectra were recorded at wavenumbers ranging from 4000 to 400 cm<sup>-1</sup> [7].

**2.7. Synthesis of Mesoporous Silica Nanoparticle.** To reach a pH of 12.3, cetyltrimethylammonium bromide (0.5 g),

2.0 M NaOH (1.75 ml), and deionized water (120 g) were heated at 80°C for 30 minutes. 2.5 ml of TEOS (tetraethyl orthosilicate) is dissolved into this transparent solution under intense stirring. Within three minutes of stirring at 550 rpm after the injection, white precipitation is noticeable. For 2 hours, the reaction temperature is maintained at 80°C. Hot filtration is used to isolate the product, which is then washed with a large volume of water and methanol (5 ml every three times). At 60°C for 6 hours, an acid extraction was carried out in methanol (100 mL) with a mixture of concentrated hydrochloric acid (1.0 mL) and *as-made* materials (1.0 g). The solid products that had been separated from the surfactant were filtered, washed with water and methanol and then dried under a vacuum.

### 3. Characterization of Nanoparticle

**3.1. UV-Vis Spectroscopy.** A 1.2 mg sample was collected after sample preparation and subjected to UV-Vis spectroscopy. A miniature fiber optic spectrometer was used to record UV-Vis spectra using versatile lamps optimized for the visible-near infrared Vis-NIR (200–500 nm). The samples had been diluted 100 times before being measured. Averaging 1000 single observations yielded the findings described here [6].

**3.2. Fourier Transform-Infrared Spectroscopy Analysis of Mesoporous Silica Nanoparticle.** After sample preparation and Fourier transform infrared spectroscopy, a sample of mesoporous silica nanoparticle 0.5 mg was taken (FT-IR). The vibrational stretch frequency of metal-oxygen bonds is revealed by Fourier transform infrared spectroscopy. A continuum source of light is used to emit light over a wide range of infrared wavelengths for Fourier transform infrared spectroscopy. Light commuting electrons are excited from their ground state to an excited state as an atom or molecule absorbs energy. The atoms in a molecule will vibrate and rotate in response to one another. These vibrations and rotations also have discrete energy levels, which can be considered as being packed on top of each electronic level. The absorption of visible or UV radiation occurs to the excitation of outer electrons [7].

**3.3. Scanning Electron Microscopy with EDAX.** Sample of mesoporous silica nanoparticle 1 g was taken after preparation of sample and scanning electron microscope. The electron beam used to probe the sample is produced by the electron gun in a scanning electron microscope. Electrons are emitted from a cathode, accelerated by electrical fields, and focused on the source's first optical image. The size and shape of the apparent source, beam acceleration, and current are the primary determinants of a scanning electron microscope's performance and resolution. Spot welded to metal posts is a bent tungsten wire filament with a diameter of around 100 micrometers. These posts are embedded in a ceramic holder and extend out the other side to provide electrical connections. In operation, the filament will be heated by passing an electrical current through it. The optimum filament temperature for the thermionic emission of electrons

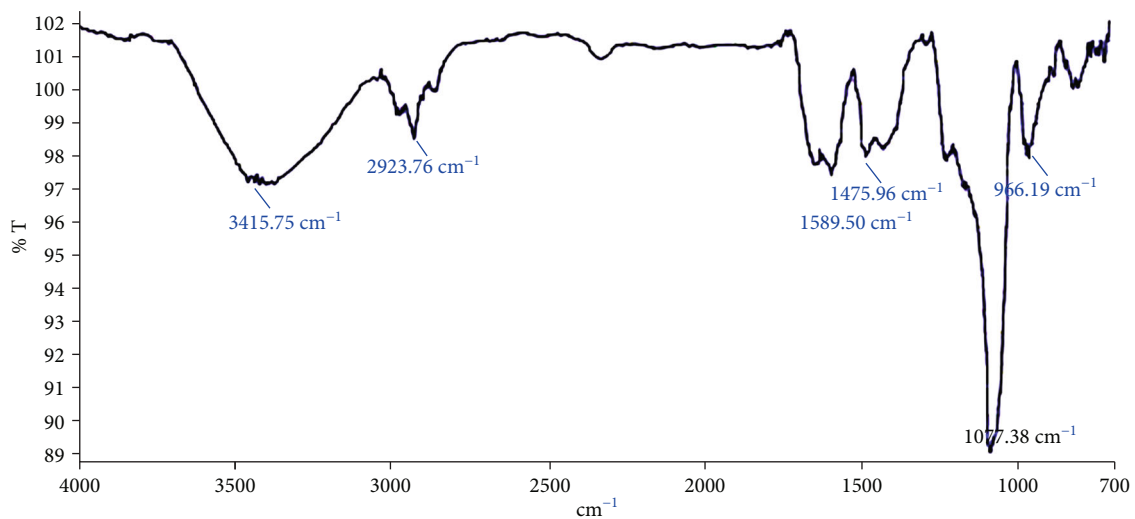
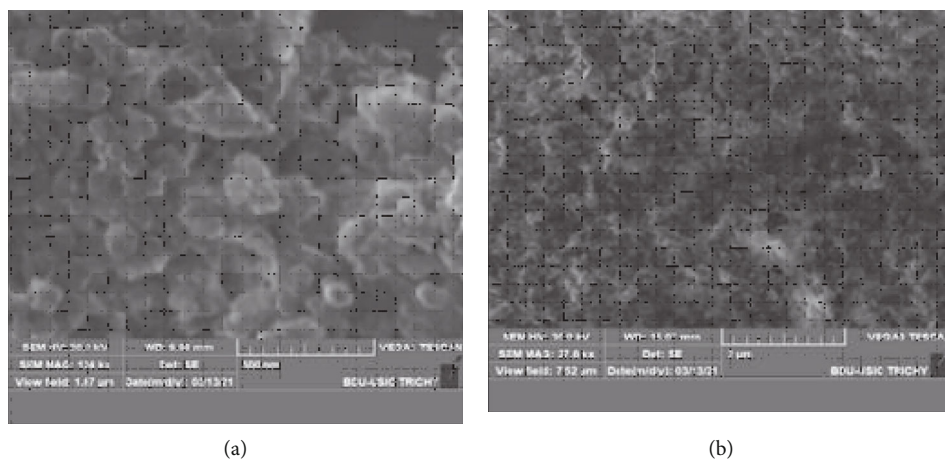


FIGURE 4: Fourier transform-infrared (FT-IR) spectrum of mesoporous silica.



(a)

(b)

FIGURE 5: (a, b) Scanning electron microscopy analysis of mesoporous silica nanoparticle.

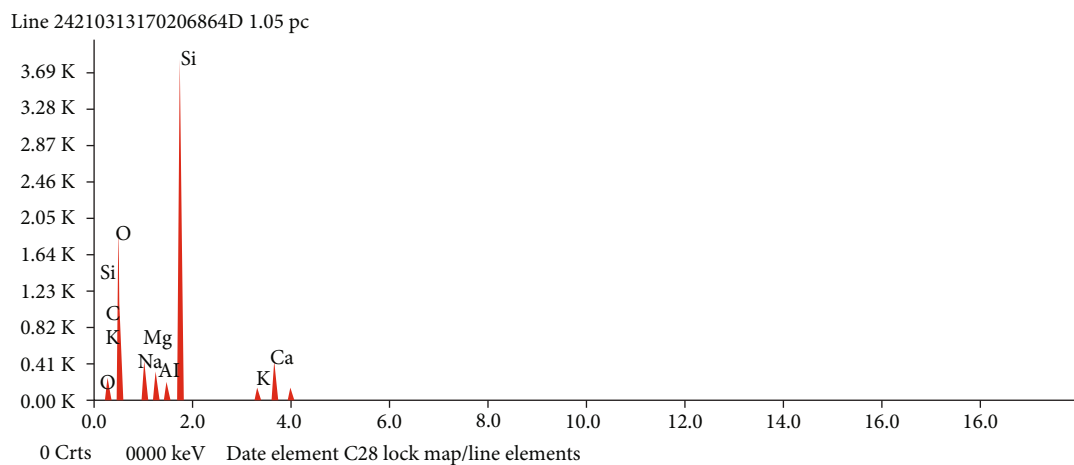


FIGURE 6: EDS analysis of synthesized mesoporous silica nanoparticles.

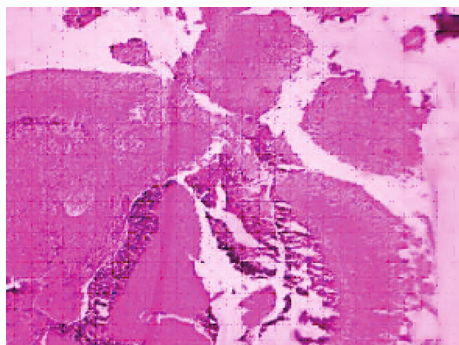


FIGURE 7: (a) Brain-group I (control) (healthy).

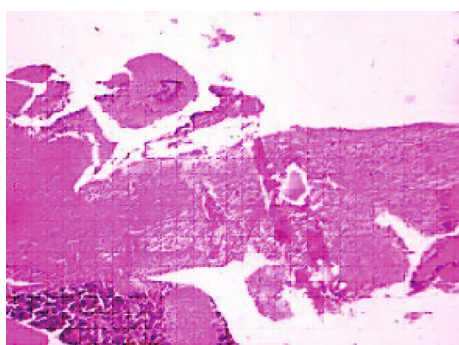


FIGURE 8: (b) Group 2: brain treated damaged (day 1: trimethyltin chloride).

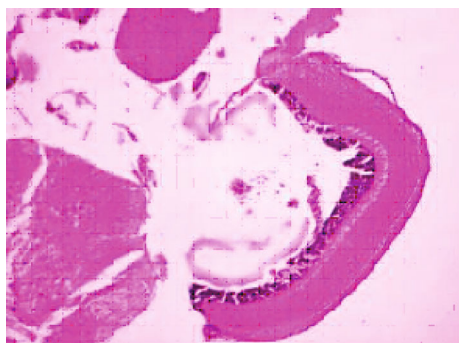


FIGURE 9: (c) Group 3: brain treated (day 2: trimethyltin chloride).

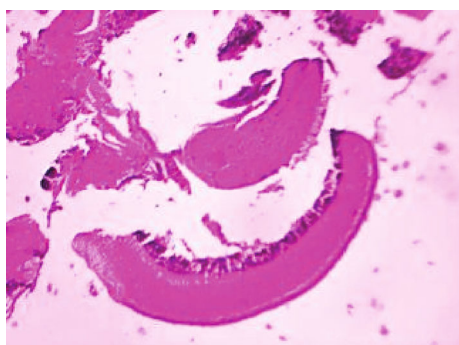


FIGURE 10: (d) Group 4: brain treated [trimethyltin chloride + FDA approved drug (donepezil)].

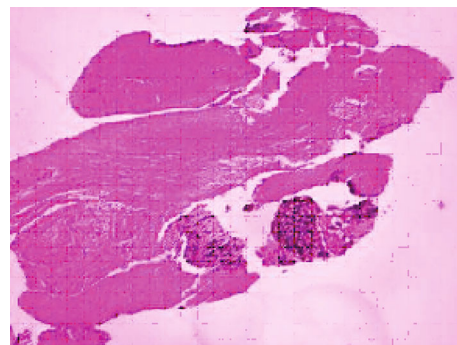


FIGURE 11: (e) Group 5: brain treated (trimethyltin chloride + charantin).

is around 2700 K. The accelerating voltage, generally, between  $-500$  volts and  $-50,000$  volts DC, is applied to the Wehnelt cylinder. Energy dispersive X-ray analysis (EDX), referred to as EDS or EDAX, is an X-ray technique used to identify the elemental composition of materials.

**3.4. Trimethyltin Chloride.** Two micromolar solutions of trimethyltin chloride are prepared by adding  $0.0003$  g in  $1000$  ml water.  $1$  h before the experiment, the zebrafish was directly placed in the above trimethyltin chloride solution.

**3.5. Donepezil.** Donepezil  $1.5$  mg was dissolved in  $1$  mL of water.  $2.5$   $\mu$ L is pipetted out into an Eppendorf tube, and  $25$   $\mu$ L water was added to it. This solution contains  $3.75$   $\mu$ g of donepezil in  $25$   $\mu$ L water. From the above solution,  $5$   $\mu$ L is sucked into a pipette and directly administered to zebrafish feed, where  $5$   $\mu$ L contains  $0.75$   $\mu$ g of donepezil.

**3.6. Model Animals.** Adult zebrafish (*Danio rerio*) weighing  $0.5$ – $1.0$  g is procured from a local aquarium pet store. They were left in housing tanks with water at a density of  $5$  animals per  $3$  L at  $14$ – $10$  h light and dark photoperiod with continuous aeration and pellet diet for about  $10$  days before the commencement of the experiment.

**3.7. Cell Viability Test.** MTT assay can be used to determine the extract's cytotoxic activity. In a summary,  $104$  murine macrophage cell line RAW 264.7 cells per well were seeded in a  $96$ -well microplate and treated for  $72$  hours with varying concentrations of *M. charantia* extracts.  $15$   $\mu$ L of MTT will be added at the end of the treatment period and incubated at  $37^{\circ}\text{C}$  for  $4$  hours. The formazan products will be dissolved in  $150$   $\mu$ L of DMSO, and their absorbance will be measured at  $370$  nm [10]. The percent cell cytotoxicity will be calculated using the formula:

$$\% \text{Cytotoxicity} = 100 - \left\{ \frac{\text{O.D control} - \text{O.D test}}{\text{O.D control}} \times 100 \right\} \quad (1)$$

**3.8. Drug Loading on Mesoporous Silica Nanoparticle.** Drug loading on mesoporous silica nanoparticles dissolves  $100$  mg of the momordica charantin drug in ethanol ( $1$  ml). Add  $100$  mg of MSNP to the clear solution of the

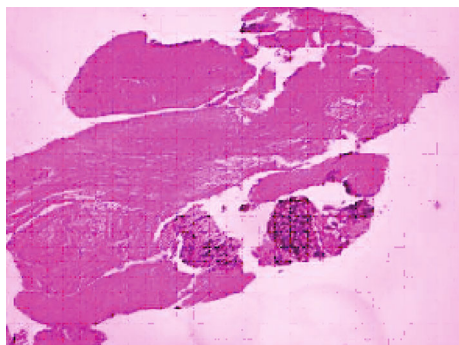


FIGURE 12: (f) Group 6: brain treated [trimethyltin chloride + (charantin + mesoporous silica nanoparticle)].

drug and the solvent. Stir the sample and MSNP mixture at 300 rpm for 24 hours [10].

**3.9. In Vivo Method Group of Fish (*Danio rario*).** This is a list of groups in untreated fish (*Danio rario*).

Group 1—control.

This is a list of groups in treated fish (*Danio rario*).

Group 2—(day 1) trimethyltin chloride.

Group 3—(day 2) trimethyltin chloride.

Group 4—trimethyltin chloride + FDA approved drug (donepezil).

Group 5—trimethyltin chloride + charantin.

Group 6—trimethyltin chloride + (charantin + mesoporous silica nanoparticle).

Histological examinations were carried out in the way described by [11], with a few modifications. Following fixation, the samples were dehydrated, embedded in paraffin wax, sliced at 3–5  $\mu\text{m}$  with a microtome, and stained with hematoxylin and eosin. DPX mountant was used to make the stained slides permanent for microscopic examinations after staining. The slides were blinded to the observer, and all serial sections were scored histopathologically. Previously, whole fish sections of untreated zebrafish were used to determine zebrafish histology. The slides were examined under a  $\times 40$  microscope.

## 4. Neurochemical and Antioxidant Estimations

**4.1. Acetylcholinesterase Activity Assay.** The AChE was made from the brain homogenate of 30 fishes, centrifuged, and the supernatant was collected and used as an enzyme source for the AChE assay. Differential concentrations (100–500 mg/mL) of aqueous extracts of *M. charantia* were incubated for 45 minutes at room temperature with 50  $\mu\text{l}$  of AChE makeup and 200  $\mu\text{l}$  of tris-HCL. 125  $\mu\text{l}$  of 3 mM DTNB was applied to the reagent mixtures, and the total volume was increased to 650  $\mu\text{l}$  with tris-HCL buffer (pH 8.0). To initiate enzyme activity, 1 mM ATCI was added to 25  $\mu\text{l}$  of the reaction mixture. A UV-visible spectrophotometer was used to detect the formation of 5-di-thio-2-nitrobenzoic acid anion, and the absorbance was measured at 405 nm. The tests were performed in triplicate. The medication donepezil was used as a standard [12].

**4.2. DPPH (2, 2-Diphenyl-1-Picrylhydrazyl) Assay.** To prepare the stock solution, 1.97 g of DPPH was dissolved in 50 mL of methanol. Various concentrations of *M. charantia* aqueous extract were analyzed using a dilution process. 100 mg–500 mg extracts were used in 10 mg in 1 mL water, and their various concentrations were prepared. The mixture was shaken and set aside for 30 minutes at room temperature. Then, at 517 nm, the absorbance was measured. All of the tests were performed in triplicates with ascorbic acid as the standard [13].

**4.3. Assay of Total Reducing Power.** Various concentrations of *M. charantia* fruit ethanol extract (10 mg/1 mL) were combined with phosphate buffer (0.5 mL, 0.2 M, pH 6) and potassium ferricyanide [ $\text{K}_3\text{Fe}(\text{CN})_6$ ] in 1 mL of distilled water (0.5 mL, 1 percent). For 20 minutes, the mixture was incubated at 50°C. Trichloroacetic acid (10%) aliquots (0.5 mL) were added to the mixture, which was then centrifuged for 10 minutes at 2500 rpm. The absorbance of the upper layer of solution (0.5 mL) was measured in a spectrophotometer at 700 nm using distilled water (0.5 mL) and ferric chloride  $\text{FeCl}_3$  (0.5 mL, 0.1%). Increased reaction mixture absorbance indicates increased reducing power.

**4.4. Assay of Lipid Peroxidation.** The peroxidation of lipids was measured using thiobarbituric acid reactive substances. The brain homogenate (10 ml) was mixed with 150 ml of acetic acid (20%), 150 ml of thiobarbituric acid (0.8%), 20 ml of sodium dodecyl sulfate (8.1%), and 50 mL of distilled water (reaction mixture); heated for 30 min at 95.8°C; and then cooled and centrifuged (3000 g during 10 min at 15°C) by adding 100 ml of water and 500 ml of n-butanol. The fluorescence of the supernatant organic phase (150 ml) was calculated in a microplate reader at the wavenumbers 515 nm–553 nm. The concentration of TBARS was determined using the standard tetra methoxy propane (TMP).

**4.5. Assay of Total Antioxidant.** The ability of the sample to reduce ferric tripridytriazine (Fe (II)-TPTZ) complex to intense blue-colored ferrous tripridytriazine (Fe (II)-TPTZ), which is read at 593 nm, is required for the FRAP assay. First, 1.5 ml of freshly prepared FRAP reagent (25 ml of 300 mM/L acetate buffer pH 3, 2.5 ml of 10 mM/L TPTZ in 40 mM/L HCL, 20 mM/L ferric chloride solution) is mixed with 50  $\mu\text{l}$  of varying concentrations of *M. charantia* (100–500  $\mu\text{l}$ ) extracted successively in different solvents and 150  $\mu\text{l}$  of distilled water. At 593 nm, absorbance was measured for 4 minutes (every 10 seconds).

## 5. Statistical Analysis

One-way ANOVA was used for data analysis and presented as a mean  $\pm$  standard error of the mean. Latencies of multiple groups were compared using Dunnett's multiple comparison test.

## 6. Results and Discussion

By exposing the ripe fruits to an orbital shaker, a sample of *M. charantia* was collected (cold extraction). It was collected

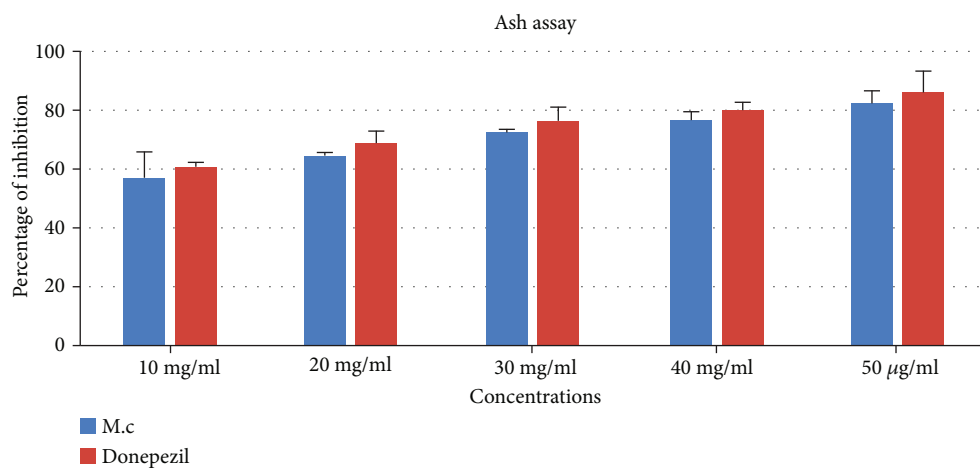


FIGURE 13: Acetylcholinesterase assay (*M. charantia*).

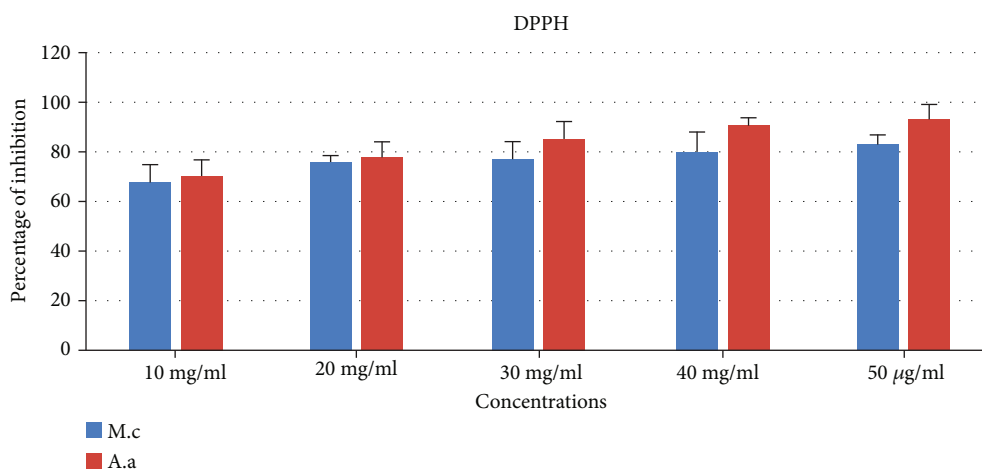


FIGURE 14: DPPH (2, 2-diphenyl-1-picrylhydrazyl) radical scavenging activity (*M. charantia*, A.a: ascorbic acid).

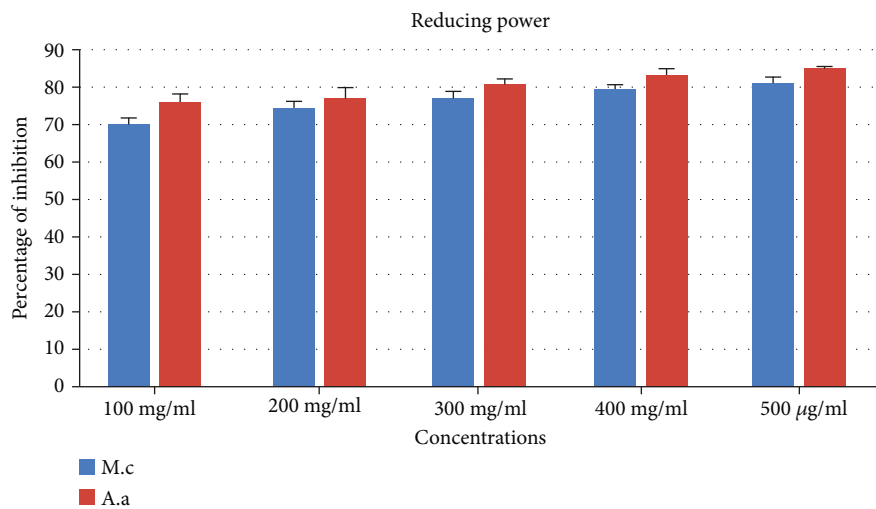


FIGURE 15: Reducing power assay (*M. charantia*, A.a: ascorbic acid).

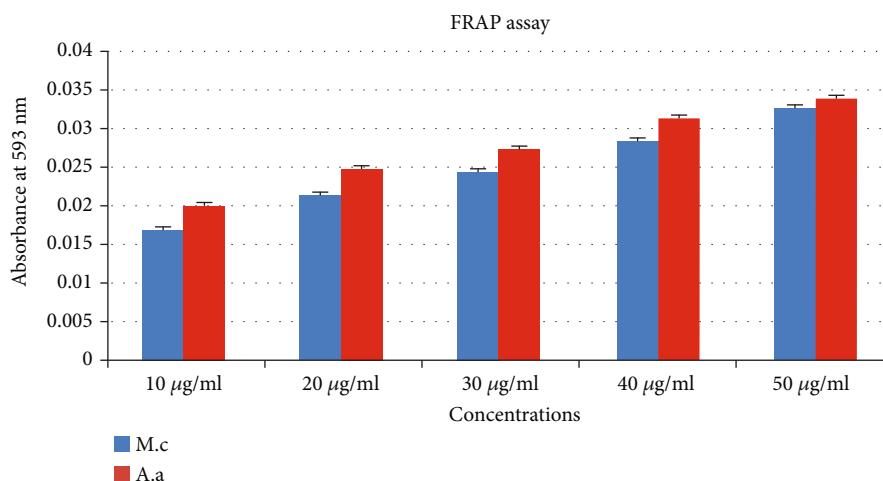


FIGURE 16: Total antioxidant assay (*M. charantia*, A.a: – ascorbic acid).

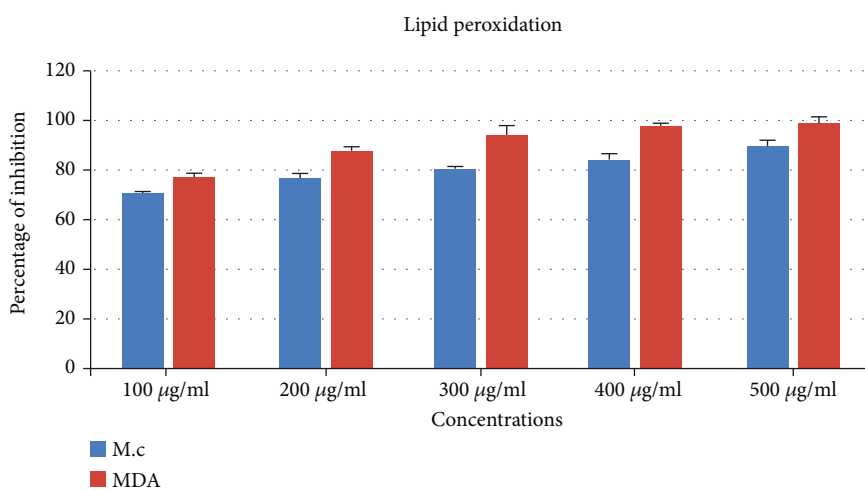


FIGURE 17: Lipid peroxidation assay (*M. charantia*, A.a: ascorbic acid).

in the form of a brownish yellow colloidal crude. Similar to [14], preliminary phytochemical screening of *M.charantia* aqueous extract revealed the presence of phytochemicals such as steroids, alkane, flavonoids, saponins, terpenoids, coumarins, and alkaloids, and reducing compounds were all included in *M.charantia* ethanol extract (Table 1). Phenols, emodols, photobatanins, tannis, and cardiac glycosides were not reported. The collected findings can be used as a starting point for identifying bioactive compounds in *M.charantia* ethanolic extract.

According to the results of High-Performance Thin-Layer (HPTLC) Identification, the  $R_f$  value of 0.44 at 700 nm reveals that the compound was stigmasterol in Figure 1(a), while the  $R_f$  value of 0.37 at 700 nm verifies that the compound was lupeol in Figure 1(b).

The unmodified *M. charantia* FTIR spectrum (Figure 2) is surprisingly clear and well assigned. Methylene ( $>CH_2$ ) was assigned to the bands at  $2923.13\text{ cm}^{-1}$ . At  $3401.91\text{ cm}^{-1}$ , the hydroxy group H-bonded OH vibrations can be seen. The C=C-C aromatic ring stretch peaks at  $1590.56\text{ cm}^{-1}$ , the C-N primary amine peaks at  $1044.38\text{ cm}^{-1}$ , and the aro-

matic secondary amine C-N stretch peaks at  $1280.08\text{ cm}^{-1}$ . The FTIR results indicate similar O-H vibrations and peak area values, according to previous findings [15].

**6.1. Synthesis of Mesoporous Silica Nanoparticle.** The formation of white shading precipitation after applying TEOS (Tetra Ethylene Ortho Silica) to the CTAB surfactant arrangement while nonstop blending confirmed the synthesis of mesoporous silica nanoparticles using the CTAB surfactant process. The MSNs are mixed at a low surfactant concentration to ensure that the organized mesophases depend heavily on the cationic surfactant's cooperation with the forming anionic oligomer orthosilicic corrosive, limiting the size of the mesophases collected. Micrometer-sized particles with circularly requested mesopores were the primary material detailed by versatile analysts.

## 6.2. Characterization of Nanoparticle

**6.2.1. UV-Visible Spectrophotometer.** The prepared mesoporous silica nanoparticles were characterized using a UV-



visible spectrophotometer, which reported a peak at 392.5 nm (Figure 3). This is likely due to the amino group found in silica nanoparticles, in similar study led by (Francesco Armetta et al., 2020). In the present study, the highest absorbance peak was observed within 200–500 nm on the UV-visible spectrophotometer, which agrees with the literature that nanoparticles were synthesized. The results of the FTIR spectrum of the mesoporous silica nanoparticle are further supported by this observation from the UV-visible spectrophotometer.

**6.2.2. Fourier Transform-Infrared (FT-IR) Spectrum Analysis of Mesoporous Silica Nanoparticle.** The Si-O stretching and asymmetric stretching vibrations bands at  $1077.38\text{ cm}^{-1}$  correspond to silica, respectively (Figure 4). Because of the presence of surfactant templates, the symmetric and asymmetric C-H motions can be seen at  $2923.76\text{ cm}^{-1}$ . However, after removing the templates, these peaks disappeared, indicating that the surfactants had been removed, and a mesoporous structure had been formed, as seen in Figure 4. N-H stretch aromatic primary amine has a peak at  $3415.75\text{ cm}^{-1}$ , >N-H secondary amine has a peak at  $1588.56\text{ cm}^{-1}$ , C-H aromatic C-H in pane bend has a peak at  $956.19\text{ cm}^{-1}$ , and methylene C-H bend has a peak at  $1475.96\text{ cm}^{-1}$ . The FTIR results suggest similar C-H vibrations and peak area values, according to prior studies [16].

**6.2.3. Scanning Electron Microscopy Analysis of Mesoporous Silica Nanoparticles.** A silica nanoparticle is a novel type of mesoporous silica nanomaterial that has a hollow spherical shape. Figures 5(a) and 5(b) show an SEM image of mesoporous silica nanoparticles. Tetraethyl orthosilicate (TEOS) as the silica precursors and cetyl trimethyl ammonium bromide (CTAB) as the pore-forming agent were used to make mesoporous silica nanoparticles with a mean diameter of around 350 nm. The solid stober spheres were successfully converted into homogeneous hollow spheres when simply treated with  $\text{Na}_2\text{CO}_3$  in the presence of CTAB at an appropriate concentration. The energy dispersive spectrum on the SEM was used to perform elemental analysis on the mesoporous silica nanoparticles. The EDS spectrum of spherical nanoparticles prepared using CTAB as a pore generating agent is shown in Figure 6. The binding energies of O and Si are shown by the peaks around 0.5 kV and 1.9 kV, respectively. Silica makes up 23.59 percent of the total weight. The EDS spectrum's remaining lines correspond to the other elements (Na, K, and Al).

**6.2.4. Drug Loading on Mesoporous Silica Nanoparticle.** Sample extract and mesoporous silica nanoparticles stirred 24 hrs. Mesoporous silica nanoparticles are used to load samples or drugs onto honey comps. It is employed in further pharmacological treatment investigations in zebrafish [17].

**6.3. Acute Toxicity Study.** Acute toxicity study of a test substance is employed as an excellent tool for assessing its toxicity risk in the human health and the environment [18]. The results of acute toxicity studies indicate that *M.charantia* did not cause any adverse behavioral changes or mortality upon

treatment. At the end of the study, all fishes were sacrificed, and the organ was collected and subjected to histopathological analysis.

**6.4. Histopathological Examination of Tissues.** The histopathological analysis was done for the organ (brain) of the fishes subjected to acute toxicity studies. Fishes from six different groups (group 1-control, group 2-(day 1) trimethyltin chloride, group 3-(day 2 trimethyltin chloride), group 4-trimethyltin chloride + FDA approved drug (donepezil), group 5-trimethyltin chloride + charantin, group 6-trimethyltin chloride + (charantin + mesoporous silica nanoparticle) were the organs were collected. Histopathology sections are viewed under  $\times 40$  and  $\times 40$  magnification photomicrograph (Figures 7–12).

**6.4.1. Group I: Brain (Control).** The section shows brain tissue with four layers, undamaged structure, and cellular morphology.

**6.4.2. Group II: Brain (Day 1: Trimethyltin Chloride).** The section shows cerebellar tissue with areas of degeneration, microinfarcts, the proliferation of ganglion cells, and diffuse inflammation.

**6.4.3. Group III: Brain (Day 2: [Trimethyltin Chloride]).** The section shows normal cerebellar tissue with focal Purkinje cell proliferation, mild edema, and degenerative changes.

**6.4.4. Group IV: Brain [Trimethyltin Chloride + FDA Approved Drug (Donepezil)].** The section shows thinned-out normal cerebellum, occasional prominent congested vessels, and neurofilaments tissue with focal very minimal degenerative changes.

**6.4.5. Group V: Brain (Trimethyltin Chloride + Charantin).** The section shows brain tissue with normal structure and cellular morphology with focal degenerative changes.

**6.4.6. Group VI: Brain [Trimethyltin Chloride + (Charantin + Mesoporous Silica Nanoparticle)].** The section shows brain tissue with thinning of Purkinje cell layer, mild edema, and preservation of rest of the normal brain tissue. The zebrafish brain was identified by the various significant studies done by Dr. Ezhilvizhi Alavandar (Pathologist), Kilpauk Medical College, Chennai, Tamilnadu.

**6.5. Acetylcholinesterase Activity Assay.** One of the various therapeutic options is the use of AChE inhibitors, which enhance the quantity of acetylcholine present in the synapses between cholinergic neurons. The AChE inhibitory activity of various concentrations (10–50 g/mL) of ethanol extract of *M.charantia* is demonstrated in strategies to enhance cholinergic functions in the brain. The results (Figure13) demonstrated that ethanol extract showed inhibitory action that was concentration-dependent. The testing results show that at a concentration of 50 g/mL, the ethanol extract of *M.charantia* exhibited significant AChE assay activity ( $81 \pm 5.86\%$ ) when compared to the standard drug ( $86 \pm 7.75\%$ ).

6.6. *DPPH (2, 2-Diphenyl-1-Picrylhydrazyl) Radical Scavenging Activity.* DPPH free radicals are very stable, and it is a widely used method for determining the antioxidant potential in less time. The capacity to scavenge was tested using different concentrations of aqueous extracts of *M. charantia* and ascorbic acid as a standard antioxidant (positive control). The results of the assay indicate that the aqueous extract of *M. charantia* exhibited significant DPPH radical scavenging activity ( $66 \pm 8.58\%$ ) at a concentration of 10 g/mL. As the concentration was raised, the percentage of inhibition went up as well ( $82 \pm 4.44$  percent) in 50 g/mL, as seen in Figure 14.

6.7. *Reducing Power Assay.* The total reducing power assay was used to assess the antioxidant potential of *M. charantia* ethanol extract. The ability to scavenge was evaluated using different concentrations of aqueous extracts of *M. charantia* and ascorbic acid as a standard antioxidant (positive control). The results of the assay indicate that the aqueous extract of *M. charantia* exhibited significant total reducing power activity ( $69 \pm 2.15$ ) at a concentration of 10 g/mL. As the concentration was increased, the percentage of inhibition went up as well ( $80 \pm 2.15$ ) in 50 g/mL, as seen in Figure 15.

6.8. *Total Antioxidant Assay.* Total antioxidant activity is a widely used method for determining the antioxidant potential of natural compounds in a short period because it is relatively stable. The ability to scavenge was evaluated using various concentrations of ethanol extracts of *M. charantia* and ascorbic acid as a standard antioxidant (positive control). The results of the assay indicate that the ethanol extract of *M. charantia* exhibited significant total antioxidant activity ( $0.168 \pm 0.00025\%$ ) at a concentration of 10 g/mL. When the extract concentration was increased, the mean was also raised ( $0.0325 \pm 0.00026$  percent) at 50 g/mL, as shown in Figure 16.

6.9. *Lipid Peroxidation Assay.* The lipid peroxidation assay was used to assess the antioxidant potential of *M. charantia* ethanol extract. Malondialdehyde was used as a standard antioxidant, and various concentrations of ethanol extracts of *M. charantia* were used to evaluate the scavenging activity. The results of the assay suggest that the ethanol extract of *M. charantia* exhibited lipid peroxidation activity at a concentration of 10 g/mL ( $69 \pm 1.313$ ). The percentage of inhibition increased when the concentration was increased ( $87 \pm 3.474$ ) in 50 g/mL, as seen in Figure 17.

## 7. Conclusion

The preliminary phytochemical analysis of the aqueous extract of *M. charantia* revealed the presence of steroids, tannins, flavonoids, terpenoids, etc., The HPTLC analysis revealed the presence of 12 compounds of steroids with bioactive potentials. The bioactive compound was confirmed and characterized by Fourier transform infrared spectroscopy. The antioxidant potential of crude aqueous extracts of *M. charantia* was assessed by DPPH (2, 2-diphenyl-1-picrylhydrazyl) radical scavenging assay, and the results suggest that

the extract showed excellent antioxidant activity. The trimethyltin chloride was subjected to Alzheimer's studies using *Danio rerio*. At the end of the Alzheimer's treatment study, the behavioral and mortality changes were assessed, and the results show that the extract did not cause any adverse effects on zebrafish, which suggests that the *M. charantia* is safe for consumption. The histopathological analysis was done for the organ (brain), and the results show that there are no pathological changes in tissues of the fish treated with the *M. charantia* extract. The effect of the ethanol extract of *M. charantia* was also analyzed by the cell viability test (MTT assay) in fibroblast (normal cell line), and the results revealed that the extract did not affect the functions of normal cells. Since the *M. charantia* showed higher antioxidant activity and anticholinesterase activity, upon further characterization and assessment, this could be a safe and potential drug candidate for neurotoxicity. In the future, the study can be developed to formulate a drug against neurotoxicity.

## Data Availability

All data used to support the findings of this study are included within the article.

## Conflicts of Interest

The authors declare that there are no conflicts of interest.

## Acknowledgments

The authors are thankful to Sri Ranga Ramanuja Centre for Advanced Research in Sciences (SRRCARs) for providing facilities to carry out this research work. The authors are would like to thank to the Management of Sathyabama Institute of Science and Technology, Chennai, for their help and cooperation.

## References

- [1] F. D. Gomez, P. Apodaca, L. N. Holloway, K. H. Pannell, and M. M. Whalen, "Effect of a series of triorganotin on the immune function of human natural killer cells," *Environmental Toxicology and Pharmacology*, vol. 23, no. 1, pp. 18–24, 2007.
- [2] X. Tang, X. Yang, G. Lai et al., "Mechanism underlying hypokalemia induced by trimethyltin chloride: inhibition of  $H^+/K^+$ -ATPase in renal intercalated cells," *Toxicology*, vol. 271, no. 1–2, pp. 45–50, 2010.
- [3] M. Liong, J. Lu, M. Kovochich et al., "Multifunctional inorganic nanoparticles for imaging, targeting, and drug delivery," *ACS Nanotechnology*, vol. 2, no. 5, pp. 889–896, 2008.
- [4] M. J. Saary and R. A. House, "Preventable exposure to trimethyl tin chloride: a case report," *Occupational Medicine*, vol. 52, no. 4, pp. 227–230, 2002.
- [5] Q. F. Zhou, G. B. Jiang, and J. Y. Liu, "Small-scale survey on the contamination status of butyltin compounds in seafoods collected from seven Chinese cities," *Journal of Agricultural Food Chemistry*, vol. 49, no. 9, pp. 4287–4291, 2001.

- [6] P. Ragavendran, D. Sophia, C. Arul Raj, and V. K. Gopalakrishnan, "Functional group analysis of various extracts of *Aerva lanata* (L.) by FTIR spectrum," *Pharmacology Online*, vol. 1, pp. 358–364, 2011.
- [7] S. Kwon, R. K. Singh, R. A. Perez, E. A. Abou Neel, H. W. Kim, and W. Chrzanowski, "Silica-based mesoporous nanoparticles for controlled drug delivery," *Journal of Tissue Engineering*, vol. 4, 2013.
- [8] S. Jia, M. Shen, F. Zhang, and J. Xie, "Recent advances in *Momordica charantia*: functional components and biological activities," *International Journal of Molecular Sciences*, vol. 18, no. 12, p. 2555, 2017.
- [9] S. Hemmalakshmi, S. Priyanga, and K. Devaki, "Phytochemical screening and HPTLC fingerprinting analysis of ethanolic extract of *Erythrina variegata* l. flowers," *International Journal of Pharmacy and Pharmaceutical Sciences*, vol. 8, pp. 210–217, 2016.
- [10] T. Becker and C. G. Becker, "Axonal regeneration in zebrafish," *Current Opinion in Neurobiology*, vol. 27, pp. 186–191, 2014.
- [11] C. Tourne-Peteilh, S. Begu, D. A. Lerner, A. Galarneau, U. Lafont, and J. M. Devoisselle, "Sol-gel one-pot synthesis in soft conditions of mesoporous silica materials ready for drug delivery system," *Journal of Solgel Science and Technology*, vol. 61, no. 3, pp. 455–462, 2012.
- [12] J. B. Harborne, *Textbook of phytochemical methods. A guide to modern techniques of plant analysis*, Chapman and Hall Ltd, London, 5th Ed edition, 1998.
- [13] F. Armetta, M. L. Saladino, C. Giordano et al., "Non-conventional Ce:YAG nanostructures via urea complexes," *Scientific Reports*, vol. 9, no. 1, p. 3368, 2019.
- [14] S. K. Srivastava, S. Trajmar, A. Chutjian, and W. Williams, "Absolute elastic differential electron scattering cross sections in the intermediate energy region. III. SF<sub>6</sub> and UF<sub>6</sub>," *The Journal of Chemical Physics*, vol. 64, no. 7, pp. 2767–2771, 1976.
- [15] T. S. Vijayakumar, S. Mahboob, G. Bupesh et al., "Facile synthesis and biophysical characterization of egg albumen-wrapped zinc oxide nanoparticles: a potential drug delivery vehicles for anticancer therapy," *Journal of Drug Delivery Science and Technology*, vol. 60, article 102015, 2020.
- [16] N. J. Borges, R. S. Manuel, C. L. Elam, and B. J. Jones, "Differences in motives between millennial and generation X medical students," *Medical Education*, vol. 44, no. 6, pp. 570–576, 2010.
- [17] J. Kim, J. Shim, S. Lee et al., "Rg3-enriched ginseng extract ameliorates scopolamine-induced learning deficits in mice," *BMC Complementary and Alternative Medicine*, vol. 16, p. 66, 2012.
- [18] A. Braca, N. de Tommasi, L. di Bari, C. Pizza, M. Politi, and I. Morelli, "Antioxidant Principles from *Bauhinia tarapotensis*," *Journal of Natural Products*, vol. 64, no. 7, pp. 892–895, 2001.

## Review Article

# Novel Nano-Based Drug Delivery Systems Targeting Hepatic Stellate Cells in the Fibrotic Liver

Devaraj Ezhilarasan <sup>1</sup>, Thangavelu Lakshmi <sup>1</sup> and Biond Raut <sup>2</sup>

<sup>1</sup>Department of Pharmacology, The Blue Lab, Molecular Medicine and Toxicology Division, Saveetha Dental College, Saveetha Institute of Medical and Technical Sciences (SIMATS), Chennai, Tamil Nadu 600077, India

<sup>2</sup>Department of Pharmacology, Kathmandu Medical College Bhaktapur Duwakot, Kathmandu University, Dhulikhel, Kavre, Nepal

Correspondence should be addressed to Thangavelu Lakshmi; [adiasdc@saveetha.com](mailto:adiasdc@saveetha.com) and Biond Raut; [rautbiond@gmail.com](mailto:rautbiond@gmail.com)

Received 26 August 2021; Revised 25 September 2021; Accepted 30 September 2021; Published 22 October 2021

Academic Editor: Venkat Kumar S

Copyright © 2021 Devaraj Ezhilarasan et al. This is an open access article distributed under the Creative Commons Attribution License, which permits unrestricted use, distribution, and reproduction in any medium, provided the original work is properly cited.

Hepatic stellate cells (HSCs) exist in the liver's perisinusoidal space, are phenotypically activated, and acquire myofibroblast-like phenotype. This phenotypic transformation is accountable for the accumulation and production of various extracellular matrix (ECM) proteins, involving different fibril-forming collagens in the perisinusoidal space, producing altered hepatic function and portal hypertension and increased vascular resistance, fibrosis, cirrhosis, and hepatocellular carcinoma. The activated HSCs/myofibroblasts are principal collagen-producing cells in the damaged liver. Therefore, fibrosis treatments are often targeting HSCs. HSCs store most of the total body's retinol in their cytoplasm, and hence, antifibrotic nanomedicines are often targeted with vitamin A decoration. Vitamin A-decorated nanomedicines with siRNAs for transforming growth factor-beta, collagen, and connective tissue growth factors target to inhibit fibrogenesis and the ECM-associated gene expressions, leading to fibrosis regression. Similarly, a variety of miRNAs play pro- and antifibrotic function. In the fibrotic liver, the profibrotic miRNAs are targeted with their respective antagomir and the antifibrotic miRNAs are targeted with their respective agomirs along with HSC-specific nanodecoration. These miRNA treatments reduce fibrogenesis by downregulation of ECM-related gene expressions. However, liver fibrosis is caused by the upregulation of a different type of profibrotic signaling pathways associated with ECM accumulation in the fibrotic liver. Therefore, specific gene silencing by siRNAs or targeting particularly miRNA may also not effectively reduce fibrosis to a greater extent. However, nanodecoration of a drug is useful to deliver drugs into activated HSCs in the injured liver. Therefore, the aim of this review is to focus on targeted drug delivery towards activated HSCs in the persistently damaged liver.

## 1. Introduction

Chronic liver diseases are the main cause of universal health problem. Approximately, 2 million annual deaths are attributed to cirrhosis and its associated complications, hepatocellular carcinoma (HCC) and viral hepatitis [1]. Hepatic fibrosis is the common sequel of chronic liver diseases. If fibrosis is not properly treated, then it progresses into cirrhosis and its related complications like portal hypertension and HCC. Cirrhosis is considered as the most advanced stage of hepatic fibrosis. Cirrhosis and HCC rank 11<sup>th</sup> and 16<sup>th</sup>, respectively, in causing global deaths. Together, HCC and cirrhosis account for 3.5% of mortalities

worldwide [1, 2]. Liver fibrosis is caused by chronic injury due to chronic ethanol intake, hepatitis infections, and metabolic disorders [3]. Fibrosis of the liver is classically distinguished by the increased synthesis and a net accumulation of a variety of extracellular matrix, comprising collagens I, III, and V, elastin, tenascin, and fibronectin in the perisinusoidal space of the liver [4]. Thus, increased ECM synthesis and scar formation are considered as the initial event of liver fibrosis mediated by the hepatic stellate cell (HSC), which is the principal collagen-producing cell in the chronically injured liver [5]. Over the last two to three decades, our understanding of the pathophysiology of fibrosis is instrumental; several studies have identified potential antifibrotic

targets either to halt progression or reverse fibrosis [6]. Chronic liver diseases are often reversible after the withdrawal of underlying etiology, and their treatment mainly focused on etiology-specific. However, presently, no accepted antifibrotic treatments are available for human use [7]. The hepatic stellate cells (HSCs) are strategically placed in the perisinusoidal area of the liver in such a way that they communicate with hepatocytes, immune cells, and sinusoidal endothelial cells in the liver. Hence, HSCs are one of the prime targets for treating fibrotic liver [8]. However, the development of natural and synthetic antifibrotic drugs targeting HSCs in the fibrotic liver has faced challenges such as poor solubility, lack of HSC-specific targeted delivery, and less effectiveness [9]. Thus, studies have principally targeted HSCs with several nanoformulations to control or regress the ongoing liver fibrosis. This review is primarily focusing on novel nano-based drug delivery systems targeting HSCs in the fibrosed liver.

## 2. Hepatic Stellate Cells

Hepatic stellate cells exist in the perisinusoidal space or Disse space in the liver. Upon chronic liver injury, HSCs are phenotypically transformed and activated into myofibroblasts. This process is termed as HSC activation [10]. The activated myofibroblasts/HSCs are liable for the expression and secretion of numerous chemokines and profibrotic cytokines [11]. Thus, activated HSCs retain the pathophysiological status of the damaged liver by expressing platelet-derived growth factors (PDGF), transforming expressing growth factor- $\beta$  (TGF- $\beta$ ), retinol binding protein (RBP) receptor, Krüppel-like factor 4, endothelin-1, and  $\alpha$ -smooth muscle actin, modulating a variety of tissue inhibitors of metalloproteinases (TIMPs) and matrix metalloproteinase (MMPs). This process is known as perpetuation. In a normal liver, HSCs are quiescence and are liable for the preservation of normal ECM homeostasis. However, the phenotypically activated myofibroblasts or activated HSCs are liable for the accumulation and synthesis of an enormous amount of ECM to substantiate the ongoing injury of the liver [12]. Anatomically, the excessive ECM deposition in the perisinusoidal space of the chronically injured liver hinders the solute transport between hepatocytes and liver sinusoidal endothelial cells (LSECs), heading to functional alteration of the liver and an increase in intrahepatic resistance-mediated portal hypertension [13]. Functionally, activated HSCs interact with several cell types in the perisinusoidal milieu by releasing PDGF, TGF- $\beta$ , TIMPs, MMPs, endothelin-1, and others [14]. These signaling molecules from activated HSCs, act on themselves via an autocrine manner also activate other cells such as quiescent HSCs, hepatocytes, and LSECs via a paracrine manner. For instance, activated HSCs and LSECs communicate each other with ET-1, leading to portal hypertension [15]. Activated HSCs induce the proliferation and activation of quiescent HSCs by expressing PDGF and TGF- $\beta$ , which increases the burden of ECM synthesis. The role of HSCs in the normal and injured liver is presented in Figure 1.

## 3. Existing Strategies Targeting Activated HSCs in the Fibrotic Liver

Since HSCs perform a pivotal role in fibrogenesis, several studies have targeted HSCs to regress fibrogenesis [16]. Accumulating experimental evidence suggests that the liver fibrosis process can be controlled by decreasing HSC activation and perpetuation. Previous studies have targeted HSCs for therapeutic purpose in the chronically injured liver by (i) decreasing the HSC proliferation via PDGF signaling, (ii) decreasing fibrogenesis through inhibition of TGF- $\beta$  signaling, (iii) targeting HSCs to promote the ECM degradation by modulating MMPs and TIMPs, (iv) inducing the clearance of activated HSCs by apoptosis, (v) inducing senescence of activated HSCs, (vi) inhibiting the proliferation of activated HSCs by halting their cell cycle, (vii) suppressing the parenchymal and qHSC activation by removal of underlying etiologies, (viii) neutralizing the oxidative stress environment of the injured liver by using antioxidants, (ix) silencing the activated HSC genes responsible for ECM synthesis, (x) targeting the profibrotic miRNAs in activated HSCs via antagomirs, (xi) decreasing epigenetic alteration in activated HSCs, and (xii) decreasing the extracellular vesicles released from activated HSCs [17–23]. The above strategies were employed by previous experimental studies by using natural and synthetic drug candidates to regulate the activated HSCs in the chronically damaged liver. However, these drugs have several disadvantages like poor bioavailability and solubility, less targeted, and off-target effects on drug delivery. The liver contains heterogenous cell population, predominantly HSCs, hepatocytes, LSECs, Kupffer cells, portal fibroblasts, and other non-resident immune cells. However, HSCs activation often leads to the overexpression of several cell surface receptors such as collagen type 4, TGF- $\beta$ , connective tissue growth factor receptors, PDGFR $\beta$ , RBP receptor, synaptophysin, cluster of differentiation 44 (CD44), insulin-like growth factor-II receptor (IGF2R), and low-density lipoprotein receptor [24]. In previous studies, these receptors have been primary targeted to direct nano-based drugs towards activated HSCs. Therefore, targeting phenotypically activated HSCs in the damaged liver by nano-based drug preparation could be one of the possible strategies to increase the targeted drug delivery to HSCs. Thus, HSC-specific nanodrug construction may direct the drug towards activated HSCs in the fibrosed liver.

## 4. Nanotargeting of Activated HSC Surface Proteins and Signaling

Conventionally, inorganic nanoparticles like silver, gold, titanium dioxide, silicon dioxide, and cerium oxide are used without targeting activated HSCs in the fibrotic liver [25, 26]. Later, nanocarriers like liposomes and hyaluronic acid micelles are used to carry antifibrotic drugs and target HSCs in the injured liver [27, 28]. These nanocarriers targetedly deliver nanoparticles into activated HSCs in the fibrotic liver. During chronic liver injury CD44 and phenotypic receptors are increasingly expressed after HSC activation. Therefore, CD44 ligands are previously targeted along with

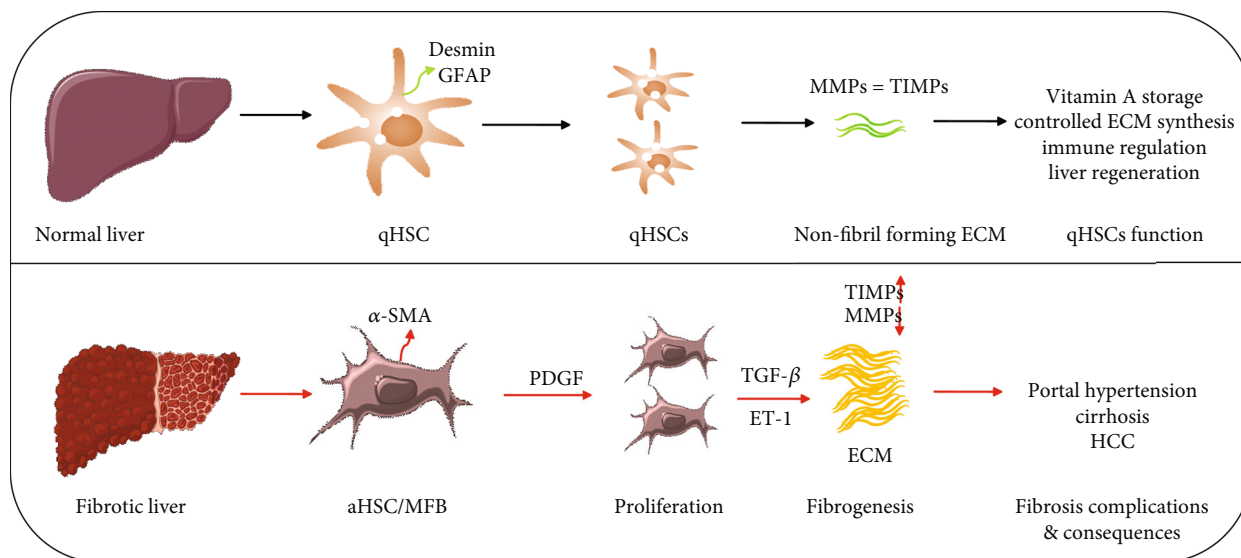


FIGURE 1: Hepatic stellate cells (HSCs) in the normal and fibrotic liver. In normal liver, quiescent HSC (qHSC) stores vitamin A and it is also responsible for the secretion of non-fibril-forming collagens, which gives functional support to the liver. In the fibrotic liver, qHSCs are phenotypically activated (activated HSCs (aHSCs)) and acquire myofibroblast (MFB) phenotype. The aHSCs are responsible for the enhanced secretion of extracellular matrix (ECM) via modulation of matrix metalloproteinases (MMPs) and tissue inhibitor of metalloproteinases (TIMPs). GFAP: glial fibrillary acidic protein;  $\alpha$ -SMA: alpha-smooth muscle actin; PDGF: platelet-derived growth factor; TGF- $\beta$ : transforming growth factor-beta; ET-1: endothelin 1; HCC: hepatocellular carcinoma.

nanoparticles to precisely deliver numerous synthetic and natural antifibrotic agents [29]. For instance,  $\alpha\beta3$  integrin is greatly expressed in activated HSCs and degradation of  $\alpha\beta3$  ligands was found in activated HSCs during the resolution of liver fibrosis. Therefore, a previous study targeted  $\alpha\beta3$  on activated HSCs [30]. Hedgehog (Hh) signaling plays a pivotal role in the pathophysiology of liver fibrosis [24]. Hedgehog signaling components and receptors Ihh, smoothed (Smo), patched (Ptc), and glioma-associated oncogene (Gli) 2 and Gli3 were highly expressed in HSCs [31]. Sterically steady liposomes that comprise the cyclic peptides (cRGDyK) with an excessive attraction to  $\alpha\beta3$  were developed to attain precise delivery to activated HSCs. cRGDyK-guided liposomes were specifically adopted into activated HSCs *in vivo* and *in vitro*. However, cRGDyK-guided liposomes uptake was minimal in quiescent HSCs, Kupffer cells, hepatocytes, biliary cells, or sinusoidal endothelial cells. Vismodegib (GDC), a Hh inhibitor loaded with cRGDyK-directed liposomes, prevented Hh signaling only in activated HSCs. *In vivo*, GDC-loaded cRGDyK-guided liposome treatment attenuated thioacetamide induced liver fibrosis in mice or attenuated bile duct ligation (BDL) [32]. Peroxisome proliferator-activated receptor  $\gamma$  (PPAR- $\gamma$ ) overexpression prevents HSC activation in the damaged liver [33]. Rosiglitazone (RGZ), a PPAR- $\gamma$  agonist, was shown to alleviate liver fibrosis via HSC activation [34]. Therefore, methoxy-polyethylene-glycol-b-poly(carbonate-co-lactide) [mPEG-b-p(CB-co-LA)] was produced and encapsulated GDC and RSZ with the encapsulation efficiency being 5.0% and 2.0% *w/w* for GDC and RSZ, respectively, to target against BDL-caused liver fibrosis in rats. Systemic administration of drug-encapsulated nanoparticles (120-130 nm-sized) protected liver injury in BDL-induced liver fibrosis by decreasing inflammatory cytokines and controlling the activation of

HSCs. GDC- and RSZ-loaded nanoparticles reduced Hh ligand molecule (Shh, Smo, Ptc-1, and Gli 1) expression and fibrosis marker expressions ( $\alpha$ -SMA, fibronectin-1, and TGF- $\beta$ 1) [35]. These studies suggest that nanoparticles with Hh inhibitor and PPAR- $\gamma$  agonist could target activated HSCs and reduce the fibrogenic potential.

Interestingly, activated HSC integrin was targeted using plant-derived active compound quercetin and along with gadolinium. RGD-hepatitis B core (Hbc)/quercetin and RGD-Hbc/quercetin-gadolinium nanocages (29.6  $\pm$  3.1 nm) were prepared with the surface-presented RGD-directing ligand. These nanocages display high binding attraction with integrin  $\alpha\beta3$  and thereby achieved targeted delivery towards activated HSCs. These nanocages effectively prevented the HSC proliferation and their activation *in vitro*. This study shows that multifunctional  $\alpha\beta3$ -directed NPs could deliver quercetin to the activated HSCs [36]. Germacrone (GMO), a major bioactive component of *Curcuma zedoaria*, and miR-29b, an antifibrotic miRNA encapsulated into nanoparticles based on poly(ethylene glycol)-block-poly(lactide-co-glycolide) (PEG-PLGA), were developed with cyclical RGD peptides (231.2 nm size) for an active ligand to integrin  $\alpha\beta3$  binding. This nanoparticle system efficiently internalized into HSCs via  $\alpha\beta3$ -mediated endocytosis. GMO and miR-29b inhibit the proliferation of activated HSCs and collagen 1 expression, and *in vivo*, this nanoparticle system ameliorated CCl<sub>4</sub>-induced liver fibrosis in mice [37].

## 5. Vitamin A- (VA-) Coupled Nanoparticles Targeting activated HSCs

HSCs store 80% of the body's total retinol existing as retinyl esters inside their lipid droplets. Vitamin A storage is a characteristic feature of HSCs [38], and therefore, this property

has been applied as a mechanism for targeting HSCs. Most of the natural antifibrotic compounds have poor solubility and bioavailability [9]. Hence, to achieve targeted drug delivery to HSCs, VA decoration may be a useful strategy to direct the antifibrotic compounds towards activated HSCs in the damaged liver [3, 39]. In a study, zein/phospholipid composite NPs coupled with VA (192 nm) were formed as a delivery platform for gallic acid (GA-CACNP/VA), a polyphenolic compound, reportedly having antifibrotic effects. These NPs showed high (60%) entrapment efficiency (EE%), selectively distributed in the liver and highly internalized into HSCs. GA-CACNP/VA evidently inhibited HSC activation, induced activated HSC apoptosis, and repressed collagen deposition [40]. This study implies that VA decoration can lead to HSC-specific efficient drug delivery in the injured liver. In a study, retinol was conjugated with polyethyleneimine, which further combined with an antisense oligonucleotide to form retinol-conjugated polyethyleneimine (RCP) nanoparticles. Retinol conjugation caused specific recruitment of retinol-connecting protein in the corona that effectively directed the nucleotide-laden nanoparticles into HSCs in the fibrotic liver. The oligonucleotide-laden RCP nanoparticles suppressed collagen 1 expression and attenuated  $\text{CCl}_4$ - and BDL-caused liver fibrosis in mice [41].

Imatinib, a second-generation tyrosine kinase inhibitor (TKI), has been significantly employed for the treatment of HCC, gastrointestinal stromal tumors, and chronic myelogenous leukemia [42]. Imatinib was shown to inhibit TGF- $\beta$  signaling and profibrotic PDGF pathways [43]. Therefore, VA-combined imatinib-rich liposomes (spherical and  $71.9 \pm 2.6$  nm-sized) have been targeted against HSCs in the fibrotic liver in rats. The VA-coupled imatinib liposomes are accumulated in the fibrotic liver when compared to the normal liver in rats. A single intraperitoneal injection of this liposome had 13.5 folds higher hepatic accumulation. Colocalization of VA-coupled liposome-rich Nile Red with immune-fluorescently labeled PDGFR $\beta$  in frozen liver tissue sections confirmed HSC directing [44]. The accumulation of different ECM in the liver perisinusoidal space is the chief pathological feature of liver fibrosis [8]. Thus, acceleration of matrix degradation is considered one of the therapeutic strategies for fibrosis regression. In a study, collagenase I, a collagen 1-degrading enzyme, and retinol-codecorated polymeric micelle that possesses nano-drill-like and HSC target function based on poly-(lactic-co-glycolic)-b-poly(ethylene glycol)-maleimide (PLGA-PEG-Mal) (CRM) was prepared. The spherical CRM ( $87.6 \pm 8.3$  nm) had a nano-drill-like function and effectively degraded pericellular collagen I. CRM loaded with nilotinib, a second-generation TKI, showed antifibrotic activity against  $\text{CCl}_4$ -induced liver fibrosis [45].

## 6. Nanotargeting of activated HSCs for Portal Hypertension

Increased intrahepatic resistance and portal hypertension are major complications of advanced fibrosis and cirrhosis. HSC activation and subsequent ET-1 release from myofibroblasts and LSECs cause portal hypertension [15]. The

influence of angiotensin II receptor antagonist, i.e., valsartan, on portal hypertensive and hepatic fibrosis has been studied in hepatic cirrhotic patients [46, 47]. Valsartan reduced portal hypertension in hepatic cirrhosis patients [48]. However, valsartan exhibits poor water-soluble (0.18 mg/ml) property and it has ~23% of oral bioavailability [49]. Therefore, liposome-based nanocarriers for valsartan were developed to improve its permeability. These valsartan-loaded liposomes (VLL) (spherical and  $169.9 \pm 2.4$  nm-sized) are coupled with VA for HSC specific targeted delivery. The orally administered VLL preferentially accumulated in the fibrotic liver for six days [50]. Further, reduced PPAR- $\gamma$  nuclear receptor expression was reported during HSC activation, while its upregulation was responsible for the regression of fibrosis and downregulation of fibrosis-associated gene expressions and fibrosis resolution [33]. VLL exhibits potential antifibrotic effects with PPAR- $\gamma$  agonistic activity and prolonged delivery [50]. Nitric oxide is a potent vasodilator, and it was shown to inhibit HSC activation and regulate portal hypertension [15]. Therefore, nitric oxide (NO) donor molecule-based drug delivery systems have been developed. For instance, silica and gold nanoparticle-arbitrated drug delivery systems containing NO donors have been tried against liver fibrosis. NO released from silica and gold nanoconjugates inhibited HSC proliferation, activation, and their vascular tube formation ability [51]. Similarly, polymeric nanoparticles incorporating nitric oxide donor molecules (S-nitrosoglutathione), conjugated with VA (25-35 nm-sized), were studied *in vitro* and *in vivo*. The VA decoration led to the polymeric nanoparticles specifically target rat primary HSCs and LX-2 cells. This nanoparticle system significantly inhibited fibrogenic marker gene expressions such as collagen and  $\alpha$ -SMA without inducing cytotoxicity in primary HSCs isolated from rats and in human HSC cell line (LX-2). Further, NO-delivering nanoparticles have reduced the ET-1 and portal pressure (approximately 20%) in BDL rats [52]. These studies indicate that gold, silver, and polymeric nanoparticle system may serve as a novel delivery platform to deliver anti-hypertensive drugs and vasodilators like NO into activated HSCs responsible for portal hypertension during chronic liver diseases.

## 7. RNA Interference-Based Targeted Drug Delivery in liver fibrosis

RNA interference is one of the valuable approaches to regress fibrosis of the liver by silencing specific gene expression in activated HSCs [53]. The activated HSCs are liable for the accumulation of a variety of ECM proteins in the perisinusoidal space of chronically injured liver, which causes liver fibrosis. Therefore, ECM-specific gene silencing may reduce the ECM accumulation in the liver, decreasing fibrosis and associated complications [54]. siRNA-based nanopreparation offers promising and targeted drug delivery. For instance, siRNA-mediated interference of poly(rC) binding protein 2 (PCBP2) gene inhibits the expression of  $\alpha$ -complex protein-2 ( $\alpha$ CP2) in HSCs, which is accountable for stabilization of collagen  $\alpha 1(I)$  mRNA. The decay rate of the collagen  $\alpha 1(I)$  mRNA was shown to increase

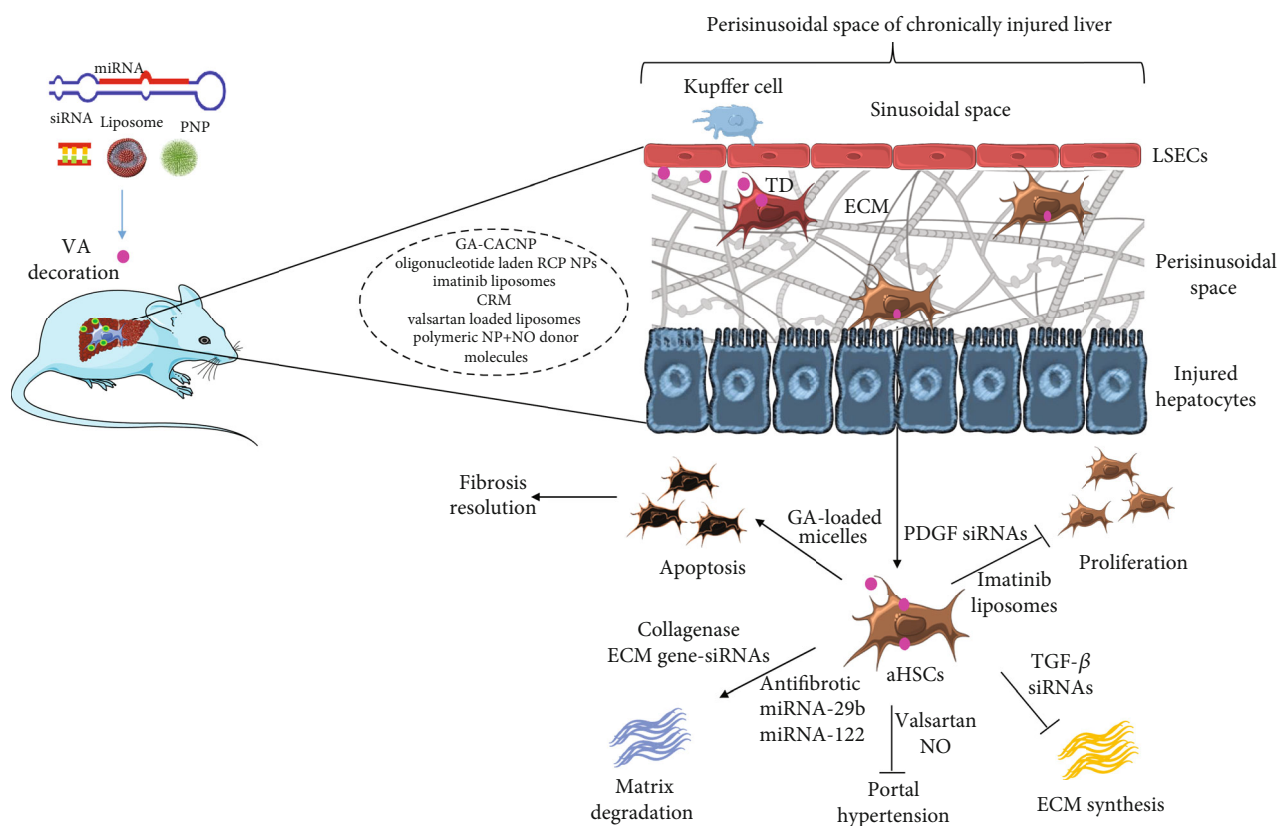


FIGURE 2: Targeted drug delivery for activated HSC (HSCs) in the fibrotic liver. miRNA: microRNA; siRNA: RNA silencing; PNP: polymeric nanoparticles (NPs); VA: vitamin A; GA-CACNP: gallic acid- (GA-) zein/phospholipid composite NPs coupled with VA; RCP NPs: retinol-conjugated polyethyleneimine nanoparticles; CRM: collagenase I and retinol codecorated polymeric micelle based on poly-(lactic-co-glycolic)-b-poly(ethylene glycol)-maleimide; NO: nitric oxide; LSECs: liver sinusoidal endothelial cells; TD: targeted delivery; ECM: extracellular matrix; PDGF: platelet-derived growth factors; TGF- $\beta$ : transforming growth factor-beta.

significantly after streptavidin, siRNA, cholesterol, and protamine (SSCP) nano-multifaced treatment in activated HSCs [55]. Later, Shukla et al. [56] demonstrated the intracellular transferring of oligonucleotide siRNA and their effective discharge into the HSC cytosol. After internalization, the siRNA nanocomplex with protamine and streptavidin entrapped in early endosomes undergoes exocytosis, entrapment in lysosomes, and endosomal escape. This caused a substantial quantity of siRNA dissociation from the nanocomplex to utilize gene silencing activity.

The IGF2R is increasingly expressed in activated HSCs. Therefore, biotin-conjugated IGF2R-specific peptide, vitamin A, and cholesterol were used as the targeting ligands for the neutravidin-based siRNA nanocomplex to deliver PCBP2 siRNA to activated HSCs. Interestingly, IGF2R-specific siRNA-neutravidin-peptide-protamine nanocomplex (228 nm) showed a maximum targeting effect to human (LX-2) and rat (HSC-T6) HSCs and activated initial rat HSCs as compared to cholesterol (191 nm) and vitamin A (167 nm) nanocomplexes. IGF2R-specific siRNA-neutravidin-peptide-protamine nanocomplex exhibited the highest liver uptake than lung and kidney in  $\text{CCl}_4$ -induced fibrotic rats. IGF2R-specific siRNA-neutravidin-peptide-protamine nanocomplex had maximum PCBP2 silencing and prevented the migration of activated HSCs [57]. Though

siRNA-neutravidin-peptide-protamine nanocomplex possesses greater than 228 nm size due to higher molecular weight of the peptide ligand, still they achieved the maximum liver intake. Vitamin A nanocomplexes have less than 200 nm size as compared to the cholesterol based nanocomplex. However, for liver directing, the average particle size was defined to be less than 200 nm, which highly promotes passive liver targeting [39]. Therefore, a study from Zhao et al. [57] suggests that nanoparticles with more than 200 nm particle size also possibly target the liver.

The chitosan is a natural, recyclable and hydrophilic polymer; it is commonly used in the development of nanoparticles (NPs) for delivery of drug, particularly for nucleic acid and protein delivery [58]. Chitosan nanoparticles have an innate affinity for ECM proteins such as collagen, suggesting that they could be used to transport drugs to fibrotic livers. A previous study developed TGF- $\beta$ -siRNA-loaded chitosan NPs (spherical shaped, zeta potential (ZP) of  $35 \pm 1$  mV, and hydrodynamic diameter (HD)  $110 \pm 6$  nm) to promote efficient delivery into activated HSCs via modification with PDGF- $\beta$  binding peptides. The addition of collagenase increased the internalization of TGF- $\beta$ -siRNA-rich chitosan NPs and delivered anti-TGF- $\beta$ 1 siRNA into activated HSCs *in vitro* and *in vivo*. Collagenase-containing nanoparticles may help to degrade the collagen-rich fibrotic scar in the



chronically injured liver [59]. Tenascin-C (TnC), an ECM protein secreted by HSCs is minimally detected in normal liver cells; however, it is transiently expressed during tissue damage and performs an important role in tumorigenesis and fibrogenesis [60]. TnC promotes HSC activation, migration, and TGF- $\beta$ -mediated type I collagen production in the chronically damaged rat liver [61]. In a study, functionalized mesoporous silica NPs (size  $40 \pm 5$  nm; HD  $157 \pm 15$  nm) were used for the efficient transport and delivery of siTnC in HSCs. Inhibition of TnC by mesoporous silica NP-loaded siTnC prevents HSC activation-mediated cell migration and prevents the elevation of proinflammatory gene expression in macrophages [62].

A wide variety of microRNA (miRNAs) is modulated during HSC activation [8]. Among these, miRNA-122 was identified as the human liver-specific miRNA and miRNA-29b was also considered a vital therapeutic focus for liver fibrosis [5]. miRNA-29b and miRNA-122 inhibit HSCs activation and proliferation and collagen synthesis via targeting profibrotic signaling pathways such as hedgehog or TGF- $\beta$ 1/Smad3 pathways [63–65]. Therefore, to selectively target and to deliver these microRNAs into activated HSCs, a pH-sensitive, magnetic resonance imaging visible VA decorated with a copolymer polyethylene glycol (PEG)–polyethylenimine-poly (N-(N',N'-diisopropylamino ethyl)-co-benzylamine) aspartamide (T-PBP) nanoparticle was developed. It was assembled into MRI contrast agent superparamagnetic iron oxide-patterned cationic micelle for miRNA-29b and miRNA-122 delivery. Due to VA decoration, T-PBP micelle efficiently delivered both miRNAs into HSCs, resulted in synergistic antifibrotic effects through downregulation of HSC activation and ECM-related marker gene expressions ( $\alpha$ -SMA and type I collagen and TIMP 1, respectively) [66].

Herbal-based hepatoprotective preparations have poor solubility, bioavailability, and rapid clearance. Therefore, to increase their solubility and bioavailability, nano-based approach is commonly used in experimental studies and tested against fibrosis models [9]. The herbal-based antifibrotic drug nanopreparation may be useful to target HSCs. For instance, a previous study designed and optimized a reverse micelle-loaded lipid nanocapsule using Box-Behnken design to deliver GA, which has antifibrotic effect, directly into activated HSCs. These  $30.35 \pm 2.34$  nm-sized GA nanoparticles had high EE ( $63.95 \pm 2.98\%$ ) with effective internalization into activated HSCs and reduced their proliferation and induced apoptosis. *In vivo*, these NPs accumulated in the liver and downregulated the fibrotic marker gene expressions [67]. San-Huang-Xie-Xin-Tang decoction containing Rhei rhizome, Coptidis rhizome, and *Scutellariae radix*, a traditional herbal medicine of China, is extensively used as hepatoprotective treatment. These dried herbal mixtures were nanoscaled using a pulsed air flow pulverizer. These pulverized nanoscale herbal mixtures induced cytotoxicity in HSCs. This nanoherbal extract has also upregulated MMP-2 gene expression and inhibited TIMP-1 gene expression [68]. However, RNA interference using siRNA and miRNAs encounters many challenges after its systemic administration. Successful and consistent siRNA delivery to activated HSCs in the fibrotic liver remains a vital

issue for the synthesis of siRNA-based therapies. The targeted drug delivery for activated HSC in the fibrotic liver is presented in Figure 2.

## 8. Conclusion and Perspectives

Undoubtedly, vitamin A-conjugated nanoparticles or siRNAs or miRNAs or drugs successfully deliver antifibrotic drugs into activated HSCs in the chronically injured liver and reduce profibrotic protein and gene expressions. Vitamin A-conjugated nitric oxide donor molecules and other antihypertensive drugs selectively deliver drugs into activated HSCs and reduce portal hypertension. To achieve better liver targeting, the average particle size was defined to be less than 200 nm, which greatly promotes passive liver targeting. However, Zhao et al. [57] developed a siRNA-neutravidin-peptide-protamine nanocomplex that achieved maximum targeted liver delivery with the particle size of 228 nm. Therefore, size is not the only factor to achieve the highest theranostic potential of a nanocomplex. Hepatic fibrosis is a consequence of the accumulation of numerous ECM proteins in the damaged liver. Therefore, targeting one protein expression via gene silencing using siRNA-based nanoconstruct may not give us efficient results and this is one of the main limitations of siRNA-based therapeutics. However, nanodecoration of HSC-specific molecules provides better siRNA delivery. Further, exocytosis is one of the main factors responsible for the transient silencing activity of non-viral siRNA delivery, and therefore, exocytosis inhibitor combination may prolong the silencing activity of siRNA. However, this approach should be studied in detail in the near future. Moreover, a variety of miRNAs are modulated during HSC activation. They have specific profibrotic and antifibrotic properties; therefore, their specific antagomir- and agomir-based nanopreparations should be studied in an elaborate manner, respectively. Thus, liver- or HSC-specific nanopreparation remains a gold standard strategy to deliver siRNA/miRNA/drugs into activated HSCs in the fibrotic liver.

## Data Availability

The data used to support the findings of this study are included within the article

## Conflicts of Interest

The authors declare that they have no conflicts of interest.

## References

- [1] S. K. Asrani, H. Devarbhavi, J. Eaton, and P. S. Kamath, “Burden of liver diseases in the world,” *Journal of Hepatology*, vol. 70, no. 1, pp. 151–171, 2019.
- [2] A. K. Singal and P. Mathurin, “Diagnosis and treatment of alcohol-associated liver disease: a review,” *Journal of the American Medical Association*, vol. 326, no. 2, pp. 165–176, 2021.
- [3] E. Devaraj and S. Rajeshkumar, “Nanomedicine for hepatic fibrosis,” in *Nanoparticles and their Biomedical Applications*, A. Shukla, Ed., Springer, Singapore, 2020.

- [4] D. Ezhilarasan, "Critical role of estrogen in the progression of chronic liver diseases," *Hepatobiliary & Pancreatic Diseases International*, vol. 19, no. 5, pp. 429–434, 2020.
- [5] D. Ezhilarasan, "MicroRNA interplay between hepatic stellate cell quiescence and activation," *European Journal of Pharmacology*, vol. 885, article 173507, 2020.
- [6] A. Khanam, P. G. Saleeb, and S. Kotttilil, "Pathophysiology and treatment options for hepatic fibrosis: can it be completely cured?," *Cell*, vol. 10, no. 5, p. 1097, 2021.
- [7] D. Schuppan, M. Ashfaq-Khan, A. T. Yang, and Y. O. Kim, "Liver fibrosis: direct antifibrotic agents and targeted therapies," *Matrix Biology*, vol. 68–69, pp. 435–451, 2018.
- [8] D. Ezhilarasan, "Oxidative stress is bane in chronic liver diseases: clinical and experimental perspective," *Arab Journal of Gastroenterology*, vol. 19, no. 2, pp. 56–64, 2018.
- [9] D. Ezhilarasan, E. Sokal, S. Karthikeyan, and M. Najimi, "Plant derived antioxidants and antifibrotic drugs: past, present and future," *Journal of Coastal Life Medicine*, vol. 2, no. 9, pp. 738–745, 2014.
- [10] T. Tsuchida and S. L. Friedman, "Mechanisms of hepatic stellate cell activation," *Nature Reviews. Gastroenterology & Hepatology*, vol. 14, no. 7, pp. 397–411, 2017.
- [11] P. Königshofer, K. Brusilovskaya, O. Petrenko et al., "Nuclear receptors in liver fibrosis," *Biochimica et Biophysica Acta - Molecular Basis of Disease*, vol. 1867, no. 12, article 166235, 2021.
- [12] C. Ortiz, R. Schierwagen, L. Schaefer, S. Klein, X. Trepap, and J. Trebicka, "Extracellular matrix remodeling in chronic liver disease," *Current Tissue Microenvironment Reports*, vol. 2, no. 3, pp. 41–52, 2021.
- [13] S. Kumar, Q. Duan, R. Wu, E. N. Harris, and Q. Su, "Pathophysiological communication between hepatocytes and non-parenchymal cells in liver injury from NAFLD to liver fibrosis," *Advanced Drug Delivery Reviews*, vol. 176, article 113869, 2021.
- [14] X. Cai, J. Wang, J. Wang et al., "Intercellular crosstalk of hepatic stellate cells in liver fibrosis: new insights into therapy," *Pharmacological Research*, vol. 155, p. 104720, 2020.
- [15] D. Ezhilarasan, "Endothelin-1 in portal hypertension: the intricate role of hepatic stellate cells," *Experimental Biology and Medicine (Maywood, N.J.)*, vol. 245, no. 16, pp. 1504–1512, 2020.
- [16] D. Ezhilarasan, "Role of microRNAs in hepatic fibrosis progression," *Journal of Applied Pharmaceutical Science*, vol. 8, no. 5, pp. 174–178, 2018.
- [17] E. Borkham-Kamphorst, J. Herrmann, D. Stoll, J. Trepap, A. M. Gressner, and R. Weiskirchen, "Dominant-negative soluble PDGF- $\beta$  receptor inhibits hepatic stellate cell activation and attenuates liver fibrosis," *Laboratory Investigation*, vol. 84, no. 6, pp. 766–777, 2004.
- [18] A. Baiocchi, C. Montaldo, A. Conigliaro et al., "Extracellular matrix molecular remodeling in human liver fibrosis evolution," *PLoS One*, vol. 11, no. 3, article e0151736, 2016.
- [19] D. Ezhilarasan, J. Evraerts, S. Brice et al., "Silibinin inhibits proliferation and migration of human hepatic stellate LX-2 cells," *Journal of Clinical and Experimental Hepatology*, vol. 6, no. 3, pp. 167–174, 2016.
- [20] H. Nishizawa, G. Iguchi, H. Fukuoka et al., "IGF-I induces senescence of hepatic stellate cells and limits fibrosis in a p53-dependent manner," *Scientific Reports*, vol. 6, no. 1, p. ???, 2016.
- [21] R. Brea, O. Motiño, D. Francés et al., "PGE<sub>2</sub> induces apoptosis of hepatic stellate cells and attenuates liver fibrosis in mice by downregulating miR-23a-5p and miR-28a-5p," *Biochimica et Biophysica Acta - Molecular Basis of Disease*, vol. 1864, no. 2, pp. 325–337, 2018.
- [22] P. Gupta, T. N. Sata, A. K. Yadav et al., "TGF- $\beta$  induces liver fibrosis via miRNA-181a-mediated down regulation of augmentor of liver regeneration in hepatic stellate cells," *PLoS One*, vol. 14, no. 6, article e0214534, 2019.
- [23] D. Ezhilarasan, J. Evraerts, B. Sid et al., "Silibinin induces hepatic stellate cell cycle arrest via enhancing p53/p27 and inhibiting Akt downstream signaling protein expression," *Hepatobiliary & Pancreatic Diseases International*, vol. 16, no. 1, pp. 80–87, 2017.
- [24] D. Ezhilarasan, "Hepatic stellate cells in the injured liver: perspectives beyond hepatic fibrosis," *Journal of Cellular Physiology*, 2021.
- [25] H. Zhang, W. Han, X. Cao et al., "Gold nanoclusters as a near-infrared fluorometric nanothermometer for living cells," *Mikrochimica Acta*, vol. 186, no. 6, p. 353, 2019.
- [26] F. Peng, J. K. Tee, M. I. Setyawati et al., "Inorganic nanomaterials as highly efficient inhibitors of cellular hepatic fibrosis," *ACS Applied Materials & Interfaces*, vol. 10, no. 38, pp. 31938–31946, 2018.
- [27] D. Yang, Y. H. Gao, K. B. Tan et al., "Inhibition of hepatic fibrosis with artificial microRNA using ultrasound and cationic liposome-bearing microbubbles," *Gene Therapy*, vol. 20, no. 12, pp. 1140–1148, 2013.
- [28] S. Poilil Surendran, R. George Thomas, M. J. Moon, and Y. Y. Jeong, "Nanoparticles for the treatment of liver fibrosis," *International Journal of Nanomedicine*, vol. 12, pp. 6997–7006, 2017.
- [29] Z. Chen, A. Jain, H. Liu, Z. Zhao, and K. Cheng, "Targeted drug delivery to hepatic stellate cells for the treatment of liver fibrosis," *The Journal of Pharmacology and Experimental Therapeutics*, vol. 370, no. 3, pp. 695–702, 2019.
- [30] X. Zhou, F. R. Murphy, N. Gehdu, J. Zhang, J. P. Iredale, and R. C. Benyon, "Engagement of  $\alpha_v\beta_3$  Integrin Regulates Proliferation and Apoptosis of Hepatic Stellate Cells\*," *The Journal of Biological Chemistry*, vol. 279, no. 23, pp. 23996–24006, 2004.
- [31] T. Li, X. S. Leng, J. Y. Zhu, and G. Wang, "Suppression of hedgehog signaling regulates hepatic stellate cell activation and collagen secretion," *International Journal of Clinical and Experimental Pathology*, vol. 8, no. 11, pp. 14574–14579, 2015.
- [32] Y. Li, S. Pu, Q. Liu et al., "An integrin-based nanoparticle that targets activated hepatic stellate cells and alleviates liver fibrosis," *Journal of Controlled Release*, vol. 303, pp. 77–90, 2019.
- [33] L. Tao, L. Wu, W. Zhang et al., "Peroxisome proliferator-activated receptor  $\gamma$  inhibits hepatic stellate cell activation regulated by miR-942 in chronic hepatitis B liver fibrosis," *Life Sciences*, vol. 253, p. 117572, 2020.
- [34] S. C. Zhi, S. Z. Chen, Y. Y. Li, J. J. Li, Y. H. Zheng, and F. X. Yu, "Rosiglitazone inhibits activation of hepatic stellate cells via up-regulating micro-RNA-124-3p to alleviate hepatic fibrosis," *Digestive Diseases and Sciences*, vol. 64, no. 6, pp. 1560–1570, 2019.
- [35] V. Kumar, V. Mundra, and R. I. Mahato, "Nanomedicines of hedgehog inhibitor and PPAR- $\gamma$  agonist for treating liver fibrosis," *Pharmaceutical Research*, vol. 31, no. 5, pp. 1158–1169, 2014.

- [36] Q. Zhang, D. Xu, Q. Guo et al., "Theranostic quercetin nanoparticle for treatment of hepatic fibrosis," *Bioconjugate Chemistry*, vol. 30, no. 11, pp. 2939–2946, 2019.
- [37] D. Ji, Q. Wang, Q. Zhao et al., "Co-delivery of miR-29b and germacrone based on cyclic RGD-modified nanoparticles for liver fibrosis therapy," *Journal of Nanobiotechnology*, vol. 18, no. 1, p. 86, 2020.
- [38] M. W. Haaker, A. B. Vaandrager, and J. B. Helms, "Retinoids in health and disease: a role for hepatic stellate cells in affecting retinoid levels," *Biochimica et Biophysica Acta - Molecular and Cell Biology of Lipids*, vol. 1865, no. 6, article 158674, 2020.
- [39] D. Ezhilarasan, "Advantages and challenges in nanomedicines for chronic liver diseases: A hepatologist's perspectives," *European Journal of Pharmacology*, vol. 893, article 173832, 2021.
- [40] S. A. A. Radwan, W. H. El-Maadawy, A. N. ElMeshad, R. A. Shoukri, and C. Yousry, "Impact of reverse micelle loaded lipid nanocapsules on the delivery of gallic acid into activated hepatic stellate cells: a promising therapeutic approach for hepatic fibrosis," *Pharmaceutical Research*, vol. 37, no. 9, p. 180, 2020.
- [41] Z. Zhang, C. Wang, Y. Zha et al., "Corona-directed nucleic acid delivery into hepatic stellate cells for liver fibrosis therapy," *ACS Nano*, vol. 9, no. 3, pp. 2405–2419, 2015.
- [42] M. C. Xiao, H. Qian, C. K. Huang et al., "Imatinib inhibits the malignancy of hepatocellular carcinoma by suppressing autophagy," *European Journal of Pharmacology*, vol. 906, article 174217, 2021.
- [43] K. Qu, Z. Huang, T. Lin et al., "New insight into the anti-liver fibrosis effect of multitargeted tyrosine kinase inhibitors: from molecular target to clinical trials," *Frontiers in Pharmacology*, vol. 6, p. 300, 2016.
- [44] N. S. El-Mezayen, W. F. El-Hadidy, W. M. El-Refaie, T. I. Shalaby, M. M. Khatib, and A. S. El-Khatib, "Hepatic stellate cell-targeted imatinib nanomedicine versus conventional imatinib: A novel strategy with potent efficacy in experimental liver fibrosis," *Journal of Controlled Release*, vol. 266, pp. 226–237, 2017.
- [45] Q. Q. Fan, C. L. Zhang, J. B. Qiao et al., "Extracellular matrix-penetrating nanodiamond micelles for liver fibrosis therapy," *Biomaterials*, vol. 230, p. 119616, 2020.
- [46] M. Yalniz, A. Demir, A. Arslan, and M. Cihangiroglu, "Short term effects of valsartan on portal blood flow in cirrhotic patients," *The Turkish Journal of Gastroenterology*, vol. 14, no. 1, pp. 18–25, 2003.
- [47] C. Fierbinteanu-Braticicevi, P. Dragomir, L. Tribus et al., "The effect of valsartan, an angiotensin II receptor antagonist, on portal and systemic hemodynamics and on renal function in liver cirrhosis," *Journal of Gastrointestinal and Liver Diseases*, vol. 15, no. 4, pp. 337–342, 2006.
- [48] L. J. Huo, Y. Liu, and S. J. Zhang, "Effect of valsartan on portal pressure and hepatic fibrosis in patients with hepatic cirrhosis," *World Chinese Journal of Digestology*, vol. 17, no. 11, pp. 1139–1142, 2009.
- [49] G. Flesch, P. Müller, and P. Lloyd, "Absolute bioavailability and pharmacokinetics of valsartan, an angiotensin II receptor antagonist, in man," *European Journal of Clinical Pharmacology*, vol. 52, no. 2, pp. 115–120, 1997.
- [50] N. S. El-Mezayen, W. F. El-Hadidy, W. M. El-Refaie, T. I. Shalaby, M. M. Khatib, and A. S. El-Khatib, "Oral vitamin-A-coupled valsartan nanomedicine: high hepatic stellate cell receptors accessibility and prolonged enterohepatic residence," *Journal of Controlled Release*, vol. 283, pp. 32–44, 2018.
- [51] A. Das, P. Mukherjee, S. K. Singla et al., "Fabrication and characterization of an inorganic gold and silica nanoparticle mediated drug delivery system for nitric oxide," *Nanotechnology*, vol. 21, no. 30, p. 305102, 2010.
- [52] H. T. Duong, Z. Dong, L. Su et al., "The use of nanoparticles to deliver nitric oxide to hepatic stellate cells for treating liver fibrosis and portal hypertension," *Small*, vol. 11, no. 19, pp. 2291–2304, 2015.
- [53] R. Omar, J. Yang, H. Liu, N. M. Davies, and Y. Gong, "Hepatic stellate cells in liver fibrosis and siRNA-based therapy," *Reviews of Physiology, Biochemistry and Pharmacology*, vol. 172, pp. 1–37, 2016.
- [54] Z. Zhao, C. Y. Lin, and K. Cheng, "siRNA- and miRNA-based therapeutics for liver fibrosis," *Translational Research*, vol. 214, pp. 17–29, 2019.
- [55] R. S. Shukla, B. Qin, Y. J. Wan, and K. Cheng, "PCBP2 siRNA reverses the alcohol-induced pro-fibrogenic effects in hepatic stellate cells," *Pharmaceutical Research*, vol. 28, no. 12, pp. 3058–3068, 2011.
- [56] R. S. Shukla, A. Jain, Z. Zhao, and K. Cheng, "Intracellular trafficking and exocytosis of a multi-component siRNA nanocomplex," *Nanomedicine*, vol. 12, no. 5, pp. 1323–1334, 2016.
- [57] Z. Zhao, Y. Li, A. Jain et al., "Development of a peptide-modified siRNA nanocomplex for hepatic stellate cells," *Nanomedicine*, vol. 14, no. 1, pp. 51–61, 2018.
- [58] R. C. Cheung, T. B. Ng, J. H. Wong, and W. Y. Chan, "Chitosan: an update on potential biomedical and pharmaceutical applications," *Marine Drugs*, vol. 13, no. 8, pp. 5156–5186, 2015.
- [59] M. Azzam, S. El Safy, S. A. Abdelgelil et al., "Targeting activated hepatic stellate cells using collagen-binding chitosan nanoparticles for siRNA delivery to fibrotic livers," *Pharmaceutics*, vol. 12, no. 6, p. 590, 2020.
- [60] A. El-Karef, M. Kaito, H. Tanaka et al., "Expression of large tenascin-C splice variants by hepatic stellate cells/myofibroblasts in chronic hepatitis C," *Journal of Hepatology*, vol. 46, no. 4, pp. 664–673, 2007.
- [61] J. C. Ma, X. Huang, Y. W. Shen et al., "Tenascin-C promotes migration of hepatic stellate cells and production of type I collagen," *Bioscience, Biotechnology, and Biochemistry*, vol. 80, no. 8, pp. 1470–1477, 2016.
- [62] J. L. Vivero-Escoto, H. Vadarevu, R. Juneja, L. W. Schrum, and J. H. Benbow, "Nanoparticle mediated silencing of tenascin C in hepatic stellate cells: effect on inflammatory gene expression and cell migration," *Journal of Materials Chemistry B*, vol. 7, no. 46, pp. 7396–7405, 2019.
- [63] J. Li, M. Ghazwani, Y. Zhang et al., "miR-122 regulates collagen production via targeting hepatic stellate cells and suppressing P4HA1 expression," *Journal of Hepatology*, vol. 58, no. 3, pp. 522–528, 2013.
- [64] J. Wang, E. S. Chu, H. Y. Chen et al., "microRNA-29b prevents liver fibrosis by attenuating hepatic stellate cell activation and inducing apoptosis through targeting PI3K/AKT pathway," *Oncotarget*, vol. 6, no. 9, pp. 7325–7338, 2015.
- [65] C. Liang, S. Bu, and X. Fan, "Suppressive effect of microRNA-29b on hepatic stellate cell activation and its crosstalk with TGF- $\beta$ 1/Smad3," *Cell Biochemistry and Function*, vol. 34, no. 5, pp. 326–333, 2016.
- [66] J. Wu, J. Huang, S. Kuang et al., "Synergistic microRNA therapy in liver fibrotic rat using MRI-visible nanocarrier targeting hepatic stellate cells," *Advanced Science*, vol. 6, no. 5, article 1801809, 2019.

- [67] S. A. A. Radwan, W. H. El-Maadawy, C. Yousry, A. N. ElMeshad, and R. A. Shoukri, "Zein/Phospholipid composite nanoparticles for successful delivery of gallic acid into aHSCs: influence of size, surface charge, and vitamin a Coupling," *International Journal of Nanomedicine*, vol. 15, pp. 7995–8018, 2020.
- [68] S. Huang, S. J. Chang, M. Yang, J. J. Chen, and W. H. Chang, "Nanoscale hepatoprotective herbal decoction attenuates hepatic stellate cell activity and chloroform-induced liver damage in mice," *International Journal of Nanomedicine*, vol. 6, pp. 1365–1371, 2011.

## Research Article

# Mycosynthesis and Physicochemical Characterization of Vanadium Oxide Nanoparticles Using the Cell-Free Filtrate of *Fusarium oxysporum* and Evaluation of Their Cytotoxic and Antifungal Activities

Mohammadhassan Gholami-Shabani <sup>1</sup>, Fattah Sotoodehnejadnematlahi <sup>1</sup>,  
Masoomeh Shams-Ghahfarokhi <sup>2</sup>, Ali Eslamifar <sup>3</sup>, and Mehdi Razzaghi-Abyaneh <sup>4</sup>

<sup>1</sup>Department of Biology, Science and Research Branch, Islamic Azad University, Tehran, Iran

<sup>2</sup>Department of Mycology, Faculty of Medical Sciences, Tarbiat Modares University, Tehran 14115-331, Iran

<sup>3</sup>Department of Clinical Research, Pasteur Institute of Iran, Tehran, Iran

<sup>4</sup>Department of Mycology, Pasteur Institute of Iran, Tehran 1316943551, Iran

Correspondence should be addressed to Fattah Sotoodehnejadnematlahi; [fattah212@gmail.com](mailto:fattah212@gmail.com)  
and Mehdi Razzaghi-Abyaneh; [mrab442@yahoo.com](mailto:mrab442@yahoo.com)

Received 27 August 2021; Revised 29 September 2021; Accepted 4 October 2021; Published 22 October 2021

Academic Editor: Shanmugam Rajeshkumar

Copyright © 2021 Mohammadhassan Gholami-Shabani et al. This is an open access article distributed under the Creative Commons Attribution License, which permits unrestricted use, distribution, and reproduction in any medium, provided the original work is properly cited.

Green nanotechnology is an expanding branch of knowledge in relation to producing efficient antifungal compounds with potential applications as nanomedicines. The aim of the current investigation was to mycosynthesize functional vanadium oxide nanoparticles ( $V_2O_5$ NPs) by *Fusarium oxysporum* cell-free filtrate using ammonium metavanadate ( $NH_4VO_3$ ) as the substrate. Various spectrometric methods and electron microscopy were used to confirm the production of mycosynthesized  $V_2O_5$ NPs. FESEM and TEM images showed that  $V_2O_5$ NPs were in the size ranging from 10 to 20 nm in a spherical shape. The XRD pattern revealed the presence of crystalline, dominantly spherical  $V_2O_5$ NPs in the sample with a size ranging from 10 to 20 nm. The XRD peaks 15.2, 20.1, 21.6, 26.1, 30.9, 32.2, 33.1, 34.2, 41.0, 41.8, 45.3, 47.2, 48.6, 51.1, 51.9, 55.4, and 58.8 can be assigned to the plane of vanadium crystals and indicate that the  $V_2O_5$ NPs were face-centered, cubic, and crystalline in nature. The FTIR results showed the presence of some biomolecules in fungal cell-free filtrate that act as a bioreducing and capping agent for  $V_2O_5$ NP mycosynthesis. DLS showed that the size of  $V_2O_5$ NPs was 10-20 nm. Zeta potential showed  $-35.09$  mV for  $V_2O_5$ NPs with a single peak. Study of antifungal activity of  $V_2O_5$ NPs against various pathogenic fungi in concentrations of 5, 25, 50, and  $100 \mu\text{g/mL}$  showed that  $V_2O_5$ NPs strongly inhibited both mycelium growth (20.3 to 67.3%) and spore germination (64.8 to 89.9%) dose-dependently.  $V_2O_5$ NPs showed strong cytotoxicity against breast cancer cell-line MCF-7 with an  $IC_{50}$  value of  $55.89 \mu\text{g/mL}$ . Microscopy images showed morphological changes and reduction of cancer cell populations in  $V_2O_5$ NP-treated MCF-7 cell-line. Taken together, our results demonstrated that bioactive  $V_2O_5$ NPs successfully synthesized by *F. oxysporum* could be considered a potential candidate in drug development against life-threatening fungal pathogens and as a feasible anticancer agent.

## 1. Introduction

Nowadays, nanoparticles (NPs) have been widely studied for their antimicrobial activities and anticancer properties and to combat any life-threatening disease as medicine [1–3]. Most of the current approaches for manufacturing NPs are

based on the usage of chemicals, including strong reducing agents, organic solvents, or surfactants [4–6]. Although chemically synthesized NPs possess unique properties with potentially broad-ranging application, there is a clear tendency toward synthesis of NPs by nontoxic safe green approaches using microorganisms and plants [7–9].

Development of clean and ecofriendly procedures is essential in the nanotechnology field, as many organisms like plant, fungi, and bacteria have the capability to produce inorganic nanostructures and organic NPs [10]. A wide array of established and newly developed physical, chemical, physicochemical, and biological methods have been successfully used for producing various NPs [11, 12].

Fungi are being employed in nanotechnology for the manufacture of NPs; biosynthesis using various fungi has displayed that this environmentally benign and renewable source can be operated as an effective bioreducing agent for the biosynthesis of NPs [13]. The biosynthesis of NPs by fungi (yeasts, molds, and mushrooms) and their subsequent application, exclusively in medical science, are studied under “myconanotechnology.” The possible use of fungi because they are simple to culture in bulk form [14]. Extracellular secretion of enzymes/proteins to produce NPs has an additional advantage in the handling of biomass and downstream processing [15]. Extracellularly secreted fungal biomolecules are able to trap heavy metals and metal salts on the cell surface and subsequently bioreducing them by enzymes/proteins to easily recover from the process, while in intracellular biosynthesis, heavy metal ions are transported into the microbial cell to produce NPs in the attendance of enzymes, and the NPs are difficult to recover in pure form [16].

Vanadium (V) metal was first isolated in 1869 by the English chemist named Henry Enfield Roscoe. V generally has diverse oxidation numbers that give various oxide structures, for instance, VO, V<sub>2</sub>O<sub>3</sub>, VO<sub>2</sub>, and V<sub>2</sub>O<sub>5</sub>, of which the latter is possibly the most investigated one, due to its thermodynamic stability. Vanadium oxide (V<sub>2</sub>O<sub>5</sub>) appears as a yellow to red crystalline powder or orange solid which plays an important role in the industry, agriculture, and medicine especially in producing biologically active nanomaterials [17–21].

Vanadium nanoparticles have received major consideration due to their unique characteristics and various applications in the structure of sensors, electrode materials for electrochemical capacitors, electrochromic and optical switching devices, and windows for solar cells [22]. Vanadium oxide nanoparticles (V<sub>2</sub>O<sub>5</sub>NPs) have been successfully synthesized by conventional approaches using chemical compounds as the base source and capping agent [23]. With the growth of knowledge in science and technology, V<sub>2</sub>O<sub>5</sub>NPs can be now biosynthesized with safe and effective green chemistry using microorganisms and plants. To our knowledge, green synthesis of V<sub>2</sub>O<sub>5</sub>NPs is still limited, for instance, to *Saccharomyces cerevisiae*, leaf extract of *Moringa oleifera*, and *Foeniculum vulgare* stem extract [24, 25].

The present study brings the information about mycosynthesis on V<sub>2</sub>O<sub>5</sub>NPs using a cell-free filtrate of the filamentous fungus, *F. oxysporum* PTCC 5115, as a bioreducing and stabilizing agent for the first time. Successfully synthesized V<sub>2</sub>O<sub>5</sub>NPs were characterized using different techniques such as UV-visible spectroscopy, Fourier transform infrared spectroscopy (FTIR), transmission electron microscopy (TEM), field emission scanning electron microscope (FESEM), X-ray diffraction (XRD), and dynamic

light scattering (DLS) techniques. Furthermore, the antifungal activity of mycosynthesized V<sub>2</sub>O<sub>5</sub>NPs was evaluated against different plant and human fungal pathogens, and their cytotoxic effects against the human breast cancer MCF-7 cell-line was investigated.

## 2. Materials and Methods

**2.1. Chemicals.** Ammonium metavanadate (NH<sub>4</sub>VO<sub>3</sub>) was purchased from Sigma-Aldrich, USA. Sabouraud dextrose agar (SDA), potato dextrose agar (PDA), potato dextrose broth (PDB), glucose, peptone, malt, and yeast extract were purchased from Merck, Germany. All other solvents and reagents were of analytical grade prepared from international companies.

**2.2. Strain, Culture Conditions, and Preparation of Fungal Cell-Free Extracts.** *Fusarium oxysporum* PTCC 5115 (CBS 620.87) was obtained from the Iran Research Organization for Science and Technology, Tehran, Iran (<https://irost.org/ptcc/ptccdb/node/649>). The fungus was grown on SDA slants for 5 days at 28°C. The mycelia were separated from the culture medium and aseptically transferred to a liquid medium containing glucose 10 g, peptone 5 g, yeast extract 3 g, malt extract 3 g, and 1000 mL distilled water [26]. The submerged cultures were incubated on a shaker incubator (LABTECH, Korea) for 4 days at 26°C with shaking (200 rpm). Fungal biomass was washed three times with sterile distilled water under aseptic conditions to remove any medium residual component from the respective biomass and subcultured to new cultures in sterile distilled water at the above conditions for 2 days. Finally, cultures were centrifuged (5000 × g, 20 min, 4°C, AWEL Centrifuge, France) to remove fungal mycelia. The clear cell-free was obtained by filtration (Whatman filter paper) and stored at –70°C for further use in V<sub>2</sub>O<sub>5</sub>NP synthesis.

**2.3. Mycosynthesis of V<sub>2</sub>O<sub>5</sub>NPs.** The extracellular mycosynthesis of the V<sub>2</sub>O<sub>5</sub>NPs was carried out using cell-free filtrate of *F. oxysporum* with some modifications [27, 28]. 1 mL of fungal cell-free filtrate was mixed with 1 mL of NH<sub>4</sub>VO<sub>3</sub> (1 mM solution). The mixture was shaken for further 96 h at room temperature under dark conditions. The secretion of large amounts of bioactive substances into the supernatant led to the mycosynthesis of V<sub>2</sub>O<sub>5</sub>NPs. Absorption spectra of the supernatant contained V<sub>2</sub>O<sub>5</sub>NPs were recorded on a PerkinElmer EZ301 UV-visible spectrophotometer.

**2.4. Characterization of Mycosynthesized V<sub>2</sub>O<sub>5</sub>NPs.** Characterization of mycosynthesized V<sub>2</sub>O<sub>5</sub>NPs was performed using different approaches including the UV-visible spectroscopy, FTIR, DLS, FESEM, and TEM.

**2.4.1. UV-Visible Spectrophotometry.** UV-Vis spectroscopy was used to confirm mycosynthesized V<sub>2</sub>O<sub>5</sub>NPs. The wavelength of green-synthesized V<sub>2</sub>O<sub>5</sub>NPs based on light absorbance (300 to 700 nm) with resolution of 1 nm was measured by loading 2 mL of sample in a quartz cuvette in a UV-Vis spectroscope (PerkinElmer, United States). The

reaction was monitored by measuring the absorbance at 1, 8, 16, 32, 48, 72, and 96 h [24, 25].

**2.4.2. DLS Analysis.** The dynamic light scattering (DLS) particle size analysis was considered a very fast, reproducible, and reliable technique to measure a wide range of NPs [29]. In the present study, the DLS (Malvern Zetasizer Nano ZEN3600, United Kingdom) was used to measure the size and distribution pattern of mycosynthesized  $V_2O_5$ NPs. A sample of 50  $\mu\text{g}$  of  $V_2O_5$ NPs was dispersed in 20 mL ultrapure water and sonicated for 20 min. 5 mL of the dispersed  $V_2O_5$ NPs was loaded on DLS to determine the size of mycosynthesized  $V_2O_5$ NPs. The stability of the  $V_2O_5$ NPs was assessed in terms of zeta potential using the above DLS allowing to run from -200 mV to +200 mV and plotting the data in a graph.

**2.4.3. FESEM Examination.** The field emission scanning electron microscope (FESEM-FEI NanoSEM 450) was used to image the  $V_2O_5$ NPs. A sample of 50  $\mu\text{g}$  of  $V_2O_5$ NPs was dispersed in 20 mL ultrapure water and sonicated for 20 min. A small drop of sample was used, and the images were captured at various magnifications [30].

**2.4.4. TEM Observations.** Transmission electron microscopy (TEM-Philips CM200) was used to image the mycosynthesized  $V_2O_5$ NPs. For the above purpose of the pasteurizing image,  $V_2O_5$ NPs were dispersed in ultrapure water and sonicated for 20 min. The resultant solution (a small drop) was placed on a 300-mesh lacy carbon-coated copper grid and dried, and the images were captured [31].

**2.4.5. XRD Analysis.** The air-dried  $V_2O_5$ NPs were coated onto an X-ray diffraction (XRD) grid and analyzed for the formation of  $V_2O_5$ NPs by a Philips PW 1390 X-ray diffractometer at a voltage of 20-100 kV. Two grams of fine-powder  $V_2O_5$ NPs with thickness of 0.2 cm in a uniform layer on one side was used for tacking diffractograms. The diffracted intensities were recorded from  $2\theta$  angles, and a graph was drawn by the standard method [24, 31].

**2.4.6. FTIR Analysis.** For the FTIR analysis, a sample of 50  $\mu\text{g}$  of  $V_2O_5$ NPs was used, and the spectra were scanned ( $400\text{--}4000\text{ cm}^{-1}$ , resolution of  $4\text{ cm}^{-1}$ ) for the characterization of chemical functional groups present over the surface of mycosynthesized  $V_2O_5$ NPs. The FTIR data measures the interaction between  $V_2O_5$  and biomolecules [24, 25].

**2.5. Effects of  $V_2O_5$ NPs on Fungal Radial Growth and Spore Germination.** The effect of the  $V_2O_5$ NPs on the growth of selected fungi *Fusarium oxysporum* PTCC 5115, *Fusarium graminearum* PFCC 573, *Aspergillus fumigatus* PTCC 5009, *Aspergillus niger* PTCC 5010, *Aspergillus flavus* PFCC 113, *Alternaria alternata* PFCC 436, and *Penicillium citrinum* PFCC 549 obtained from Iran Research Organization for Science and Technology, Tehran, Iran (PTCC strains), and Pathogenic Fungi Culture Collection of the Pasteur Institute of Iran, Tehran, Iran (PFCC strains), was studied using the food-poisoning process [32].  $V_2O_5$ NPs at variable concentrations were poured into each sterile Petri dish; a

PDA medium was added to each sterile Petri dish which gave a PDA- $V_2O_5$ NP mixture with corresponding 5, 25, 50, and 100  $\mu\text{g}/\text{mL}$   $V_2O_5$ NP concentrations. These Petri dishes were softly rotated to ensure dispersion of the  $V_2O_5$ NPs. The agar- $V_2O_5$ NP combination was allowed to solidify. All Petri dishes were inoculated at the center with a thickness of 4 mm diameter agar containing a pure culture of each fungus. The control trial was used with distilled water without the addition of  $V_2O_5$ NPs. Then, Petri dishes were incubated at  $28^\circ\text{C}$  for 5 days. Finally, the fungal growth inhibition induced by  $V_2O_5$ NPs was calculated according to the technique described by Ebadzadsahrai et al. [32].

The effect of various concentrations of the  $V_2O_5$ NPs on spore germination of selected fungi was investigated. Spore suspensions of selected pathogenic fungi were prepared from 7-day-old pure cultures on potato dextrose agar (PDA) slants by gentle rubbing of culture surfaces using a sterile glass rod. Spore suspension of each fungus ( $10^3$  spores/mL) was exposed to  $V_2O_5$ NPs in various concentrations (5, 25, 50, and 100  $\mu\text{g}/\text{mL}$ ) in Falcon tubes containing potato dextrose broth (PDB). After 30 min incubation of tubes at  $28^\circ\text{C}$ , one drop of lactophenol cotton blue was separately added to the spore suspension of each fungus on glass slides, and the percentage of spore germination was recorded under microscope ( $\times 400$ ) according to Begum et al. [33].

## 2.6. Cytotoxicity Effect of Mycosynthesized $V_2O_5$ NPs

**2.6.1. MTT Assay of Mycosynthesized  $V_2O_5$ NPs.** The cytotoxicity effect of  $V_2O_5$ NPs was determined by the MTT assay [34]. The MCF-7 cell-lines were obtained from the National Cell Bank (NCBI), Pasteur Institute of Iran, Tehran, Iran. The cancerous MCF-7 cell-lines were cultured into Dulbecco's modified Eagle's medium (DMEM) containing fetal bovine serum (10%, FBS), glutamine (2 mM), and antibiotics (amphotericin B, penicillin G, and streptomycin, 50, 60, and 100 mg/L, respectively) under a relatively humid atmosphere ( $37^\circ\text{C}$ , 5%  $\text{CO}_2$ ). Briefly,  $1 \times 10^5$  cells/well were treated with diverse concentrations of  $V_2O_5$ NPs (10-100  $\mu\text{g}/\text{mL}$ ). After a 24 h incubation, the cells were washed two times by sterile phosphate-buffered saline (PBS), and 3-[4, 5-dimethylthiazol-2-yl]-2, 5-triphenyltetrazolium bromide (MTT or thiazolyl blue; 0.5 mg/mL PBS) was added to the wells and incubated at  $37^\circ\text{C}$  for 4 h. The blue formazan crystals that formed were dissolved through adding dimethyl sulfoxide (100  $\mu\text{L}/\text{well}$ ), and the absorbance was read by a microplate scanning spectrophotometer at 570 nm (ELISA reader, Organon Teknika, Netherlands). The  $\text{IC}_{50}$  values of  $V_2O_5$ NPs on cancerous cells lines were then determined.

**2.6.2. Cell Cytotoxicity Analysis by Optical Microscopy.** Optical microscopic evaluation of the MCF-7 cells was performed to observe the morphological changes after exposure to  $V_2O_5$ NPs [35, 36]. MCF-7 cells were grown in a well plate and treated with  $V_2O_5$ NPs at the  $\text{IC}_{50}$  concentration for 24 h. The morphological changes of cells were observed under an invert optical microscope (Olympus, Japan).

**2.6.3. Cell Cytotoxicity Analysis Using AO/EB Staining.** Study of acridine orange (AO)/ethidium bromide (EB) fluorescent staining was performed according to the previous method with a few modifications [35]. Briefly, the MCF-7 cells ( $1 \times 10^5$ /well) were deposited in a plate and treated by the  $IC_{50}$  concentration of  $V_2O_5$ NPs at  $37^\circ C$  for 24 h. The cells were collected, washed once with sterile PBS, and then suspended with sterile PBS. For AO/EB fluorescent staining,  $1 \mu L$  of AO/EB (Sigma) dye mixture (10 mg/mL of AO/EB in PBS) was added to  $9 \mu L$  of cell suspension and then covered with a cover slip on a clean slide. After incubation for 3 min, the cells were observed under a fluorescence microscope (Olympus, Japan).

**2.6.4. Cell Cytotoxicity Analysis Using SEM and TEM.** MCF-7 cells were prepared for scanning (SEM) and transmission electron microscopy (TEM) analysis according to the previous method with a few modifications [37]. Briefly, the cells were incubated for 24 h with mycosynthesized  $V_2O_5$ NPs at the  $IC_{50}$  concentration. The cells were harvested and fixed in 2.5% glutaraldehyde, washed with sodium cacodylate buffer, postfixed with 1% osmium tetroxide, dehydrated using gradual concentrations of ethanol, and dried using hexamethyldisilazane. Finally, the morphological changes of the cells were observed using SEM and TEM microscopy.

**2.6.5. Cell Cytotoxicity Analysis by DNA Fragmentation.** DNA fragmentation was performed according to a previous method [35]. An amount of  $1 \times 10^5$  MCF-7 cells was exposed to  $V_2O_5$ NPs at  $IC_{50}$  concentrations at  $37^\circ C$  for 24 h. After slight harvesting with centrifugation, the cells were suspended in 10 mL of 10 mM TE buffer solution (pH 8.0, 10 mM EDTA, 10 mM Tris-HCl, 2% SDS, and 20 mg/mL proteinase K). The mixture was incubated for 3 h at  $37^\circ C$ , followed by DNA extraction. The DNA was treated with DNase-free RNase (20 mg/mL concentration,  $4^\circ C$  for 45 min) and precipitated with sodium acetate (100 mL, 2.5 M) and three volumes of absolute ethanol. A DNA fragmentation study was carried out with  $10 \mu L$  of DNA prepared from treated cells by mycosynthesized  $V_2O_5$ NPs at the  $IC_{50}$  concentration and analyzed by electrophoresis on 1.5% agarose gel containing ethidium bromide for a period of 45 min at 100 V.

**2.7. Statistical Analysis.** The data were analyzed using the GraphPad Prism software Version 9.0, and  $P$  values under 0.05 were considered significant.

### 3. Results

**3.1. Mycosynthesis of  $V_2O_5$ NPs.** Exposure of the cell-free fungal culture filtrate of *F. oxysporum* to  $NH_4VO_3$  (1 mM final concentration) resulted in a time-dependent color change of the reaction mixture from light-yellowish to dark-brown, suggesting the successful biosynthesis of  $V_2O_5$ NPs. The change in color indicated the completion of reaction with vanadium ions. The intensity of color was correlated with the increase in the number of mycosynthesized  $V_2O_5$ NPs. At the same condition, the fungal culture filtrate (positive

control) and the  $NH_4VO_3$  solution (negative control) did not show any visual alteration.

#### 3.2. Characterization of Mycosynthesized $V_2O_5$ NPs

**3.2.1. UV-Visible Spectrophotometric Results.** The absorption peak was obtained in the visible range at 410 nm after 96 h (Figure 1(a)). The UV scan of mycosynthesized  $V_2O_5$ NPs revealed an absorbance peak of 410 nm, implying that  $V_2O_5$ NPs were successfully synthesized. Figure 1(b) shows the absorption peak of fungal cell-free filtrate and the  $NH_4VO_3$  solution.

**3.2.2. DLS Observations.** The DLS data has revealed that the size of mycosynthesized  $V_2O_5$ NPs was around 10–20 nm (Figure 2(a)). Further zeta potential of  $V_2O_5$ NPs was found to be  $-35.09$  mV indicating its good stability of the bioreduced  $V_2O_5$ NPs (Figure 2(b)). The negative zeta potential value could be due to the capping of natural compounds present in the fungal cell-free filtrate. This negative value has indicated the strong repellent forces between particles due to high electrical charge on the surface of  $V_2O_5$ NPs, which in turn results in higher stability by preventing the aggregation of  $V_2O_5$ NPs.

**3.2.3. FESEM and TEM Observations.** Figures 3(a)–3(c) show the FESEM images of the mycosynthesized  $V_2O_5$ NPs in three magnifications implying that  $V_2O_5$ NPs were mostly spherical in shape with the estimated size ranging around 10–20 nm. Figure 3(d) shows the TEM analysis of the mycosynthesized  $V_2O_5$ NPs. TEM confirmed that the  $V_2O_5$ NPs were spherical in shape with the size ranging around 10–20 nm.

**3.2.4. XRD Results.** The crystallographic nature of the mycosynthesized  $V_2O_5$ NPs was determined through XRD analysis, and the obtained results are demonstrated in Figure 4. The distinctive major diffraction peaks appeared at  $2\theta = 15.2, 20.1, 21.6, 26.1, 30.9, 32.2, 33.1, 34.2, 41.0, 41.8, 45.3, 47.2, 48.6, 51.1, 51.9, 55.4,$  and  $58.8$  that corresponded to  $hkl$ , (200), (001), (101), (110), (310), (011), (111), (310), (002), (102), (411), (600), (302), (020), (601), (121), and (611) index planes. The obtained consequences were in good agreement with their standard JCPDS card No. 41-1426.

**3.2.5. FTIR Spectroscopy.** The  $V_2O_5$ NPs mycosynthesized by the cell-free fungal filtrate of *F. oxysporum* were not in direct contact, signifying stabilization of the NPs by a capping agent which was confirmed using the FTIR analysis. Figure 5 shows the FTIR spectrum of *F. oxysporum* cell-free filtrate,  $NH_4VO_3$ , and mycosynthesized  $V_2O_5$ NPs. The FTIR spectrum of mycosynthesized  $V_2O_5$ NPs showed five distinct peaks, 1311, 1759, 2090, 2521, and  $3403 \text{ cm}^{-1}$ .

**3.3. Effects of  $V_2O_5$ NPs on Fungal Radial Growth and Spore Germination.** The results of antifungal activity of  $V_2O_5$ NPs are summarized in Table 1 which shows the inhibition of fungal growth in the range of 20.3 to 67.3%. As shown in Figure 6, the dose-dependent inhibition of mycelium growth was observed for all tested fungi compared with nontreated controls. The  $V_2O_5$ NPs were able to inhibit the spore



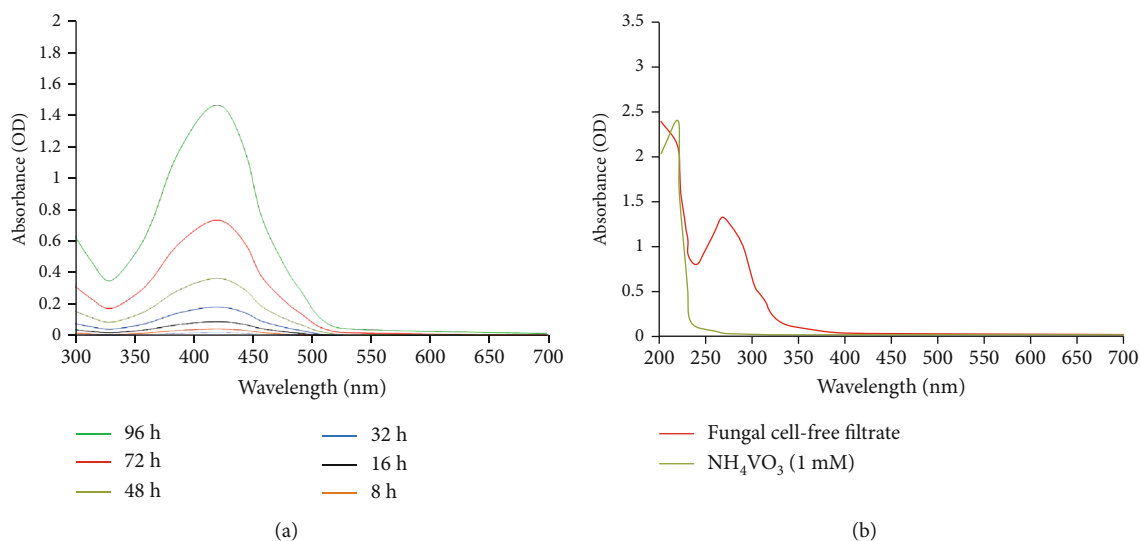


FIGURE 1: (a) The UV-Vis spectrum of extracellular fungal filtrate reaction with 1 mM  $\text{NH}_4\text{VO}_3$  solution ( $\text{V}_2\text{O}_5\text{NPs}$ ). Mycosynthesized  $\text{V}_2\text{O}_5\text{NPs}$  showed the maximum absorption peak at around 410 nm after 96 h. (b) Extracellular fungal filtrate and 1 mM  $\text{NH}_4\text{VO}_3$  solution.

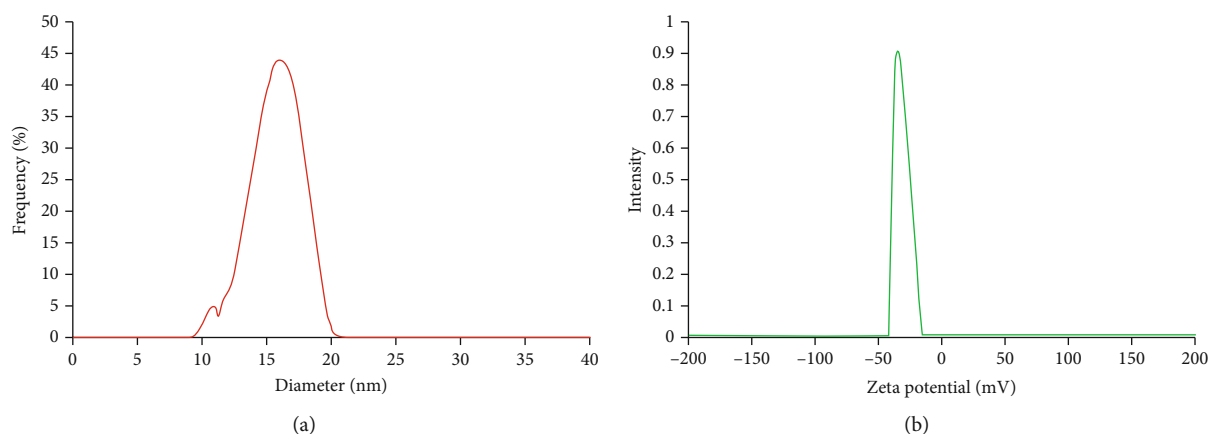


FIGURE 2: (a) DLS (particle size analysis) of mycosynthesized  $\text{V}_2\text{O}_5\text{NPs}$ . The size of mycosynthesized  $\text{V}_2\text{O}_5\text{NPs}$  was around 10–20 nm. (b) The zeta potential analysis of mycosynthesized  $\text{V}_2\text{O}_5\text{NPs}$ . The zeta potential was found to be  $-35.09$  mV demonstrating good stability of the bio-reduced  $\text{V}_2\text{O}_5\text{NPs}$ .

germination of all selected fungi in the range of 64.8 to 89.9% with the maximum inhibition at the  $100 \mu\text{g}/\text{mL}$  concentration (Table 1). The highest inhibition in spore germination was reported for *Aspergillus fumigatus*.

### 3.4. Cytotoxic Effect of Mycosynthesized $\text{V}_2\text{O}_5\text{NPs}$

**3.4.1. In Vitro Cytotoxicity in MTT Assay.** Figure 7 indicates the results obtained by MTT on MCF-7 cells exposed to  $1$ – $100 \mu\text{g}/\text{mL}$  of  $\text{V}_2\text{O}_5\text{NPs}$  after 24 h. A concentration-dependent reduction in the viability of MCF-7 cancer cell-line was reported in the range of 10.74% to 85.45% which was significant compared to the nontreated control at all concentrations. The  $\text{IC}_{50}$  of the  $\text{V}_2\text{O}_5\text{NPs}$  for MCF-7 was calculated as  $55.89 \mu\text{g}/\text{mL}$ .

**3.4.2. Cell Cytotoxicity Results in Optical Microscopy.** As indicated in Figure 8, the chromatids of cancer cells were condensed in a sample treated with the  $\text{IC}_{50}$  concentration of  $\text{V}_2\text{O}_5\text{NPs}$ . Progressive structural modification and reduction of cancer cell populations were also evident.

**3.4.3. Cell Cytotoxicity Observations by AO/EB Staining.** As shown in Figure 8, the morphology of the necrotic/dead, apoptotic, and normal/untreated cells of MCF-7 cells was recognized separately using fluorescence microscopy after staining by AO/EB based on the cell-membrane integrity. MCF-7 cells displayed a green fluorescence color that shows the presence of live cells in controls (untreated cells). Orange/yellow-colored cells contain proapoptotic bodies and red necrotic/dead cells found in the mycosynthesized  $\text{V}_2\text{O}_5\text{NP}$ -

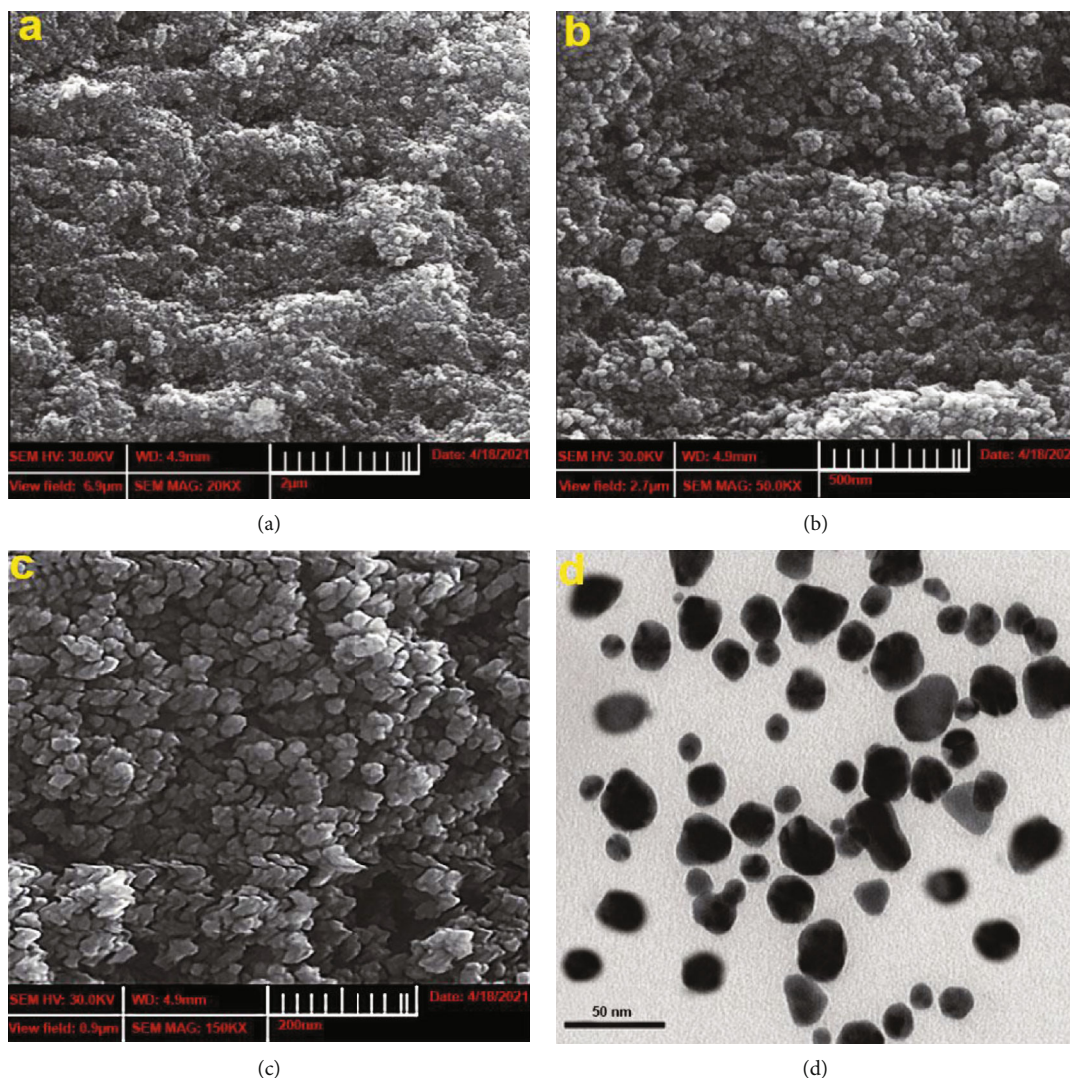


FIGURE 3: (a–c) The FESEM image of mycosynthesized  $V_2O_5$ NPs in different magnifications. The image indicates that  $V_2O_5$ NPs were mostly spherical in shape with the estimated size ranging around 10–20 nm. (d) TEM image of  $V_2O_5$ NPs mycosynthesized by fungal cell-free filtrate confirmed the FESEM image.

treated MCF-7 cell-lines (Figure 8). Microscopic observation indicated that the untreated viable cells were detected to be green because of the binding of AO into cell membranes, whereas proapoptotic cells were detected as orange/yellow-colored bodies due to the shrinkage of nuclei and nuclear blebbing because of the induction of EB into cells. However, the dead/necrotic cells were turned into a red color due to their loss of outer membrane integrity using mycosynthesized  $V_2O_5$ NPs.

**3.4.4. Cell Cytotoxicity Results by SEM and TEM.** After treatment with mycosynthesized  $V_2O_5$ NPs, the morphological changes were observed in treated MCF-7 cell-lines and also compared with normal/untreated cells. Figure 8 shows the SEM and TEM micrographs of the MCF-7 cell-line. The SEM micrograph shows that normal MCF-7 cancer cells (untreated) are round in shape and are characterized using short lamellipodia, whereas  $V_2O_5$ NP-treated cells show a semiflattened surface structure containing microvilli with

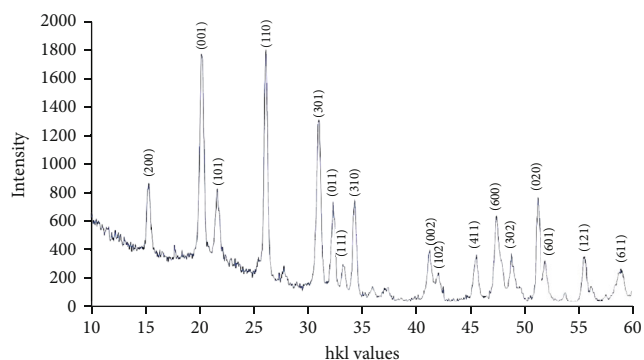


FIGURE 4: XRD spectra of  $V_2O_5$ NPs mycosynthesized by extracellular fungal filtrate. The typical main diffraction peaks appeared at  $2\theta = 15.2, 20.1, 21.6, 26.1, 30.9, 32.2, 33.1, 34.2, 41.0, 41.8, 45.3, 47.2, 48.6, 51.1, 51.9, 55.4, \text{ and } 58.8$  corresponding to  $hkl$ , (200), (001), (101), (110), (301), (011), (111), (310), (002), (102), (411), (600), (302), (020), (601), (121), and (611) index planes.

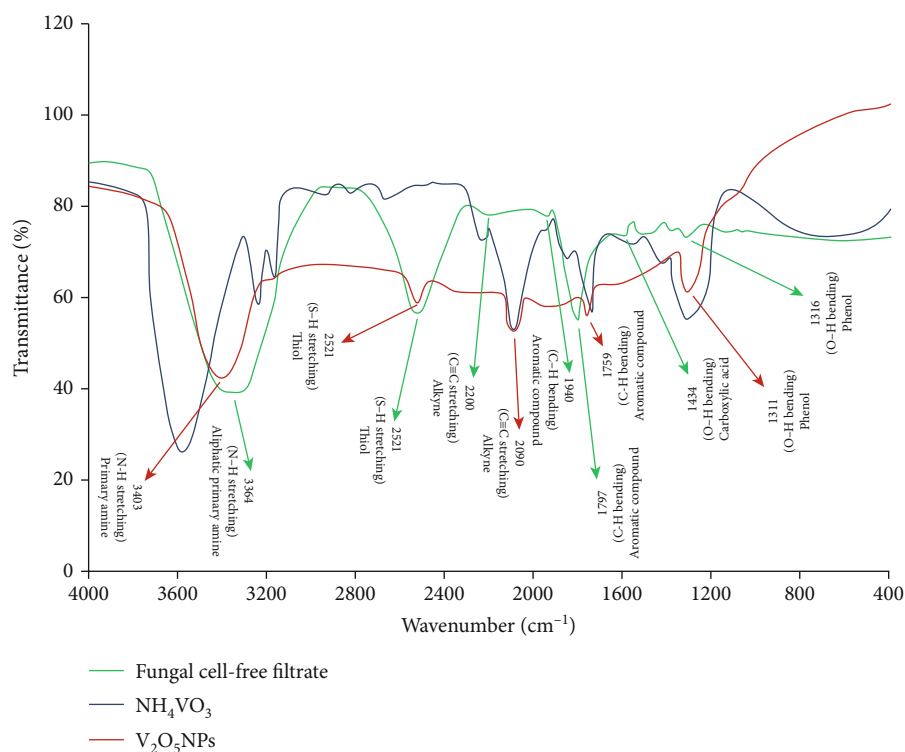


FIGURE 5: The FTIR spectrum of fungal cell-free filtrate,  $\text{NH}_4\text{VO}_3$ , and  $\text{V}_2\text{O}_5\text{NPs}$  mycosynthesized by extracellular fungal filtrate. For fungal cell-free filtrate, the peak at  $3364\text{ cm}^{-1}$  was associated with N-H stretching, peak at  $2521\text{ cm}^{-1}$  with S-H stretching, peaks at  $2200\text{ cm}^{-1}$  with  $\text{C}\equiv\text{C}$  stretching, peaks at  $1940$  and  $1797\text{ cm}^{-1}$  with C-H bending, and peaks at  $1434$  and  $1316\text{ cm}^{-1}$  with O-H bending. For mycosynthesized  $\text{V}_2\text{O}_5\text{NPs}$ , the peak at  $3403\text{ cm}^{-1}$  was associated with N-H stretching, peak at  $2521\text{ cm}^{-1}$  with S-H stretching, peaks at  $2090\text{ cm}^{-1}$  with  $\text{C}\equiv\text{C}$  stretching, peak at  $1759\text{ cm}^{-1}$  with C-H bending, and peak at  $1311\text{ cm}^{-1}$  with O-H bending. It was also confirmed that the carbonyl group from the protein and amino acid had stronger ability to bind with  $\text{V}_2\text{O}_5\text{NPs}$  or act as capping and stabilizing agents.

TABLE 1: Effect of  $\text{V}_2\text{O}_5\text{NPs}$  on spore germination (%) and radial mycelium growth (% of inhibition) of pathogenic fungi in comparison with non- $\text{V}_2\text{O}_5\text{NP}$ -treated control.

Fungi	$\text{V}_2\text{O}_5\text{NP}$ concentration ( $\mu\text{g/mL}$ )							
	5	25	50	100	5	25	50	100
	Spore germination (%)				Inhibition of mycelia growth (%)			
<i>Fusarium oxysporum</i>	31.3	22.6	15.4	12.2	20.3	28.6	46.1	67.3
<i>Fusarium graminearum</i>	33.2	26.5	17.8	16.3	25.2	30.5	52.0	62.2
<i>Aspergillus fumigatus</i>	29.7	23.2	15.6	10.1	28.3	32.1	46.6	61.0
<i>Aspergillus niger</i>	27.2	21.4	17.1	19.7	26.2	30.4	43.3	55.7
<i>Aspergillus flavus</i>	34.7	31.2	25.5	20.6	28.1	33.4	40.5	48.6
<i>Alternaria alternata</i>	35.2	27.2	22.8	18.3	32.2	43.2	56.1	57.0
<i>Penicillium citrinum</i>	32.3	27.9	19.6	14.3	28.2	48.2	52.5	58.0

Control: sterile distilled water.

extending lamellipodia known as membrane ruffles. The TEM micrograph displays morphological change in apoptotic characters in the mycosynthesized  $\text{V}_2\text{O}_5\text{NP}$ -treated MCF-7 cells. The cells show shrinkage, chromatin condensation, and integrity of plasma membrane.

#### 3.4.5. Cell Cytotoxicity Observations by DNA Fragmentation.

Study of DNA fragmentation/damage was carried out to detect whether the death of MCF-7 cells had occurred outstanding to the cytotoxic effect of mycosynthesized  $\text{V}_2\text{O}_5\text{NP}$  treatment. As shown in Figure 9, DNA ladder for-

mation with low molecular weight was detected in the  $\text{V}_2\text{O}_5\text{NP}$ -treated cells, while an intact DNA band was noticed in the control (normal/untreated) cell with high molecular weight.

## 4. Discussion

Like many other transition metals, vanadium possesses useful optical, electronic, magnetic, and catalytic properties. Vanadium nanoparticles have received major consideration in recent years due to use in developing of compounds with

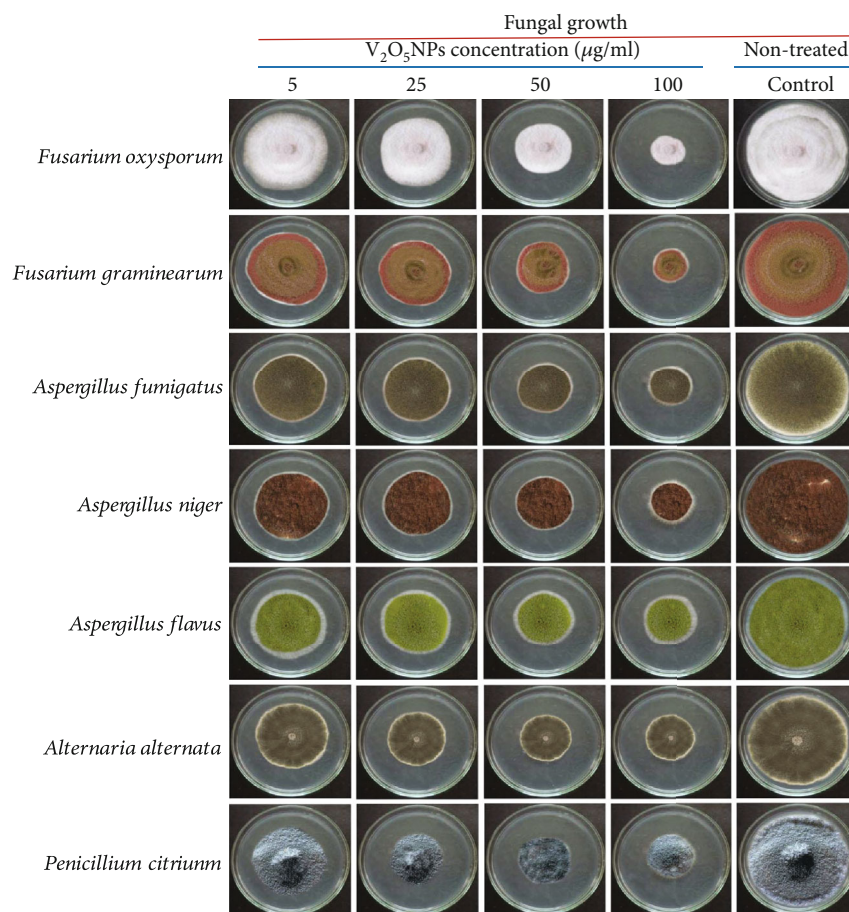


FIGURE 6: The radial growth of fungal mycelia of different pathogenic fungi exposed to various concentrations of V<sub>2</sub>O<sub>5</sub>NPs. A dose-dependent inhibition of fungal growth is evident for all tested fungi in comparison with nontreated controls. The highest inhibition of fungal growth is evident for 100 μg/mL of V<sub>2</sub>O<sub>5</sub>NP concentration.

novel biological applications and pharmacological properties [23].

In the present study, V<sub>2</sub>O<sub>5</sub>NPs were successfully synthesized by a green approach using *F. oxysporum* as a fungal cell factory. Synthesized V<sub>2</sub>O<sub>5</sub>NPs showed maximum absorption peak at around 410 nm. They were mostly spherical with size around 10–20 nm with a zeta potential value of -35.09 mV, indicating that capped biomolecules have a highly negatively charged surface. FTIR confirmed that the carbonyl group from the protein(s) and amino acid has a stronger ability to bind with V<sub>2</sub>O<sub>5</sub>NPs or acts as capping and stabilizing agents. Synthesized V<sub>2</sub>O<sub>5</sub>NPs showed strong antifungal properties against a wide variety of pathogenic fungi, cell cytotoxicity toward MCF-7 cancer cell-line which showed shrinkage, chromatin condensation, integrity of plasma membrane, and DNA fragmentation indicating possible cancer cell apoptosis.

Although biosynthesis of various metal nanoparticles by *F. oxysporum* has been reported and confirmed by different researchers [38–41], little has been documented about green synthesis of V<sub>2</sub>O<sub>5</sub>NPs using fungi. Likewise, in most cases, the biological activity of synthesized V<sub>2</sub>O<sub>5</sub>NPs has not been studied.

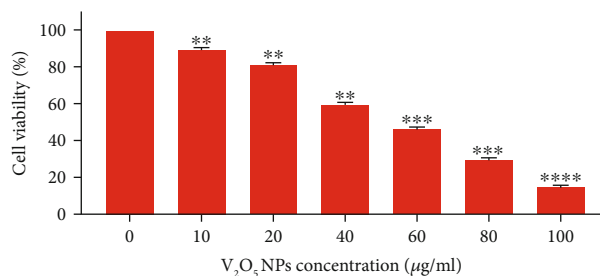


FIGURE 7: *In vitro* cytotoxicity of V<sub>2</sub>O<sub>5</sub>NPs for MCF-7 cell-lines examined by the MTT assay. All data were obtained from three independent ( $N = 3$ ) biological replicates in two separate experiments. Meaningful dose-dependent reduction in cell viability in the range of 10.74% to 85.45% is evident for all concentrations compared to nontreated control (\*\* $P \leq 0.01$ , \*\*\* $P \leq 0.001$ , \*\*\*\* $P \leq 0.0001$ ).

Aliyu et al. [25] reported green synthesis of vanadium nanoparticles with spherical shape by leaf extract of *Moringa oleifera* [25]. Synthesized NPs showed antibacterial activity toward *Escherichia coli* and *Salmonella typhi*, but they did not show any obvious antifungal activity against *Candida tropicalis* and *Candida albicans*. Prasad et al. [42] reported

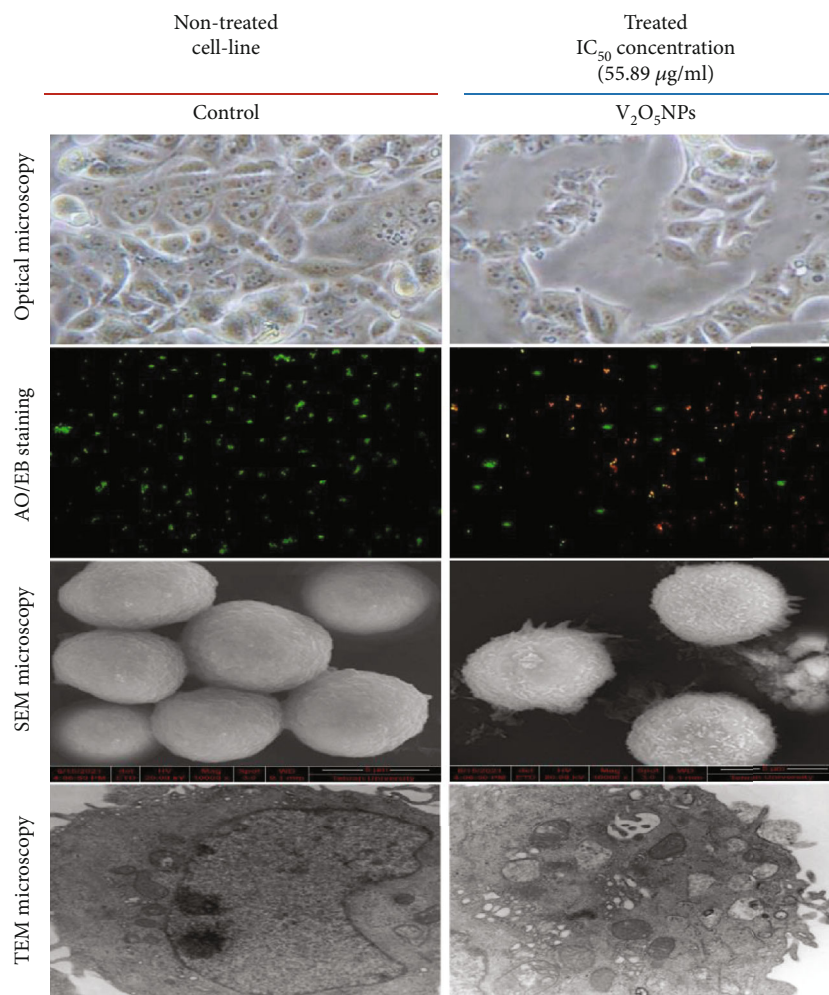


FIGURE 8: The optical, fluorescence, SEM, and TEM microscopy images of mycosynthesized V<sub>2</sub>O<sub>5</sub>NP-treated using IC<sub>50</sub> concentration (55.89  $\mu\text{g}/\text{mL}$ ) and normal/untreated MCF-7 cells. The morphological changes and reduction of cancer cell populations were observed in treated MCF-7 cell-line exposed to V<sub>2</sub>O<sub>5</sub>NPs compared with normal/nontreated cells. Optical microscopy showed that chromatids of cancer cells were condensed, when treated with the IC<sub>50</sub> concentration of V<sub>2</sub>O<sub>5</sub>NPs. AO/EB staining displayed that the nontreated proapoptotic cells and dead/necrotic cells were detected to be green, orange, or yellow, and because of the binding of AO into cell membranes, proapoptotic cells were detected as orange/yellow red color, respectively. TEM and SEM showed cell shrinkage, chromatin condensation, and integrity of plasma membrane after being treated with V<sub>2</sub>O<sub>5</sub>NPs.

green synthesis of vanadium oxide (10-60 nm) nanorods using *Phyllanthus amarus* [42]. They found that synthesized NPs had antibreast cancer properties. Farahmandjou and Abaeiyan [23] synthesized vanadium oxide NPs by a simple chemical technique using sodium metavanadate as a precursor and cetyltrimethylammonium bromide as the surfactant [23]. Synthesized NPs were in the range size of 5-10 nm.

Jabbar et al. [24] synthesized V<sub>2</sub>O<sub>5</sub>NPs using the *Foeniculum vulgare* stem. Synthesized NPs were around 78 nm with cubic-like agglomerated morphology. The maximum absorbance of the NPs was 452 nm at 50 minutes. The FTIR of their NPs showed three peaks at 940  $\text{cm}^{-1}$ , 835  $\text{cm}^{-1}$ , and 718  $\text{cm}^{-1}$ . NPs showed 2 peaks at  $2\theta = 20^\circ$  and  $26^\circ$  with the structural planes (001) and (101) in XRD [24].

Wasmi et al. [43] synthesized vanadium pentoxide NPs by the solvothermal synthesis process that has almost perfect rods with 60-90 nm in size [43]. Taylor et al. [44] synthesized vanadium pentoxide NPs using pulsed laser ablation.

Synthesized NPs have nearly spherical and flower-like morphologies. The colloidal solution of NPs had a zeta potential of  $-51$  mV. Indeed, solutions with zeta potential smaller than  $-30$  mV or larger than  $+30$  mV were considered stable [44].

Pinto et al. [45] synthesized vanadium NPs with size around 7 nm on activated carbon by the reduction of VCl<sub>3</sub> salt. Rasheed et al. [46] green-synthesized vanadium oxide-zirconium oxide nanocomposite using *Daphne alpine* leaf extracts. The size of their NPs was 41.74 nm with different shapes. The diffraction bands appeared at the  $2\theta$  position with corresponding  $hkl$  value positions of 21.40 (200), 28.16 (103), 34.04 (004), 36.67 (213), 42.80 (303), 43.68 (400), and 56.43 (501). The FTIR of their NPs was showed stretching vibration of the OH group at around 3499  $\text{cm}^{-1}$ . The peaks at around 3000 and 2942  $\text{cm}^{-1}$  are for C-H bending, whereas the band at 1725  $\text{cm}^{-1}$  may be due to the carbonyl group of ester and carboxylic acid. The bands at

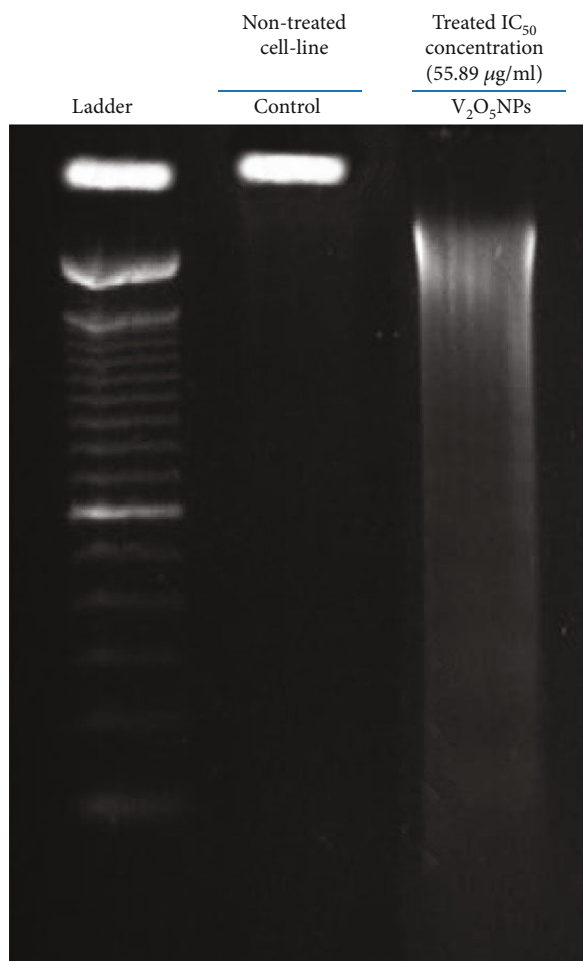


FIGURE 9: DNA fragmentation analysis of MCF-7 cell-lines. First line: 100 bp DNA ladder, second line: DNA from untreated/normal MCF-7 cell-line, and third line: DNA from mycosynthesized  $V_2O_5$ NP-treated MCF-7 cell-line. It was clear when the DNA of MCF-7 cell-line was treated with mycosynthesized  $V_2O_5$ NPs, DNA fragmentation has occurred compared with nontreated cell-line.

1433 and  $1220\text{ cm}^{-1}$  are attributed to the N=O bending mode and carbonyl stretching, respectively [46].

## 5. Conclusions

In the present study, we successfully synthesized biologically active  $V_2O_5$ NPs by a green approach using an extracellular fungal filtrate from a hyaline hyphomycete, *F. oxysporum*, in a single-step bioreduction of vanadium ions for the first time. Our green-synthesized  $V_2O_5$ NPs displayed strong inhibitory activity toward the growth and spore germination of a wide variety of pathogenic fungi indicating that they may be considered as potential therapeutic agents in drug development against life-threatening fungal pathogens. Furthermore, cytotoxic effects of  $V_2O_5$ NPs against the breast cancer MCF-7 cell-line make them suitable in the line of anticancer studies. Further works on *in vivo* cytotoxicity and antifungal activity of green-synthesized  $V_2O_5$ NPs in animal experimental models are recommended.

## Data Availability

All data generated or analyzed during this study are included in this published article.

## Conflicts of Interest

The authors declare that they have no competing interests.

## Authors' Contributions

M.G-S and M.R-A conceived, designed, and validated the study and wrote the manuscript. M.G-S., M.S-G, F.S, A.E, and M.R-A conducted the experiments and performed the data curation. All authors read and approved the final manuscript. M.R-A and F.S supervised the study.

## Acknowledgments

The research reported in this publication was supported by the Elite Researcher Grant Committee under award numbers 958634 and 963646 from the National Institute for Medical Research Development (NIMAD), Tehran, Iran, to M.R-A.

## References

- [1] A. Aygun, F. Gülbagca, L. Y. Ozer et al., "Biogenic platinum nanoparticles using black cumin seed and their potential usage as antimicrobial and anticancer agent," *Journal of Pharmaceutical and Biomedical Analysis*, vol. 179, article 112961, 2020.
- [2] S. Roy, T. Mukherjee, S. Chakraborty, and T. K. Das, "Biosynthesis, characterisation & antifungal activity of silver nanoparticles synthesized by the fungus *Aspergillus foetidus* mtcc8876," *Digest Journal of Nanomaterials and Biostructures*, vol. 8, pp. 197–205, 2013.
- [3] G. Baskar, J. Chandhuru, K. Sheraz Fahad, A. S. Praveen, M. Chamundeeswari, and T. Muthukumar, "Anticancer activity of fungal L-asparaginase conjugated with zinc oxide nanoparticles," *Journal of Materials Science: Materials in Medicine*, vol. 26, no. 1, p. 5380, 2015.
- [4] A. Gade, A. Ingle, C. Whiteley, and M. Rai, "Mycogenic metal nanoparticles: progress and applications," *Biotechnology Letters*, vol. 32, no. 5, pp. 593–600, 2010.
- [5] M. E. Castro, L. Cottet, and A. Castillo, "Biosynthesis of gold nanoparticles by extracellular molecules produced by the phytopathogenic fungus *Botrytis cinerea*," *Materials Letters*, vol. 115, pp. 42–44, 2014.
- [6] D. El-Kahky, M. Attia, S. M. Easa, N. M. Awad, and E. A. Helmy, "Biosynthesized of zinc oxide nanoparticles using *Aspergillus terreus* and their application as antitumor and antimicrobial activity," *Global Advanced Research Journal of Agricultural Science*, vol. 8, pp. 90–100, 2019.
- [7] M. Gholami-Shabani, Z. Gholami-Shabani, M. Shams-Ghahfarokhi, A. Akbarzadeh, G. Riazi, and M. Razzaghi-Abyaneh, "Biogenic approach using sheep milk for the synthesis of platinum nanoparticles: the role of milk protein in platinum reduction and stabilization," *International Journal of Nanoscience and Nanotechnology*, vol. 12, pp. 199–206, 2016.



- [8] D. W. Hobson, "Commercialization of nanotechnology," *Wiley Interdisciplinary Reviews: Nanomedicine and Nanobiotechnology*, vol. 1, no. 2, pp. 189–202, 2009.
- [9] M. H. Hulikere and C. G. Joshi, "Characterization, antioxidant and antimicrobial activity of silver nanoparticles synthesized using marine endophytic fungus-*Cladosporium cladosporioides*," *Process Biochemistry*, vol. 82, pp. 199–204, 2019.
- [10] A. Bhargava, N. Jain, K. A. Khan, V. Pareek, R. V. Dilip, and J. Panwar, "Utilizing metal tolerance potential of soil fungus for efficient synthesis of gold nanoparticles with superior catalytic activity for degradation of rhodamine B," *Journal of Environmental Management*, vol. 183, pp. 22–32, 2016.
- [11] S. Abel, J. L. Tesfaye, R. Shanmugam et al., "Green synthesis and characterizations of zinc oxide (ZnO) nanoparticles using aqueous leaf extracts of coffee (*Coffea arabica*) and its application in environmental toxicity reduction," *Journal of Nanomaterials*, vol. 2021, Article ID 3413350, 6 pages, 2021.
- [12] M. Thiruvengadam, I. M. Chung, T. Gomathi et al., "Synthesis, characterization and pharmacological potential of green synthesized copper nanoparticles," *Bioprocess and Biosystems Engineering*, vol. 42, no. 11, pp. 1769–1777, 2019.
- [13] E. Priyadarshini, S. S. Priyadarshini, B. G. Cousins, and N. Pradhan, "Metal-fungus interaction: review on cellular processes underlying heavy metal detoxification and synthesis of metal nanoparticles," *Chemosphere*, vol. 274, article 129976, 2021.
- [14] S. M. Joshi, S. de Britto, S. Jogaiah, and S. I. Ito, "Mycogenic selenium nanoparticles as potential new generation broad spectrum antifungal molecules," *Biomolecules*, vol. 9, no. 9, p. 419, 2019.
- [15] P. Khandel and S. K. Shahi, "Mycogenic nanoparticles and their bio-prospective applications: current status and future challenges," *Journal of Nanostructure in Chemistry*, vol. 8, no. 4, pp. 369–391, 2018.
- [16] P. Suryavanshi, R. Pandit, A. Gade, M. Derita, S. Zachino, and M. Rai, "*Colletotrichum* sp.-mediated synthesis of sulphur and aluminium oxide nanoparticles and its *in vitro* activity against selected food-borne pathogens," *LWT-Food Science and Technology*, vol. 81, pp. 188–194, 2017.
- [17] D. Rehder, "The future of/for vanadium," *Dalton Transactions*, vol. 42, no. 33, pp. 11749–11761, 2013.
- [18] M. Liu, B. Su, Y. Tang, X. Jiang, and A. Yu, "Recent advances in nanostructured vanadium oxides and composites for energy conversion," *Advanced Energy Materials*, vol. 7, no. 23, article 1700885, 2017.
- [19] S. Kumar, A. Qadir, F. Maury, and N. Bahlawane, "Visible thermochromism in vanadium pentoxide coatings," *ACS Applied Materials and Interfaces*, vol. 9, no. 25, pp. 21447–21456, 2017.
- [20] D. Rehder, "The potentiality of vanadium in medicinal applications," *Future Medicinal Chemistry*, vol. 4, no. 14, pp. 1823–1837, 2012.
- [21] S. Chakraborty, B. E. Petel, E. Schreiber, and E. M. Matson, "Atomically precise vanadium-oxide clusters," *Nanoscale Advances*, vol. 3, no. 5, pp. 1293–1318, 2021.
- [22] B. Kim, C. H. Kim, K. S. Yang, A. Rahy, and D. J. Yang, "Electrospun vanadium pentoxide/carbon nanofiber composites for supercapacitor electrodes," *Electrochimica Acta*, vol. 83, pp. 335–340, 2012.
- [23] M. Farahmandjou and N. Abaeiyan, "Chemical synthesis of vanadium oxide ( $V_2O_5$ ) nanoparticles prepared by sodium metavanadate," *Journal of Nanomedicine Research*, vol. 5, no. 1, article 00103, 2017.
- [24] J. L. Al Jabbar, D. O. Apriandanu, Y. Yulizar, and S. Sudirman, "Synthesis, characterisation and catalytic activity of  $V_2O_5$  nanoparticles using *Foeniculum vulgare* stem extract," *IOP Conference Series: Materials Science and Engineering*, vol. 763, article 01203, 2020.
- [25] A. O. Aliyu, S. Garba, and O. Bognet, "Green synthesis, characterization and antimicrobial activity of vanadium nanoparticles using leaf extract of *Moringa oleifera*," *International Journal of Chemical Sciences*, vol. 16, p. 231, 2017.
- [26] M. Obiedallah, M. Aboul-Nasr, and S. Mohamed, "A study of extracellular proteins produced by *Aspergillus oryzae*," *Journal of Environmental Studies*, vol. 18, pp. 25–31, 2018.
- [27] S. S. Salem and A. Fouda, "Green synthesis of metallic nanoparticles and their prospective biotechnological applications: an overview," *Biological Trace Element Research*, vol. 199, no. 1, pp. 344–370, 2021.
- [28] A. Ingle, M. Rai, A. Gade, and M. Bawaskar, "*Fusarium solani*: a novel biological agent for the extracellular synthesis of silver nanoparticles," *Journal of Nanoparticle Research*, vol. 11, no. 8, pp. 2079–2085, 2009.
- [29] N. Farkas and J. A. Kramar, "Dynamic light scattering distributions by any means," *Journal of Nanoparticle Research*, vol. 2, p. 120, 2021.
- [30] M. N. Owaid, J. Raman, H. Lakshmanan, S. S. S. al-Saeedi, V. Sabaratnam, and I. A. Abed, "Mycosynthesis of silver nanoparticles by *Pleurotus cornucopiae* var. *citrinopileatus* and its inhibitory effects against *Candida* sp.," *Materials Letters*, vol. 153, pp. 186–190, 2015.
- [31] S. Mourdikoudis, R. M. Pallares, and N. T. Thanh, "Characterization techniques for nanoparticles: comparison and complementarity upon studying nanoparticle properties," *Nanoscale*, vol. 10, no. 27, pp. 12871–12934, 2018.
- [32] G. Ebadzadsahrai, E. A. Higgins Keppler, S. D. Soby, and H. D. Bean, "Inhibition of fungal growth and induction of a novel volatile in response to *Chromobacterium vaccinii* volatile organic compounds," *Frontiers in Microbiology*, vol. 11, article 1035, 2020.
- [33] M. F. Begum, M. F. Mahal, and M. S. Alam, "Inhibition of spore germination and mycelial growth of three fruit rot pathogens using some chemical fungicides and botanical extracts," *Journal of Life and Earth Science*, vol. 5, pp. 23–27, 2011.
- [34] H. Mohammadi, A. Abedi, A. Akbarzadeh et al., "Evaluation of synthesized platinum nanoparticles on the MCF-7 and HepG-2 cancer cell lines," *International Nano Letters*, vol. 3, no. 1, p. 28, 2013.
- [35] G. Prasannaraj and P. Venkatachalam, "Green engineering of biomolecule-coated metallic silver nanoparticles and their potential cytotoxic activity against cancer cell lines," *Advances in Natural Sciences: Nanoscience and Nanotechnology*, vol. 8, no. 2, article 025001, 2017.
- [36] S. N. S. A. Rahman, N. A. Wahab, and S. N. A. Malek, "*In vitro* morphological assessment of apoptosis induced by antiproliferative constituents from the rhizomes of *Curcuma zedoaria*," *Evidence-Based Complementary and Alternative Medicine*, vol. 2013, Article ID 257108, 14 pages, 2013.
- [37] X. M. Hu, Z. X. Li, R. H. Lin et al., "Guidelines for regulated cell death assays: a systematic summary, a categorical comparison, a prospective," *Frontiers in Cell and Developmental Biology*, vol. 9, p. 368, 2021.

- [38] N. Naimi-Shamel, P. Pourali, and S. Dolatabadi, "Green synthesis of gold nanoparticles using *Fusarium oxysporum* and antibacterial activity of its tetracycline conjugant," *Journal de Mycologie Medicale*, vol. 29, pp. 7–13, 2019.
- [39] M. Gholami-Shabani, A. Akbarzadeh, D. Norouzian et al., "Antimicrobial activity and physical characterization of silver nanoparticles green synthesized using nitrate reductase from *Fusarium oxysporum*," *Applied Biochemistry and Biotechnology*, vol. 172, no. 8, pp. 4084–4098, 2014.
- [40] A. Syed and A. Ahmad, "Extracellular biosynthesis of platinum nanoparticles using the fungus *Fusarium oxysporum*," *Colloids and Surfaces B: Biointerfaces*, vol. 97, pp. 27–31, 2012.
- [41] A. Ahmad, P. Mukherjee, D. Mandal et al., "Enzyme mediated extracellular synthesis of CdS nanoparticles by the fungus, *Fusarium oxysporum*," *Journal of the American Chemical Society*, vol. 124, no. 41, pp. 12108–12109, 2002.
- [42] K. S. Prasad, C. Shivamallu, G. Shruthi, and M. Prasad, "A novel and one-pot green synthesis of vanadium oxide nanorods using a phytomolecule isolated from *Phyllanthus amarus*," *ChemistrySelect*, vol. 3, no. 13, pp. 3860–3865, 2018.
- [43] B. Wasmi, A. A. al-Amiery, A. A. H. Kadhum, M. S. Takriff, and A. B. Mohamad, "Synthesis of vanadium pentoxide nanoparticles as catalysts for the ozonation of palm oil," *Ozone: Science & Engineering*, vol. 38, no. 1, pp. 36–41, 2016.
- [44] P. Taylor, M. Kusper, T. Hesabizadeh et al., "Synthesis of naked vanadium pentoxide nanoparticles," *Nanoscale Advances*, vol. 3, no. 7, pp. 1954–1961, 2021.
- [45] S. Pinto, L. D'Ornelas, and P. Betancourt, "Synthesis and characterization of vanadium nanoparticles on activated carbon and their catalytic activity in thiophene hydrodesulphurization," *Applied Surface Science*, vol. 254, no. 17, pp. 5390–5393, 2008.
- [46] P. Rasheed, S. Haq, M. Waseem et al., "Green synthesis of vanadium oxide-zirconium oxide nanocomposite for the degradation of methyl orange and picloram," *Materials Research Express*, vol. 7, article 025011, 2020.



## Review Article

# Applications of Nanomaterials in Agrifood and Pharmaceutical Industry

**Hiwa M. Ahmed** <sup>1</sup>, **Arpita Roy** <sup>2</sup>, **Muhammad Wahab**,<sup>3</sup> **Mohammed Ahmed**,<sup>4</sup> **Gashaw Othman-Qadir**,<sup>5</sup> **Basem H. Elesawy**,<sup>6</sup> **Mayeen Uddin Khandaker**,<sup>7</sup> **Mohammad Nazmul Islam**,<sup>8</sup> and **Talha Bin Emran**<sup>9</sup>

<sup>1</sup>Sulaimani Polytechnic University, Slemani, 46001 Kurdistan Region, Iraq

<sup>2</sup>Department of Biotechnology, School of Engineering & Technology, Sharda University, Greater Noida, India

<sup>3</sup>Food Science and Quality Control Department, College of Agricultural Engineering Science, University of Sulaimani, Slemani, Kurdistan Region, Iraq

<sup>4</sup>Department of Horticulture, University of Raparin, Ranya, Kurdistan Region, Iraq

<sup>5</sup>Newcastle Center for Natural Therapy, Slemani, Ranya, 46012 Kurdistan Region, Iraq

<sup>6</sup>Department of Pathology, College of Medicine, Taif University, P.O. Box 11099, Taif 21944, Saudi Arabia

<sup>7</sup>Centre for Applied Physics and Radiation Technologies, School of Engineering and Technology, Sunway University, 47500 Selangor, Malaysia

<sup>8</sup>Department of Pharmacy, International Islamic University Chittagong, Chittagong 4318, Bangladesh

<sup>9</sup>Department of Pharmacy, BGC Trust University Bangladesh, Chittagong 4381, Bangladesh

Correspondence should be addressed to Hiwa M. Ahmed; [hiwa2009@yahoo.com](mailto:hiwa2009@yahoo.com)

Received 22 August 2021; Accepted 13 September 2021; Published 7 October 2021

Academic Editor: Shanmugam Rajeshkumar

Copyright © 2021 Hiwa M. Ahmed et al. This is an open access article distributed under the Creative Commons Attribution License, which permits unrestricted use, distribution, and reproduction in any medium, provided the original work is properly cited.

Nanotechnology recently emerged among the most exciting science-related innovations. Nanotechnology-produced metal nanoparticles got a lot of attention. This is emerging as a rapidly developing field due to its effective applications that targeted the manufacturing of new materials at the nanoscale level. There is considerable interest in the application of nanomaterials in many areas of industry including agrifood and biomedical products. In the agrifood area, nanomaterials have benefits in diverse areas which include fertilizers, herbicides, pesticides, sensors, and quality stimulants, among other food processing, food packaging, and nutraceuticals to improve nutritional value. These applications in agriculture result in enhanced quality and crop yield, reduction in pollution caused by various chemicals, etc. In the pharmaceutical area, nanomaterials are claimed to ameliorate drug safety and efficacy, as well as bioavailability. They are utilized for targeting various drugs to a specific location in the body. However, there are also concerns that some nanoparticles may have adverse effects on human health. These include titanium dioxide, copper oxides, and other nanomaterials which lead to liver damage, skin damage, lung damage, and various other human health-related problems. This review is aimed at presenting a briefing on the state of the art in the application of nanotechnology in food and human nutrition and drug administration, consumer attitudes, and their challenges and opportunities with future perspectives.

## 1. Introduction

In today's society, consumer demand for higher quality, safer, and healthier food and natural products is increasing [1–3]. Nanotechnology may play a significant role to protect and conveyance active compounds (hydrophobic and

hydrophilic) through incorporation into food products, to enhance nutraceuticals, functional foods [4, 5]. Nanotechnology typically refers to the use of nanomaterials between 1 and 100 nm in size [6–9]. The fundamentals of nanotechnology consist of materials adopting alternative and often more beneficial properties at their nanosize when

TABLE 1: Types of nanoparticles and their applications in biomedicine and food industry [25–29].

Type of nanoparticle	Structure	Properties	Functions	Application
Liposome	Phospholipid bilayer in an aqueous environment	(i) Biocompatibility (ii) Biodegradability	(i) Drug and gene delivery (ii) Texture in cosmetic products (iii) Application in dairy products	(i) Medicine (ii) Cosmetic industry (iii) Food industry
Polymer	Can be either polymer-protein conjugates or polymer-drug conjugates	(i) Polymer protein enhances protein stability (ii) Polymer drug promotes tumour targeting	(i) Drug delivery systems (ii) Functional foods	(i) Medicine (ii) Food industry
Carbon (i) Fullerenes (ii) Nanotubes	Many points of attachment for binding	(i) High symmetry (i) Electrical conductivity and strength (ii) Can be single or multiwalled	(i) Cleave DNA (ii) Drug delivery (i) Delivery of therapeutic molecules (ii) Uses in milk and other proteins	(i) Medicine (i) Medicine (ii) Food industry
Quantum dots	Coated in other materials to prevent leakage of toxic materials	(i) Semiconductors (ii) Fluorescent	(i) Cell tracking	(i) Medicine
Metal nanoparticles	Can be spherical, triangular, hexagonal, rod-shaped, polyhedral, cubic, etc.	(i) Biocompatibility (ii) Biodegradability	—	(i) Application in food industry (ii) Medicine
Metal oxide nanoparticles	Can be spherical, hexagonal, triangular, rod-shaped, polyhedral, cubic, etc.	(i) Biocompatibility (ii) Biodegradability	—	(i) Application in environmental remediation (ii) Pharmaceutical

N.B. Applications in medicine may also include nutritional supplements.

compared to their normal size, due to an increase in surface area [10–13]. Nanomaterials can be created in one (nanoscale), two (nanowires and nanotubes), or three dimensions (nanoparticles) [14–16]. There are several techniques used to form nanomaterials; these include bottom-up and top-down approaches [17]. Bottom-up approaches involve the self-assembly of individual atoms using scanning tunnel microscopy; this process is time-consuming due to the vast number of atoms to be assembled. Top-down approaches are also used to create nanomaterials; large materials are transformed into smaller ones via atomic force microscopy. Current funding is supplied on a yearly basis; apart from a few expensive pieces of equipment, nanotechnology is relatively inexpensive [18]. Nanomaterials include nanofilms, nanotubes, and nanoparticles among others [17, 18]. Nanoparticles are a particular type of nanomaterial that can occur naturally, be created unintentionally, or indeed be engineered on purpose. Although benefits of these engineered nanoparticles (ENPs) are well recognised in many industries, more attention is needed on potential toxicity and its adverse effects [19]. Nanotechnology can be applied in a number of fields including medicine, agriculture, food science, food technology, recreation, and civil engineering [20–22]. There is exciting potential of nanotechnology in these areas, and some applications are already of great benefit to industries and consumers. Engineers have used nanotechnology to create substances for products, which are stronger, lighter, rustproof, and stain/fire resistant [23]. Advances in nanotechnology have been made in a number of areas; however,

development and acceptance of the technology are slow in the food industry [23]. This is mainly due to a mixed consensus from the public; many are unaware and do not understand nanotechnology as a science [24]. Nevertheless, consumers need to recognise that both natural and processed foods already contain nanoparticles. Milk is characterised as a nanofood, and meat is composed of nanosized protein fibres. Meat processing procedures practiced for many years alter the nanostructure of muscle [23]. In addition to that, we are exposed to naturally occurring and engineered nanoparticles every day (Table 1). This study will provide an overview of the current state of the art in the use of nanotechnology in food and human nutrition, medication administration, consumer attitudes, difficulties, and possibilities, as well as future prospects.

## 2. Applications of Nanomaterials in Agrifood Industry

Nowadays, with growing population, food demand is on the rise and food safety is a matter of concern. Nanoscience has emerged as one of the most innovative technologies in the field of agriculture and food industry chain. Nanomaterials can be utilized in the agrifood industries as nanoformulations for crop improvement, in crop protection for the identification of diseases, nanodevices for the genetic manipulation of plants, plant disease diagnostics, etc. [30]. A number of nanoparticles (mostly metal-based and carbon-based nanomaterials) have been exploited to improve the growth

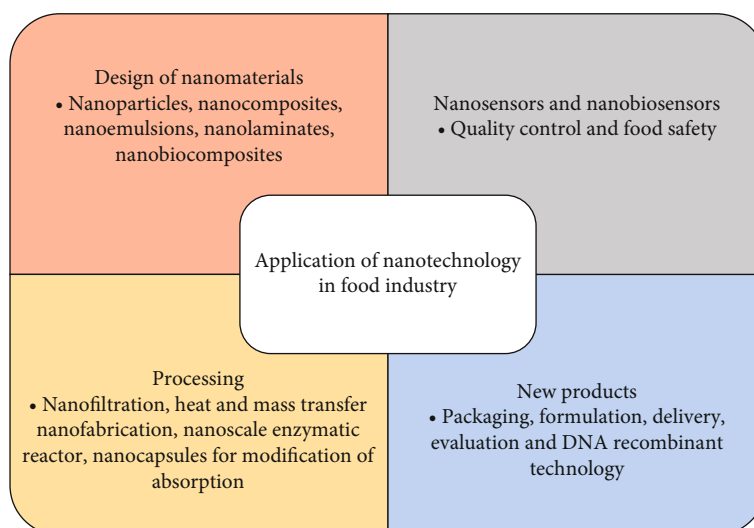


FIGURE 1: Application matrix of nanotechnology in the food industry.

and development of crop food plants [31]. This positive impact has led to enhanced germination percentage, biomass production along with enhancement of physiological parameters such as photosynthesis and nitrogen metabolism in many food crops including alfalfa, cucumber, corn, lettuce, onion, pumpkin, ryegrass, rape, radish, spinach, soybean, tomato, and wheat [32]. Nanomaterial has given a promise in plant protection, via genetically modified crops to produce a plant disease resistance to pathogen infections and is crucial to ensure sustainable food and agriculture [33]. Nanoencapsulation displays the advantage of more efficient use and safer handling of pesticides, fertilizers, and vaccines with less exposure to the environment that guarantees eco-protection [34]. Nanofertilizers have unique features like ultrahigh absorption which is a route to enrich the soil with adequate essential nutrients gradually, thus preventing pollution of water resources and it is well known to improve the quantity of fruit and biological production [35].

### 3. Applications of Nanomaterials in Food Industry

Nanotechnology has much potential to improve and produce new food concepts beyond capabilities in the current domain. It can be applied to all aspects of the food sector including agriculture, food processing, food packaging, and supplements. Food packaging may be developed in order to prevent the invasion of microorganisms or alert consumers if food is no longer edible via nanosensors. Through nanotechnology, food can also be made healthier for consumers [6]. However, such scientific breakthroughs may not be utilized if the public is uncertain about the technology. Applications in packaging are currently more accepted than uses in food itself; trust issues occur concerning naturalness. Nonetheless, it is predicted that nanotechnology will become increasingly important in the future [6]. Much research into nanotechnology is still warranted, especially in relation to food applications. Nanomaterials in food can

be described as both “soft” and “hard.” Soft nanomaterials are formed from natural ingredients or components of food during processing; examples include homogenised milk, ricotta cheese, and coenzyme Q10 (use in supplements). Hard nanomaterials however are more of a concern to the Food Standards Agency (FSA). Such materials are insoluble, and little is known regarding the properties in which they possess. Metals, among others, are characterised as hard nanomaterials [36]. As outlined by the FSA, current approval of nanotechnology foods and processes would be required in line with the “Novel Foods Regulation” (Regulation (EC) No. 258/97) [37].

Existing hazards associated with nanotechnology in the food industry are somewhat unknown. The EFSA expressed concern over the lack of methods in which to detect and measure engineered nanomaterials and the effect they may have on both consumers and livestock. Toxicity levels must be defined along with ways to identify engineered nanomaterial concentrations in food, feed, and biological tissues [38]. There is a need for greater awareness and understanding of nanotechnology; this will result in more productive and informed decisions. Following this, consumers may also perceive nanotechnology in a more positive light. Nanotechnology has wide range of applications within the food industry (Figure 1). However, some applications could fall into the arbitrary grey regions where overlapping of these categories occurs.

Table 2 shows specific examples of their potential usage into the four main categories related to agriculture, food processing, food packaging, nutraceuticals, and biomedicine [34, 36, 39]. Despite most of these applications being in the research and development (R&D) stages, food industries have been very careful in making decisions on whether or not to adopt these technologies due to concerns on consumer perceptions, which will be discussed in the later sections [39]. Advancing knowledge within this field in order to set the appropriate regulatory measures appears to be even more complex as it involves confidentiality, openness,

TABLE 2: Examples of current and potential nanotechnology application in the agrifood and biomedicine industry [49–53].

	Food processing	Food packaging	Nutraceuticals	Biomedicine
Agriculture				
Nanocapsules for the delivery of pesticides, fertilizers, vaccines, and other agrichemicals	Fumed silica (E551) as anticaking agent and carriers	Nanoclay embedded between PET layers for enhanced mechanical strength, heat resistance, gas permeability, and transparency	Nanosized powders for increased absorption of nutrients	Liposomes exploited in drug and gene delivery
Nanocapsules in the delivery of growth hormones in a controlled fashion	Nanosprayed dried salt with increased perception of saltiness as means to reduce salt levels in food	Nanosilver coated in reusable containers to inhibit microorganism growth	Cellulose nanocrystal composites as drug carriers	Dendrimers for targeted drug delivery
Nanosensors to detect animal and plant pathogens	Nanoparticles with selective binding properties to remove chemicals or pathogens in food	Titanium nitride in food packaging improving rigidity and strength	Nanodroplets with better vitamin absorption	Nanoshells for targeted cancer cells
Nanosensors to identify and preservation	Nanocapsule infusions of plant steroids as replacement of cholesterol	Nanoparticles with fluorescent properties with attached antibodies for detecting chemicals or foodborne pathogens	Nanocochleates for drug and nutrient delivery into the body	Quantum dots, gold nanoparticles, nanowires, and fullerenes as targeting and imaging agents
Nanosensors for soil condition monitoring and plant growth	Nanocapsule for flavour enhancers	Electrochemical nanosensors for detecting ethylene		Carbon nanotube for gene and drug delivery towards tumour cell
Nanotechnology for DNA molecular detection	Nanocapsules improving bioavailability of nutraceuticals			Nanobiosensors for diagnosis and detection of cancer agents
Nanochips for identity preservation and tracking	Nanotubes as gelation and viscosifying agents			

and transparency issues relating to commercial interests as addressed by [40]. Nowadays, consumers are increasingly demanding high-quality, safe, and healthy food products. Nanofood has the potential to change the whole food industry chain and is often associated with colour and flavour improvement, storage, preservation, pathogen detection, antimicrobial properties, and intelligent packaging [41].

#### 4. Nutritional Benefits of Using Nanoparticles

Foodborne microbial pathogens can potentially cause illness and fatality; this problem is hard to solve due to the increasing resistance of microbial strains [42, 43]. Nanotechnology can play a role in the detection of pathogens or pesticides in food. They can also monitor the temperature and pH of foods to prevent the presence of these unwanted organisms through the use of nanosensors [44]. Thin inorganic coatings act as protective layers on food products to enhance shelf life, by producing moisture- or oxygen-resistant materials. This knowledge led scientists and researchers to use similar methods to prevent spoilage by microbes and oxidation to prolong shelf life, using nanocomposite materials in food storage [42]. Nanocomposite materials favour conventional food packaging materials due to their superior polymeric properties reinforced by nanoparticles. This structure gives an advantage to food storage because it is less permeable to gases than other materials. Therefore, oxidation and consequently food spoilage are reduced. Nanocomposites with added nanoparticles can maintain resistance to these gases at half the thickness of others, meaning production costs are also reduced [42]. Macro- and micronutrients of low bioavailability have limited absorption in the body. However, by making these smaller with the use of nanotechnology, the particles can enhance bioavailability due to the increased surface area, improving absorption rates in the stomach and small intestine [42]. Therefore, nanotechnology has the potential to alter nutrient intakes through enriched and fortified food products [45]. Nanodrops have been used as an additive in canola oil which is designed to carry vitamins, minerals, and phytochemicals through the digestive system and urea [15].

Iron is the fourth most abundant mineral on earth, yet iron deficiency is the most common mineral deficiency in the world as over 2 billion people worldwide are anaemic [46]. It does not help that iron has an estimated lower bioavailability than other nutrients at 14–18% for mixed diets and 5–12% for vegetarian diets in subjects with no iron stores [47]. One solution to this could be to fortify foods with iron; however, this is often challenging because it can seriously affect the taste, smell, and appearance of foods [48]. Scientists in Switzerland addressed the problem of iron deficiencies and came up with a solution to enrich food with iron using nanotechnology. Iron was first dissolved in water then sprayed over a fire. The intense heat evaporated the water leaving minute iron crystals each about 10 nm in size. These nanoparticles can then be added to foods, and it was reported that they did not alter food in any way. However, this experiment was carried out in rats, so it is hard to determine if the taste of food was affected [48].

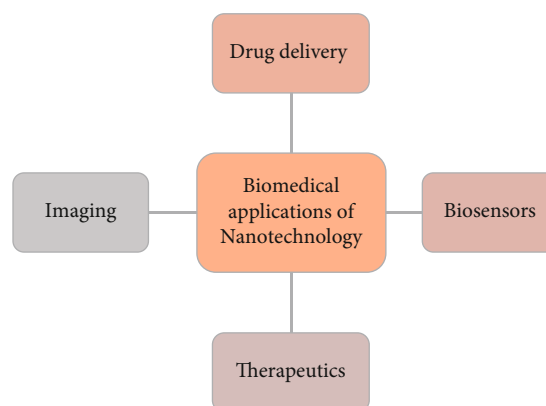


FIGURE 2: Application of nanotechnology in the biomedical sector.

#### 5. Nanotechnology in Biomedical Application

Nanotechnology plays a significant role in biomedical and pharmaceutical products as it facilitates from syndrome diagnoses to drug delivery to human organs in order to target infectious diseases. Nanoparticles have unique biological properties which can be used for detection, prevention, and treatment of diseases, drug delivery, and gene therapy of cancer as well as pulmonary diseases [54, 55] (Figure 2), due to having capability to bind, absorb, and carry small-molecule drugs, DNA, RNA, and proteins with high efficiency [15]. Indeed, liposomal drug formulations (i.e., doxorubicin) are widely used for the treatment of breast and ovarian cancers and Kaposi's sarcoma successfully [56]. Incorporation of liposomal drug formulations to amphotericin and hamycin cancer drugs exhibited much better efficacy and safety as compared to conventional preparations [57]. Quantum dots are inorganic nanoparticles that consist of 10–50 atoms, and their diameter ranges from 2 to 10 nm [15]. Because of their high-sensitivity and multicontrast imaging properties, they have been used for the detection and diagnosis of cancer cells in *in vivo* conditions [58]. In addition to that, nanobiosensors can be employed for the early detection of leading causes of cancer such as environmental pollutants, pathogens, and carcinogenic gases [59, 60]. Nanomaterials have been incorporated into a drug formulation, such as active constituent (nanocrystals), excipients (drug-metal complexes), drug carriers (liposomes), or as complexes/conjugates (drug-protein) [54]. Nanotechnology may also have future nutritional health benefits. People with type one diabetes are expected to be able to consume a nanoengineered biodegradable material containing insulin, which can be released as a response to high blood glucose concentrations [61]. There is also interest in the application of nanotechnology-derived anti-inflammatory agents to the mucosal lining of patients with inflammatory bowel disease or Crohn's disease. It is also thought that the use of nanotechnology on some nutrients can enable individuals to expand their limited food tolerances or choices. There are various nanoparticle-based delivery systems that have been exploited for diagnostic and therapeutic applications as illustrated in Tables 1 and 2.

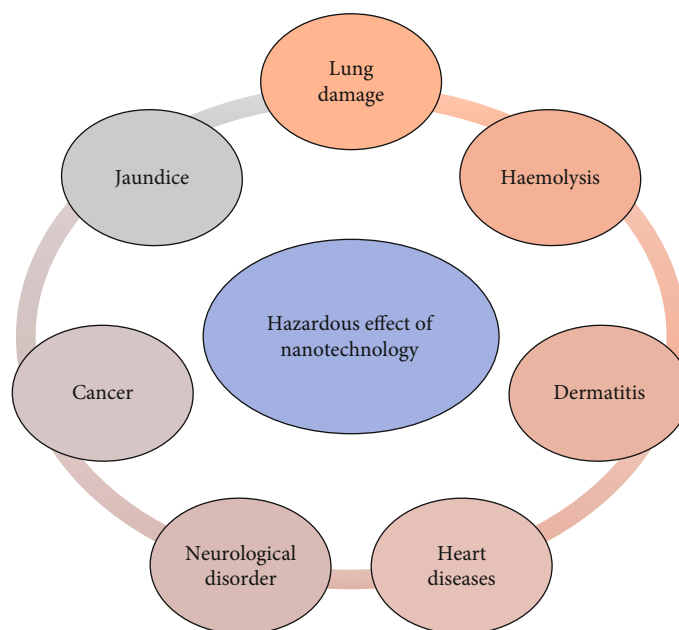


FIGURE 3: Hazardous effect of nanotechnology in human health.

## 6. Potential Hazards in the Use of Nanotechnology/Nanomaterials for Human Health

Although an increase in certain micronutrient intakes may be beneficial, it is also important to realise that the overconsumption of these nutrients can lead to toxicity, which may result in more severe problems (Figure 3). There are several potential challenges derived from the emergence of the use of nanotechnology. This includes toxicity and environment, health, social, ethical, legal, and cultural implications [62]. Nanoparticles are widely produced from nanotechnology and are presently utilized in a broad range of industrial sectors. These sectors include agriculture, healthcare, materials, and energy, therefore increasing the likelihood of exposure to consumers and workers [20]. Humans can be exposed to ENPs (engineered nanoparticles) from various pathways such as ingestion, inhalation, absorption through skin, and direct injection for medicinal purposes [63].

The detriments caused by inhalation of nanoparticles, titanium dioxide ( $\text{TiO}_2$ ) taken in food in rats and humans [64] and also in sunscreen and carbon nanoparticles in rodents [65, 66], were subject to investigation by researchers and found that inhaled particles into the lungs can lead to damage and scarring and this especially with long-term exposure could affect the lung wall, reduce absorbed oxygen, decrease carbon dioxide, and then trigger breathing difficulties [63]. Despite the lack of evidence for toxicity, results suggest that potential hazards of carbon nanotubes may cause inflammation in the lungs [65]. This is very similar to the process by which asbestos fibres cause asbestosis [63]. However, little research is known about toxicity of cerium oxide nanoparticles ( $\text{CeO}_2$  NPs), which are used to increase fuel efficiency and reduce its emissions of car, but a recent study revealed it may cause lung cancer [67]. Studies

show that by reducing the surface area from large scale to nanoscale enables its toxicity to damage organs and the best example is nanocopper particles ingested by mice induce severely toxicological effects on the liver, kidney, and spleen [68]. Similarly, copper nanoparticles can enter the human body through food, water, drugs, cosmetics on the skin, nails, hair, [69], etc. If the intake of copper exceeds the capacity of the human body, it will result in toxic effects such as haemolysis, jaundice, and even death [68].

Furthermore, particles 7000 nm or smaller can penetrate the skin and have the ability to impair them [70]. Nanoparticles or nanoemulsions are used to manufacture sports equipment, biomedical applications, electronic components [71], clothing, cosmetics, shaving creams, sunscreens, shampoos, and toothpastes. Many of these are produced to deal with the skin and to treat damaged skin or hair and therefore can penetrate the skin. Such diseases such as dermatitis, acne, and psoriasis, as a result of simple actions, for instance, injuries (sunburns, cuts, or scrapes) or shaving, can lead to more cutaneous permeability [66]. Once particles are absorbed through the skin, they can be toxic to cellular and subcellular levels and damage the DNA [72].

However, the risks of toxicity of nanotechnology-derived food and food packaging for consumers are largely not very well understood [73], but recent studies demonstrate that silver nanoparticles (AgNPs) can be applied to food, food packaging, and other consumer products due to their antibacterial properties. These smaller AgNPs (AgNPs-5) can enter human cells much more easily than bigger ones (AgNPs-20 and AgNPs-50) which may lead to higher toxic effects than silver ions in cells [63, 74]. Research demonstrates that ENPs are able to cross the blood-brain barrier and induce direct damage to neuronal cells, neuroinflammation, and prooxidant changes because of their nanosizes [20]. It has been proposed that not all nanomaterials will

TABLE 3: Literature studies on potential nanotechnology-related health hazards.

Exposure via	Study outcomes	References
<i>Inhalation</i>	Inhaled titanium dioxide (TiO <sub>2</sub> ) particles from food colouring into the lungs can lead to breathing difficulties.	[63, 79]
<i>Ingestion</i>	Little known about toxicity of carbon nanotubes (CNTs) which may cause to inflammation in the lungs.	[65]
	Intake of TiO <sub>2</sub> particles (150–500 nm) through food can translocate to the blood, liver, and spleen.	[64]
	Copper nanoparticles enter the human body by ingestion from food and consumer product, leading to haemolysis, jaundice, and death.	[68]
	AgNPs-5 may lead to higher toxic effects than AgNPs-20 and AgNPs-50 in cells; ENPs cross the blood-brain barrier and cause damage to neuronal cells, neuroinflammation, and prooxidant changes.	[20]
<i>Skin penetration</i>	Particles size of 7000 nm or smaller can penetrate the skin and have ability to damage DNA.	[70]
	May be toxic to cellular and subcellular levels and damage to DNA; inconclusive data to show toxicity.	[66]

have adverse effects on human health due to differences in their surface, size, and formulation of the material in the products [75]. Although there are appropriate techniques available to assess many of the risks related to the consumer products and processes in which nanoparticles are involved, it seems to be not adequate to address all the hazards. Therefore, more studies should be done.

There are toxicity concerns with nanoparticles and ultra-fine particles in particular, due to their increased surface area and potential to bioaccumulate in cells [76]. The potential problems are unknown as they do not normally occur with bulk materials. However, most of this research is limited to animal models due to ethical reasons. Nanotechnology packaging also has its concerns due to the possibility of particle migration into foods [77]. Currently, safe limits are not defined by legislation due to limited knowledge in this area. Therefore, it is unknown if the levels used in food packaging or the food itself may be detrimental to health. Table 3 gives an overview of the potential hazards of exposure to nanomaterials via different routes. Assessment methods to detect the level of nanomaterials are limited; therefore, it is difficult to establish toxicity and exposure levels. For this reason, the development of technology is needed to establish a valid method of assessing nanomaterial exposure levels. Due to the novelty of this technology in food-related applications, long-term risks are not fully understood. Short-term studies must be considered carefully as their reliability is questionable [78].

## 7. Consumer Attitudes to Nanotechnology

Consumer perceptions of nanotechnology applications in the food industry are varied. This mixed consensus is thought to be largely accounted to limited awareness and understanding of the emerging nanotechnology science. Numerous studies have shown that consumer attitudes towards nanotechnology in the food industry differ according to the application [79]. Research carried out in France by [6] suggested that French citizens were sceptical about both nanotechnology food and packaging applications. However, research in Switzerland suggested consumers tended to accept the concept of nanotechnology packaging

but not the application of nanotechnology in food. These two pieces of research could suggest that the consumer's attitude towards nanotechnology has changed within the time period between the two studies. Conversely, it could be that different cultures have different perceptions of nanotechnology, creating a need for cultural perceptions to be addressed individually.

The consumers' opposition to nanotechnology applications in the food industry is thought to be multifactorial:

- (i) Poor knowledge of the concept of nanotechnology
- (ii) Lack of trust in governmental agencies
- (iii) Low perceived level of naturalness
- (iv) Limited knowledge of the benefits

It is advisable to acknowledge sceptical consumer outlooks in the early stage of developing nanotechnology products in order to gain consumer trust. To encourage public approval of nanotechnology, the government and NGOs will need to address the subject appropriately to ensure the public develops an informed view of the technology [6]. Consumer willingness to buy health beneficial foods, produced using nanotechnology, has recently been investigated [80]. The finding displayed evidence for naturalness has been a very important factor in deciding whether or not to purchase functional food. Hence, as consumers currently view nanotechnology as unnatural, they will need to be convinced that the concept is natural before they willingly purchase nanotechnology functional foods. Vandermoere et al. [24] completed a study using risk-benefit trade-offs to distinguish supporters (benefit > risk), doubters (risk = benefits), and opponents (risk > benefit) of nanotechnology food packaging and nanotechnology food.

When familiarity of nanotechnology was accounted for, there were no differences in opinion between gender and/or educational background. Prior to the survey, 57.6% of the participants were not aware of what nanotechnology was and only 5.1% reported having good knowledge of nanotechnology. This demonstrates the limited public knowledge of nanotechnology and provides evidence that there is a need to educate the public about nanotechnology. There

are fears that consumers may express negativity towards nanotechnology applications as it becomes commercialised; this concern stems from the adverse public reaction to GM (genetically modified) applications. Therefore, the learnings as to why consumers did not trust GM when the concept was released must be unraveled and where possible applied in the context of nanotechnology in order to reduce the potential negativity which is speculated [79]. Currently, there is no legislation regarding labelling of nanotechnology products, although it is often discussed. One study investigated how labelling nanotechnology products affected consumer perception. The findings suggested that labelling sunscreen as “nanotechnology sunscreen” was reason of a higher level of perceived risk and a lower level of perceived benefits. Although this is not a food product, consideration is needed as the consumer attitude would likely be similar for food [81].

## 8. Conclusion

Nanotechnology plays a significant role in biomedical and pharmaceutical products. Nanomaterials are an efficient tool for the improvement of agricultural and pharmaceutical industry. They are utilized for the protection of plants, crop improvement, drug delivery, biosensors, etc. Though it shows different activities, nanotoxicological effects need to be found out. Different factors may be responsible for the negative impact of nanomaterials. Therefore, research is needed to clarify a number of issues including knowledge and understanding from both industry and consumer perspectives, detection methods of nanomaterial exposure levels, and effects of long-term exposure to consumers. If these problems are addressed appropriately, the public may start to accept the use of nanomaterials for industrial purposes.

## Data Availability

The data used to support the findings of this study are included within the article.

## Conflicts of Interest

The authors declare no conflict of interest.

## Authors' Contributions

Hiwa M. Ahmed wrote the first draft of the manuscript; Arpita Roy revised the manuscript and added; Muhammad Wahab, Mohammed Ahmed, Gashaw Othman-Qadir, Basem H. Elesawy, Mayeen Uddin Khandaker, Mohammad Nazmul Islam, and Talha Bin Emran have read and improved the whole manuscript and supported. All authors read and agreed to the final submitted version.

## Acknowledgments

The authors acknowledge the support of Taif University Researchers Supporting Project number TURSP-2020/127, Taif University, Taif, Saudi Arabia.

## References

- [1] H. M. Ahmed, “Ethnopharmacobotanical study on the medicinal plants used by herbalists in Sulaymaniyah Province, Kurdistan, Iraq,” *Journal of Ethnobiology and Ethnomedicine*, vol. 12, no. 1, pp. 1–17, 2016.
- [2] R. Prasad and V. Kumar, *Nanotechnology: Food and Environmental Paradigm*, M. Kumar, Ed., Springer, 2017.
- [3] R. Prasad, A. K. Jha, and K. Prasad, Eds., *Exploring the Realms of Nature for Nanosynthesis*, Springer International Publishing, Cham, 2018.
- [4] H. M. Ahmed, S. Nabavi, and S. Behzad, “Herbal drugs and natural products in the light of nanotechnology and nanomedicine for developing drug formulations,” *Mini Reviews in Medicinal Chemistry*, vol. 21, no. 3, pp. 302–313, 2021.
- [5] N. Saglam, F. Korkusuz, and R. Prasad, *Nanotechnology Applications in Health and Environmental Sciences*, Springer International Publishing, 2021.
- [6] M. Siegrist, N. Stampfli, H. Kastenholz, and C. Keller, “Perceived risks and perceived benefits of different nanotechnology foods and nanotechnology food packaging,” *Appetite*, vol. 51, no. 2, pp. 283–290, 2008.
- [7] A. Roy, “Synthesis of silver nanoparticles from medicinal plants and its biological application: a review,” *Research & Reviews in BioSciences*, vol. 12, no. 4, p. 138, 2017.
- [8] A. Roy and N. Bharadvaja, “Silver nanoparticle synthesis from *Plumbago zeylanica* and its dye degradation activity,” *Bioinspired, Biomimetic and Nanobiomaterials*, vol. 8, no. 2, pp. 130–140, 2019.
- [9] E. K. Tian, Y. Wang, R. Ren, W. Zheng, and W. Liao, “Gold nanoparticle: recent progress on its antibacterial applications and mechanisms,” *Journal of Nanomaterials*, vol. 2021, Article ID 2501345, 18 pages, 2021.
- [10] H. Sarma, S. J. Joshi, R. Prasad, and J. Jampilek, *Biobased Nanotechnology for Green Applications*, Springer International Publishing, 2021.
- [11] R. Prasad, “Synthesis of silver nanoparticles in photosynthetic plants,” *Journal of Nanoparticles*, vol. 2014, Article ID 963961, 8 pages, 2014.
- [12] A. Roy and N. Bharadvaja, “Silver nanoparticles synthesis from a pharmaceutically important medicinal plant *Plumbago zeylanica*,” *MOJ Bioequiv Availab*, vol. 3, no. 5, article 00046, 2017.
- [13] S. Raina, A. Roy, and N. Bharadvaja, “Degradation of dyes using biologically synthesized silver and copper nanoparticles,” *Environmental Nanotechnology, Monitoring & Management*, vol. 13, article 100278, 2020.
- [14] F. Findik, “Nanomaterials and their applications,” *Periodicals of Engineering and Natural Sciences (PEN)*, vol. 9, no. 3, pp. 62–75, 2021.
- [15] Y. Chu, S. Jing, D. Liu, J. Liu, and Y. Zhao, “Morphological control and kinetics in three dimensions for hierarchical nanostructures growth by screw dislocations,” *Acta Materialia*, vol. 162, pp. 284–291, 2019.
- [16] A. Roy, “Plant derived silver nanoparticles and their therapeutic applications,” *Current Pharmaceutical Biotechnology*, vol. 22, no. 14, pp. 1834–1847, 2020.
- [17] N. Chausali, J. Saxena, and R. Prasad, “Nanobiochar and biochar based nanocomposites: advances and applications,” *Journal of Agriculture and Food Research*, vol. 5, article 100191, 2021.



- [18] N. Aziz, M. Faraz, M. A. Sherwani, T. Fatma, and R. Prasad, "Illuminating the anticancerous efficacy of a new fungal chas-sis for silver nanoparticle synthesis," *Frontiers in chemistry*, vol. 7, no. 65, 2019.
- [19] N. Prajitha, S. S. Athira, and P. V. Mohanan, "Bio-interactions and risks of engineered nanoparticles," *Environmental Research*, vol. 172, pp. 98–108, 2019.
- [20] K. Radad, M. Al-Shraim, R. Moldzio, and W. D. Rausch, "Recent advances in benefits and hazards of engineered nanoparticles," *Environmental Toxicology and Pharmacology*, vol. 34, no. 3, pp. 661–672, 2012.
- [21] A. Roy and N. Bharadvaja, "Qualitative analysis of phytocompounds and synthesis of silver nanoparticles from *Centella asiatica*," *Innovative Techniques in Agriculture*, vol. 1, no. 2, pp. 88–95, 2017.
- [22] P. Nagore, S. Ghotekar, K. Mane, A. Ghoti, M. Bilal, and A. Roy, "Structural properties and antimicrobial activities of *Polyalthia longifolia* leaf extract-mediated CuO nanoparticles," *BioNanoScience*, vol. 11, no. 2, pp. 579–589, 2021.
- [23] V. Amenta, K. Aschberger, M. Arena et al., "Regulatory aspects of nanotechnology in the agri/feed/food sector in EU and non-EU countries," *Regulatory Toxicology and Pharmacology*, vol. 73, no. 1, pp. 463–476, 2015.
- [24] F. Vandermoere, S. Blanchemanche, A. Bieberstein, S. Marette, and J. Roosen, "The public understanding of nanotechnology in the food domain: the hidden role of views on science, technology, and nature," *Public Understanding of Science*, vol. 20, no. 2, pp. 195–206, 2011.
- [25] Y. Panahi, M. Farshbaf, M. Mohammadhosseini et al., "Recent advances on liposomal nanoparticles: synthesis, characterization and biomedical applications," *Artificial cells, nanomedicine, and biotechnology*, vol. 45, no. 4, pp. 788–799, 2017.
- [26] V. R. Rai, J. A. Bai, S. Ötleş, and B. Y. Şahyar, "Use of nanopolymers, nanocomposites, and nanostructured coatings in food packaging," in *Nanotechnology Applications in the Food Industry*, pp. 97–106, CRC Press, 2018.
- [27] M. Azizi-Lalabadi, H. Hashemi, J. Feng, and S. M. Jafari, "Carbon nanomaterials against pathogens; the antimicrobial activity of carbon nanotubes, graphene/graphene oxide, fullerenes, and their nanocomposites," *Advances in Colloid and Interface Science*, vol. 284, article 102250, 2020.
- [28] H. Fan, M. Zhang, B. Bhandari, and C. H. Yang, "Food waste as a carbon source in carbon quantum dots technology and their applications in food safety detection," *Trends in Food Science & Technology*, vol. 95, pp. 86–96, 2020.
- [29] P. Devi, S. Saini, and K. H. Kim, "The advanced role of carbon quantum dots in nanomedical applications," *Biosensors and Bioelectronics*, vol. 141, article 111158, 2019.
- [30] R. Prasad and M. Kumar, *Nanotechnology: An Agricultural Paradigm*, V. Kumar, Ed., Springer, 2017.
- [31] S. Agrawal and P. Rathore, "Nanotechnology pros and cons to agriculture: a review," *International Journal of Current Microbiology and Applied Sciences*, vol. 3, no. 3, pp. 43–55, 2014.
- [32] H. M. Ahmed, "Phytochemical screening, total phenolic content and phytotoxic activity of corn (*Zea mays*) extracts against some indicator species," *Natural Product Research*, vol. 32, no. 6, pp. 714–718, 2018.
- [33] R. Nair, S. H. Varghese, B. G. Nair, T. Maekawa, Y. Yoshida, and D. S. Kumar, "Nanoparticulate material delivery to plants," *Plant Science*, vol. 179, no. 3, pp. 154–163, 2010.
- [34] A. Yaktine, *Nanotechnology in Food Products: Workshop Summary*, L. Pray, Ed., National Academies Press, 2009.
- [35] M. R. Naderi and A. Danesh-Shahraki, "Nanofertilizers and their roles in sustainable agriculture," *International Journal of Agriculture and Crop Sciences*, vol. 5, no. 19, p. 2229, 2013.
- [36] T. Mennini, "Nanotechnology-enabled foods and food contact materials on the UK market," *Nutrafoods*, vol. 12, no. 1, pp. 29–29, 2013.
- [37] European Food Safety Authority, "Nanotechnology," 2012, <https://www.food.gov.uk/safety-hygiene/genetically-modified-foods>.
- [38] European Food Safety Authority (EFSA), "The potential risks arising from nanoscience and nanotechnologies on food and feed safety," *EFSA Journal*, vol. 7, no. 3, p. 958, 2009.
- [39] K. Groves and P. Titoria, "Nanotechnology and the food industry," *Food Science & Technology*, vol. 23, no. 2, pp. 22–24, 2009.
- [40] European Food Safety Authority (EFSA), "A review of potential implications of nanotechnologies for regulations and risk assessment in relation to food," 2008, <http://www.food.gov.uk/multimedia/pdfs/nanoregreviewreport.pdf>.
- [41] A. Acevedo-Fani, R. Soliva-Fortuny, and O. Martín-Belloso, "Nanostructured emulsions and nanolaminates for delivery of active ingredients: improving food safety and functionality," *Trends in Food Science & Technology*, vol. 60, pp. 12–22, 2017.
- [42] S. Sonkaria, S. H. Ahn, and V. Khare, "Nanotechnology and its impact on food and nutrition: a review," *Recent Patents on Food, Nutrition & Agriculture*, vol. 4, no. 1, pp. 8–18, 2012.
- [43] H. M. Ahmed and A. M. A. Al-Zubaidy, "Exploring natural essential oil components and antibacterial activity of solvent extracts from twelve *Perilla frutescens* L. Genotypes," *Arabian Journal of Chemistry*, vol. 13, no. 10, pp. 7390–7402, 2020.
- [44] M. C. Powell and M. S. Kanarek, "Nanomaterial health effects-part 2: uncertainties and recommendations for the future," *Wisconsin Medical Journal*, vol. 105, no. 3, pp. 18–23, 2006.
- [45] R. Prasad, A. Bhattacharyya, and Q. D. Nguyen, "Nanotechnology in sustainable agriculture: recent developments, challenges, and perspectives," *Frontiers in Microbiology*, vol. 8, p. 1014, 2017.
- [46] M. Tkaczyszyn, J. Comin-Colet, A. A. Voors et al., "Iron deficiency and red cell indices in patients with heart failure," *European Journal of Heart Failure*, vol. 20, no. 1, pp. 114–122, 2018.
- [47] R. Hurrell and I. Egli, "Iron bioavailability and dietary reference values—," *The American Journal of Clinical Nutrition*, vol. 91, no. 5, pp. 1461S–1467S, 2010.
- [48] M. Zimmermann, F. Rohner, F. Ernst et al., "Synthesis, characterization and bioavailability of ferric phosphate nanoparticles," *The FASEB Journal*, vol. 21, no. 6, pp. A1113–A11A1, 2007.
- [49] B. S. Sekhon, "Nanotechnology in agri-food production: an overview," *Nanotechnology, Science and Applications*, vol. 7, p. 31, 2014.
- [50] N. A. Singh, "Nanotechnology innovations, industrial applications and patents," *Environmental Chemistry Letters*, vol. 15, no. 2, pp. 185–191, 2017.
- [51] R. Kalpana Sastry, S. Anshul, and N. H. Rao, "Nanotechnology in food processing sector—an assessment of emerging trends," *Journal of Food Science and Technology*, vol. 50, no. 5, pp. 831–841, 2013.

- [52] A. R. Singh, P. K. Desu, R. K. Nakkala et al., "Nanotechnology-based approaches applied to nutraceuticals," *Drug Delivery and Translational Research*, pp. 1–15, 2021.
- [53] W. Jian, D. Hui, and D. Lau, "Nanoengineering in biomedicine: current development and future perspectives," *Nanotechnology Reviews*, vol. 9, no. 1, pp. 700–715, 2020.
- [54] S. R. D'Mello, C. N. Cruz, M. L. Chen, M. Kapoor, S. L. Lee, and K. M. Tyner, "The evolving landscape of drug products containing nanomaterials in the United States," *Nature Nanotechnology*, vol. 12, no. 6, pp. 523–529, 2017.
- [55] V. P. Nguyen, H. Le Trung, T. H. Nguyen, D. Hoang, and T. H. Tran, "Synthesis of biogenic silver nanoparticles with eco-friendly processes using *Ganoderma lucidum* extract and evaluation of their theranostic applications," *Journal of Nanomaterials*, vol. 2021, Article ID 6135920, 11 pages, 2021.
- [56] A. Di Paolo, "Liposomal anticancer therapy: pharmacokinetic and clinical aspects," *Journal of chemotherapy*, vol. 16, supplement 4, pp. 90–93, 2004.
- [57] K. M. Tyner, N. Zheng, S. Choi et al., "How has CDER prepared for the nano revolution? A review of risk assessment, regulatory research, and guidance activities," *The AAPS Journal*, vol. 19, no. 4, pp. 1071–1083, 2017.
- [58] K. J. Morrow, R. Bawa, and C. Wei, "Recent advances in basic and clinical nanomedicine," *Medical Clinics of North America*, vol. 91, no. 5, pp. 805–843, 2007.
- [59] S. Sugumar, M. F. Jamlos, M. N. Ahmad, C. S. Bellan, and D. Schreurs, "Nanostructured materials with plasmonic nanobiosensors for early cancer detection: a past and future prospect," *Biosensors and Bioelectronics*, vol. 100, pp. 361–373, 2018.
- [60] J. F. Buyel, "Plants as sources of natural and recombinant anticancer agents," *Biotechnology Advances*, vol. 36, no. 2, pp. 506–520, 2018.
- [61] N. A. Peppas and N. J. Kavimandan, "Nanoscale analysis of protein and peptide absorption: insulin absorption using complexation and pH-sensitive hydrogels as delivery vehicles," *European Journal of Pharmaceutical Sciences*, vol. 29, no. 3–4, pp. 183–197, 2006.
- [62] P. R. Srinivas, M. Philbert, T. Q. Vu et al., "Nanotechnology research: applications in nutritional sciences," *The Journal of Nutrition*, vol. 140, no. 1, pp. 119–124, 2010.
- [63] M. Cushen, J. Kerry, M. Morris, M. Cruz-Romero, and E. Cummins, "Nanotechnologies in the food industry - Recent developments, risks and regulation," *Trends in Food Science & Technology*, vol. 24, no. 1, pp. 30–46, 2012.
- [64] P. J. Borm, D. Robbins, S. Haubold et al., "The potential risks of nanomaterials: a review carried out for ECETOC," *Particle and Fibre Toxicology*, vol. 3, no. 1, p. 11, 2006.
- [65] J. Muller, F. Huaux, N. Moreau et al., "Respiratory toxicity of multi-wall carbon nanotubes," *Toxicology and Applied Pharmacology*, vol. 207, no. 3, pp. 221–231, 2005.
- [66] A. Nasir, "Nanotechnology and dermatology: Part II—risks of nanotechnology," *Clinics in Dermatology*, vol. 28, no. 5, pp. 581–588, 2010.
- [67] P. Rosenkranz, M. L. Fernández-Cruz, E. Conde et al., "Effects of cerium oxide nanoparticles to fish and mammalian cell lines: an assessment of cytotoxicity and methodology," *Toxicology In Vitro*, vol. 26, no. 6, pp. 888–896, 2012.
- [68] Z. Chen, H. Meng, G. Xing et al., "Acute toxicological effects of copper nanoparticles in vivo," *Toxicology Letters*, vol. 163, no. 2, pp. 109–120, 2006.
- [69] J. J. Powell, R. S. J. Harvey, P. Ashwood, R. Wolstencroft, M. E. Gershwin, and R. P. H. Thompson, "Immune potentiation of ultrafine dietary particles in normal subjects and patients with inflammatory bowel disease," *Journal of Autoimmunity*, vol. 14, no. 1, pp. 99–105, 2000.
- [70] D. D. Verma, S. Verma, G. Blume, and A. Fahr, "Particle size of liposomes influences dermal delivery of substances into skin," *International Journal of Pharmaceutics*, vol. 258, no. 1–2, pp. 141–151, 2003.
- [71] S. Sharifi, S. Behzadi, S. Laurent, M. Laird Forrest, P. Stroeve, and M. Mahmoudi, "Toxicity of nanomaterials," *Chemical Society Reviews*, vol. 41, no. 6, pp. 2323–2343, 2012.
- [72] A. Nel, T. Xia, L. Mädler, and N. Li, "Toxic potential of materials at the nanolevel," *Science*, vol. 311, no. 5761, pp. 622–627, 2006.
- [73] Q. Chaudhry, M. Scotter, J. Blackburn et al., "Applications and implications of nanotechnologies for the food sector," *Food Additives and Contaminants*, vol. 25, no. 3, pp. 241–258, 2008.
- [74] W. Liu, Y. Wu, C. Wang et al., "Impact of silver nanoparticles on human cells: effect of particle size," *Nanotoxicology*, vol. 4, no. 3, pp. 319–330, 2010.
- [75] A. Grobe, O. Renn, and A. Jaeger, *Risk governance of nanotechnology applications in food and cosmetics*, International Risk Governance Council (IRGC), 2008.
- [76] N. Sozer and J. L. Kokini, "Nanotechnology and its applications in the food sector," *Trends in Biotechnology*, vol. 27, no. 2, pp. 82–89, 2009.
- [77] European Food Safety Authority (EFSA), "The potential risks arising from nanoscience and nanotechnologies on food and feed safety," 2010, <http://www.efsa.europa.eu/en/events/documents/corporate101124-ax1.pdf>.
- [78] Q. Saquib, A. A. Al-Khedhairy, M. A. Siddiqui, F. M. Abou-Tarboush, A. Azam, and J. Musarrat, "Titanium dioxide nanoparticles induced cytotoxicity, oxidative stress and DNA damage in human amnion epithelial (WISH) cells," *Toxicology In Vitro*, vol. 26, no. 2, pp. 351–361, 2012.
- [79] N. Gupta, A. R. Fischer, I. A. van der Lans, and L. J. Frewer, "Factors influencing societal response of nanotechnology: an expert stakeholder analysis," *Journal of Nanoparticle Research*, vol. 14, no. 5, p. 857, 2012.
- [80] M. Siegrist, N. Stampfli, and H. Kastenholz, "Acceptance of nanotechnology foods: a conjoint study examining consumers' willingness to buy," *British Food Journal*, vol. 111, no. 7, pp. 660–668, 2009.
- [81] M. Siegrist and C. Keller, "Labeling of nanotechnology consumer products can influence risk and benefit perceptions," *Risk Analysis*, vol. 31, no. 11, pp. 1762–1769, 2011.

## Research Article

# Citrus Lemon Juice Mediated Preparation of AgNPs/Chitosan-Based Bionanocomposites and Its Antimicrobial and Antioxidant Activity

S. Rajeshkumar 

Nanobiomedicine Lab, Department of Pharmacology, Saveetha Dental College and Hospitals, SIMATS, Chennai 600077, India

Correspondence should be addressed to S. Rajeshkumar; [ssrajeshkumar@hotmail.com](mailto:ssrajeshkumar@hotmail.com)

Received 2 July 2021; Revised 15 September 2021; Accepted 24 September 2021; Published 6 October 2021

Academic Editor: Ali Khorsand Zak

Copyright © 2021 S. Rajeshkumar. This is an open access article distributed under the Creative Commons Attribution License, which permits unrestricted use, distribution, and reproduction in any medium, provided the original work is properly cited.

Nanoparticles are important advanced materials with numerous uses in a variety of fields. Novel antibacterial nanocomposites with synergistic capabilities can be created by combining metal nanoparticles with biopolymers of various functionalities. This research evaluates an antimicrobial and antioxidant-rich chitosan-based silver nanocomposite synthesized by using citrus lemon extract as a reducing and capping agent. UV-vis spectrophotometer, scanning electron microscope, elemental dispersive analysis, X-ray diffraction assay, atomic force microscope, Fourier transform infrared spectroscopy, UV-near infrared spectroscopy, and transmission electron microscopy were used to characterize the chitosan-based silver nanocomposite (CS-Ag nanocomposite). The nanocomposite synthesized is used to demonstrate antioxidant and antimicrobial activity against fungal pathogens.

## 1. Introduction

Nanoparticles and nanocomposites are employed in a variety of applications across a wide range of industries. Silver nanoparticles have a wide range of applications as antimicrobial agents, including wastewater treatment, food preservation, clothe and textile preservation, detergents, and medical implants [1]. Plant extracts can be used to make silver nanoparticles that are both environmentally friendly and cost-effective [2]. Plant extracts such as *Boerhavia diffusa* leaves [3], *Piper nigrum* stem and leaf [4], *Avicennia marina* mangrove plant [5], *Cissus quadrangularis* [6], *Parthenium hysterophorus* [7], *Manilkara zapota* seeds [6], and Chrysanthemum flower extracts [8] and fruit extracts of pomegranate [9], *Dillenia indica* [10], *Solanum xanthocarpum* [11], and *Crataegus douglasii* [12] were employed, and it was used for antibacterial, antifungal, and antioxidant properties. Chitosan is a harmless, biodegradable polymer found in natural resources such as crab and prawn shells, as well as other marine and terrestrial invertebrates. Because of its excellent antibacterial and biocompatibility qualities, it has a wide range of biological uses [13]. Once silver nanoparticles are mixed with other polymers, they

can generate nanocomposites with a variety of benefits. The antimicrobial activity of silver with agar against *Listeria monocytogenes* and *Escherichia coli* [14], the antimicrobial activity of polysulfone with silver to inhibit biofilm growth on downstream membrane surfaces [15], and the bacterial cellulose with silver magnetic nanocomposites are used for high antimicrobial activity against the model microbes *Escherichia coli* and *Bacillus subtilis* [16], and agar-based silver nanocomposite films are prepared using red alga *Gracilaria dura* to control *Bacillus pumilis* bacterial growth [17]. Chitosan-based silver nanocomposites, which include chitosan with silver nanoparticles, are being developed for a variety of commercial uses. The *Bacillus subtilis*-based silver nanocomposites were tested against disease-causing pathogens such as *Staphylococcus aureus*, *Pseudomonas aeruginosa*, *Aspergillus niger*, and *Candida albicans* [18], and the chitosan-based silver and fluoride nanocomposites were tested against disease-causing pathogens such as *Staphylococcus aureus*, *Escherichia coli*, and *Candida albicans* using microdilution technique [19]. In this research, we employed citrus lemon juice to synthesize chitosan-based silver nanocomposites (CS-Ag nanocomposite). UV-vis spectrophotometer, scanning electron

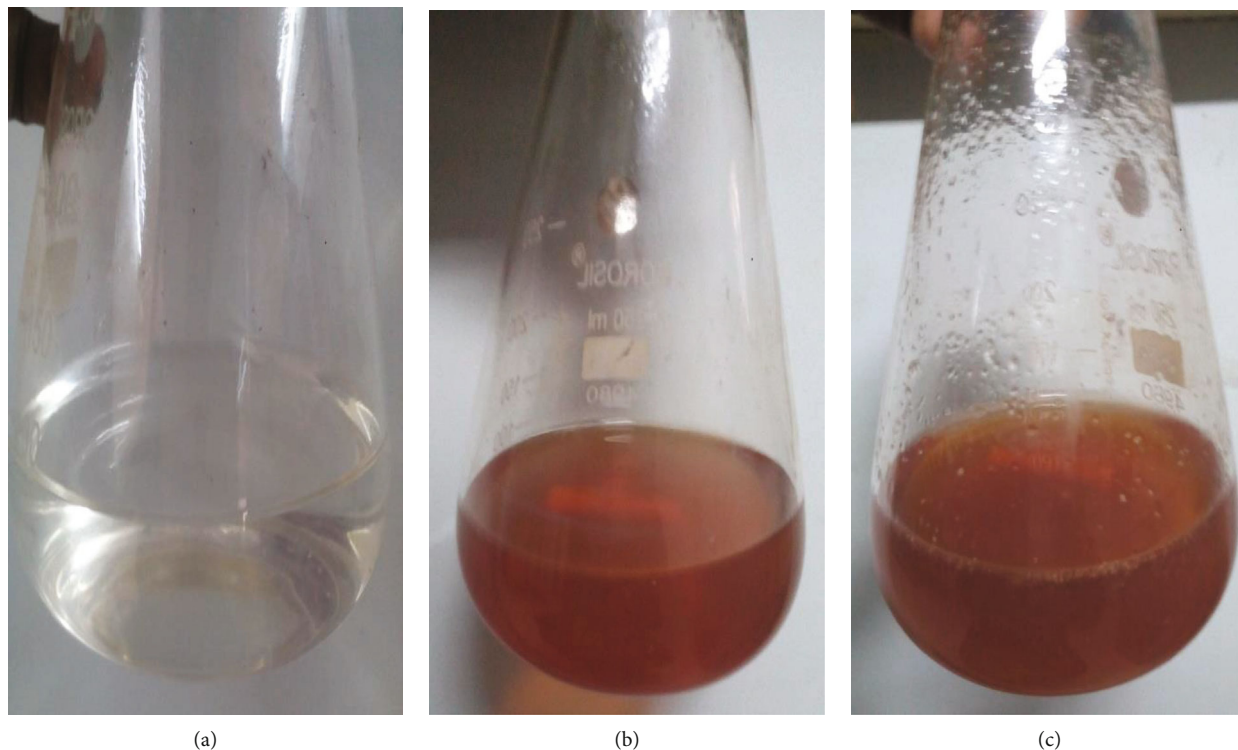


FIGURE 1: Visual observation: (a) initial observation of lemon extract and  $\text{AgNO}_3$ ; (b) color change after 2 hours; (c) color change after adding chitosan.

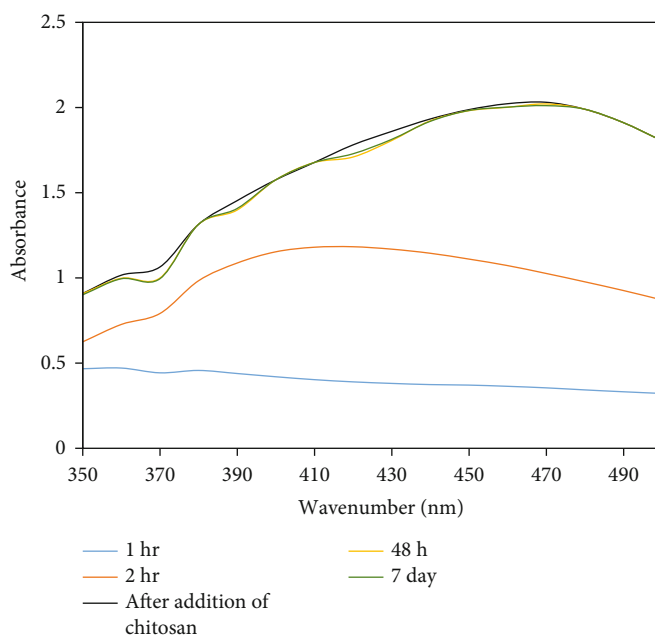


FIGURE 2: UV-spectrum of CS-Ag nanocomposites.

microscope, elemental dispersive analysis, X-ray diffraction assay, atomic force microscope, Fourier transform infrared spectroscopy, and UV-near infrared spectroscopy were used to characterize the nanocomposites. Finally, antioxidant and antibacterial activity against fungal infections is performed to the nanocomposites which have been synthesized.

## 2. Materials and Methods

**2.1. Preparation of Fruit Extract.** Lemon fruit was purchased from Vellore market and washed thoroughly under tap water. The lemons were cut into four pieces, and the fresh juice was extracted, filtered using Whatman No.1 filter paper.

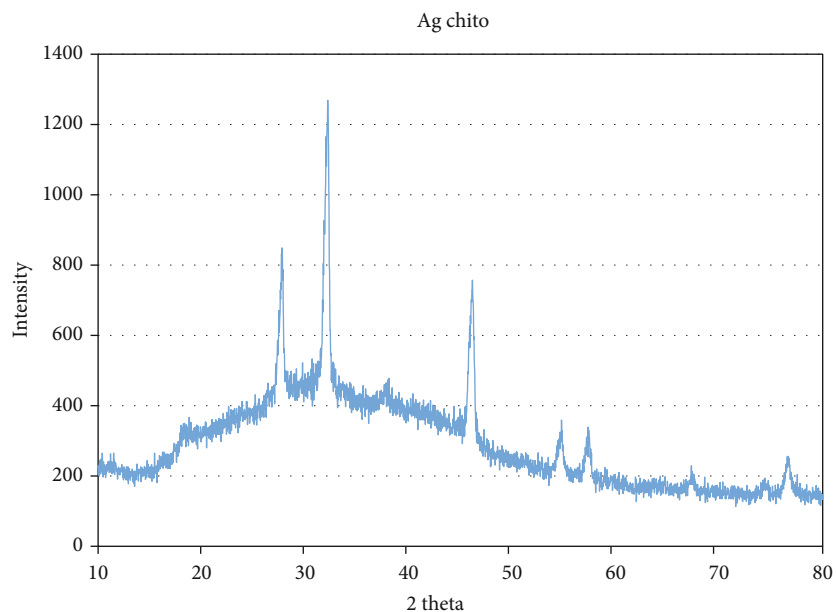


FIGURE 3: XRD spectrum of CS-Ag nanocomposite which showed broadened peak due to the presence of chitosan polymer.

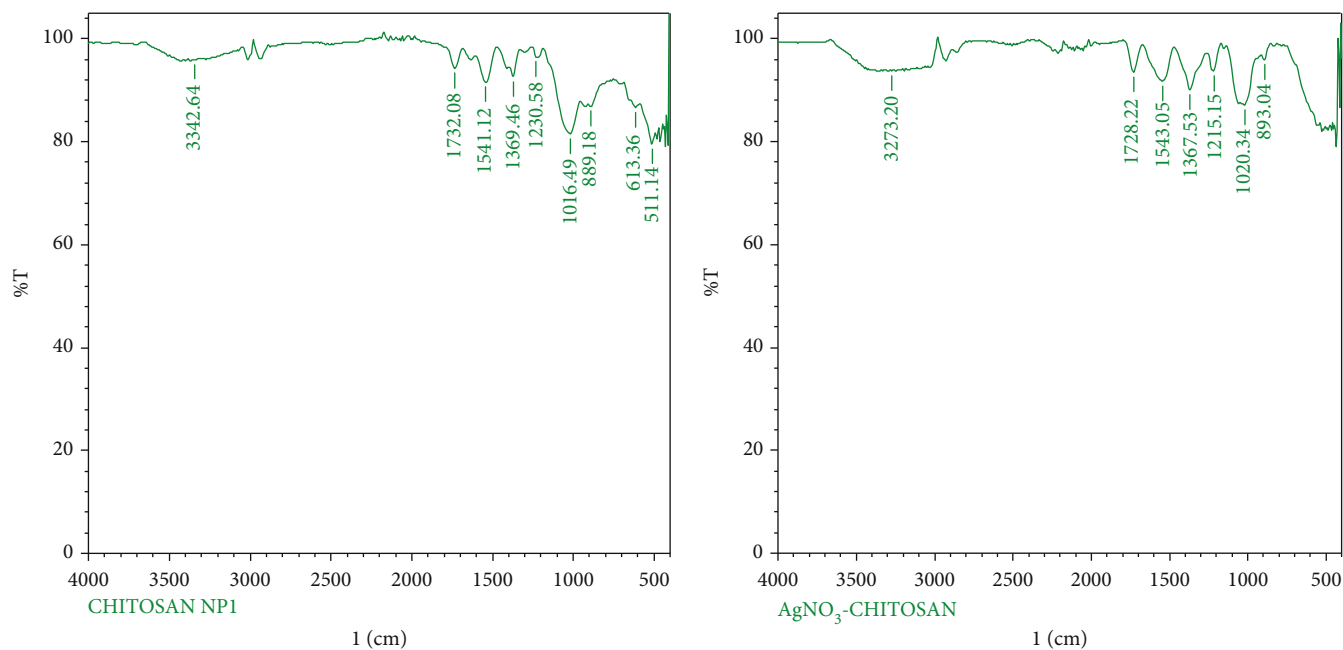


FIGURE 4: FTIR spectra of chitosan and chitosan-based silver nanocomposites.

**2.2. Synthesis of CS-Ag Nanocomposite.** To synthesize CS-Ag nanocomposite, 1 mM of silver nitrate was added to 95 ml of distilled water. 5 ml of filtered fresh lemon juice extract was added to 95 ml of silver nitrate solution. The reaction mixture was placed on a magnetic stirrer at 700 rpm for 3 h to detect color changes. Figure 1 depicts a visual observation of the synthesized silver nanoparticle solution. After 3 h, 0.25 g of chitosan was added to the solution and stirred for 3 h in a magnetic stirrer at 700 rpm. The CS-Ag nanocomposite solution was then centrifuged for 10 minutes at 8000 rpm. The pellet was collected after centrifugation, and the supernatant was discarded.

**2.3. Characterization of CS-Ag Nanocomposite.** During the reduction of  $\text{Ag}^+$  to Ag NPs, UV-vis absorption analysis was carried. It was often scanned in the 300-500 nm wavelength range. XRD measurements at 40 kV and 30 mA, equipped with a Cu anode and a ceramic X-ray tube, were used to assess the crystalline nature and structure of AgNPs incorporated with chitosan. The functional groups present in the CS-Ag nanocomposite were analyzed using FT-IR in the range of  $4000\text{-}500\text{ cm}^{-1}$ . The microstructure of lemon extract mediated CS-Ag nanocomposite was analyzed using a scanning electron microscope (SEM) and atomic force microscope (AFM) to determine the size shape and

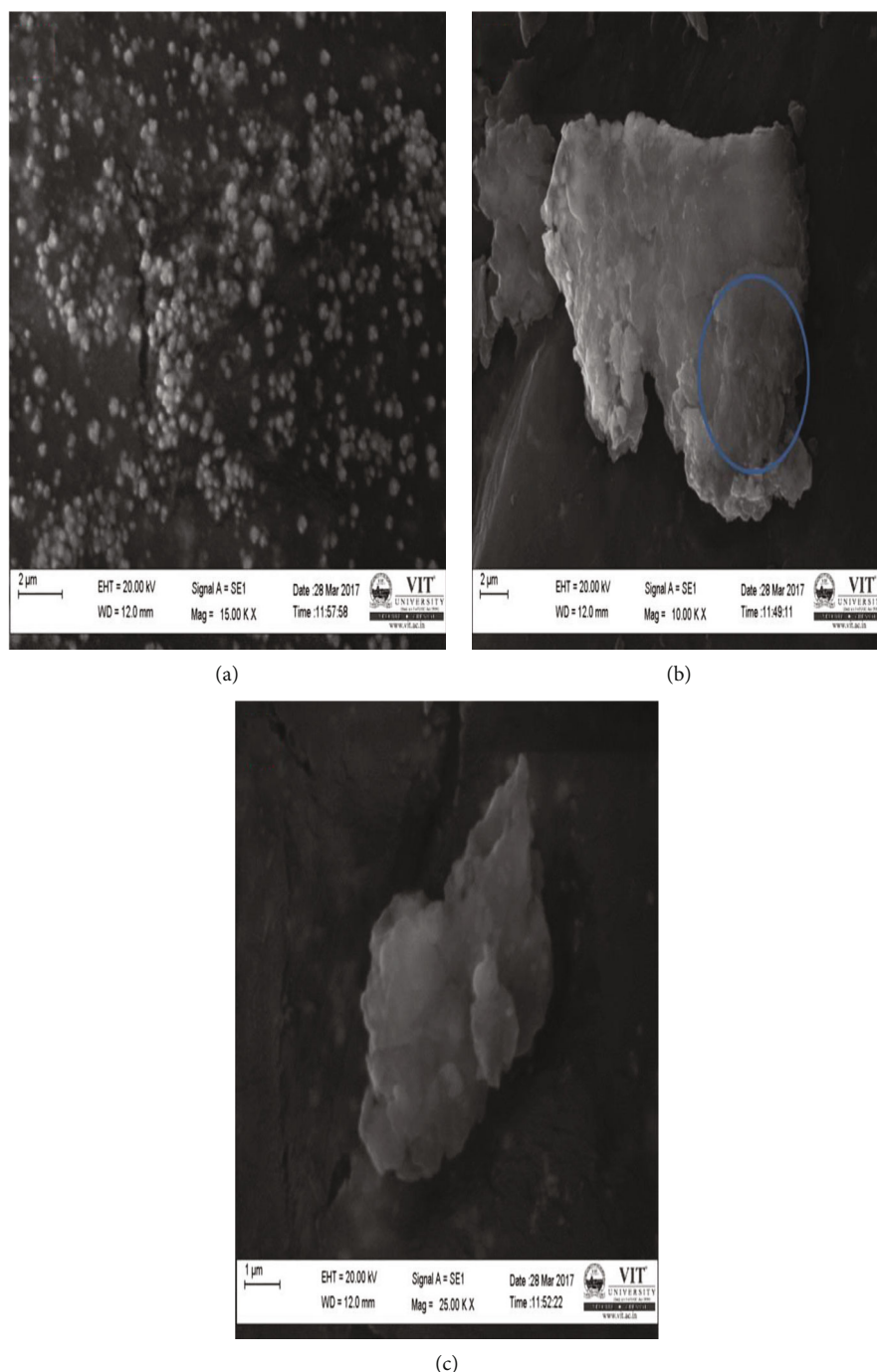


FIGURE 5: SEM images of CS-Ag nanocomposites: (a) chitosan-silver nanoparticles with the size range of 200 nm; (b) SEM image of silver nanoparticles embedded in chitosan polymer; (c) SEM image of chitosan polymer.

morphology of the CS-Ag nanocomposite. Energy-dispersive X-ray analysis spectrum was also recorded.

**2.4. Antibacterial Activity.** The agar well diffusion method was used to test antibacterial activity. The Mueller-Hinton agar was sterilized and prepared. The Muller-Hinton agar was poured and solidified in aseptic condition on clean and sterilized Petri plates. Swabs of pathogenic organisms such as *Streptococcus sp*, *Rhizobium radiobacter*, *Klebsiella pneumoniae*, and *Escherichia coli* were cultured in liquid

broth. After 5 minutes, wells were punched in the agar plate with a 5 mm gel puncher. The results were seen after different concentrations of nanoparticles of 25  $\mu\text{l}$ , 50  $\mu\text{l}$ , and 75  $\mu\text{l}$  were loaded into each well and incubated for 24 hours. The antibacterial activity was determined by measuring the diameter of the inhibitory zone generated around the well and recording the mean results.

**2.5. Antifungal Activity.** The agar well diffusion method was used to test antifungal activity. Rose Bengal Agar was

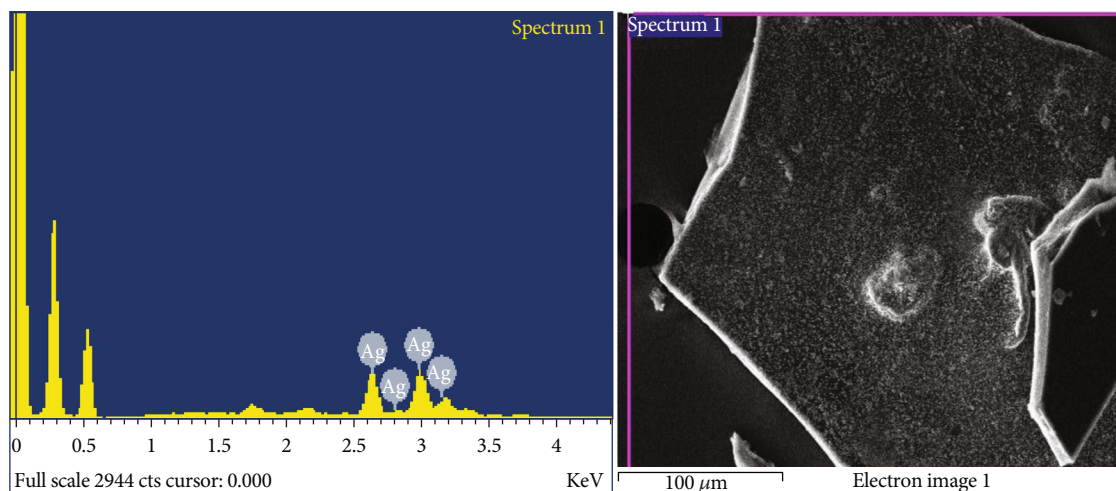


FIGURE 6: EDX spectra of chitosan-silver nanocomposites.

sterilized and prepared. The Rose Bengal Agar was poured and solidified in sterile conditions on clean and sterilized plates. Cultures of pathogenic organisms like *Aspergillus niger*, *Fusarium oxysporum*, and *Aspergillus fumigatus* were inoculated and swabbed. After 5 minutes, wells were punched in the agar plate with a 5 mm gel puncher. Different concentrations of nanoparticles of 25  $\mu\text{l}$ , 50  $\mu\text{l}$ , and 75  $\mu\text{l}$  were loaded into each well and incubated for 24 hours before the data were analyzed. The antifungal activity was determined by measuring the diameter of the inhibitory zone that formed around the well and recording the mean results.

**2.6. Antioxidant Activity of Nanocomposites.** Based on previous findings [8], the free radical scavenging activity of the lemon juice mediated CS-Ag nanocomposite was evaluated using the 1,1-diphenyl-2-picrylhydrazyl (DPPH) assay. 0.78 mg of DPPH was added to 10 ml of methanol to make DPPH. Five different concentrations of extracts (20  $\mu\text{l}$ , 40  $\mu\text{l}$ , 60  $\mu\text{l}$ , 80  $\mu\text{l}$ , and 100  $\mu\text{l}$ ) were added to 2 ml of this DPPH solution. The antioxidant ascorbic acid was utilized as a standard. The samples were incubated for 30 min in dark. The absorbance was measured using a spectrophotometer at 517 nm. The blank was prepared without the addition of extract. Lower absorbance of the reaction mixture indicates higher free radical scavenging activity. The capability to scavenge the DPPH radical was calculated using the following equation:

$$\text{DPPH Scavenged (\%)} = \frac{A_{\text{control}} - A_{\text{test}} \times 100}{A_{\text{control}}}, \quad (1)$$

where  $A_{\text{control}}$  is the absorbance of the control reaction and  $A_{\text{test}}$  is the absorbance in the presence of the sample of the extracts.

### 3. Result and Discussion

**3.1. Color Change and Visual Observation.** Figure 1(a) shows the silver nitrate solution, which changed color from pale yellow to brown after adding lemon juice, indicating the syn-

thesis of silver nanoparticles. Fruit extracts are a great source for making silver nanoparticles because they quickly change the color of silver nitrate solution into silver nanoparticles [9]. AgNPs were expected to form in the CS-Ag nanocomposite as a result of  $\text{AgNO}_3$  reduction. Depending on the concentration of AgNPs, the chitosan films loaded with AgNPs turned from pale brown to dark brown. Figure 1(c) depicts the color change of silver nanoparticles in chitosan solution to turbid solution.

**3.2. UV-Visible Spectroscopy.** The UV-vis absorption spectra of Ag nanoparticles and AgNP-based chitosan nanocomposites are shown in Figure 2. Figure 2 displays a peak at 420 nm, due to the plasma vibrations of silver nanoparticles and another peak at 470 nm showing some possible interaction between chitosan and silver nanoparticles. The absorption peaks of the UV-vis spectra shifted to a longer wavelength when the particle diameters were increased [20]. Based on the size of the AgNPs, the SPR band at 420–460 nm represents silver nanoparticles, and the peak increases when chitosan is added to the solution [21, 22]. The nanocomposite was again analyzed for its surface plasmon resonance at 48 h and 7<sup>th</sup> day. The peaks are near to the value of after the addition of chitosan values confirms the stability of nanocomposites.

**3.3. X-Ray Diffraction Analysis.** Figure 3 shows the XRD patterns of the CS-Ag nanocomposite spheres. The (111), (121), and (200), crystallographic planes of the face-centered cubic silver crystals might be attributed to three distinctive peaks of silver nanoparticles corresponding to  $2\theta = (28.01^\circ)$ ,  $(32.18^\circ)$ , and  $(46.16^\circ)$ . The position and relative intensity of all the diffraction peaks of the samples were compatible with the crystalline pattern of silver, indicating that the produced nanoparticles were silver nanoparticles. Furthermore, the chitosan utilized in the synthesis procedure did not induce silver oxides to develop. Since the chitosan polymer and silver nanoparticles were present, the shape of each peak was broadened.

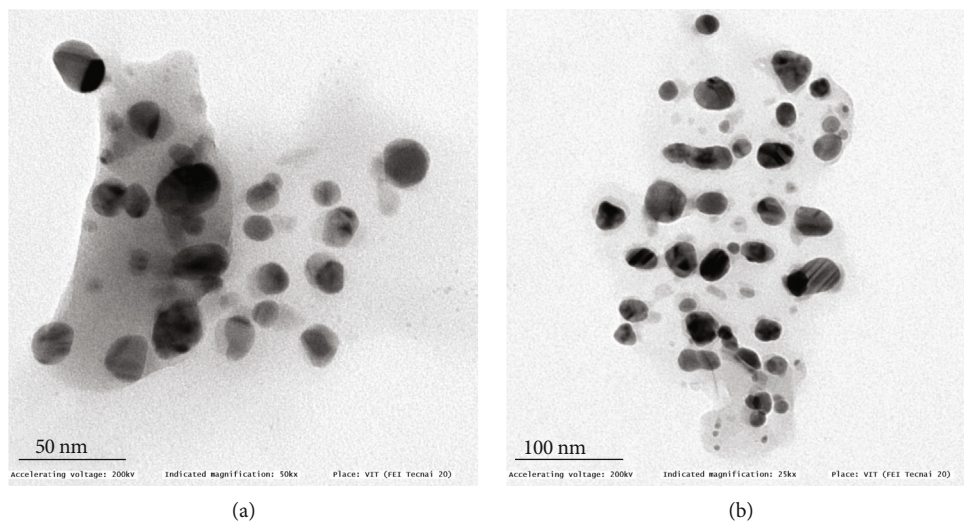


FIGURE 7: Silver nanoparticles embedded with chitosan nanocomposite: (a) 50 nm and (b) 100 nm.

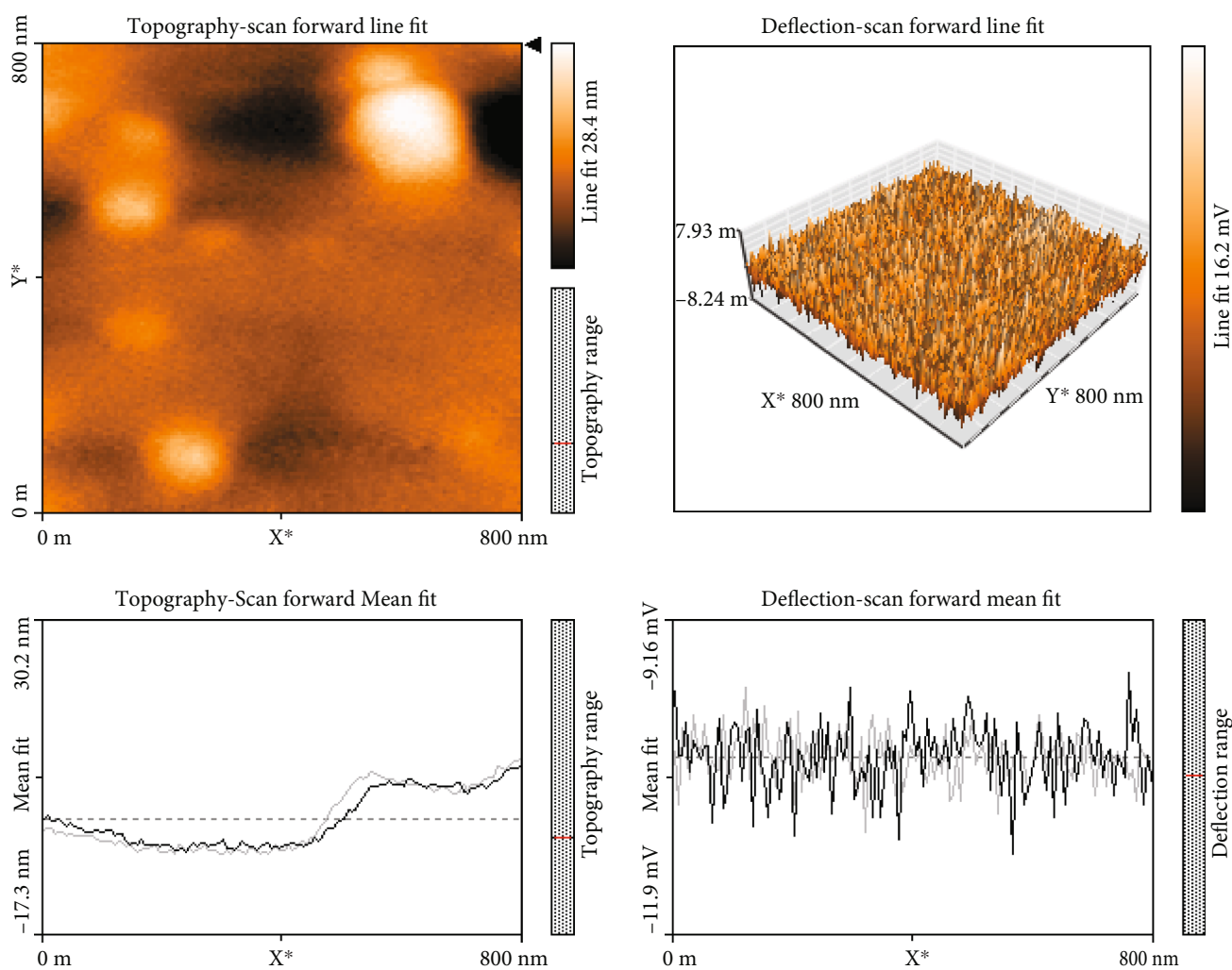


FIGURE 8: Topographical image by AFM.

**3.4. FTIR Spectroscopy.** FTIR spectra of CS-Ag nanocomposites are shown in Figure 4. The band between  $3273.20\text{ cm}^{-1}$  was related to the stretching vibration of =C-H from the

alkyne group. The band between  $1728.22\text{ cm}^{-1}$  was related to stretching vibration of C=O from ester groups. The band between  $1543.05\text{ cm}^{-1}$  was related to the bending vibration of



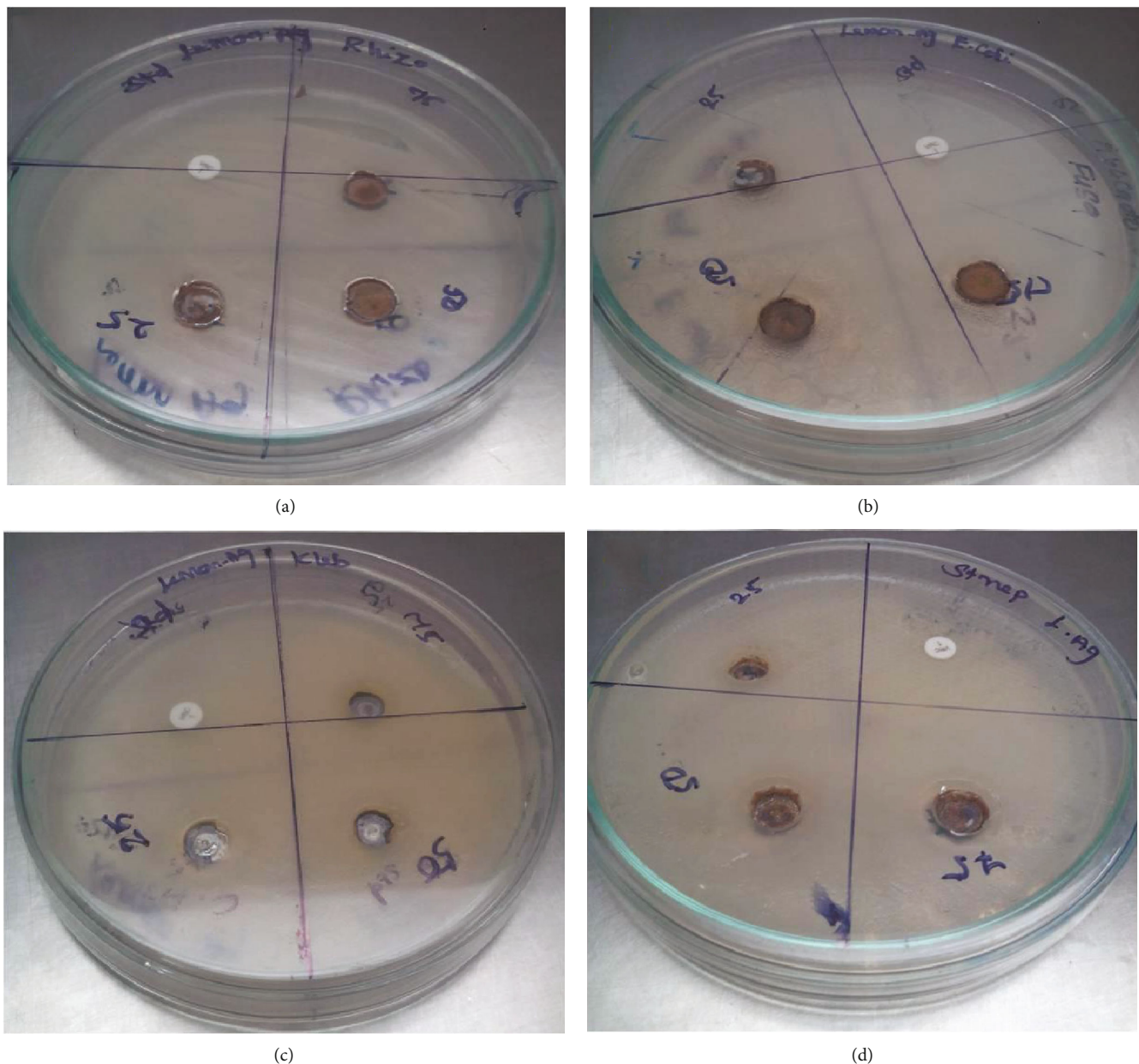


FIGURE 9: Antimicrobial activity of CS-Ag nanocomposite against (a) *Rhizobium radiobacter*, (b) *Escherichia coli*, (c) *Klebsiella pneumoniae*, and (d) *Streptococcus* sp.

N-H from the amine secondary group. The band between  $1367.53\text{ cm}^{-1}$  was related to bending vibration of N=O from the nitro group. The band between  $1215.15\text{ cm}^{-1}$  and  $1020.34\text{ cm}^{-1}$  was related to the stretching vibration of C-O from the ester group. The silver nanoparticles were bonded by protein, which served as a stabilizing agent, either through the free amine group or cysteine residues. These proteins could reduce  $\text{AgNO}_3$  ions to form silver nanoparticles [4, 23].

**3.5. Scanning Electron Microscopy.** SEM analysis was used to determine the size and shape of nanocomposites. Figure 5(a) clearly shows the SEM micrograph of the silver nanocomposite. The composite particle has an average diameter of about 200 nm and a uniform particle size. The morphology

of the chitosan spheres is shown in Figure 5(b), which have relatively smooth structures when compared to the CS-Ag nanocomposite spheres. The background of chitosan and silver nanoparticle binding is clearly shown in Figures 5(b) and 5(c). Youssef et al. previously reported to synthesize chitosan-based silver and gold nanocomposites [18] in which SEM images clearly show the binding of chitosan and silver nanoparticles.

**3.6. EDX Spectrum Analysis.** The EDX analysis was used to determine the elements in chitosan-based silver nanocomposites, and the results are shown in Figure 6. The EDX analysis confirmed that the nanocomposites contained approximately 15% silver and chitosan, 35% carbon, 44% oxygen, and 4% nitrogen. The metallic element, Ag, was

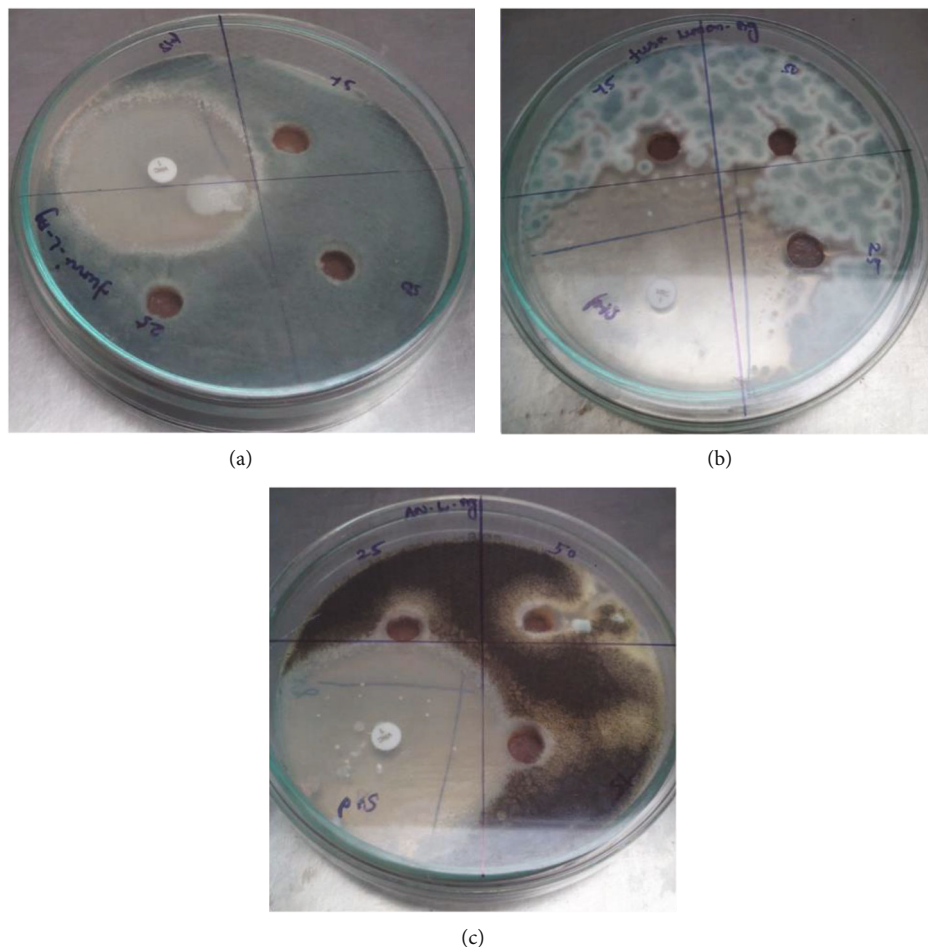


FIGURE 10: Antifungal activity of chitosan/silver nanocomposite against (a) *Aspergillus fumigatus*, (b) *Fusarium oxysporum*, and (c) *Aspergillus niger*.

present in all of the chitosan-based silver nanocomposite films, and the amount of elemental silver in the CS-Ag nanocomposite films increased as the content of AgNP increased.

**3.7. TEM Analysis.** The morphology of nanoparticles and nanocomposites prepared using green synthesis methods is greatly aided by TEM analysis [24, 25]. The various shapes and sizes produced by silver nanoparticles with chitosan are clarified by TEM analysis. Silver nanoparticles with sizes ranging from 15 to 25 nm have been discovered, and the size of the nanocomposite is 150 to 200 nm. The chitosan nanocomposites were clearly observed to be embedded with silver nanoparticles, confirming the nanocomposite formation. Figures 7(a) and 7(b) show different spherical-shaped nanoparticles and the background light color, which was discovered to be chitosan.

**3.8. AFM Analysis.** AFM was used to perform topographical imaging on the surface roughness of the film sample. In Figure 8, an AFM image of silver nanoparticles with chitosan-formed nanocomposites clearly matches the SEM and TEM images.

**3.9. Antibacterial Activity.** Figure 9 depicts the antibacterial activity of CS-Ag nanocomposite against bacterial pathogens. At a concentration of 75  $\mu\text{l}$ , the maximum zone of inhibition was obtained in the gram-positive bacteria *Streptococcus*, with a zone diameter of  $12.47 \pm 0.26$ . At a concentration of 25  $\mu\text{l}$ , the gram-negative bacteria *Klebsiella pneumoniae* had the smallest zone of inhibition, with a zone diameter of  $10.27 \pm 0.18$ . The difference in inhibition is due to the arrangement of cell walls in gram-positive and gram-negative organisms. *Streptococcus pneumoniae*, which causes pneumonia, wound infection, and skin infection, can be killed by CS-Ag nanocomposites. Silver nanoparticles are an excellent antibacterial agent, and when combined with chitosan, they may be even more effective against other bacterial pathogens [21, 22, 26].

**3.10. Antifungal Activity.** Figure 10 depicts the antifungal activity of chitosan/silver nanocomposites against fungus. It had the highest fungal activity against *Aspergillus niger* and the smallest inhibition zone against *Aspergillus fumigatus* and *Fusarium oxysporum*. The fungus' cell wall is very strong, and it may prevent fungal growth from being killed. Silver nanoparticles have been shown to suppress fungal infections on their own [27].

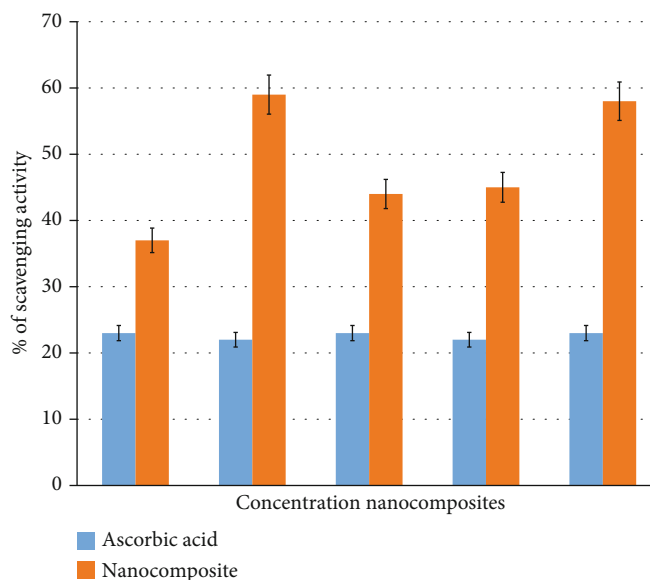


FIGURE 11: Graphical representation of antioxidant activity by DPPH assay.

**3.11. Antioxidant Activity by DPPH Assay.** The silver nanoparticles synthesized using plant extracts are having very good antioxidant property [8, 28]. DPPH has been used extensively as a stable free to evaluate reducing substances, and it is a useful reagent for investigating free radical scavenging activity of the component. The free radical scavenging activity by DPPH in graphical representation is shown in Figure 11. It demonstrates the highest antioxidant activity at higher concentration such as  $100 \mu\text{l}$  which implies a dose-dependent manner (Bedlovicova et al.,2020).

## 4. Conclusion

Lemon juice extract was shown to form a silver nanoparticle-based chitosan nanocomposite. Characterization of the material using XRD, UV-vis spectroscopy, and FT-IR techniques confirmed the production of the nanocomposite. AFM, SEM, and TEM were used to analyze the morphology of nanocomposite. The nanocomposites were found to be spherical using SEM. The synthesis of the nanocomposite was confirmed by the formation of chitosan in the presence of silver nanoparticles in TEM. Agar well diffusion was used to test the antibacterial properties of nanocomposites against *Streptococcus*, *Rhizobium radiobacter*, *Klebsiella pneumoniae*, and *Escherichia coli*. The findings demonstrated that silver nanoparticles with chitosan layer exhibited outstanding antibacterial and antioxidant properties, suggesting that they could be used as advanced biomedicine in the future.

## Data Availability

The data used to support the findings of this study are included within the article.

## Conflicts of Interest

The authors declare that there is no conflict of interest.

## Authors' Contributions

SR designed, carried out research, and wrote the manuscript.

## Acknowledgments

The study is funded by DST-SERB (file no. YSS/2014/000931), New Delhi, India.

## References

- [1] M. J. Sweet and I. Singleton, "Silver nanoparticles: a microbial perspective," *Advances in Applied Microbiology*, vol. 77, pp. 115–133, 2011.
- [2] S. Ahmed, M. Ahmad, B. L. Swami, and S. Ikram, "A review on plants extract mediated synthesis of silver nanoparticles for antimicrobial applications: a green expertise," *Journal of Advanced Research*, vol. 7, no. 1, pp. 17–28, 2016.
- [3] U. Kanagavalli, A. M. Sadiq, Sathishkumar, and S. Rajeshkumar, "Plant assisted synthesis of silver nanoparticles Using *Boerhaavia diffusa* Leaves extract and evolution of antibacterial activity," *Research Journal of Pharmacy and Technology*, vol. 9, no. 8, p. 1064, 2016.
- [4] K. Paulkumar, G. Gnanajobitha, M. Vanaja et al., "*Piper nigrum* leaf and stem assisted green synthesis of silver nanoparticles and evaluation of its antibacterial activity against agricultural plant pathogens," *Scientific World Journal*, vol. 2014, article 829894, pp. 1–9, 2014.
- [5] M. Gnanadesigan, M. Anand, S. Ravikumar et al., "Antibacterial potential of biosynthesised silver nanoparticles using *Avicennia marina* mangrove plant," *Applied Nanoscience*, vol. 2, no. 2, pp. 143–147, 2012.
- [6] M. Vanaja, G. Gnanajobitha, K. Paulkumar, S. Rajeshkumar, C. Malarkodi, and G. Annadurai, "Phytosynthesis of silver

- nanoparticles by *Cissus quadrangularis*: influence of physico-chemical factors,” *Journal of Nanostructure in Chemistry*, vol. 3, no. 1, p. 17, 2013.
- [7] P. Rajiv, S. Rajeshwari, and R. Venkatesh, “Bio-Fabrication of zinc oxide nanoparticles using leaf extract of *Parthenium hysterophorus* L. and its size-dependent antifungal activity against plant fungal pathogens,” *Spectrochimica Acta Part A: Molecular and Biomolecular Spectroscopy*, vol. 112, pp. 384–387, 2013.
- [8] S. Rajeshkumar, “Antioxidant activity of characterized silver nanoparticles synthesized using flower extracts of *Chrysanthemum indicum*,” *Research Journal of Biotechnology*, vol. 12, no. 8, pp. 38–43, 2017.
- [9] G. Gnanajobitha, S. Rajeshkumar, G. Annadurai, and C. Kannan, “Preparation and characterization of fruit-mediated silver nanoparticles using pomegranate extract and assessment of its antimicrobial activities,” *Journal of Environmental Nanotechnology*, vol. 2, no. 1, pp. 20–27, 2013.
- [10] S. Singh, J. P. Saikia, and A. K. Buragohain, “A novel ‘green’ synthesis of colloidal silver nanoparticles (SNP) using *Dillenia indica* fruit extract,” *Colloids and Surfaces B: Biointerfaces*, vol. 102, pp. 83–85, 2013.
- [11] M. Amin, F. Anwar, M. R. S. A. Janjua, M. A. Iqbal, and U. Rashid, “Green synthesis of silver nanoparticles through reduction with *Solanum xanthocarpum* L. Berry extract : characterization, antimicrobial and urease inhibitory activities against *Helicobacter pylori*,” *International Journal of Molecular Sciences*, vol. 13, no. 8, pp. 9923–9941, 2012.
- [12] M. Ghaffari-Moghaddam and R. Hadi-Dabanlou, “Plant mediated green synthesis and antibacterial activity of silver nanoparticles using *Crataegus douglasii* fruit extract,” *Journal of Industrial and Engineering Chemistry*, vol. 20, no. 2, pp. 739–744, 2014.
- [13] W. L. Du, Z. R. Xu, X. Y. Han, Y. L. Xu, and Z. G. Miao, “Preparation, characterization and adsorption properties of chitosan nanoparticles for eosin Y as a model anionic dye,” *Journal of Hazardous Materials*, vol. 153, no. 1-2, pp. 152–156, 2008.
- [14] J. Rhim, L. Wang, Y. Lee, and S. Hong, “Preparation and characterization of bio-nanocomposite films of agar and silver nanoparticles: Laser ablation method,” *Carbohydrate Polymers*, vol. 103, pp. 456–465, 2014.
- [15] J. S. Taurozzi, H. Arul, V. Z. Bosak et al., “Effect of filler incorporation route on the properties of polysulfone-silver nanocomposite membranes of different porosities,” *Journal of Membrane Science*, vol. 325, no. 1, pp. 58–68, 2008.
- [16] M. Sureshkumar, D. Y. Siswanto, and C. Lee, “Magnetic antimicrobial nanocomposite based on bacterial cellulose and silver nanoparticles,” *Journal of Materials Chemistry*, vol. 20, no. 33, pp. 6948–6955, 2010.
- [17] M. K. Shukla, R. P. Singh, C. R. K. Reddy, and B. Jha, “Synthesis and characterization of agar-based silver nanoparticles and nanocomposite film with antibacterial applications,” *Biore-source Technology*, vol. 107, pp. 295–300, 2012.
- [18] A. M. Youssef, M. S. Abdel-aziz, and S. M. El-sayed, “Chitosan nanocomposite films based on Ag-NP and Au-NP biosynthesis by *Bacillus Subtilis* as packaging materials,” *International Journal of Biological Macromolecules*, vol. 69, pp. 185–191, 2014.
- [19] P. L. L. Freire, A. J. R. Albuquerque, I. A. P. Farias et al., “Antimicrobial and cytotoxicity evaluation of colloidal chitosan - silver nanoparticles - fluoride nanocomposites,” *International journal of biological macromolecules*, vol. 93, no. Part A, pp. 896–903, 2016.
- [20] J. W. Rhim, L. F. Wang, and S. I. Hong, “Preparation and characterization of agar/silver nanoparticles composite films with antimicrobial activity,” *Food Hydrocolloids*, vol. 33, no. 2, pp. 327–335, 2013.
- [21] P. Kaur, A. Choudhary, and R. Thakur, “Synthesis of chitosan-silver nanocomposites and their antibacterial activity,” *International Journal of Scientific and Engineering Research*, vol. 4, pp. 869–872, 2013.
- [22] A. Nithya, H. L. JeevaKumari, K. Rokesh, K. Ruckmani, K. Jeganathan, and K. Jothivenkatachalam, “A versatile effect of chitosan-silver nanocomposite for surface plasmonic photocatalytic and antibacterial activity,” *Journal of Photochemistry & Photobiology, B : Biology*, vol. 153, pp. 412–422, 2015.
- [23] G. Gnanajobitha, M. Vanaja, K. Paulkumar, and S. Rajeshkumar, “Green synthesis of silver nanoparticles using *Millingtonia hortensis* and evaluation of their antimicrobial efficacy,” *International Journal of Nanomaterials and Biostructures*, vol. 3, no. 1, pp. 21–25, 2013.
- [24] C. Krishnaraj, P. Muthukumaran, R. Ramachandran, M. D. Balakumaran, and P. T. Kalaichelvan, “*Acalypha indica* Linn: Biogenic synthesis of silver and gold nanoparticles and their cytotoxic effects against MDA-MB-231, human breast cancer cells,” *Biotechnology Reports*, vol. 4, pp. 42–49, 2014.
- [25] N. Nigam, S. Kumar, T. Ghosh, and P. K. Dutta, “Preparation of chitosan based silver nanocomposites by a facile method,” in *International Conference on Optics and Photonics*, pp. 1–4, Chandigarh: CSIO, 2009.
- [26] K. Sharneli, M. B. Ahmad, Z. W. Yunis et al., “Green synthesis of silver/montmorillonite/chitosan bionanocomposites using the UV irradiation method and evaluation of antibacterial activity,” *International journal of nanomedicine*, vol. 5, pp. 875–887, 2010.
- [27] S. Rajeshkumar, C. Malarkodi, K. Paulkumar, M. Vanaja, G. Gnanajobitha, and G. Annadurai, “Algae mediated green fabrication of silver nanoparticles and examination of its antifungal activity against clinical pathogens,” *International Journal of Metalcasting*, vol. 2014, article 692643, pp. 1–8, 2014.
- [28] N. J. Reddy, D. Nagoor Vali, M. Rani, and S. S. Rani, “Evaluation of antioxidant, antibacterial and cytotoxic effects of green synthesized silver nanoparticles by *Piper longum* fruit,” *Materials Science and Engineering: C*, vol. 34, pp. 115–122, 2014.

## Research Article

# Green versus Chemical Precipitation Methods of Preparing Zinc Oxide Nanoparticles and Investigation of Antimicrobial Properties

Bulcha Bekele,<sup>1</sup> Anatol Degefa,<sup>2</sup> Fikadu Tesgera,<sup>1</sup> Leta Tesfaye Jule,<sup>1,3</sup> R. Shanmugam,<sup>4</sup> L. Priyanka Dwarampudi,<sup>5</sup> N. Nagaprasad ,<sup>6</sup> and Krishnaraj Ramasamy <sup>3,7</sup>

<sup>1</sup>Department of Physics, College of Natural and Computational Science, Dambi Dollo University, Ethiopia

<sup>2</sup>Department of Mathematics, College of Natural and Computational Science, Dambi Dollo University, Ethiopia

<sup>3</sup>Centre for Excellence-Indigenous Knowledge, Innovative Technology Transfer and Entrepreneurship, Dambi Dollo University, Ethiopia

<sup>4</sup>TIFAC, CORE-HD, JSS College of Pharmacy, JSS Academy of Higher Education & Research, Ooty, Nilgiris, Tamil Nadu, India

<sup>5</sup>Department of Pharmacognosy, JSS College of Pharmacy, JSS Academy of Higher Education & Research, Ooty, Nilgiris, Tamil Nadu, India

<sup>6</sup>Department of Mechanical Engineering, ULTRA College of Engineering and Technology, Madurai, 625104 Tamilnadu, India

<sup>7</sup>Department of Mechanical Engineering, College of Engineering, Dambi Dollo University, Ethiopia

Correspondence should be addressed to Krishnaraj Ramasamy; [prof.dr.krishnaraj@dadu.edu.et](mailto:prof.dr.krishnaraj@dadu.edu.et)

Received 16 July 2021; Revised 5 August 2021; Accepted 3 September 2021; Published 20 September 2021

Academic Editor: Shanmugam Rajeshkumar

Copyright © 2021 Bulcha Bekele et al. This is an open access article distributed under the Creative Commons Attribution License, which permits unrestricted use, distribution, and reproduction in any medium, provided the original work is properly cited.

Comparison of green and chemical precipitation method syntheses of zinc oxide nanoparticles (ZnO NPs) was performed, and antimicrobial properties were investigated. Avocado, mango, and papaya fruit extracts were carried out for the green synthesising methods, while the chemical precipitation method was chosen from chemical synthesis methods. Zinc nitrate was used as a salt precursor, whereas leaf extract was served as a reducing agent for green synthesising methods. In addition, sodium hydroxide, polyvinyl alcohol, and potassium hydroxide were used as reducing agents in the case of chemical precipitation synthesis methods. ZnO NPs were characterised by characterizing techniques such as Fourier transform infrared (FT-IR), X-ray diffraction (XRD), and scanning electron microscopy (SEM). The antimicrobial activities of prepared nanoparticles were evaluated on *Bacillus subtilis* (*B. subtilis*), *Staphylococcus aureus* (*S. aureus*), and *Salmonella typhimurium* (*S. typhimurium*). The particle sizes of the prepared samples which were evaluated by the Scherrer equation were in the range of 11-21 nm for green synthesis, while 30-40 nm for chemical precipitation synthesis methods. Small agglomerations were observed from SEM results of prepared ZnO NPs from both methods. Prepared ZnO NPs were showed strong antimicrobial properties. From the result, the inhibition zone was in the range of 15-24 mm for the green route and 7-15 mm for chemical precipitation methods, where the standard drugs have 25 mm of the zone of inhibition. A green synthesised method of preparing ZnO NPs gives promising antimicrobial properties compared to chemical synthesis and is also eco-friendly and safe compared to the chemical synthesis.

## 1. Introduction

In the previous period, nanoscience and technology of nanocomposite materials are emerging in material science fields. It manipulates matter at the atomic scale that produces a nanoproduct of new novel properties [1]. Nanomaterials

are manufacturing and engineering materials that are characterised at least in one dimension in nanoscale (1 nm–100 nm). It is useful to develop structures and devices of various materials [2]. Nanoparticles are the parts of nanometres widely used in the application of medicine [3], environmental protection [1, 3], sunscreen [4], and cosmetics

technology. Biomaterials make challenges while researchers are studying material science fields. Researcher loses a lot of time to generate a new idea, especially on biomaterials in medicine applications on antibiotic resistance microorganism [1, 3, 4]. Physical and chemical differences of characterisation of nanocomposite materials include mechanical and biological properties [5]. A nanoparticle gave greater properties than bulk materials and had an appreciation application in human life. It has a lower surface area to volume ratio and shows essential properties like versatility, high strength, and electrical conductivity; in comparison to bulk material with the same chemical makeup, this material has superior strength and affinity [6]. New materials with innovative purposes can be created by manipulating the shape and size of atoms and molecules on the nanoscale. [7] Nanoparticles (NPs) have a wide range of applications along with memory schematics and cordless electronic logic as well as chemical sensing and electrometers as well as computer transistors. They also have antibacterial and catalytic behaviour as well as magnetic characteristics, mechanical resistance, and conductivity. Those nanoparticles can also be used in various other fields, such as tumour heating, medicine administration, filtration, nanocomposites, and diagnostic scanning, to name a few. Since the last few generations, there has been much interest in inorganic NPs with increased characteristics [8]. Through the use of NP characterisation, it is possible to determine the direction, fractal sizes, crystallinity, and a number of the interactivities.

ZnO NPs are used as supercapacitors because of their high energy density, electrochemical activity, environmental friendliness, abundant availability, and inexpensive cost. Because of its large surface area, ZnO nanoparticles (ZnO NPs) have been used to eliminate arsenic and sulphur from water. ZnO nanopowders are commonly employed in sectors such as blue laser diodes, solar cells, and conductive thin films [2, 4–8]. When compared to green synthetic methods, these methods have some disadvantages, such as being challenging to operate, costly, emitting radiation, requiring very high pressure, and being toxic [9]. The medical uses of some technologies are harmed by the adsorption of hazardous chemical species on the surface. Green synthesis has been developed to prevent chemical toxicity and an intense environment of physical and chemical processes. They are suitable for biomedical applications due to their characteristics. The shape of the NPs is influenced by a variety of factors during green synthesis, including plant extract content, pH, temperature, reaction duration, and solvent [10]. Because of the existence of useful photochemicals such as ascorbic acids, phenols, and carboxylic acids, plant biodiversity was being extensively employed in the production of green synthesis. Therefore, the aims of this study are to synthesise ZnO NPs by green and chemical precipitation methods and examine its antimicrobial properties.

## 2. Experimental Details

*2.1. Materials and Chemical Used in Green Synthesis.* Here, avocado, papaya, and mango fruits were collected from the

land farm of Kellem Wollega Zone, Mugi Woreda. In addition, zinc nitrate hexahydrate  $\text{Zn}(\text{NO}_3)_2 \cdot 6\text{H}_2\text{O}$ , zinc acetate dihydrate  $(\text{Zn}(\text{CH}_3\text{COO})_2 \cdot 2\text{H}_2\text{O})$ , zinc sulphate heptahydrate  $(\text{ZnSO}_4 \cdot 7\text{H}_2\text{O})$  of 99% pure, sodium hydroxide (NaOH), polyvinyl alcohol (PVA), potassium hydroxide (KOH), and ethanol were purchased from Addis Ababa Chemical Shop, Piazza. Different types of glasses of double-distilled water were used for washing.

*2.2. Green Synthesis/Methods of Extractions.* The green synthesis methods were developed from the procedure developed in Safavinia et al. (2021). Avocado fruit sizes were reduced using a knife by cutting and washed six times by double distilled and three times by ethanol. 16 g of avocado was mixed with 170 mL of double-distilled water and then continuously heated for the duration of 30 min on a magnetic stirrer. The aqueous solution of avocado extractions was obtained and filtered by Whatman paper and stored at normal temperature for later use. 10 g of  $\text{Zn}(\text{NO}_3)_2 \cdot 6\text{H}_2\text{O}$  were measured by triple beam balance and dissolved in 30 mL of double-distilled water by using a high-speed magnetic stirrer at constant temperature for 30 min. Then, 1.75 M of avocado extract were added to  $\text{Zn}(\text{NO}_3)_2 \cdot 6\text{H}_2\text{O}$  combination mixture and continuously stirred for 1 hr. The solutions were now settled for 24 hr at normal temperature. Similar procedures were repeated for papaya and mango.

*2.3. Chemical Precipitation Methods of Zinc Oxide Nanoparticles.* The chemical precipitation methods used in the chemical synthesis were  $\text{Zn}(\text{NO}_3)_2 \cdot 6\text{H}_2\text{O}$ ,  $\text{Zn}(\text{CH}_3\text{COO})_2 \cdot 2\text{H}_2\text{O}$ , and  $\text{ZnSO}_4 \cdot 7\text{H}_2\text{O}$  as salt precursor, while NaOH, PVA, and KOH are reducing agents. According to the procedure developed in Bekele et al. (2021), zinc oxide nanoparticles were prepared. All zinc salts and reducing agents were measured by beam balance. 12 gm of the sodium hydroxide (NaOH) solution was blended in 70 mL of twice distilled water and agitated. Under gentle magnetic stirrer for 30 min. Again, 4 gm of  $\text{Zn}(\text{NO}_3)_2 \cdot 6\text{H}_2\text{O}$  was dissolved into double-distilled water of 30 mL and stirred continuously for 20 min. Slowly drop by drop,  $\text{Zn}(\text{NO}_3)_2 \cdot 6\text{H}_2\text{O}$  solution was added to NaOH solution and stirred continuously for 2 hr at 60°C. At this stage, gel-like solutions were formed and left to cure in an oven at a temperature of 160°C for 10 hr overnight. Then, the sample was taken furnace (Model: MC2-5/5/10-12, BIOBASE, China) and calcinated at 300°C for 6 hrs. Similar procedures were followed for other salt precursors, zinc acetate  $(\text{Zn}(\text{CH}_3\text{COO})_2 \cdot 2\text{H}_2\text{O})$ , and zinc sulphate hydrate  $(\text{ZnSO}_4 \cdot 7\text{H}_2\text{O})$ .

*2.4. Characterisation Techniques.* In order to report the presence of functional groups attached to a surface of the synthesised nanoparticles, the Perkin Elmer FT-IR spectrum was used in the scanning region of 4000-400  $\text{cm}^{-1}$  and a resolution of 4  $\text{cm}^{-1}$  for the analysis of the connected functional groups to the exterior of the synthesised ZnO NPs. The X-ray diffraction (XRD) distribution of ZnO nanoparticles was acquired utilising an XPERT-PROX-ray diffractometer

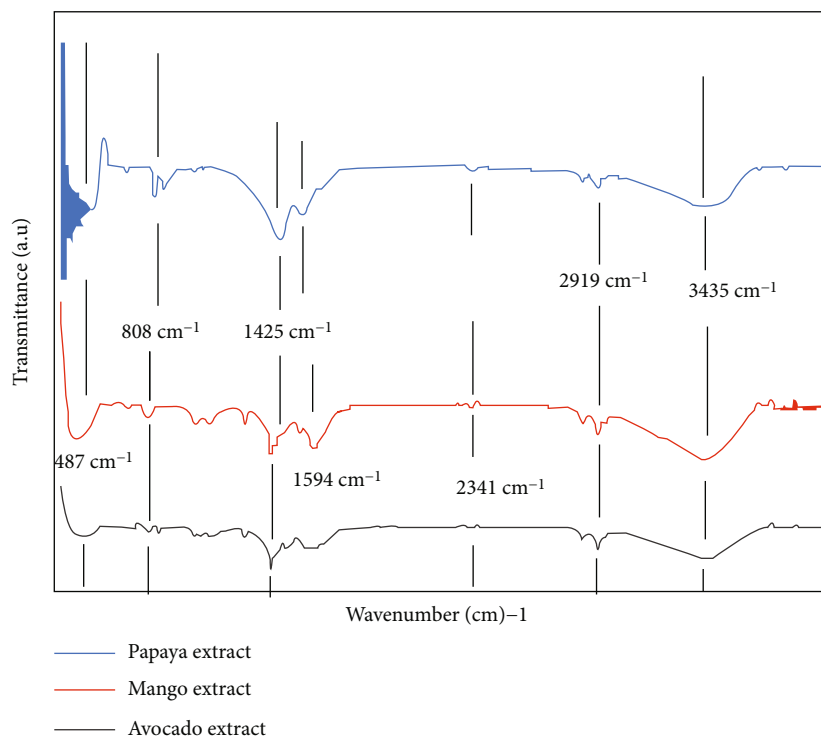
that generated Cu-K radiation (with an angular resolution of 1.5418 angstroms). It is being employed to evaluate the crystalline particle size that has been manufactured. For the purposes of characterisation, a tiny quantity of powder samples was used. At room temperature, when the X-ray generators were working at 40 kV and transmitting a charge of 30 mA to the target, it was considered a successful hit. Properties were measured at room temperature in steps of 0.02, over an ambient temperature of 100 to 800 degrees Celsius, with the diffractometer connected to a computer for the collection of data and presentation of characterisation results. It was necessary to authenticate the structure of the crystal by comparing its peak positions with those of the existing standard data. For each sample, about 0.4 g of produced ZnO NPs were grinded to tiny powders and quantified using a beam balance before being transferred to a metal plate. Once the nanoparticles had been formed, it was discovered that the nanoparticle morphology might be investigated using a scanning electron microscope (Hitachi, H-7600), which functions under extreme vacuum as well as have magnifications varying between 20x to around 30,000x, with resolutions varying between 50 and 100 nm. Increased magnification of the ZnO NPs was achieved by reducing the raster width of the specimen, and vice versa, for the ZnO NPs with fixed sizes. A quartz cuvette with a diameter of 1 cm has been used to examine the absorbance spectra of produced ZnO NPs utilising UV-vis spectroscopy (Perkin Elmer Lambda 950), which was run over a wavelength range of 200-500 nm. The ZnO NPs were combined using double-distilled water until being placed in a quartz cuvette to produce their solutions, which were then analysed. After that, the cuvette was placed in an ultraviolet-visible spectrophotometer, where the absorption spectra of ZnO NPs were determined.

**2.5. Antimicrobial Activity.** The green and hydrothermal methods of synthesised zinc oxide nanoparticles were evaluated for antibacterial activities through disc-diffusion methods as developed in literature [11–14]. A growing media was created, autoclaved, and then moved to a putrefaction Petri plate in order to execute the technique. It was necessary to prepare the growing media, autoclave it, and transfer it aseptically to sterilised Petri plates. Slants of test tube media were transferred to Petri plate media, and sterile and dried paper discs (6 mm) were inoculated with 10 L of freshly prepared ZnO NPs, either through a 0.45-millipore filter or through a 0.45-millipore filter with freshly prepared ZnO NPs for both the synthetic and the synthesis methods. The discs that had been impregnated were cured in a laminar flow cabinet. Controls and discs were planted on newly seeded microbial lawns in conjunction with the experimental discs. Negative controls included sterile water (10 L per disc) and streptomycin (1 per cent per disc), while positive controls included 1 per cent streptomycin (10 L per disc). Several investigations were carried out in triplicate to ensure accuracy. With a zone reader, the regions of inhibition or antimicrobial activities were counted in millimetres (mm) on the Petri plates after they had been incubated at their respective temperatures.

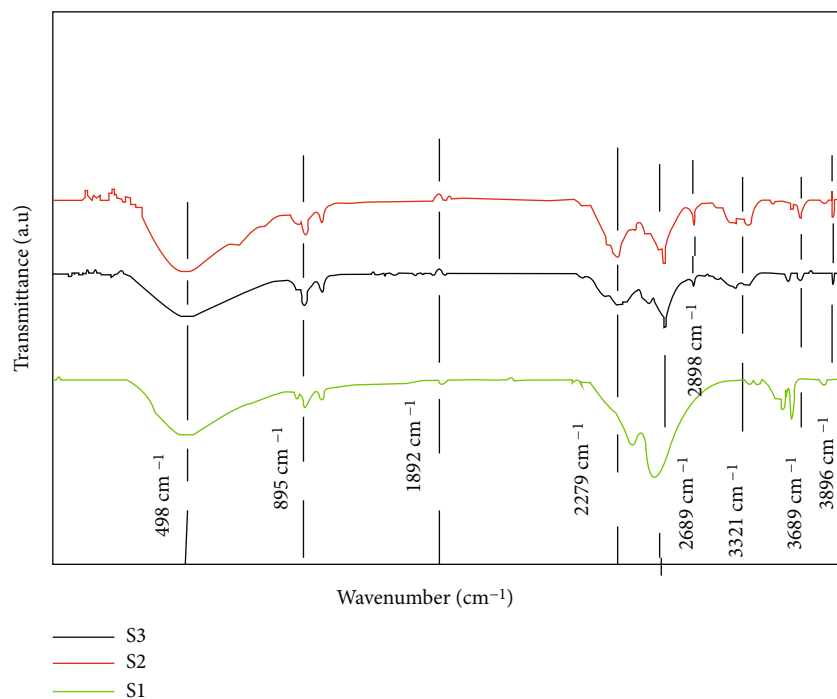
### 3. Results and Discussion

**3.1. FT-IR Spectral Analysis of ZnO NPs.** ZnO NPs were prepared by green and chemical precipitation synthesised techniques. Green synthesising methods of ZnO NPs from avocado, mango, and papaya extracts and chemical synthesis by hydrothermal methods were depicted in Figures 1(a) and 1(b), respectively. ZnO NPs were prepared by hydrothermal methods from zinc nitrate hexahydrate ( $\text{Zn}(\text{NO}_3)_2 \cdot 6\text{H}_2\text{O}$ ) and sodium hydroxide (NaOH), zinc sulphate heptahydrate ( $\text{ZnSO}_4 \cdot 7\text{H}_2\text{O}$ ) and polyvinyl alcohol (PVA), and zinc acetate dihydrate ( $\text{Zn}(\text{CH}_3\text{COO})_2 \cdot 2\text{H}_2\text{O}$ ) and potassium hydroxide (KOH) as S1, S2, and S3, respectively. The FT-IR spectrum shows the transmission band around 487, 808, 1425, 1594, 2341, 2919, and 3435  $\text{cm}^{-1}$  in the region of 400–4000  $\text{cm}^{-1}$ . The transmission band observed at 487 and 808  $\text{cm}^{-1}$  shows the presence of ZnO NPs for all extracts [13]. The peak observed at 1425, 1594, and 2341  $\text{cm}^{-1}$  shows the presence of carbonyl ( $-\text{C}=\text{O}$ ) groups are stretching vibration, CN stretching, and  $\text{COO}^-$  antisymmetric stretching, respectively [14]. The peak observed around 2919 and 3435  $\text{cm}^{-1}$  depicts the presence of C-H stretching vibrations to  $\text{CH}_2$  and  $\text{CH}_3$  [15]. Bioactive compounds were also found in the region between 808 and 1425  $\text{cm}^{-1}$ . Similarly, broad transmission peaks were depicted from chemical synthesis by the hydrothermal method. FT-IR spectrum shows transmission peaks at 498, 895, 1892, 2279, 2689, 3321, 3689, and 3896  $\text{cm}^{-1}$  for all chemical synthesis of S1, S2, and S3. ZnO NPs were observed at and around the 498 and 895  $\text{cm}^{-1}$ , where the textile bond and oxygen vacancies were observed [15]. The peaks observed at 1892 and 2279  $\text{cm}^{-1}$  represents symmetrical stretching of zinc carboxylate for all samples. The peaks observed at 2689 and 3321  $\text{cm}^{-1}$  represents the O-H hydroxyl group's fluctuation [16]. In addition, the transmission band observed at 3689 and 3896  $\text{cm}^{-1}$  depicts the valence vibrations of water molecules. The broad peaks of ZnO NPs were observed in chemical synthesis methods than in the green synthesis methods. As the dimension of zinc oxide nanoparticles increases, the content of the impurities attached to the samples were decreased for both synthesising methods.

**3.2. XRD Spectral Analysis.** ZnO NPs were synthesised through green and chemical precipitation methods (as shown in Figures 2(a) and 2(b)). The XRD pattern of ZnO NPs was generated using avocado, mango, and papaya extracts in green synthesis methods and S1, S2, and S3 samples of zinc nitrate, zinc acetate, and zinc sulphate salts with their corresponding reducing agents of sodium hydroxide, polyvinyl alcohol, and potassium hydroxide, respectively. In accordance with JCPDS card no. 36-1451, many of the XRD diffraction patterns of ZnO NPs are in perfect agreement with the hexagonal wurtzite structure (hexagonal phase, crystal structure P63mc) with lattice parameters of  $a = b = 3.249$  and  $c = 5.206$  as reported in the recovered products [17]. Nine well-defined spectral peaks were observed at 31°, 34°, 36°, 47°, 56°, 62°, 66°, 68°, and 69° with their corresponding reflection (100), (002), (101), (102), (110), (103), (200), (112), and (201) crystal planes, respectively, for green



(a)



(b)

FIGURE 1: FT-IR spectral analysis of (a) green synthesis of ZnO NPs from avocado, mango, and papaya extract. (b) Chemical precipitation synthesis of ZnO NPs from  $\text{Zn}(\text{NO}_3)_2 \cdot 6\text{H}_2\text{O}$  (S1),  $\text{Zn}(\text{CH}_3\text{COO})_2 \cdot 2\text{H}_2\text{O}$  (S2), and  $\text{ZnSO}_4 \cdot 7\text{H}_2\text{O}$  (S3) salt precursors.

synthesis methods for mango and papaya extracts. There is a shift towards a smaller angle in the case of the avocado extract by ten degrees when compared to the other extracts. From the graph, the narrow and sharp peaks of diffractions were observed that the prepared nanoparticles are well crys-

tallised. The diffraction peaks of chemical precipitation synthesising methods for samples S1, S2, and S3 of zinc salt precursors correspond to Bragg reflections with two theta values of 17.29°, 35.08°, 38.39°, 40.12°, 47.95°, 53.93°, 62.95°, 70.77°, and 76.10° to their corresponding Miller Bravais



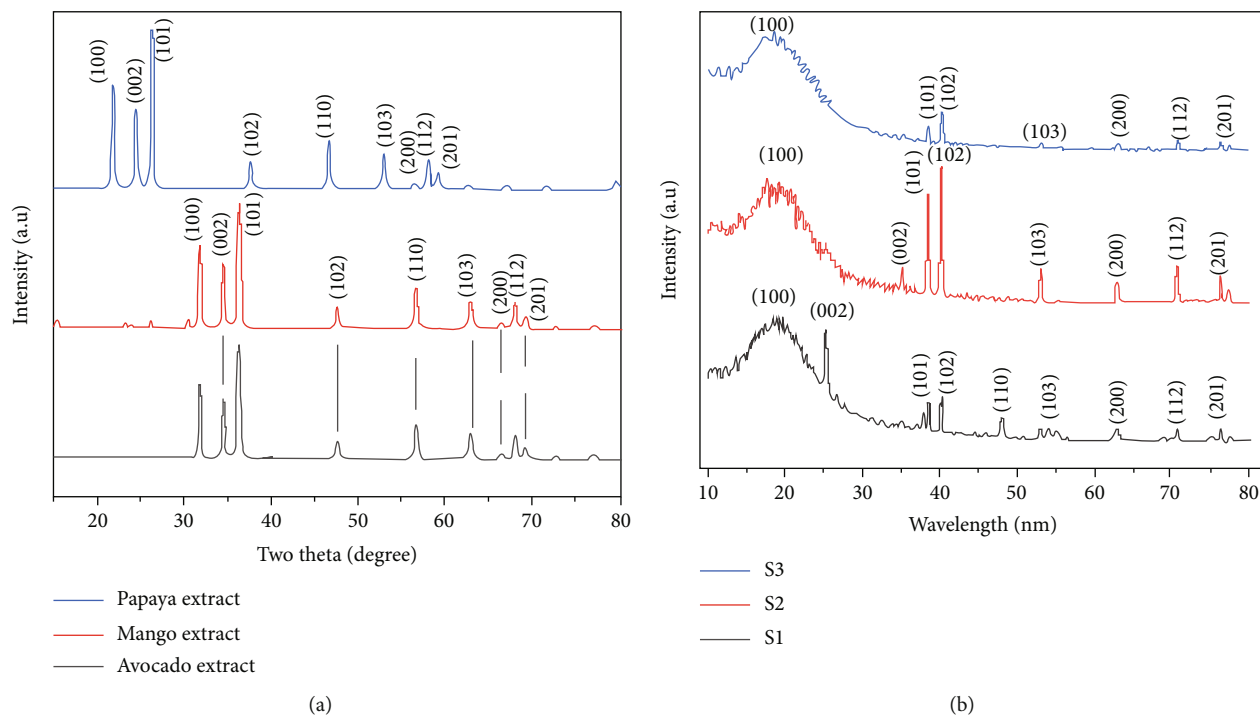


FIGURE 2: XRD spectral analysis of (a) green synthesis of ZnO NPs by avocado, mango, and papaya extract. (b) Hydrothermal synthesis of ZnO NPs from  $\text{Zn}(\text{NO}_3)_2 \cdot 6\text{H}_2\text{O}$  (S1),  $\text{Zn}(\text{CH}_3\text{COO})_2 \cdot 2\text{H}_2\text{O}$  (S2), and  $\text{ZnSO}_4 \cdot 7\text{H}_2\text{O}$  (S3) zinc salt precursors.

indices (100), (002), (101), (102), (110), (103), (200), (112), and (201) planes of hexagonal structure phases of ZnO, respectively. These XRD patterns of the samples are in good agreement with the standard data of the hexagonal ZnO wurtzite structure of standard JCPDS card 36-1451. Sharp and intense peaks of chemically prepared nanoparticles were indicated that ZnO NPs with highly crystalline were successfully prepared. The average particle sizes of green and chemically prepared ZnO NPs were calculated by the Scherrer equation.

$$t = \frac{0.9\lambda}{\beta \cos \theta}, \quad (1)$$

whereby  $t$  is the mean dimension of nanoparticles,  $k$  is the frequency of radiation,  $\beta$  is the whole width half peak in radians, and  $\theta$  is the degree diffraction [15–18]. Avocado, mango, and papaya extracts of green methods have been used to synthesis nanoparticles with mean sizes of 11 nm, 16 nm, and 21 nm, respectively. The average sizes of the nanoparticles produced with avocado, mango, and papaya extracts are tabulated in Table 1.

The average sizes of the zinc oxide nanoparticles produced by chemical precipitation methods are seen in Table 2. Based on the foregoing findings, it can be inferred that throughout the instance, green synthesising methods gave smaller nanoparticles which is more applicable for biomedical application [18, 19].

**3.3. SEM Analysis of ZnO NPs.** Figure 3(a) shows the scanning electron microscope (SEM) morphology of green synthesised ZnO NPs from avocado, mango, and papaya

TABLE 1: Average particle size, FWHM, and angle of diffraction of avocado, mango, and papaya extracted of green synthesis methods of ZnO NPs.

Green synthesis methods	2 theta	FWHM ( $\beta$ )	Average particle size ( $t$ )
Avocado	38.33	0.0995	$11 \pm 20$ nm
Mango	38.33	0.0673	$16 \pm 30$ nm
Papaya	26.29	0.0568	$21 \pm 10$ nm

TABLE 2: Average particle size, FWHM, and angle of diffraction of chemical precipitation method synthesis of ZnO NPs.

Chemical precipitation methods	2 theta	FWHM ( $\beta$ )	Average particle size ( $t$ )
$\text{Zn}(\text{NO}_3)_2 \cdot 6\text{H}_2\text{O} + \text{NaOH}$ (S1)	38.33	0.03345	$40 \pm 10$ nm
$\text{Zn}(\text{CH}_3\text{COO})_2 \cdot 2\text{H}_2\text{O} + \text{PVA}$ (S2)	38.33	0.02931	$36 \pm 20$ nm
$\text{ZnSO}_4 \cdot 7\text{H}_2\text{O} + \text{KOH}$ (S3)	26.29	0.02134	$31 \pm 20$ nm

extracts. An avocado extract of SEM image depicts that the prepared nanoparticle is rod-like images, while flower images were observed in the case of mango extract with small agglomerations. It is noticed that small agglomeration of green synthesis methods were probability obtained from the escape of volatile substances or gases during the calcination process. Nanotube-like images without any agglomeration were also seen from SEM results of papaya extracts, and the same results were reported in the literature of [20].

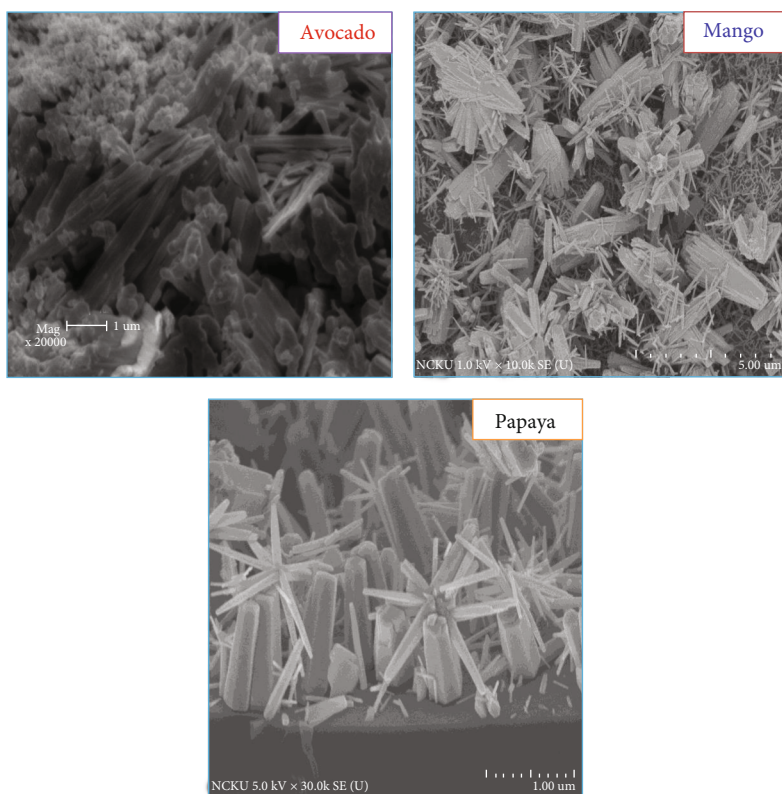


FIGURE 3: SEM images of ZnO NPs synthesised by green methods from avocado, mango, and papaya extracts.

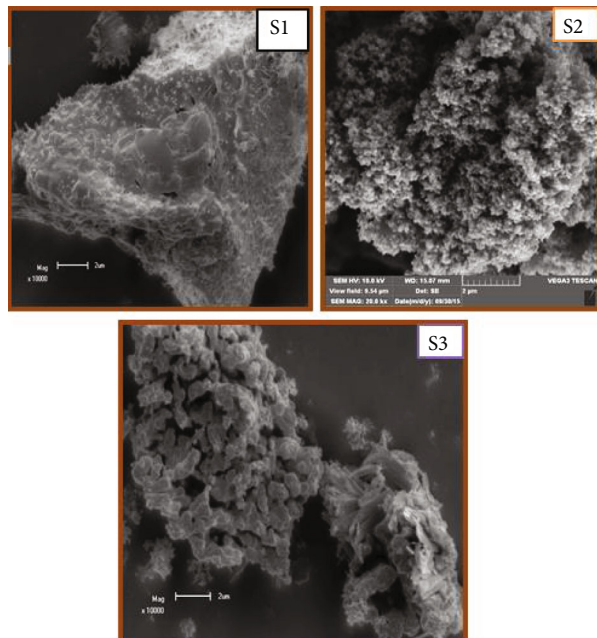


FIGURE 4: SEM morphology of ZnO NPs prepared by chemical precipitation methods of  $\text{Zn}(\text{NO}_3)_2 \cdot 6\text{H}_2\text{O} + \text{NaOH}$  (S1),  $\text{Zn}(\text{CH}_3\text{COO})_2 \cdot 2\text{H}_2\text{O} + \text{PVA}$  (S2), and  $\text{ZnSO}_4 \cdot 7\text{H}_2\text{O} + \text{KOH}$  (S3)

Figure 4 depicts SEM morphology of ZnO NPs by chemical precipitation method from zinc nitrate hexahydrate, zinc acetate dehydrate, and zinc sulphate heptahydrate from sodium hydroxide, polyvinyl alcohol, and potassium

hydroxide as reducing agents, respectively. Highly magnified semispherical shape of prepared nanostructured was seen in case of S1 and uniform distributed spherical shape in S2 prepared sample. In addition, an almost nearly spherical shape was observed in the case of sample S3. In both green and chemical synthesising methods, SEM results confirm the crystalline nature of the ZnO NPs [21].

**3.4. Antimicrobial Investigations of ZnO NPs.** The antibacterial investigation of green and chemical precipitation methods of prepared ZnO NPs was estimated on three bacteria such as *B. subtilis* (*Bacillus subtilis*), *S. aureus* (*Staphylococcus aureus*), and *S. Typhimurium* (*Salmonella Typhimurium*) as shown in Tables 3. It is known that some bacteria consist of the cell membrane, cytoplasm, and cell wall. Especially, peptidoglycan membrane cell is found in Gram-positive bacteria and has hard cell wall 20-80 nm [22]. In addition, Gram-negative bacteria have a double cell membrane, i.e., plasma and outer cell, which have 7-8 thickness [19, 21]. But ZnO NPs able to penetrate easily through this hard, strong cell membrane. ZnO NPs exert antimicrobial action and destroy bacterial growth [23].

In this study, green synthesis methods of ZnO NPs from avocado, mango, and papaya extracts were subjected to antibacterial activity to investigate antimicrobial activities which are shown in Figure 5. From all extracted samples, avocado extract has more inhibition potential on all bacterial strains. ZnO NPs applied on *Bacillus subtilis* show high inhibition potential than others. In other words, because the particle size of these strains has been in the nanoscale, which can

TABLE 3: Chemical precipitation of ZnONPs.

Zone of inhibition (mm)	Green synthesis of ZnONPs			Chemical		
	Avocado	Mango	Papaya	S1	S2	S3
precipitation of ZnONPs						
Bacteria stains						
<i>Bacillus subtilis</i>	24	20	16	12	15	12
<i>Staphylococcus aureus</i>	20	18	17	11	13	10
<i>Salmonella typhimurim</i>	17	16	15	9	14	7

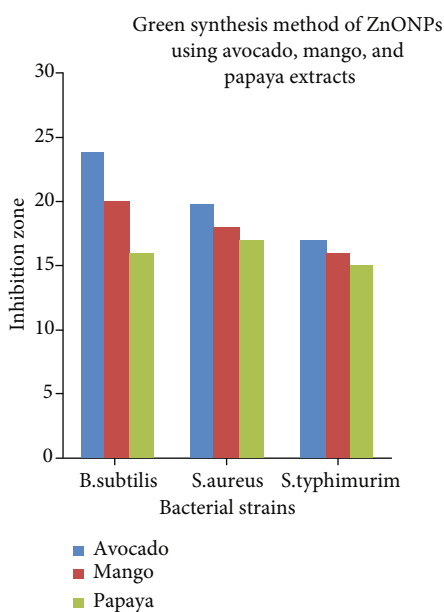


FIGURE 5: Antimicrobial activities of ZnO NPs prepared by green methods from avocado, mango, and papaya extracts.

easily impede the development of these strains, the inhibition of such strains did not take particle size into consideration [24]. Figure 6 illustrates the antimicrobial activities of ZnO NPs prepared by chemical precipitation methods of S1, S2, and S3 samples of zinc salt precursors. These results have good agreements with standard references of antimicrobial activities (streptomycin).

As shown in Figure 6, The sample S1 is the most effective of the inhibitors when compared to the other salt precursors. Antimicrobial activities of sample S3 were low compared to S1 and S2. Chemical precipitation methods of ZnO NPs have more inhibition potential on the bacterial strains of *S. aureus*. ZnO NPs prepared by both chemical and green synthesis have been found to be key interest in antimicrobial activities [25–28]. ZnO NPs prepared by green synthesis methods were found to be more active against this selected *B. subtilis*, *S. aureus*, and *S. Typhimurium* compared to chemical precipitation methods and have highly antibacterial agents. The results of this finding have a good agreement with previous studies [27]. Furthermore, ZnO NPs prepared from avocado, mango, and papaya extract were highly active

Chemical precipitation method of prepared ZnONPs as sample S1, S2, and S3

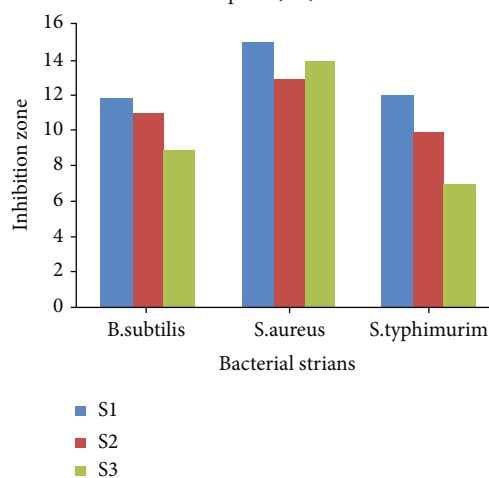


FIGURE 6: Antimicrobial activities of ZnO NPs prepared by chemical precipitation methods of S1, S2, and S3 samples of zinc salt precursors.

antimicrobial properties with slight differences. Hence, fabrication of ZnO NPs from avocado, mango, and papaya extracts are highly recommended rather than chemical synthesis for microbial agents. In the green route, bioactive compounds were present as stabilising, reducing, and capping agents [28–30]. Furthermore, green extracts produce several biomolecules, including carbohydrates and proteins; accompanying prime metabolites and secondary metabolites that have been linked to the elimination of metal ions and stability has been linked to nucleic acids [31–40]. Not only antimicrobial agents but also green synthesis is also needed for environmental pollution protections by developing and adopting benign eco methods [41–50].

#### 4. Conclusions

Comparison of green and chemical precipitation method synthesis of zinc oxide nanoparticles (ZnO NPs) was performed, and antimicrobial properties were calculated. Avocado, mango, and papaya fruit extracts were carried out for the green synthesising methods, while the chemical precipitation method was chosen from chemical synthesis methods. Zinc nitrate was used as a salt precursor, whereas fruit extracts were served as reducing agents for green synthesising methods. In addition, sodium hydroxide, polyvinyl alcohol, and potassium hydroxide were used as reducing agents in the case of chemical precipitation synthesis methods. ZnO NPs were characterised by characterizing techniques such as Fourier transform infrared (FT-IR), X-ray diffraction (XRD), and scanning electron microscopy (SEM). The antimicrobial activities of prepared nanoparticles were evaluated on *E. coli* and *S. aureus*. The particle sizes of the prepared samples which were evaluated by the Scherrer equation were in the range 11–21 nm for green synthesis, while 30–40 nm for chemical precipitation synthesis methods. Small agglomerations were observed from SEM results of prepared ZnO

NPs from both methods. Prepared ZnO NPs showed strong antimicrobial properties. From the result, the inhibition zones were in the range of 15-24 mm for the green route and 7-15 mm for chemical precipitation methods, where the standard drugs have 25 mm of the zone of inhibition. A green synthesised method of preparing ZnO NPs gives promising antimicrobial properties compared to chemical synthesis and is also eco-friendly and safe compared to the chemical synthesis. The results of this finding have good agreement with previous studies. Furthermore, ZnO NPs prepared from avocado, mango, and papaya extract were highly active antimicrobial properties with slight differences. Hence, fabrication of ZnO NPs from avocado, mango, and papaya extracts is highly recommended rather than chemical synthesis for microbial agents.

### Data Availability

The data used to support the findings of this study are included within the article.

### Conflicts of Interest

The authors declare that there are no conflicts of interest.

### References

- [1] G. Sangeetha, S. Rajeshwari, and R. Venkatesh, "Green synthesis of zinc oxide nanoparticles by *aloe barbadensis miller* leaf extract: Structure and optical properties," *Materials Research Bulletin*, vol. 46, no. 12, pp. 2560–2566, 2011.
- [2] K. Rambabu, G. Bharath, F. Banat, and P. Loke Show, "Green synthesis of zinc oxide nanoparticles using *Phoenix dactylifera* waste as bioreductant for effective dye degradation and antibacterial performance in wastewater treatment," *Journal of Hazardous Materials*, vol. 402, p. 123560, 2021.
- [3] E. F. el-Beley, M. Farag, H. A. Said et al., "Green synthesis of zinc oxide nano-particles (ZnO-NPs) using *Arthrospira platensis* (class: Cyanophyceae) and evaluation of their biomedical activities," *Nanomaterials*, vol. 11, no. 1, p. 95, 2021.
- [4] E. M. Isa, K. Shameli, N. C. Jusoh, S. M. Sukri, and N. A. Ismail, "Variation of green synthesis techniques in fabrication of zinc oxide nanoparticles—a mini review," in *IOP Conference Series: Materials Science and Engineering*, vol. 1051, 2021no. 1, Article ID 012079.
- [5] K. G. Akpomie, S. Ghosh, M. Gryzenhout, and J. Conradie, "One-pot synthesis of zinc oxide nanoparticles via chemical precipitation for bromophenol blue adsorption and the antifungal activity against filamentous fungi," *Scientific reports*, vol. 11, no. 1, article 8305, pp. 1–17, 2021.
- [6] L. A. Kolahalam, K. R. Prasad, P. Murali Krishna, and N. Supraja, "*Saussurea lappa* plant rhizome extract-based zinc oxide nanoparticles: synthesis, characterization and its antibacterial, antifungal activities and cytotoxic studies against Chinese Hamster Ovary (CHO) cell lines," *Heliyon*, vol. 7, no. 6, article e07265, 2021.
- [7] A. Rana, K. Yadav, and S. Jagadevan, "A comprehensive review on green synthesis of nature-inspired metal nanoparticles: mechanism, application and toxicity," *Journal of Cleaner Production*, vol. 272, article 122880, 2020.
- [8] B. Bekele, L. T. Jule, and A. Saka, "The effects of annealing temperature on size, shape, structure and optical properties of synthesised zinc oxide nano-particles by sol-gel methods," *Digest Journal of Nanomaterials & Biostructures*, vol. 16, no. 2, pp. 471–478, 2021.
- [9] A. M. Awwad, M. W. Amer, N. M. Salem, and A. O. Abdeen, "Green synthesis of zinc oxide nanoparticles (ZnO-NPs) using *Ailanthus altissima* fruit extracts and antibacterial activity," *Chemistry International*, vol. 6, no. 3, pp. 151–159, 2020.
- [10] A. Belay, B. Bekele, and A. C. Reddy, "Effects of temperature and polyvinyl alcohol concentrations in the synthesis of zinc oxide nano-particles," *Digest Journal of Nanomaterials & Biostructures*, vol. 14, no. 1, pp. 51–60, 2019.
- [11] Q. Tang, H. Xia, W. Liang, X. Huo, and X. Wei, "Synthesis and characterization of zinc oxide nanoparticles from *Morus nigra* and its anticancer activity of AGS gastric cancer cells," *Journal of Photochemistry and Photobiology B: Biology*, vol. 202, article 111698, 2020.
- [12] D. Rehana, D. Mahendiran, R. S. Kumar, and A. K. Rahiman, "Evaluation of antioxidant and anticancer activity of copper oxide nanoparticles synthesized using medicinally important plant extracts," *Biomedicine & Pharmacotherapy*, vol. 89, pp. 1067–1077, 2017.
- [13] K. Ali, S. Dwivedi, A. Azam et al., "*Aloe vera* extract functionalized zinc oxide nanoparticles as nanoantibiotics against multi-drug resistant clinical bacterial isolates," *Journal of Colloid and Interface Science*, vol. 472, pp. 145–156, 2016.
- [14] S. M. E. Sepasgozar, S. Mohseni, B. Feizyadeh, and A. Morsali, "Green synthesis of zinc oxide and copper oxide nanoparticles using *Achillea Nobilis* extract and evaluating their antioxidant and antibacterial properties," *Bulletin of Materials Science*, vol. 44, no. 2, pp. 1–13, 2021.
- [15] E. Y. Shaba, J. O. Jacob, J. O. Tijani, and M. A. T. Suleiman, "A critical review of synthesis parameters affecting the properties of zinc oxide nano-particle and its application in wastewater treatment," *Applied Water Science*, vol. 11, no. 2, pp. 1–41, 2021.
- [16] E. D. M. Isa, K. Shameli, N. W. C. Jusoh, and R. Hazan, "Rapid photodecolorization of methyl orange and rhodamine B using zinc oxide nano-particles mediated by pullulan at different calcination conditions," *Journal of Nanostructure in Chemistry*, vol. 11, no. 1, pp. 187–202, 2021.
- [17] K. Dulta, G. Koşarsoy Ağçeli, P. Chauhan, R. Jasrotia, and P. K. Chauhan, "A novel approach of synthesis zinc oxide nanoparticles by *bergenia ciliata* rhizome extract: antibacterial and anticancer potential," *Journal of Inorganic and Organometallic Polymers and Materials*, vol. 31, no. 1, pp. 180–190, 2021.
- [18] A. Kurian and P. Elumalai, "Study on the impacts of chemical and green synthesized (*Leucas aspera* and oxy-cyclodextrin complex) dietary zinc oxide nanoparticles in Nile tilapia (*Oreochromis niloticus*)," *Environmental Science and Pollution Research*, vol. 28, no. 16, pp. 20344–20361, 2021.
- [19] S. N. A. M. Sukri, K. Shameli, E. D. M. Isa, and N. A. Ismail, "Green synthesis of zinc oxide-based nanomaterials for photocatalytic studies: a mini review," in *IOP Conference Series: Materials Science and Engineering*, vol. 1051, 2021no. 1, Article ID 012083.
- [20] M. Irfan, H. Munir, and H. Ismail, "*Moringa oleifera* gum based silver and zinc oxide nanoparticles: green synthesis, characterization and their antibacterial potential against MRSA," *Biomaterials research*, vol. 25, no. 1, pp. 1–8, 2021.

- [21] G. S. Thirumoorthy, O. Balasubramaniam, P. Kumaresan, P. Muthusamy, and K. Subramani, "Tetraselmis indica mediated green synthesis of zinc oxide (ZnO) nano-particles and evaluating its antibacterial, antioxidant, and hemolytic activity," *BioNanoScience*, vol. 11, no. 1, pp. 172–181, 2021.
- [22] L. Safavinia, M. R. Akhgar, B. Tahamipour, and S. Ahmadi, "Green synthesis of highly dispersed zinc oxide nanoparticles supported on silica gel matrix by Daphne oleoides extract and their antibacterial activity," *Iranian Journal of Biotechnology*, vol. 19, no. 1, pp. 86–95, 2021.
- [23] G. Yashni, A. al-Gheethi, R. Mohamed, M. S. Hossain, A. F. Kamil, and V. Abirama Shanmugan, "Photocatalysis of xenobiotic organic compounds in greywater using zinc oxide nano-particles: a critical review," *Water and Environment Journal*, vol. 35, no. 1, pp. 190–217, 2021.
- [24] S. M. el-Megharbel, M. Alsawat, F. A. al-Salmi, and R. Z. Hamza, "Utilizing of (Zinc Oxide Nano-Spray) for Disinfection against "SARS-CoV-2" and Testing Its Biological Effectiveness on Some Biochemical Parameters during (COVID-19 Pandemic)–"ZnO Nanoparticles Have Antiviral Activity against (SARS-CoV-2)," *Coatings*, vol. 11, no. 4, p. 388, 2021.
- [25] S. Alamdari, M. Sasani Ghamasari, C. Lee et al., "Preparation and Characterization of zinc oxide Nanoparticles using leaf extract of *Sambucus ebulus*," *Applied Sciences*, vol. 10, no. 10, p. 3620, 2020.
- [26] A. K. Worku, D. W. Ayele, N. G. Habtu et al., "Structural and thermal properties of pure and chromium doped zinc oxide nano-particles," *SN Applied Sciences*, vol. 3, no. 7, pp. 1–10, 2021.
- [27] T. F. Hassanein, A. S. Mohammed, W. S. Mohamed, R. Sobh, and M. K. Zahran, "Optimized synthesis of biopolymer-based zinc oxide Nanoparticles and evaluation of their antibacterial activity," *Egyptian Journal of Chemistry*, vol. 64, no. 7, pp. 3767–3790, 2021.
- [28] H. Moradpoor, M. Safaei, H. Mozaffari et al., "An overview of recent progress in dental applications of zinc oxide nano-particles," *RSC Advances*, vol. 11, no. 34, pp. 21189–21206, 2021.
- [29] V. A. Spirescu, C. Chircov, A. M. Grumezescu, B. Ş. Vasile, and E. Andronescu, "Inorganic nanoparticles and composite films for antimicrobial therapies," *International Journal of Molecular Sciences*, vol. 22, no. 9, p. 4595, 2021.
- [30] T. Khalafi, F. Buazar, and K. Ghanemi, "Phycosynthesis and Enhanced Photocatalytic Activity of Zinc Oxide Nanoparticles Toward Organosulfur Pollutants," *Scientific Reports*, vol. 9, no. 1, article 6866, pp. 1–10, 2019.
- [31] A. Sajjad, S. H. Bhatti, Z. Ali et al., "Photoinduced fabrication of zinc oxide nanoparticles: transformation of morphological and biological response on light irradiance," *ACS Omega*, vol. 6, no. 17, pp. 11783–11793, 2021.
- [32] E. D. Mohamed Isa, N. W. Che Jusoh, R. Hazan, and K. Shameli, "Photocatalytic degradation of methyl orange using pullulan-mediated porous zinc oxide microflowers," *Environmental Science and Pollution Research*, vol. 28, no. 5, article 10939, pp. 5774–5785, 2021.
- [33] S. M. Taghizadeh, N. Lal, A. Ebrahimezhad et al., "Green and economic fabrication of zinc oxide (ZnO) nanorods as a broadband UV blocker and antimicrobial agent," *Nanomaterials*, vol. 10, no. 3, p. 530, 2020.
- [34] W. Ahmad and D. Kalra, "Green synthesis, characterization and anti microbial activities of ZnO nanoparticles using *Euphorbia hirta* leaf extract," *Journal of King Saud University-Science*, vol. 32, no. 4, pp. 2358–2364, 2020.
- [35] M. F. S. Hermandy, M. Z. M. Yusoff, M. S. Yahya, and M. R. Awal, "The green synthesis of nanoparticle zinc oxide (ZnO) using aloe vera leaf extract: structural and optical characterization reviews," *International Journal*, vol. 8, no. 10, pp. 6896–6902, 2020.
- [36] M. J. Haque, M. M. Bellah, M. R. Hassan, and S. Rahman, "Synthesis of ZnO nanoparticles by two different methods & comparison of their structural, antibacterial, photocatalytic and optical properties," *Nano Express*, vol. 1, no. 1, article 010007, 2020.
- [37] A. Jayachandran, T. R. Aswathy, and A. S. Nair, "Green synthesis and characterization of zinc oxide nanoparticles using Cayratia pedata leaf extract," *Biochemistry and Biophysics Reports*, vol. 26, article 100995, 2021.
- [38] M. Bandeira, M. Giovanela, M. Roesch-Ely, D. M. Devine, and J. da Silva Crespo, "Green synthesis of zinc oxide nanoparticles: a review of the synthesis methodology and mechanism of formation," *Sustainable Chemistry and Pharmacy*, vol. 15, article 100223, 2020.
- [39] K. M. Ezealisiji, X. Siwe-Noundou, B. Maduelosi, N. Nwachukwu, and R. W. M. Krause, "Green synthesis of zinc oxide nanoparticles using *Solanum torvum* (L) leaf extract and evaluation of the toxicological profile of the ZnO nanoparticles–hydrogel composite in Wistar albino rats," *International Nano Letters*, vol. 9, no. 2, pp. 99–107, 2019.
- [40] D. Gnanasangeetha and M. Suresh, "A review on green synthesis of metal and metal oxide nanoparticles," *Nature Environment and Pollution Technology*, vol. 19, no. 5, pp. 1789–1800, 2020.
- [41] M. G. Demissie, F. K. Sabir, G. D. Edossa, and B. A. Gonfa, "Synthesis of zinc oxide nanoparticles using leaf extract of *lip-pia adoensis* (koseret) and evaluation of its antibacterial activity," *Journal of Chemistry*, vol. 2020, Article ID 7459042, 9 pages, 2020.
- [42] A. Singh and P. K. Dutta, "Green synthesis, characterization and biological evaluation of chitin glucan based zinc oxide nanoparticles and its curcumin conjugation," *International Journal of Biological Macromolecules*, vol. 156, pp. 514–521, 2020.
- [43] M. Ijaz, M. Zafar, A. Islam, S. Afsheen, and T. Iqbal, "A review on antibacterial properties of biologically synthesized zinc oxide nanostructures," *Journal of Inorganic and Organometallic Polymers and Materials*, vol. 30, no. 8, pp. 2815–2826, 2020.
- [44] V. Hoseinpour, M. Souri, and N. Ghaemi, "Green synthesis, characterisation, and photocatalytic activity of manganese dioxide nanoparticles," *Micro & Nano Letters*, vol. 13, no. 11, pp. 1560–1563, 2018.
- [45] M. Mandal, "The use of aloe vera gel functionalized biogenic zinc-oxide nanoparticles against fish putative pathogens," *Aquatic Sciences and Engineering*, vol. 36, no. 3, pp. 101–108, 2021.
- [46] S. Thakur, M. Shandilya, and G. Guleria, "Appraisalment of antimicrobial zinc oxide nanoparticles through *Cannabis Jatropha curcusa* Alovera and *Tinosporacordifolia* leaves by green synthesis process," *Journal of Environmental Chemical Engineering*, vol. 9, no. 1, article 104882, 2021.
- [47] J. D. O. Primo, C. Bittencourt, S. Acosta et al., "Synthesis of zinc oxide nanoparticles by ecofriendly routes: adsorbent for copper removal from wastewater," *Frontiers in Chemistry*, vol. 8, p. 1100, 2020.
- [48] V. Koutu, L. Shastri, and M. M. Malik, "Effect of temperature gradient on zinc oxide nano particles synthesized at low

reaction temperatures,” *Materials Research Express*, vol. 4, no. 3, article 035011, 2017.

- [49] S. Abel, J. L. Tesfaye, R. Shanmugam et al., “Green synthesis and characterizations of zinc oxide (ZnO) nanoparticles using aqueous leaf extracts of coffee (*Coffea arabica*) and its application in environmental toxicity reduction,” *Journal of Nanomaterials*, vol. 2021, Article ID 3413350, 6 pages, 2021.
- [50] A. Degefa, B. Bekele, L. T. Jule et al., “Green Synthesis, Characterization of Zinc Oxide Nanoparticles, and Examination of Properties for Dye-Sensitive Solar Cells Using Various Vegetable Extracts,” *Journal of Nanomaterials*, vol. 2021, Article ID 3941923, 9 pages, 2021.

## Research Article

# Ecofriendly/Rapid Synthesis of Silver Nanoparticles Using Extract of Waste Parts of Artichoke (*Cynara scolymus* L.) and Evaluation of their Cytotoxic and Antibacterial Activities

Ayşe Baran,<sup>1</sup> Mehmet Firat Baran,<sup>2</sup> Cumali Keskin ,<sup>2</sup> Sevgi Irtegun Kandemir,<sup>3</sup> Mahbuba Valiyeva,<sup>4</sup> Sevil Mehraliyeva,<sup>4</sup> Rovshan Khalilov ,<sup>5,6,7</sup> and Aziz Eftekhari <sup>7,8</sup>

<sup>1</sup>Department of Biology, Graduate Education Institute, Mardin Artuklu University, Mardin, Turkey

<sup>2</sup>Medical Laboratory Techniques, Vocational Higher School of Healthcare Studies, Mardin Artuklu University, Mardin, Turkey

<sup>3</sup>Department of Medical Biology, Faculty of Medicine, Dicle University, Diyarbakir, Turkey

<sup>4</sup>Department of Pharmaceutical Technology and Management, Azerbaijan Medical University, Baku, Azerbaijan

<sup>5</sup>Department of Biophysics and Biochemistry, Baku State University, Baku, Azerbaijan

<sup>6</sup>Institute of Radiation Problems, National Academy of Sciences of Azerbaijan, Baku, Azerbaijan

<sup>7</sup>Department of Biology and Chemistry, Drohobych Ivan Franko State Pedagogical University, Drohobych, Ukraine

<sup>8</sup>Toxicology and Pharmacology Department, Maragheh University of Medical Sciences, Maragheh, Iran

Correspondence should be addressed to Cumali Keskin; ckeskinoo@gmail.com and Aziz Eftekhari; ftekhari@ymail.com

Received 5 August 2021; Revised 18 August 2021; Accepted 1 September 2021; Published 14 September 2021

Academic Editor: Shanmugam Rajeshkumar

Copyright © 2021 Ayşe Baran et al. This is an open access article distributed under the Creative Commons Attribution License, which permits unrestricted use, distribution, and reproduction in any medium, provided the original work is properly cited.

Recycling wastes and providing their use in useful fields attract attention every day. In our study, with the extract prepared from the parts of the *Cynara scolymus* L. (artichoke) plant that is not suitable for human consumption, silver nanoparticles were easily synthesized in an ec-friendly, energy-free way. Characterization of the obtained nanoparticles was done with a UV-visible spectrophotometer (UV-Vis.), fourier transform infrared spectroscopy (FTIR), X-ray diffraction diffractometer (XRD), scanning electron microscope (SEM), transmission electron microscopy (TEM), and zeta potential analysis data. In these data, it was determined that AgNPs have a maximum absorbance at 458.8 nm wavelength, a crystal nanosize of 28.78 nm, and a spherical appearance. The zeta potential of (-) 16.9 mV indicates that silver nanoparticles exhibit a stable structure. Particles show antimicrobial effects on pathogenic species at concentrations of 0.03-0.25 µg/ml, and it was determined by using the minimum inhibition concentration (MIC) microdilution method. By examining their cytotoxic effects on U118, CaCo-2, and Skov-3 cancer cell lines and healthy HDF cell lines by the MTT method, concentrations of inhibitive effects on survival were determined.

## 1. Introduction

Metallic nanoparticles are valuable materials with their wide-spread use. Nanoparticles such as silver (Ag), gold (Au), iron (Fe), and zinc (Zn) are some of them. There are different methods such as heat treatment and photochemical and chemical processes in obtaining them [1]. Although the application stages of these methods are difficult, they also bring high costs. Another disadvantage is that it contains toxic chemicals in the process. Against these methods, the synthesis of

metallic nanoparticles with ecofriendly biological methods has recently attracted considerable attention [2].

Silver nanoparticles (AgNPs) are used in many different fields such as medical [3], bioremediation studies [4], catalysis applications [5], food [6], cosmetics industry [7], agricultural activities [8], and electronics [9]. Biological resources such as algae [10], bacteria [11], fungi [12], and plants [13] are used in the synthesis of AgNPs by biological methods. Among these, the use of plant sources, when compared to other organisms, to obtain a greater amount of

nanoparticles, the more stable particles obtained [14], the simpler and more economical application steps [15] increase the preference for this field. Plants' leaves [16], fruits [17], roots [18], flowers [19], and aboveground parts of the plant [20] are structures used for the synthesis of AgNPs.

Bioactive components such as alcohols, flavonoids, phenols, and terpenoids found in the structure of plant sources form AgNPs by reducing Ag<sup>+</sup> ions in the aqueous structure to the Ago form [21].

*Cynarascolymus L.* (artichoke) is a herbaceous plant cultivated in the Mediterranean region since ancient times. Today, it is widely cultured in many parts of the world. The leaf contains caffeinated quinic acid derivatives, flavonoids, lactones, tannin, and inulin. It prevents lipid peroxidation through polyphenols and flavonoids in artichoke content. It is known that this effect is caused by strong antioxidants such as cynarin and silymarin [22]. The head part is the popular vegetable consumed. It is consumed by making salads, jams, and canned food [23]. It creates a large amount of waste, except for the consumed part.

This study is aimed at synthesizing and characterizing AgNPs by using the extract obtained with the parts of the artichoke in a waste state economically and simply, with an eco-friendly method, and to examine their antimicrobial and cytotoxic activities.

## 2. Material and Method

**2.1. Plant Material.** Artichoke (*Cynarascolymus*) is a perennial herb with purple flowers belonging to the *Asteraceae* (Compositae) family. Artichoke, which is rich in antioxidants, is often grown in Mediterranean countries. As the study material, the parts of the artichoke fruit that are not consumed as food were used [23].

**2.2. Instruments.** The analysis was made by using, respectively, PerkinElmer one UV-visible spectrophotometer (UV-Vis.), Rad B-DMAX II computer-controlled X-ray diffractometer (XRD), EVO 40 LEQ scanning electron microscopy (SEM), and Jeol Jem. 1010 transmission electron microscopy (TEM), RadB-DMAX II computer-controlled energy dispersive X-ray diffraction (EDX), and Malvern zeta potential devices were used to determine the formation, presence, crystal structure, dimensions, morphological appearance, and surface structures of AgNPs. Besides, PerkinElmer one fourier transform infrared spectroscopy (FTIR) device was used to evaluate the bioactive groups in the extract participating in reduction. The OHAUS FC 5706 model refrigerated centrifuge (6000 rpm) was used to separate the AgNPs from the extract at the end of synthesis.

Sigma-Aldrich brand solid compound form of % 98.8 AgNO<sub>3</sub> (silver nitrate) was used. Commercially purchased vancomycin, colistin, and fluconazole were used as standard antibiotics.

**2.3. Plant Extract and Solution Preparation.** The edible part of the 3 kg artichoke fruit is approximately 500 g. The rest is in the waste state as it is not consumed. After weighing 200 g of the parts to be discarded, they were cut into small

pieces and dried under room conditions for use as material. It undergoes a series of washing processes to purify it from material residues. The extraction process was carried out at room temperature using a heated magnetic stirrer (150 rpm). In the extraction process, after the mixture reaches boiling temperature, it is left to boil for 5 minutes. Then, it was cooled at room temperature and then the extract and residue are separated using Whatman no. 1 filter paper. The obtained extract was made ready to use for synthesis.

A solution with a concentration of 20 mM (millimolar) was prepared from the AgNO<sub>3</sub> salt.

**2.4. Synthesis of AgNPs and Characterization.** 500 ml of plant extract and 20 mM AgNO<sub>3</sub> solution was transferred into a 2000 ml glass flask. It was left on a stable surface at room conditions after simple mixing. Observations were made depending on the time. Samples were taken according to the color change, wavelength, and absorbance measurements were made in the UV-vis spectrophotometer.

To detect the formation and presence of AgNP analyses, the UV-visible spectrophotometer was used. Functional groups of bioactive components involved in reduction were evaluated with FTIR analysis data. A high-speed centrifuge was used to separate the AgNPs from the liquid phase after synthesis. After the reaction was finished, the dark solution was centrifuged at 6000 rpm for 25 minutes. The centrifuge process was repeated several times by adding distilled water. Then, the removed particles from the residue were left to dry at 80°C. The dried and powdered material was used in FTIR analysis. XRD analysis results were examined to determine the crystal sizes and structures. SEM, TEM, and EDX data were evaluated to determine the morphological structure and element composition content. The zeta potential analysis results were examined in the surface analysis of nanoparticles and in determining the charge distribution.

**2.5. Determination of Antimicrobial Activity Using the Minimum Inhibition Concentration (MIC) Microdilution Method.** *Staphylococcus aureus* (*S.aureus*) ATCC 25923, *Escherichia coli* (*E. coli*) ATCC25922 strains, and *Candida albicans* (*C.albicans*) clinic isolate were obtained from İnönü University Medical Faculty Hospital Microbiology Laboratory, and *Bacillus subtilis* (*B. subtilis*) ATCC 11774 and *Pseudomonas aeruginosa* (*P. aeruginosa*) ATCC27853 were obtained from Artuklu University Microbiology Research Laboratory.

Gram-positive (*S. aureus* and *B. subtilis*) and Gram-negative (*P. aeruginosa* and *E. coli*) bacteria were inoculated on a nutrient agar medium. *C. Albicans* yeast was inoculated on sabouraud dextrose agar medium and left to grow in an oven at 37°C overnight. Following the growth control the next day, microorganism suspensions were prepared according to McFarland standard 0.5 [24] (the colony in 1.5 × 10<sup>8</sup> units (CFU) ml<sup>-1</sup>) concentration for each of the microorganisms grown from the plates in solid form.

Muller Hinton broth (for bacteria), RPMI (Roswell Park Memorial Institute) broth for yeast, and AgNP solution prepared at concentrations of 20 µg/ml<sup>-1</sup> were added to 96 well microplates. A series of dilutions were made to the first well



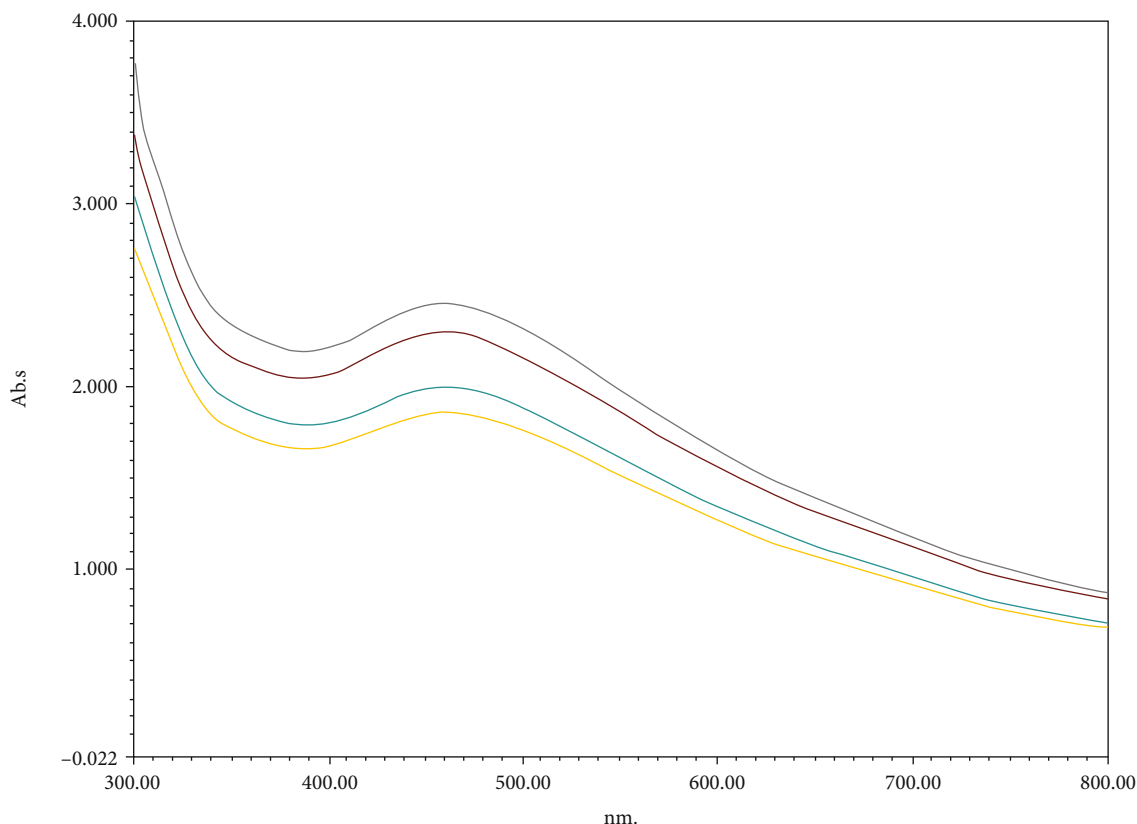


FIGURE 1: UV-vis showing the formation and presence of AgNPs: spectrophotometer data.

and then the other wells. Then, suspension prepared for each microorganism was added to each diluted well.

To compare the effects of AgNPs, the same application steps were repeated using vancomycin for Gram-positive strains, colistin for Gram-negative, and finally fluconazole antibiotics for the yeast *C. albicans*. Microplates were allowed to grow at 37°C for 24 hours. At the end of the period, the concentration of the well before the well where the growth started was determined as the minimum inhibition concentration.

**2.6. Analyzing of Cytotoxic Effects of AgNPs.** Cytotoxic effect application was made in Dicle University Scientific Research Centre Cell Culture Laboratory with human dermal fibroblast (HDF), glioblastoma (U118), human colorectal adenocarcinoma (CaCo-2), and ovarian sarcoma (Skov-3) cells obtained from the American Type Culture Collection (ATCC).

The 3 cell types used were cultured in Dulbecco's Modified Eagle's Medium (DMEM) 75 t-flasks that include 10% FBS, 100 U/ml penicillin-streptomycin (Penstrep.), and 2 mM L-glutamine. Over sarcoma (Skov-3) cells were cultured in Roswell Park Memorial Institute (RPMI) 75 t-flasks that include %10 FBS and 100 U/ml penstrep.

The cultured flasks were incubated at 37°C, 5% CO<sub>2</sub>, 95% air, and humidity conditions. After the cells reached approximately 80% confluence in the hemocytometer measurement, they were suspended in different concentrations, transferred to 96 well microplates, and subjected to an overnight incubation. The next day, cells were treated with nanoparticles with concentrations of 200 µg/ml, 100 µg/ml,

50 µg/ml, and 25 µg/ml and incubated for 48 hours. After waiting, MTT solution was added to the plate wells, 3 hours of incubation, and then DMSO was added and left at room temperature for 15 minutes. The absorbance of the microplates at 540 nm wavelength was measured using the Multi ScanGo, Thermo instrument.

Using these absorbance values, the concentration in which the percentage of viability of AgNPs is inhibited on cells was calculated: %viability =  $U/C \times 100$  [25, 26].

U defines absorbances of cells treated with AgNPs, and C defines the absorbance values of control cells.

### 3. Result and Discussion

**3.1. UV-vis. Spectrophotometer Data.** Colour transformation from yellow to dark brown was observed one hour after mixing the plant extract and 20 mM AgNO<sub>3</sub> solution [2]. This color change is caused by the reduction of Ag<sup>+</sup> ions to Ago while transforming to AgNPs and the occurrence of vibrations (SPR) on the plasma surface [27, 28]. On the UV vis. device readings of samples taken regarding color changes, maximum absorbance value was found at 458.8 nm wavelength (Figure 1). It refers to the samples taken every two minutes in the UV-Vis spectrophotometer.

These peaks represent the maximum absorption of samples taken at different times.

The results of color change and maximum absorbance wavelength are the data showing the formation and presence of AgNPs in the dark-colored liquid [24, 29].

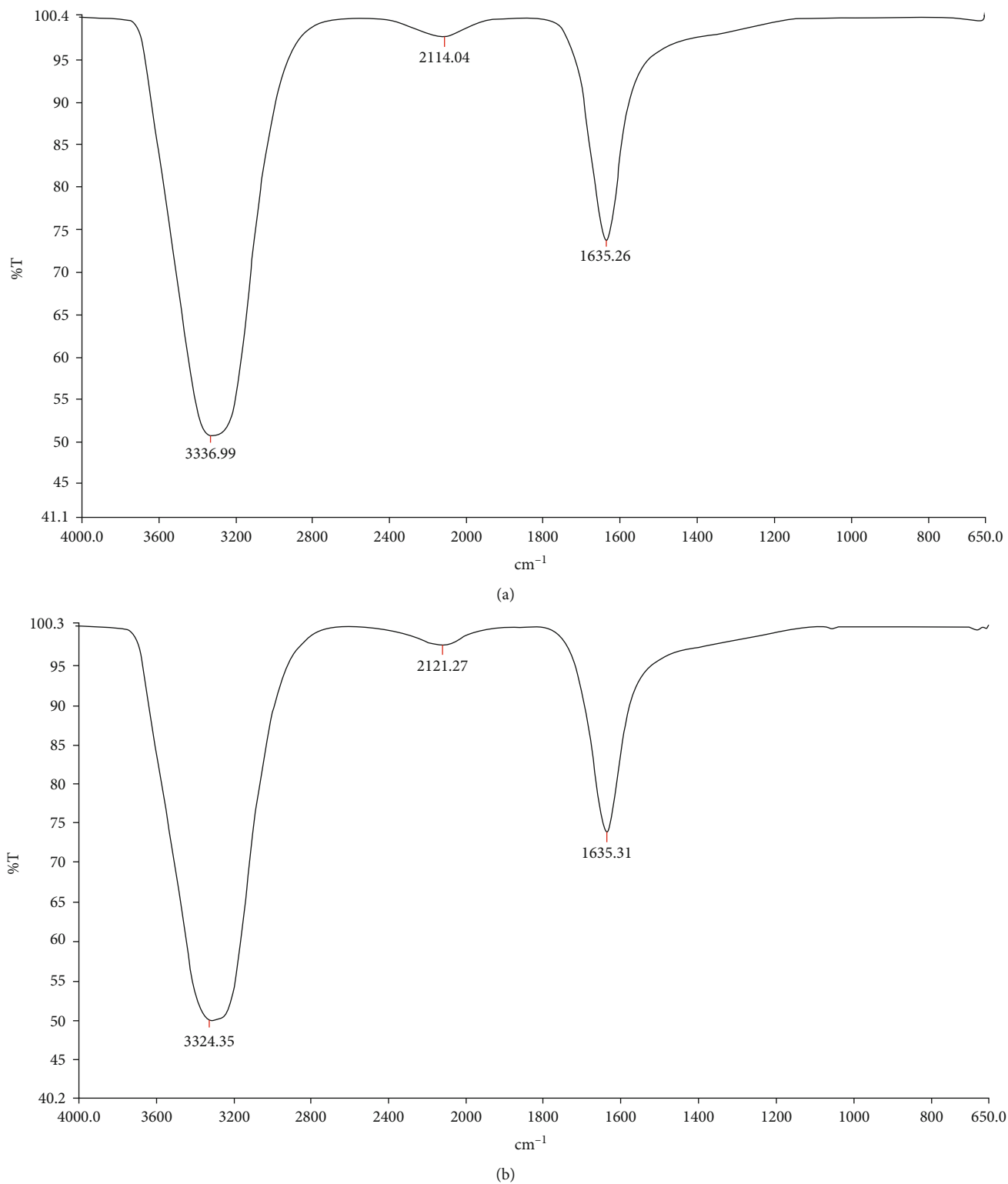


FIGURE 2: Infrared spectra of (a) extract of *Cynara scolymus* L. and (b) the reducing functional groups that play a role in the formation of AgNPs.

In synthesis studies using plant extracts, the maximum absorbance wavelength results of 460 nm [30] and 453 nm [9] have been associated with the presence of AgNPs.

**3.2. FTIR Analysis Data.** The functional groups involved in reduction were evaluated by looking at the FTIR results. Frequency shifts occurred at 3336.99-3324.35  $\text{cm}^{-1}$ , 1635.26-

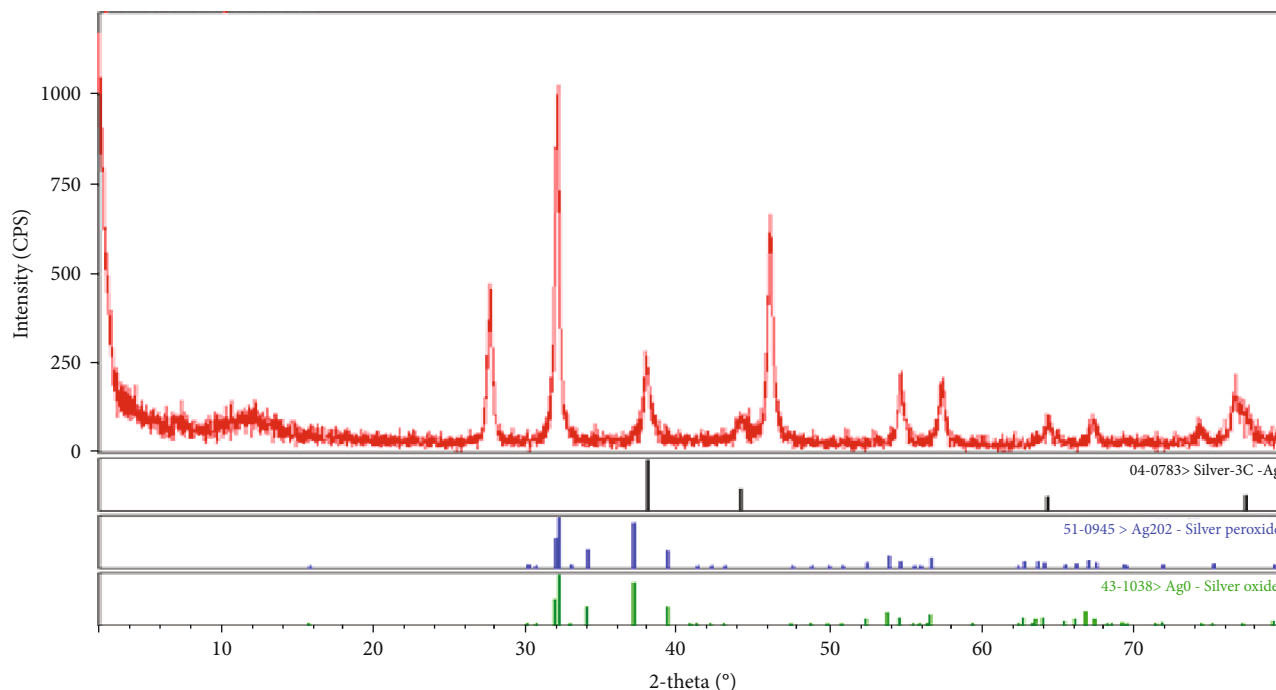


FIGURE 3: X-ray diffraction data of the crystal pattern of AgNPs.

1635.31  $\text{cm}^{-1}$ , and 2114.04–2121.27  $\text{cm}^{-1}$ . The shifts in these frequencies suggest that -OH (hydroxyl) groups [15], N-H amine groups [31], and  $\text{C}\equiv\text{C}$  alkyne groups [32] are functional groups involved in the reduction (Figure 2).

**3.3. XRD Analysis Data.** At  $2\theta$ , in the XRD results, it was seen that the crystal structure of silver was cubic, and the peaks belong to  $111^\circ$ ,  $200^\circ$ ,  $220^\circ$ , and  $311^\circ$  [33]. The values of these peaks were read as 32.16, 46.10, 64.44, and 76.68, respectively (Figure 3).

Using the peak values, the crystal nanosize was calculated according to the Debye-Scherrer equation ( $D = K\lambda / (\beta \cos \theta)$ ) [33].

The meanings of the symbols in this equation are  $D$  is the particle size,  $K$  is the constant value (0.90), X-ray wavelength  $\lambda$  value (1.5418 Å),  $\beta$  value of peak at maximum height (FWHM), and Bragg  $\theta$  angle of a high peak. As a result of the calculation, it was concluded that it has a crystal nanosize of 28.78 nm. In other studies calculating the crystal nanosize of AgNPs using the Debye-Scherrer equation, 35 nm [18] and 40 nm [34] crystal nanosizes were calculated.

**3.4. SEM, TEM, and EDX Analysis Data.** SEM, TEM, and EDX analysis data were used to determine the morphological structures and element compositions of AgNPs obtained after synthesis (Figure 4). It was determined that obtained AgNPs are in spherical view [34, 35]. Strong peaks of silver in EDX data indicate that the element composition is largely silver content and the presence of AgNPs [36]. Weak C and O peaks are due to contamination from extract [37] (Figure 4).

**3.5. Zeta Potential of AgNPs.** In the zeta potential analyses made to determine the surface charges of AgNPs, it was

examined whether AgNPs were negatively or positively charged. As seen in Figure 5, the zeta potentials of AgNPs obtained were measured as -16.9 mV. When AgNPs are in positive and negative charges, they show clustering and clumping features [26]. The (-)16.9 mV value we obtained shows that AgNPs have only negative charges and exhibit a stable structure. Since the silver nanoparticles we synthesize are of plant origin, it is natural to have a negative zeta potential. We think that this is due to the negatively charged structures in the plant structure. Having only a negative charge indicates that there is no clustering and clumping [38]. These negative charges may be due to the extract. The zeta potentials of AgNPs were found to be -14 mV [25] and -19 mV [26] in the studies. In a synthesis study, a zeta potential value of +5.68 mV was found, and it was reported that AgNPs exhibit clustering and clumping character [2].

**3.6. Evaluation of Antimicrobial Activities of AgNPs.** When we evaluated the activities of AgNPs, we obtained on pathogen species, and we determined that concentrations of 0.12 and 0.25  $\mu\text{g}/\text{ml}$  and were effective on Gram-positive *S. aureus* and *B. subtilis* bacteria, respectively. We determined that the concentration of 0.07 and 0.13  $\mu\text{g}/\text{ml}$  was effective on *P. aeruginosa* and *E. coli* in Gram-negative bacteria, respectively. The lowest concentration where AgNPs are effective is the concentration of 0.03  $\mu\text{g}/\text{ml}$  on *C. albicans* yeast. When we compared the effects of AgNPs obtained with silver nitrate solution and antibiotics, we concluded that they were effective at lower concentrations against these groups (Figure 6 and Table 1).

Silver ions ionize in an aqueous structure and show a high level of reactivity. Positive silver ions interact with the negatively charged cell membranes of microorganisms with an electrostatic attraction force. After this interaction, they

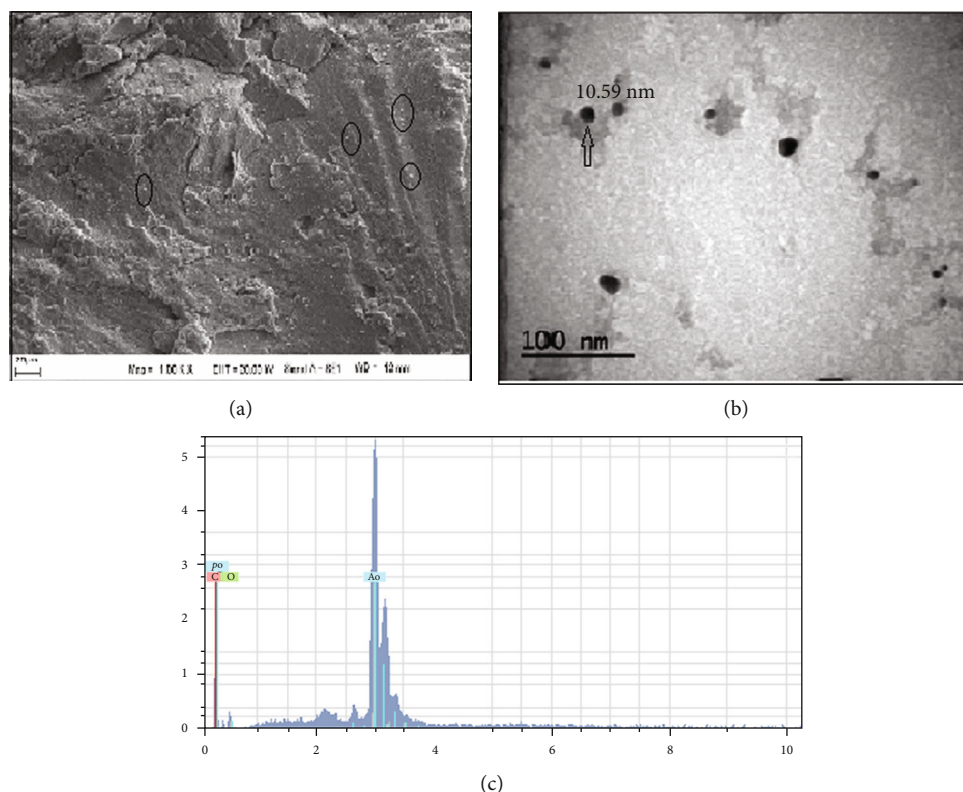


FIGURE 4: Morphological images and element composition of AgNPs: (a) SEM, (b) TEM images, and (c) EDX profile element.

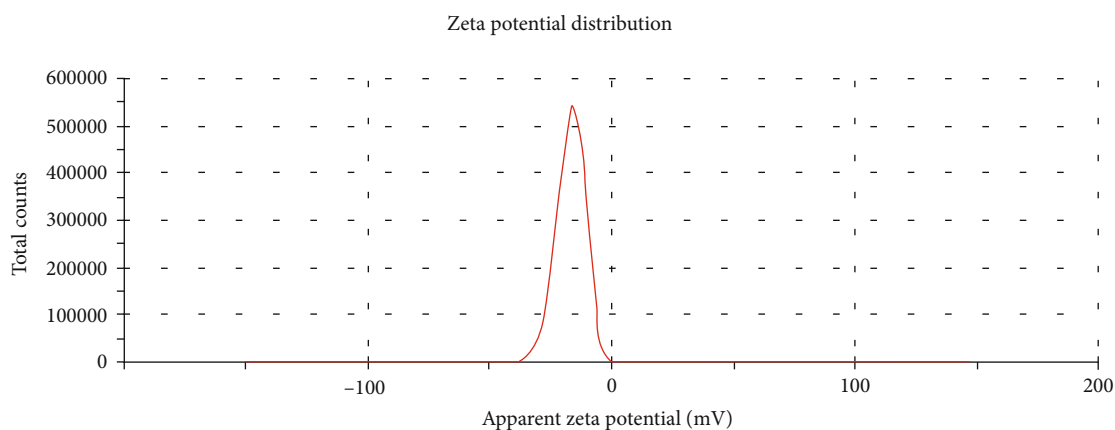


FIGURE 5: The zeta potential data of the surface charge distributions of AgNPs.

cause an increase in reactive oxygen species (ROS). With the increase of ROS, the cell wall structure is disrupted. The functions of the cell membrane and the nucleus membrane are impaired and undergo structural changes. The functions of structures such as DNA, RNA, and protein synthesis that have an affinity for these species are disrupted. Cell death occurs with cellular destruction [39–42].

When we examined some researches on the antimicrobial effects of AgNPs, it was found that the AgNPs are obtained using the plant extract of *Pistacia vera L.*, and it was observed to be effective on *S. aureus*, *E. coli*, and *C. albi-*

*cans* species at concentrations of 0.04, 0.66, and 0.16  $\mu\text{g/ml}$ , respectively [15]. In a study aimed at obtaining AgNPs in different sizes, it was determined that those with 5 nm sizes were effective on *B. subtilis*, *S. aureus*, and *E. coli* with concentrations of 0.8–6  $\mu\text{g/ml}$  [43]. In another study, it was emphasized that AgNPs were effective at 30  $\mu\text{g/ml}$  concentration on *P. aeruginosa* [24].

AgNPs may show different effects in different strains. Among the factors that affect their activities, characteristics such as concentration, size, shape, microorganism wall structure, temperature, and pH play a decisive role [42, 44].

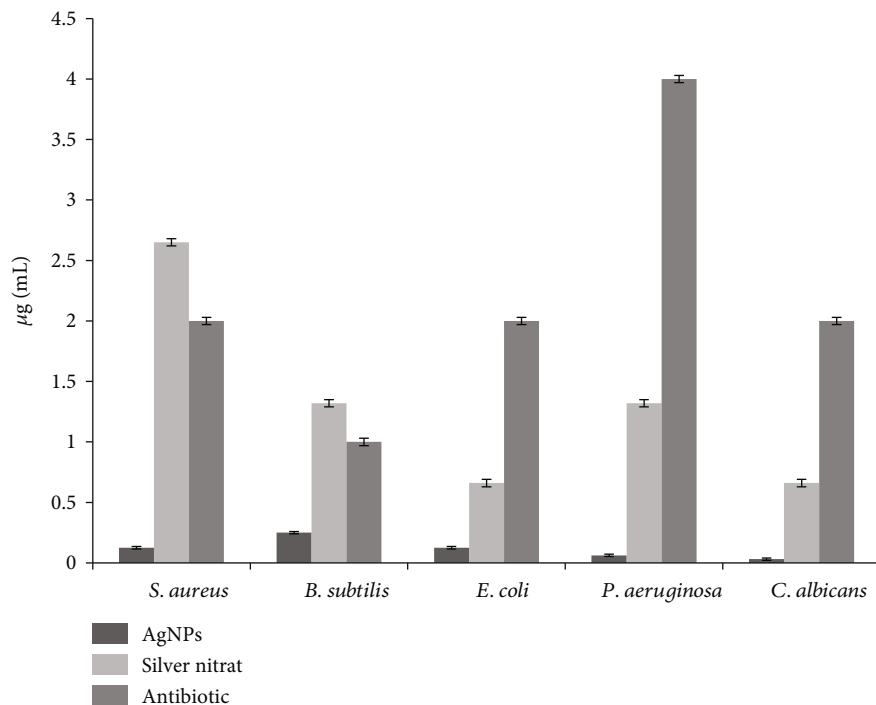


FIGURE 6: MIC values of AgNPs, silver nitrate solution, and antibiotics on the growth of pathogenic microorganisms.

TABLE 1: MIC values where AgNPs, silver nitrate, and antibiotics are effective in antimicrobial activity.

Tested organism	AgNPs $\mu\text{g/ml}$	Silver nitrate $\mu\text{g/ml}$	Antibiotic $\mu\text{g/ml}$
<i>S. aureus</i> ATCC 29213	0.12	2.65	2
<i>B. subtilis</i> ATCC 11773	0.25	1.32	1
<i>E. coli</i> ATCC25922	0.13	0.66	2
<i>P. aeruginosa</i> ATCC27833	0.07	1.32	4
<i>C. albicans</i>	0.03	0.66	2

**3.7. Cytotoxic Activities of AgNPs.** The data on the cytotoxic activities of the AgNPs we obtained on U118, HDF, CaCo-2, and Skov-3 cell lines are presented in Figure 7 and Table 2. 44.76% viability was seen on HDF cells at a concentration of 25  $\mu\text{g/ml}$ . On the U118 and Skov-3 cell lines, 58.98% and 74.55% viability was determined at a concentration of 25  $\mu\text{g/ml}$ , respectively. A concentration of 25  $\mu\text{g/ml}$  was toxic in the U118 and CaCo-2 cell lines. The increase in the percentage of viability versus the concentration of AgNPs in the U118 cell line is due to the proliferative properties of cancer cells [45].

AgNPs exhibit strong oxidative properties. The release of the Ag<sup>+</sup> form may induce immunological, cytotoxic, and genotoxic responses in biological environments; therefore, it is of great importance to examine its effects [46]. AgNPs settle at different points in the cells. These spots are the cell membrane, nucleus, and mitochondria. AgNPs show toxic effects by inducing apoptosis with ROS increase [45, 47].

In cell line studies on the cytotoxicity of AgNPs, it was determined that CaCo-2 cells at 3.75  $\mu\text{g/ml}$  [46] and Skov-3 cells at 9.4  $\mu\text{g/ml}$  [25] had toxic effects. In a study conducted on HDF cell lines, it was stated that a concentration of 100  $\mu\text{g/ml}$  has a toxic effect [48].

Several parameters can have a significant effect on the toxicity of nanomaterials. Some of them are concentration, exposure time, charge, the chemistry of surface composition, degree of deposition, shape, and size [41].

The different cytotoxic concentrations of AgNPs we obtained in all these studies and ourselves maybe since AgNPs are synthesized from different sources and have different sizes and morphological structures.

## 4. Conclusion

Artichoke (*Cynara scolymus* L.) is a plant that cannot be used except for the edible part and generates a large amount of agricultural waste. We synthesized AgNPs with an easy, economical, and ecofriendly method with the extract we prepared from these parts to transform these wastes into useful fields for human life. We characterized the AgNPs obtained with UV-vis., FTIR, SEM, TEM, EDX, XRD, and zeta potential analysis data. According to the results of the XRD analysis, the average nanosize was calculated to be 28.78 nm. As can be seen from the SEM images, it was determined that the silver nanoparticles were spherical, and the AgNPs averaged 10.59 in the TEM analysis. It was determined that AgNPs showed antimicrobial effects at low concentrations such as 0.03-0.25  $\mu\text{g/ml}$ . It is important to examine and determine the toxic effects of AgNPs for their use as anticancer and antimicrobial agents in medicine. Cytotoxic effects of AgNPs on U118, HDF, CaCo-2, and Skov-3 cell lines were

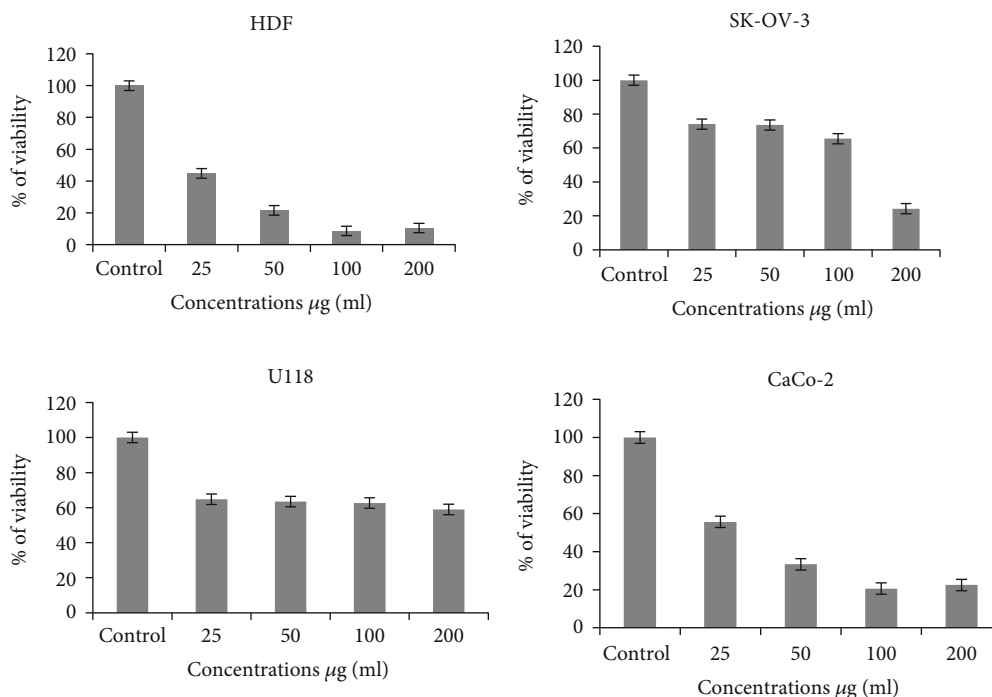


FIGURE 7: Viability rates of HDF, U118, CaCo-2, and Skov-3 cell lines 48 hours after interaction with AgNPs.

TABLE 2: Viability-suppressing concentrations of AgNPs on HDF, U118, CaCo-2, and Skov-3 cell lines.

Cell lines	25 µg/ml	50 µg/ml	100 µg/ml	200 µg/ml
HDF	44.76	21.52	8.61	10.44
U118	58.98	62.65	63.52	64.70
CaCo-2	55.64	33.37	20.624	22.50
Skov-3	74.15	73.62	65.57	24.25

examined. We determined an approximately 50% inhibition on cancer cell lines at a concentration of 25 µg/ml. These rates can be increased by developing method steps. It can be qualified to supply the demand for antimicrobial and anticancer agents.

## Data Availability

All data used to support the findings of this study are included within the article.

## Conflicts of Interest

The authors declare that there are no conflicts of interest regarding the publication of this paper.

## Acknowledgments

The authors are thankful to Mardin Artuklu University for providing all necessary research facilities to carry out this research.

## References

- [1] F. Mohammadi, M. Yousefi, and R. Ghahremanzadeh, "Green synthesis, characterization and antimicrobial activity of silver nanoparticles (AgNPs) using leaves and stems extract of some plants," *Advanced Journal of Chemistry-Section A*, vol. 2, no. 4, pp. 266–275, 2019.
- [2] Z. A. Ali, R. Yahya, S. D. Sekaran, and R. Puteh, "Green synthesis of silver nanoparticles using apple extract and its antibacterial properties," *Advances in Materials Science and Engineering*, vol. 2016, Article ID 4102196, 6 pages, 2016.
- [3] J. Y. Song and B. S. Kim, "Rapid biological synthesis of silver nanoparticles using plant leaf extracts," *Bioprocess and Biosystems Engineering*, vol. 32, no. 1, pp. 79–84, 2009.
- [4] B. Thomas, B. S. M. Vithiya, T. A. A. Prasad et al., "Antioxidant and photocatalytic activity of aqueous leaf extract mediated green synthesis of silver nanoparticles Using *Passiflora edulis f. flavicarpa*," *Journal of Nanoscience and Nanotechnology*, vol. 19, no. 5, pp. 2640–2648, 2019.
- [5] P. Rani, V. Kumar, P. P. Singh et al., "Highly stable AgNPs prepared via a novel green approach for catalytic and photocatalytic removal of biological and non-biological pollutants," *Environment International*, vol. 143, 2020.
- [6] J. A. Gudadhe, A. Yadav, A. Gade, P. D. Marcato, N. Durán, and M. Rai, "Preparation of an agar-silver nanoparticles (A-AgNp) film for increasing the shelf-life of fruits," *IET Nanobiotechnology*, vol. 8, no. 4, pp. 190–195, 2014.
- [7] A. C. P. Dias, G. Marslin, Selvakesavan, F. Gregory, and B. Sarmento, "Antimicrobial activity of cream incorporated with silver nanoparticles biosynthesized from *Withania somnifera*," *International Journal of Nanomedicine*, vol. 10, pp. 5955–5963, 2015.
- [8] S. D. Gupta, A. Agarwal, and S. Pradhan, "Phytostimulatory effect of silver nanoparticles (AgNPs) on rice seedling growth:

- an insight from antioxidative enzyme activities and gene expression patterns,” *Ecotoxicology and Environmental Safety*, vol. 161, pp. 624–633, 2018.
- [9] S. Sampaio and J. C. Viana, “Production of silver nanoparticles by green synthesis using artichoke (*Cynara scolymus*L.) aqueous extract and measurement of their electrical conductivity,” *Advances in Natural Sciences: Nanoscience and Nanotechnology*, vol. 9, no. 4, pp. 1–10, 2018.
- [10] S. N. Sinha, D. Paul, N. Halder, D. Sengupta, and S. K. Patra, “Green synthesis of silver nanoparticles using fresh water green alga *Pithophora oedogonia* (Mont.) Wittrock and evaluation of their antibacterial activity,” *Applied Nanoscience*, vol. 5, no. 6, pp. 703–709, 2015.
- [11] K. Gopalu, J. Matheswaran, G. Alexander, A. L. T. Juan, K. Evgeny, and K. Denis, “Rapid biosynthesis of AgNPs using soil bacterium *Azotobacter vinelandii* with promising antioxidant and antibacterial activities for biomedical applications,” *Journal of the Minerals, Metals and Materials Society*, vol. 69, pp. 1206–1212, 2017.
- [12] G. Li, D. He, Y. Qian et al., “Fungus-mediated green synthesis of silver nanoparticles using *aspergillus terreus*,” *International Journal of Molecular Sciences*, vol. 13, no. 1, pp. 466–476, 2012.
- [13] C. Luna, V. H. G. Chávez, E. D. Barriga-Castro, N. O. Núñez, and R. Mendoza-Reséndez, “Biosynthesis of silver fine particles and particles decorated with nanoparticles using the extract of *Illicium verum* (star anise) seeds,” *Spectrochimica Acta Part A: Molecular and Biomolecular Spectroscopy*, vol. 141, pp. 43–50, 2015.
- [14] O. A. Ojo, B. E. Oyinloye, A. B. Ojo et al., “Green synthesis of silver nanoparticles (AgNPs) using *Talinum triangulare* (Jacq.) Willd. leaf extract and monitoring their antimicrobial activity,” *Journal of Bionanoscience*, vol. 11, pp. 292–296, 2017.
- [15] M. F. Baran, “Synthesis, Characterization And Investigation Of Antimicrobial Activity Of Silver Nanoparticles From *Cydonia oblonga* Leaf,” *Applied Ecology and Environmental Research*, vol. 17, no. 2, pp. 2583–2592, 2019.
- [16] S. Francis, S. Joseph, E. P. Koshy, and B. Mathew, “Green synthesis and characterization of gold and silver nanoparticles using *Mussaenda glabrata* leaf extract and their environmental applications to dye degradation,” *Environmental Science and Pollution Research*, vol. 24, no. 21, pp. 17347–17357, 2017.
- [17] B. Kumar, K. Smita, L. Cumbal, and A. Debut, “Green synthesis of silver nanoparticles using Andean blackberry fruit extract,” *Saudi Journal of Biological Sciences*, vol. 24, no. 1, pp. 45–50, 2015.
- [18] C. Sudhakar, K. Selvam, M. Govarthanan et al., “*Acorus calamus* rhizome extract mediated biosynthesis of silver nanoparticles and their bactericidal activity against human pathogens,” *Journal, Genetic Engineering & Biotechnology*, vol. 13, no. 2, pp. 93–99, 2015.
- [19] G. Karunakaran, M. Jagathambal, M. Venkatesh et al., “*Hydrangea paniculata* flower extract-mediated green synthesis of MgNPs and AgNPs for health care applications,” *Powder Technology*, vol. 305, pp. 488–494, 2017.
- [20] M. F. Baran, “Synthesis and antimicrobial applications of silver nanoparticles from *artemisia absinthium* plant,” *Biological and Chemical Research*, vol. 6, pp. 96–103, 2019.
- [21] S. K. Srikar, D. D. Giri, D. B. Pal, P. K. Mishra, and S. N. Upadhyay, “Green synthesis of silver nanoparticles : a review,” *Green and Sustainable Chemistry*, vol. 6, no. 1, pp. 34–56, 2016.
- [22] A. Mandegary, A. Saeedi, A. Eftekhari, V. Montazeri, and E. Sharif, “Hepatoprotective effect of silymarin in individuals chronically exposed to hydrogen sulfide; modulating influence of TNF- $\alpha$  cytokine genetic polymorphism,” *DARU Journal of Pharmaceutical Sciences*, vol. 21, no. 1, 2019.
- [23] B. Biswas, K. Rogers, F. McLaughlin, D. Daniels, and A. Yadav, “Antimicrobial Activities of Leaf Extracts of Guava (*Psidium guajava* L.) on Two Gram-Negative and Gram-Positive Bacteria,” *International Journal of Microbiology*, vol. 2013, Article ID 746165, 7 pages, 2013.
- [24] W. R. Rolim, M. T. Pelegrino, B. de Araújo Lima et al., “Green tea extract mediated biogenic synthesis of silver nanoparticles: characterization, cytotoxicity evaluation and antibacterial activity,” *Applied Surface Science*, vol. 463, pp. 66–74, 2019.
- [25] C. D. Fahrenholtz, J. Swanner, M. Ramirez-Perez, and R. N. Singh, “Heterogeneous responses of ovarian cancer cells to silver nanoparticles as a single agent and in combination with cisplatin,” *Journal of Nanomaterials*, vol. 2017, Article ID 5107485, 11 pages, 2017.
- [26] I. Al-Ogaidi, M. I. Salman, F. I. Mohammad et al., “Antibacterial and cytotoxicity of silver nanoparticles synthesized in green and black tea,” *World*, vol. 5, no. 1, pp. 39–45, 2017.
- [27] M. J. Ahmed, G. Murtaza, F. Rashid, and J. Iqbal, “Eco-friendly green synthesis of silver nanoparticles and their potential applications as antioxidant and anticancer agents,” *Drug Development and Industrial Pharmacy*, vol. 45, no. 10, pp. 1682–1694, 2019.
- [28] M. F. Baran, “Green synthesis of silver nanoparticles (AGNPs) using *Pistacia Terebinthus* leaf extract: antimicrobial effect and characterization,” *International Journal of Mathematics and Mathematical Sciences*, vol. 5, no. 2, 2018.
- [29] W. Zhang and W. Jiang, “Antioxidant and antibacterial chitosan film with tea polyphenols- mediated green synthesis silver nanoparticle via a novel one-pot method,” *International Journal of Biological Macromolecules*, vol. 155, pp. 1252–1261, 2020.
- [30] A. D. Dwivedi and K. Gopal, “Biosynthesis of silver and gold nanoparticles using *Chenopodium album* leaf extract,” *Colloids and Surfaces A: Physicochemical and Engineering Aspects*, vol. 369, no. 1–3, pp. 27–33, 2010.
- [31] G. Das, H. Shin, A. Kumar, C. N. Vishnuprasad, and J. K. Patra, “Photo-mediated optimized synthesis of silver nanoparticles using the extracts of outer shell fibre of *Cocos nucifera* L. fruit and detection of its antioxidant, cytotoxicity and antibacterial potential,” *Saudi Journal of Biological Sciences*, vol. 28, no. 1, pp. 980–987, 2021.
- [32] M. M. Alkhulaifi, J. H. Alshehri, M. A. Alwehaibi et al., “Green synthesis of silver nanoparticles using Citrus Limon peels and evaluation of their antibacterial and cytotoxic properties,” *Saudi Journal of Biological Sciences*, vol. 27, no. 12, pp. 3434–3441, 2020.
- [33] A. Eren and M. F. Baran, “Green Synthesis, Characterization and Antimicrobial Activity of Silver Nanoparticles (AgNPs) from Maize (*ZEA mays* L.),” *Applied Ecology and Environmental Research*, vol. 17, no. 2, pp. 4097–4105, 2019.
- [34] K. R. G. G. J. A. and G. M., “Rapid green synthesis of silver nanoparticles (AgNPs) using (*Prunus persica*) plants extract: exploring its antimicrobial and catalytic activities,” *Journal of Nanomedicine & Nanotechnology*, vol. 8, no. 4, pp. 1–8, 2017.
- [35] J. Wongpreecha, D. Polpanich, T. Suteewong, C. Kaewsaneha, and P. Tangboriboonrat, “One-pot, large-scale green synthesis of silver nanoparticles-chitosan with enhanced antibacterial

- activity and low cytotoxicity,” *Carbohydrate Polymers*, vol. 199, pp. 641–648, 2018.
- [36] V. Kumar, R. K. Gundampati, D. K. Singh, D. Bano, M. V. Jagannadham, and S. H. Hasan, “Photoinduced green synthesis of silver nanoparticles with highly effective antibacterial and hydrogen peroxide sensing properties,” *Journal of Photochemistry and Photobiology B: Biology*, vol. 162, pp. 374–385, 2016.
- [37] D. Arumai Selvan, D. Mahendiran, R. Senthil Kumar, and A. Kalilur Rahiman, “Garlic, green tea and turmeric extracts-mediated green synthesis of silver nanoparticles: Phytochemical, antioxidant and *in vitro* cytotoxicity studies,” *Journal of Photochemistry and Photobiology B: Biology*, vol. 180, pp. 243–252, 2018.
- [38] M. P. Patil, R. D. Singh, P. B. Koli et al., “Antibacterial potential of silver nanoparticles synthesized using *Madhuca longifolia* flower extract as a green resource,” *Microbial Pathogenesis*, vol. 121, pp. 184–189, 2018.
- [39] V. Gopinath, S. Priyadarshini, M. F. Loke et al., “Biogenic synthesis, characterization of antibacterial silver nanoparticles and its cell cytotoxicity,” *Arabian Journal of Chemistry*, vol. 10, no. 8, pp. 1107–1117, 2017.
- [40] P. Singh, A. Garg, S. Pandit, V. R. S. S. Mokkaapati, and I. Mijakovic, “Antimicrobial effects of biogenic nanoparticles,” *Nanomaterials*, vol. 8, no. 12, pp. 1009–1019, 2018.
- [41] M. K. Swamy, M. S. Akhtar, S. K. Mohanty, and U. R. Sinniah, “Synthesis and characterization of silver nanoparticles using fruit extract of *Momordica cymbalaria* and assessment of their *in vitro* antimicrobial, antioxidant and cytotoxicity activities,” *Spectrochimica Acta Part A: Molecular and Biomolecular Spectroscopy*, vol. 151, pp. 939–944, 2015.
- [42] N. Durán, M. Durán, M. B. JesusDe, A. B. Seabra, W. J. Fávaro, and G. Nakazato, “Silver nanoparticles: a new view on mechanistic aspects on antimicrobial activity,” *Nanomedicine: Nanotechnology, Biology and Medicine*, vol. 12, no. 3, pp. 789–799, 2016.
- [43] J. Li, K. Rong, H. Zhao, F. Li, Z. Lu, and R. Chen, “Highly selective antibacterial activities of silver nanoparticles against *Bacillus subtilis*,” *Journal of Nanoscience and Nanotechnology*, vol. 13, no. 10, pp. 6806–6813, 2013.
- [44] S. Rajeshkumar and L. V. Bharath, “Mechanism of plant-mediated synthesis of silver nanoparticles – a review on biomolecules involved, characterisation and antibacterial activity,” *Chemico-Biological Interactions*, vol. 273, pp. 219–227, 2017.
- [45] M. Morais, A. L. Teixeira, F. Dias, V. Machado, R. Medeiros, and J. A. V. Prior, “Cytotoxic effect of silver nanoparticles synthesized by green methods in cancer,” *Journal of Medicinal Chemistry*, vol. 63, no. 23, pp. 14308–14335, 2020.
- [46] A. Mohamed, S. Hassan, A. Fouda, M. Elgamal, and S. Salem, “Extracellular biosynthesis of silver nanoparticles using *aspergillus* sp. and evaluation of their antibacterial and cytotoxicity,” *Journal of Applied Life Sciences International*, vol. 11, no. 2, pp. 1–12, 2017.
- [47] A. R. Gliga, S. Skoglund, I. Odnevall Wallinder, B. Fadeel, and H. L. Karlsson, “Size-dependent cytotoxicity of silver nanoparticles in human lung cells: the role of cellular uptake, agglomeration and Ag release,” *Particle and Fibre Toxicology*, vol. 11, no. 1, pp. 1–17, 2014.
- [48] Y. Zhang, D. Yang, Y. Kong, X. Wang, O. Pandoli, and G. Gao, “Synergetic antibacterial effects of silver nanoparticles@aloe vera prepared via a green method,” *Nano Biomedicine and Engineering*, vol. 2, no. 4, pp. 252–257, 2010.



## Research Article

# Green Synthesis, Characterization of Zinc Oxide Nanoparticles, and Examination of Properties for Dye-Sensitive Solar Cells Using Various Vegetable Extracts

Anatol Degefa,<sup>1</sup> Bulcha Bekele,<sup>2</sup> Leta Tesfaye Jule,<sup>2,3</sup> Boka Fikadu,<sup>2</sup> Shanmugam Ramaswamy,<sup>4</sup> Lalitha Priyanka Dwarampudi,<sup>5</sup> N. Nagaprasad ,<sup>6</sup> and Krishnaraj Ramaswamy <sup>3,7</sup>

<sup>1</sup>Department of Mathematics, College of Natural and Computational Science, Dambi Dollo University, Ethiopia

<sup>2</sup>Department of Physics, College of Natural and Computational Science, Dambi Dollo University, Ethiopia

<sup>3</sup>Centre for Excellence-Indigenous Knowledge, Innovative Technology Transfer and Entrepreneurship, Dambi Dollo University, Ethiopia

<sup>4</sup>TIFAC CORE HD, Department of Pharmacognosy, JSS Academy of Higher Education and Research, JSS College of Pharmacy, Ooty, Tamil Nadu, India

<sup>5</sup>Department of Pharmacognosy, JSS Academy of Higher Education and Research, JSS College of Pharmacy, Ooty, Tamil Nadu, India

<sup>6</sup>Department of Mechanical Engineering, ULTRA College of Engineering and Technology, Madurai, Tamil Nadu, India

<sup>7</sup>Department of Mechanical Engineering, College of Engineering, Dambi Dollo University, Ethiopia

Correspondence should be addressed to Krishnaraj Ramaswamy; [prof.dr.krishnaraj@dadu.edu.et](mailto:prof.dr.krishnaraj@dadu.edu.et)

Received 8 July 2021; Revised 29 July 2021; Accepted 7 August 2021; Published 26 August 2021

Academic Editor: Shanmugam Rajeshkumar

Copyright © 2021 Anatol Degefa et al. This is an open access article distributed under the Creative Commons Attribution License, which permits unrestricted use, distribution, and reproduction in any medium, provided the original work is properly cited.

The production of zinc oxide nanoparticles (ZnO NPs) utilizing different vegetable extracts (onion, cabbage, carrot, and tomato) was performed in this research owing to its excellency over other methods of synthesis, namely, simplicity, environmental friendliness, and the elimination of harmful compounds. Fresh extracted onion, cabbage, carrot, and tomato of ZnO NPs are characterized by Fourier transform infrared (FTIR), X-ray diffraction (XRD), scanning electron microscopy (SEM), and UV-visible spectroscopy. FTIR findings demonstrate that the prepared nanoparticles were observed in the spectrum of  $626\text{ cm}^{-1}$ – $1219\text{ cm}^{-1}$  with some other functional groups. Wurtzite hexagonal structure of the prepared ZnO NPs was observed from XRD results. In addition, the prepared nanoparticles were failed into nanoscales (17 nm, 18 nm, 24 nm, and 15 nm) calculated from Scherrer's equation. Nearly spherical shapes were seen from SEM image for onion and tomato extraction while rod and tube for carrot and cabbage, respectively. Two broad peaks were observed from UV-vis spectroscopy results for each extract. The presence of a wide range of energy bandgaps in the region of 3–4 eV was detected, indicating that ZnO NP material can be employed in metal oxide semiconductor-based systems. The dye-sensitive solar cell based on ZnO NPs has been successfully synthesized, and the efficiency of the device has been evaluated by measuring the current density-voltage behaviour under the presence of artificial sunshine. The increased effectiveness of the manufactured dye-sensitive solar cell is attributable to a large improvement in dye molecular adsorption onto the surface of ZnO NPs. Thus, the usage of the green produced ZnO NPs with creating dye sensitivity solar cell is a simple and viable way for the well-being of our future.

## 1. Introduction

Power originates in numerous forms as a result of burning forests to produce fire in ancient times to electrical produc-

tions in the contemporary era. Its usage is among the most significant aspects in everyday living interaction of human beings. Nevertheless, the primary resources of energy that human beings utilized in the reaping have exhibited signs

of insufficiency due to the rise in industrial development in a large number of countries. As an outcome, growing concerns about energy crisis, global warming, lack in fossil fuels, and environmental problems are encouraging the research work to produce clean, affordable, and sustainable sources of the energy that will propel the world into the future [1]. Latest advancement in solar energy transformation innovations that use biosemiconductors as the light harvesting layer makes use of metallic oxide semiconductor (MOS) nanostructures for reliability. Both electrode and the biomolecules are involved in charge extraction and transportation, according to the National Renewable Energy Laboratory [2]. Nanoscience is a broad topic that concerns of the research and implementation of materials on a nanoscale. It is becoming increasingly popular. When compared to their bulk counterparts, nanoparticles (NPs) demonstrate new and enhanced qualities as a result of changes in their characteristics such as form size, size distribution, and a greater measure of the relationship between surface area and volume [3]. Metal nanoparticles (metal NPs) have found a wide range of applications in the fields of science and innovation in recent years, owing to their distinctive electrical, mechanical, optical, and magnetic characteristics [1–3]. Because of its vital applications as antibacterial agents, photovoltaic cells, textile fabrics, and polymers to eradicate microorganisms, zinc oxide nanoparticles (ZnO NPs) have garnered a considerable deal of interest from researchers in recent years [3].

The need for environmentally friendly energy sources has prompted extensive study into nanomaterials to meet these needs. When it comes to technology, nanotechnology is a branch that analyzes diverse materials on a nanometric scale. Its applications can be discovered in materials science, engineering, and electronic engineering. Nanoparticles exhibit a wide range of magnetic and optoelectronic properties that are influenced by their size and form distribution, as well as their composition. Due to the fact that this technique of synthesis eliminates the need for harmful chemicals, as well as its ease and environmental friendliness, the synthesis of nanoparticles employing vegetable extract is becoming increasingly popular [3–5]. In addition to its unique characteristics and high excitonic binding energy, zinc oxide (ZnO) is used in this application [1–5].

It is routinely possible to synthesize ZnO NPs using various methods, including but not limited to hydrothermal, solvothermal, sol-gel, direct oxidation, chemical vapour deposition (CVD), electrodeposition (ED), sonochemical, chemical bath deposition (CBD), microwave, and other approaches [5]. These approaches, on the other hand, are expensive, hazardous, and unfriendly to the natural environment. Nowadays, there is a growing demand for developing ZnO that has excellent yielding, has moderate cost, and is nontoxic by utilizing biological sources and environmentally acceptable techniques of exploration and production. To synthesize zinc oxide nanoparticles using a green synthesis approach, environmentally friendly resources including such plant extracts (leaf/flower/bark/root/seed/peel) and also the bacteria/fungi/enzymes are used for the manufacture of zinc oxide nanoparticles [6]. Vegetable removal was employed in this investigation due to its plentiful affordability. It has been observed that diverse vegetable extracts can be used to pro-

duce zinc oxide nanoparticles [6–8]. Different scholars have documented the usage of ZnO NPs in the production of dye-sensitive solar cells in their research. The green synthesis of zinc oxide nanoparticles employing onion, cabbage, carrot, and tomatoes as a resource for dye-sensitive solar cell implementation has not been documented, and no comparisons have been done between them. In the present research, ZnO nanoparticles are synthesized using the green synthesis technique, with preparations of tomato, onion, cabbage, and carrot serving as reducing and stabilising agents in addition to the ZnO. The nanoparticles that were synthesized were analyzed using a variety of techniques, including Fourier transform infrared, X-ray diffraction, scanning electron microscopy, and an ultraviolet/visible spectroscope. One of the objectives of this research is to synthesize and analyze zinc oxide nanoparticles based on extracts of onion and cabbage. Another is in order to look into the use of zinc oxide nanoparticles in the manufacture of dye-sensitive solar cells utilizing extracts of carrot and tomato.

## 2. Experimental Details

*2.1. Synthesis Methods.* Fresh onion, carrot, cabbage, and tomato were acquired in a market of Dambi Dollo Town. Zinc acetate dihydrates (99.7%) and ethanol (99.5%) as a solvent were also purchased from the market. First, the onion, cabbage, carrot, and tomato were chopped into tiny slices and rinsed three times with distilled water. Next, the onion, cabbage, carrot, and tomato were weighed and blended into the distilled water, and the process was repeated three more times. Aqueous extracts were obtained after mixing 22 grams of onion powder, 30 grams of cabbage powder, 20 grams of carrot powder, and 22 grams of tomato powder in 200 millilitres of distilled water in various beakers for 20 minutes at a time until the mixtures came to a boil. Following freezing, the combinations were filtered through what man paper and kept at 40°C until they were needed for another application. The green syntheses of ZnO NPs were performed out in accordance with published procedures [9]. 2 M concentration of zinc acetate dihydrate  $\text{Zn}(\text{CH}_3\text{COO})_2 \cdot 2\text{H}_2\text{O}$  was made in a beaker using sonication to dissolve 15 g of  $\text{Zn}(\text{CH}_3\text{COO})_2 \cdot 2\text{H}_2\text{O}$  in 1 litre of distilled water. The mixture was stored in the refrigerator until it was needed. The preparations of onion (10 mL), tomato (10 mL), cabbage (10 mL), and carrot (10 mL) were combined with a 10 mL solution of  $\text{Zn}(\text{CH}_3\text{COO})_2 \cdot 2\text{H}_2\text{O}$  in a beaker using a stirrer for 10 minutes and then allowed to stand at room temperature for 24 h before testing. The decrease of Zn-ion was seen as a change in colour from white to pale brown and then to a deep brown over time, as shown by the shifting of colour to white to light brown and then to dark brown. Because of the manufacture of ZnO NPs, the texture of the mixture had been changing. In the following 24 hours, the produced nanoparticles were whirled at 12000 rpm for 15 minutes and rinsed six times using ethanol and distilled water before being used. Following collection of the samples, they were moved to a Petri dish and dried for 12 hours at 70°C in a vacuum oven.

## 2.2. Characterization Techniques

**2.2.1. FTIR Analysis.** In order to study and characterize the connected functional groups to a surface of the synthesized ZnO nanoparticles, the PerkinElmer FTIR Spectrum One was used with a scanning spectrum of 4000–400  $\text{cm}^{-1}$  and a resolution of 4  $\text{cm}^{-1}$  for the analysis of the connected functional groups to the exterior of the synthesized ZnO nanoparticles. For both the FTIR evaluations, the specimen was consistently and appropriately mixed with solid KBr, which was squeezed to settle down on an extremely thin film, and this relatively thin film was used for the FTIR analysis, which was stored in the scanning chamber of the instrument.

**2.2.2. X-Ray Diffraction and SEM Analysis.** The X-ray diffraction (XRD) distribution of ZnO nanoparticles was acquired using an X'Pert Pro X-ray diffractometer that generated Cu  $K\alpha$  radiation (with an angular resolution of 1.5418 angstrom). It is being employed to evaluate the crystalline particle sizes that have been manufactured. For the purposes of characterization, a tiny quantity of powder sample was used. At room temperature, X-ray generators were running at a voltage of 40 kV and applying a current of 30 mA to the target. Temperature-dependent strengths were recorded at ambient temperature in steps of 0.02, throughout a range of 100 to 800°C, with the diffractometer attached to a computer for data collection and characterization displays. It was necessary to authenticate the structure of the crystal by comparing its peak positions with those of the existing standard data. For each sample, about 0.6 g of the produced ZnO NPs was ground to tiny powders and quantified using a beam balance before being transferred to a metal plate. Once the nanoparticles had been formed, the particle morphology was examined by utilizing a scanning electron microscope (Hitachi, H-7600) that operates under high vacuum and has magnifications ranging from 20x to about 30,000x, as well as spatial resolutions of 50 to 100 nm. Greater magnification of ZnO NPs was attained by decreasing the raster width of the sample, and vice versa, for the fixed sizes of the ZnO NPs. A quartz cuvette with a diameter of 1 cm was used to measure the absorbance spectra of obtained ZnO NPs employing UV-vis spectroscopy (PerkinElmer LAMBDA 950), which was operated throughout a wavelength range of 200–500 nm. Approximately 0.3 g of ZnO NPs was mixed with double distilled water before being placed into a quartz cuvette to form their solutions. After that, the cuvette was placed in an ultraviolet visible spectrophotometer, where the absorption spectra of ZnO NPs were determined.

## 3. Results and Discussion

**3.1. FTIR Analysis.** In order to identify the probable functional groups in biomolecules contained with the presence of a natural extract that are due to the reduction of the zinc ion into ZnO NPs, a Fourier transform infrared spectral analysis (FTIR) was performed. FTIR spectra of the prepared ZnO NPs with vegetable extracts are observed in Figure 1. FTIR spectrum of ZnO NPs synthesized with onion, cab-

bage, carrot, and tomato extracts demonstrated almost the absorption peaks at 626, 1219, 1392, 1744, and 2361  $\text{cm}^{-1}$ . The N-H, O-H, and H-bonded phenols and alcohols stretching oscillations of amide groups are represented because of the powerful and broad peak at 1500–2000  $\text{cm}^{-1}$ , which corresponds to the N-H, O-H, and H-bonded phenols and alcohols stretching vibrations of amide groups, respectively. The C-O stretch oscillations are represented by the bands that occur in the vicinity of 2361  $\text{cm}^{-1}$ . The appearance of a band in the spectrum in the ranges of 626  $\text{cm}^{-1}$  to 1219  $\text{cm}^{-1}$  indicates the formation of ZnO NPs, and the results are in great deal with the literature [10–12].

**3.2. X-Ray Diffraction Analysis.** The XRD pattern of ZnO NPs that were generated utilizing samples of onion, cabbage, carrot, and tomato is presented in Figure 2, and it can be seen in Figure 3. In accordance with JCPDS card no. 36-1451, all XRD diffraction profiles of ZnO NPs are all in excellent accordance with the hexagonal wurtzite architecture (hexagonal phase, space group P63mc) having lattice parameters of  $a = b = 3.249$  and  $c = 5.206$  as described in the retrieved products [10, 12, 13]. Two broad diffraction peaks were observed at 27.39° and 40.64° with corresponding crystal planes of (100) and (002), respectively. Here, the onion-extracted nanoparticles have shown two broad peaks only. In addition, 47.31°, 53.60°, 72.63°, and 73.75° were observed with (101), (102), (200), and (112) of crystal planes, respectively, in all the extracted samples except in the case of onion. The most intense peak was observed at (100) and shows the preferred growth plane; therefore, it demonstrated to the high level of purity of ZnO NP products. The XRD pattern of green synthesized ZnO NPs reported in the literature [14] is incongruous in accordance with the trend illustrated in Figure 2. Thus, utilizing XRD, the formation of ZnO NPs was established. The dimensions of the nanoparticles were determined using the assistance of the following Scherrer's equation.

$$t = \frac{0.9\lambda}{\beta \cos \theta}, \quad (1)$$

where  $t$  is the mean dimension of nanoparticles,  $k$  is the frequency of radiation,  $\beta$  is the whole width half peak in radians, and  $\theta$  is the degree diffraction [12–14].

Onion, cabbage, carrot, and tomato preparations have been used to synthesize nanoparticles with mean sizes of 17 nm, 18 nm, 24 nm, and 15 nm, respectively. The average sizes of the nanoparticles produced with onion, cabbage, carrot, and tomato extracts are seen in Table 1. Based on the foregoing findings, it can be inferred that throughout the instance of tomato extracts, smaller nanoparticles are generated.

**3.3. SEM Analysis.** Figure 3 demonstrates the SEM morphology of the extracted ZnO nanoparticles synthesized by onion, cabbage, carrot, and tomato, respectively. SEM images depict the spherical surface morphology in the case of onion and tomato extractions, while nearly nanorod and nanotube are synthesized using carrot and cabbage,

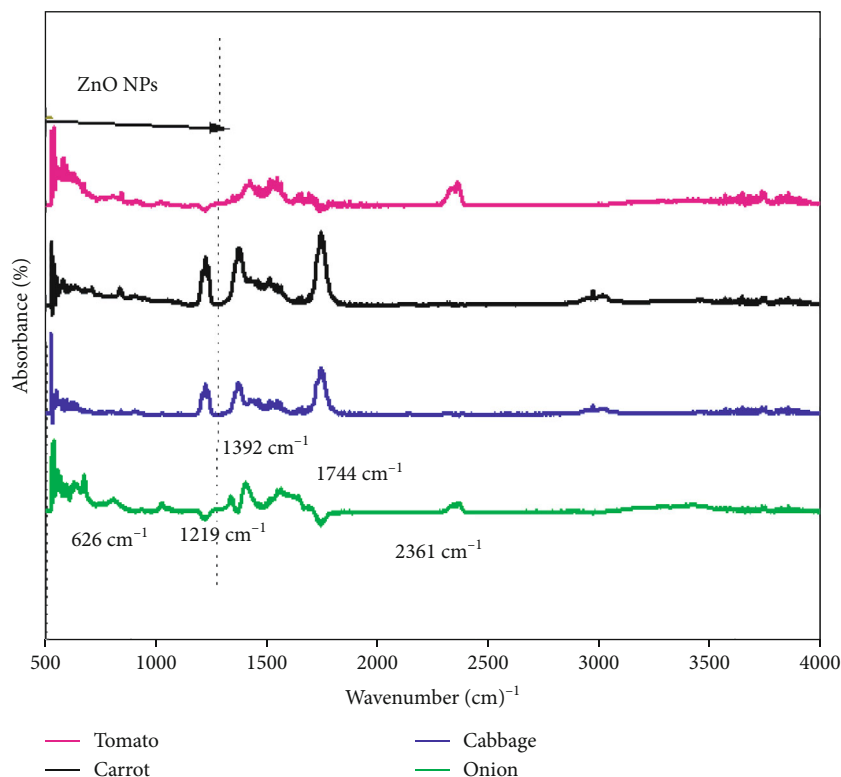


FIGURE 1: FTIR spectra of onion-, cabbage-, carrot-, and tomato-extracted ZnO NPs by green synthesizing methods.

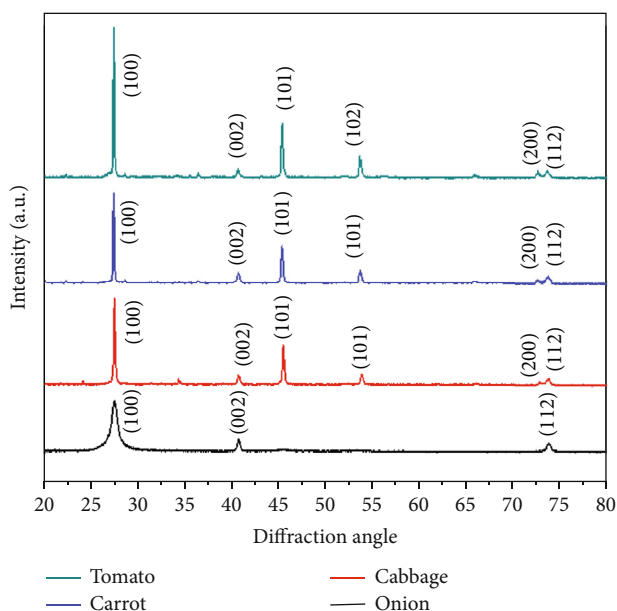


FIGURE 2: XRD spectral analysis of the prepared ZnO NPs extracted from onion, cabbage, carrot, and tomato.

respectively. Because of their small size, the green synthesized structures are uniform in nature, with little aggregation. Instead of using costly and harmful capping agents to minimize agglomeration, plant extract works as a reducing agent as well as a capping agent. As a result, this process is

more cost-effective and environmentally benign than the other certain technique of producing ZnO NPs. The narrow assimilation SEM image in onion and tomato extracts of the prepared ZnO NPs depicts detail wurtzite hexagonal structure where their adjacent contacting surface is smooth and has well-defined shapes [15–18].

The optical bandwidth of the produced ZnO NPs was studied using UV-vis spectroscopy [16, 18]. To obtain a homogeneous solution, the produced ZnO NPs were scattered evenly in the triple filtered water employing an ultrasonicator for 5 minutes. The UV-visible spectrum of the green produced ZnO NPs retrieved from onion, cabbage, carrot, and tomato is shown in Figure 4. The spectrum reveals a wide absorption peak at 276 nm and 375 nm for onion-extracted nanoparticles. In addition, 217 nm and 310 nm, 214 nm and 338 nm, and 215 nm and 343 nm are for cabbage-, carrot-, and tomato-extracted zinc oxide nanoparticles, respectively. These peaks are caused by ZnO NPs' surface plasmon absorption characteristics. When electromagnetic waves impact the surface plasmon absorption, a phenomenon happens owing to the cumulative oscillation of the open conduction band electrons [17, 18].

This current study of UV-visible absorption peak for ZnO NPs is similar to prior results [19]. Planck's equation was used to compute the bandgap energy ( $E$ ) of the produced ZnO nanoparticles.

$$E = \frac{hc}{\lambda}, \quad (2)$$

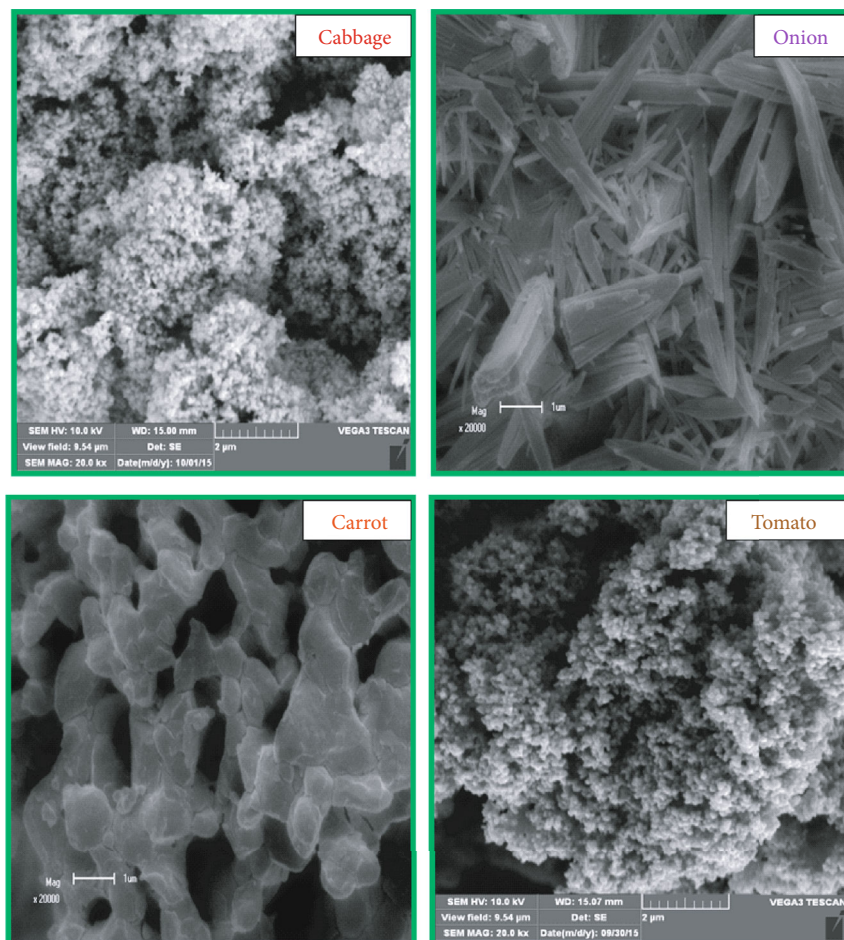


FIGURE 3: SEM images of the extracted ZnO NPs from onion, cabbage, carrot, and tomato through green synthesis methods.

TABLE 1: Average particle size, FWHM, and angle of diffraction of onion, cabbage, carrot, and tomato extracted from the prepared ZnO NPs.

Extracted samples	2 theta	FWHM ( $\beta$ )	Average particle size ( $t$ )
Onion	40.64	0.07345	17.10
Cabbage	40.64	0.05325	18.20
Carrot	40.64	0.04687	24.20
Tomato	40.64	0.08767	15.20

where  $E$  is the energy bandgap,  $h$  is the Planck constant =  $6.626 \times 10^{-34}$  Js,  $c$  is the speed of light =  $3 \times 10^8$  nm s $^{-1}$ , and  $\lambda$  is the wavelength.

Conversion of electron volt to joule is calculated as  $1 \text{ eV} = 1.6 \times 10^{-19}$  J [20]. Table 2 shows the computed bandgap energy value for greatest wavelengths. ZnO's inherent bandgap absorption is caused by electron transitions between the valences to the conduction bands. Because ZnO nanoparticles absorb UV light, they can be employed in medicinal purposes such as sunscreen protection or anti-bacterial ointments [16]. A wide range of energy bandgaps was discovered in the 3-4 eV range, indicating that ZnO NP powder can be employed in metal oxide semiconductor-based systems [19].

The characterization of the extracted zinc oxide nanoparticles was calculated using fill factor for dye-sensitive solar cell by using the following equation:

$$ff = \frac{J_{\max} \times V_{\max}}{J_{sc} \times V_{oc}}, \quad (3)$$

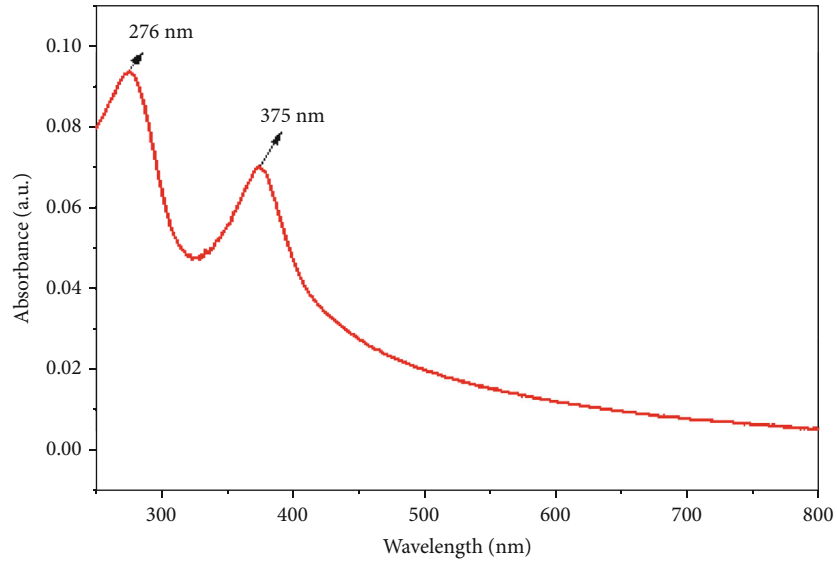
where  $J_{\max}$ ,  $V_{\max}$ ,  $J_{sc}$ , and  $V_{oc}$  represent the peak power point current density and voltage, small current density ( $J_{sc}$ ) of an observed current at 0 V, and open-circuit voltage ( $V_{oc}$ ), respectively [21].

The following Equation (4) calculates the energy conversion efficiency ( $n$  percent), which is the ratio of maximum power ( $p_{\max}$ ) to electrical input power ( $p_{in}$ ):

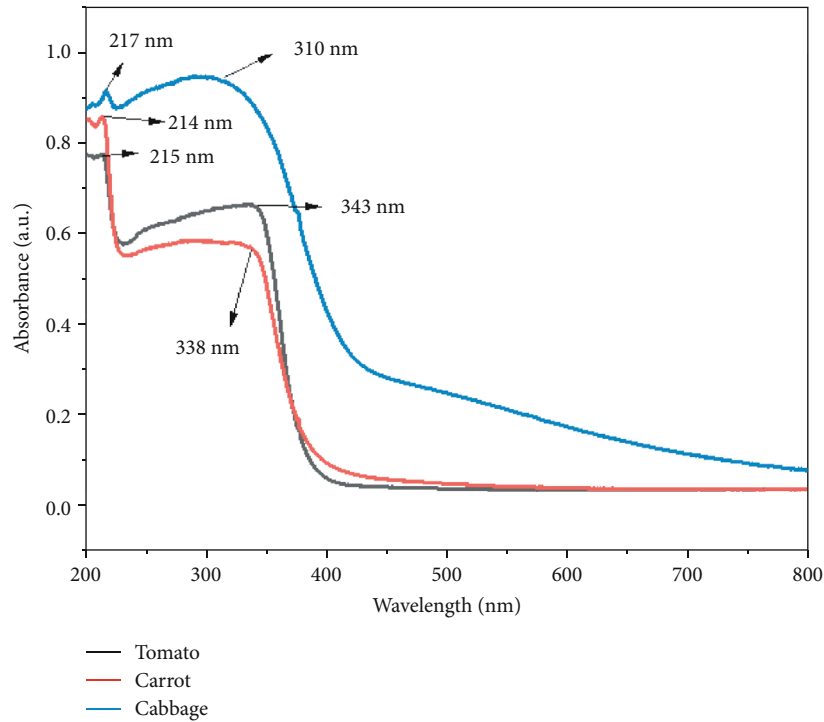
$$n = \frac{ff \times V_{oc} \times J_{sc}}{s \times p_{in}}, \quad (4)$$

where "s" is the area of dye-sensitive solar cell [22].

Figure 1 shows the electrical density ( $j$ - $v$ ) curve of a dye-sensitive solar module based on zinc oxide nanoparticles at various light intensities (a, b). DSSC variables like open voltage ( $V_{oc}$ ), shorter-circuit current density ( $J_{sc}$ ), fill factor ( $ff$ ), and efficiency ( $n$ ) were determined from the  $j$ - $v$  curves



(a)



(b)

FIGURE 4: UV-visible absorbance spectra of the prepared ZnO NPs at (a) onion extraction and (b) cabbage, carrot, and tomato extractions.

TABLE 2: Energy bandgap of the prepared ZnO NPs extracted from onion, cabbage, carrot, and tomato.

Extracted sample	Maximum wavelength	Energy bandgap
Onion	375 nm	3.31 eV
Cabbage	310 nm	4.01 eV
Carrot	338 nm	3.68 eV
Tomato	343 nm	3.62 eV

using Equations (3) and (4). Table 1 shows the computed values for the DSSC parameters [23–33].

When compared to research having comparable ZnO nanoparticle architectures in the literature, it was discovered that the ZnO-based DSSC made  $n$  percent quite good [22]. The immersion duration of ZnO NPs together into sensitizing dye had been demonstrated to be an important factor in the solar cell properties of the ZnO-based DSSC [34]. When compared to similar research [12–15], the manufactured ZnO-based DSSC showed better performance in a lesser

TABLE 3: Performance parameter of DSSC by the extracted ZnO NPs through green synthesizing methods.

Extracted sample	$J_{sc}$ ( $A\ cm^{-2}$ )	$V_{oc}$ (V)	$J_{max}$ ( $A\ cm^{-2}$ )	$V_{max}$ (V)	$ff$	$n\%$
Onion	$6.22 \times 10^{-5}$	0.38	$3.20 \times 10^{-5}$	0.26	0.38	0.0055
Cabbage	$8.43 \times 10^{-5}$	0.22	$4.21 \times 10^{-5}$	0.19	0.34	0.0069
Carrot	$2.99 \times 10^{-4}$	0.37	$3.01 \times 10^{-4}$	0.30	0.70	0.080
Tomato	$6.01 \times 10^{-4}$	0.36	$0.40 \times 10^{-4}$	0.28	0.61	0.122

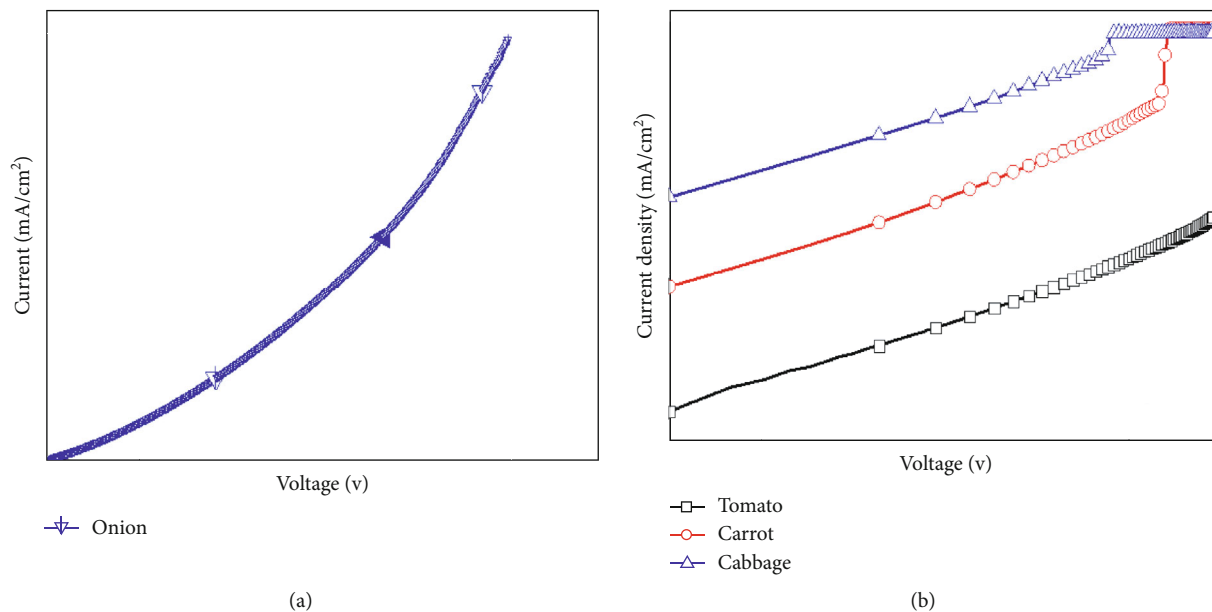


FIGURE 5: Current versus voltage curves of green synthesized ZnO NPs by (a) onion extract and (b) cabbage, carrot, and tomato extracts.

period of sinking time [35–44]. The enhanced absorption due to the larger amount and the better performance can also be expressed by the dye molecules that have been adsorbed onto the ZnO surface which can also express the better performance. As a result of the simplicity of the approach and the ease with which the specimens can be generated, through utilization of ZnO nanoparticles in photovoltaics seems to hold long-term prospects. The current density was discovered to be considerably lower. The photocurrent is the greatest significant parameter that defines the system's total performance limit. Then, because of their high surface area, parental substances act differently, and surface energy increases when the particle dimension is going towards that of a nanoscale [23, 24, 34]. The average crystallite dimensions of the ZnO nanoparticles were generated to be within 15 nm and 20 nm. As a result, we can anticipate considerable photochemical characteristics. A low hardness factor, reflection or dispersion, minimal injection performance, and charge collecting efficiency can all contribute to a low [16–18]. As the light intensity rose, the short-circuit voltage output grew progressive to near-saturation levels. Increased photogenerated excitons were linked to the linear increase in  $J_{sc}$  [20–22, 34, 45]. As a result, at greater light intensities, larger electron densities were transmitted to ZnO. Table 3 shows that “ $n$ ” and “ $J_{sc}$ ” readings improved even as applied light density has improved. The

improvement in charge generation is a result of an elevation in light intensity. Comparable outcomes had previously been reported for ZnO-based DSSC materials [19, 20, 45]. These findings reveal that increasing the intensity of illumination to  $100\ mW\ cm^{-2}$  has no effect on transport, injection, or recombination mechanisms as shown in Figure 5.

#### 4. Conclusion

ZnO NPs were completely synthesized through simple and eco-friendly vegetable-mediated green synthesizing technique from onion, cabbage, carrot, and tomato fruit extraction. FTIR, XRD, SEM, and UV-visible spectroscopy were accustomed to characterize the produced nanopowders. The crystal structures of synthesized ZnO NPs were with particle sizes where observed from XDR results. According to Scherrer's equation, the produced ZnO NPs have a single-phase hexagonal geometry having mean particle sizes of 17 nm, 18 nm, 24 nm, and 15 nm. Small agglomeration of the extracted nanoparticles was observed from SEM results. Because extract capping agents are poisonous, they were not employed to minimize the clustering; nonetheless, the vegetable retrieving itself would work as a diminishing agent or a capping agent depending on the situation. As a result, the green synthesizing process is more cost-effective and environmentally friendly than conventional ways for

producing ZnO NPs. The ZnO NP UV-visible spectroscopy revealed a large surface plasmon resonance absorption spike of the dye-sensitive solar cell based on ZnO NPs was effectively manufactured, and its performance was studied using current density-voltage behaviour below the influence of artificial sunlight. Due to a significant enhancement in dye molecule absorption upon this surface of ZnO NPs, a significant rise in the performance of the produced DSSC can be attributed to this. As a result, the employment of the green produced ZnO nanoparticles in the construction of dye-sensitive solar cells is a simple and promising strategy for the future's well-being. ZnO nanoparticles can be used as intelligent weapons toward a wide range of drug-resistant microbes, as well as a capable antibiotic replacement.

### Data Availability

The data used to support the findings of this study are included within the article.

### Conflicts of Interest

The authors declare that there are no conflicts of interest

### References

- [1] H. Ahmad, K. Venugopal, K. Rajagopal et al., "Green synthesis and characterization of zinc oxide nanoparticles using Eucalyptus globules and their fungicidal ability against pathogenic fungi of apple orchards," *Biomolecules*, vol. 10, no. 3, p. 425, 2020.
- [2] O. J. Nava, C. A. Soto-Robles, C. M. Gómez-Gutiérrez et al., "Fruit peel extract mediated green synthesis of zinc oxide nanoparticles," *Journal of Molecular Structure*, vol. 1147, pp. 1–6, 2017.
- [3] S. Thakur, M. Shandilya, and G. Guleria, "Appraisal of antimicrobial zinc oxide nanoparticles through Cannabis Jatropha curcusa Alovera and Tinosporacordifolia leaves by green synthesis process," *Journal of Environmental Chemical Engineering*, vol. 9, no. 1, article 104882, 2021.
- [4] S. Faisal, H. Jan, S. A. Shah et al., "Green synthesis of zinc oxide (ZnO) nanoparticles using aqueous fruit extracts of Myristica fragrans: their characterizations and biological and environmental applications," *ACS Omega*, vol. 30, pp. 9709–9722, 2021.
- [5] L. A. Kolahalam, K. R. Prasad, P. M. Krishna, and N. Supraja, "Saussurea lappa plant rhizome extract-based zinc oxide nanoparticles: synthesis, characterization and its antibacterial, anti-fungal activities and cytotoxic studies against Chinese Hamster Ovary (CHO) cell lines," *Heliyon*, vol. 7, no. 6, article e07265, 2021.
- [6] K. M. Ezealisiji, X. Siwe-Noundou, B. Maduelosi, N. Nwachukwu, and R. W. M. Krause, "Green synthesis of zinc oxide nanoparticles using Solanum torvum (L) leaf extract and evaluation of the toxicological profile of the ZnO nanoparticles–hydrogel composite in Wistar albino rats," *International Nano Letters*, vol. 9, no. 2, pp. 99–107, 2019.
- [7] B. Bekele, L. T. Jule, and A. Saka, "The effects of annealing temperature on size, shape, structure and optical properties of synthesized zinc oxide nanoparticles by sol-gel methods," *Digest Journal of Nanomaterials & Biostructures*, vol. 16, no. 2, 2021.
- [8] L. T. Jule, R. Krishnaraj, B. Bekele, A. Saka, and N. Nagaprasad, "Experimental investigation on the impacts of annealing temperatures on titanium dioxide nanoparticles structure, size and optical properties synthesized through sol-gel methods," *Materials Today: Proceedings*, vol. 45, pp. 5752–5758, 2021.
- [9] A. Belay, B. Bekele, and A. C. Reddy, "Effects of temperature and polyvinyl alcohol concentrations in the synthesis of zinc oxide nanoparticles," *Digest Journal of Nanomaterials & Biostructures*, vol. 14, no. 1, 2019.
- [10] Q. Tang, H. Xia, W. Liang, X. Huo, and X. Wei, "Synthesis and characterization of zinc oxide nanoparticles from *Morus nigra* and its anticancer activity of AGS gastric cancer cells," *Journal of Photochemistry and Photobiology B: Biology*, vol. 202, article 111698, 2020.
- [11] D. Rehana, D. Mahendiran, R. S. Kumar, and A. K. Rahiman, "Evaluation of antioxidant and anticancer activity of copper oxide nanoparticles synthesized using medicinally important plant extracts," *Biomedicine & Pharmacotherapy*, vol. 89, pp. 1067–1077, 2017.
- [12] K. Ali, S. Dwivedi, A. Azam et al., "Aloe vera extract functionalized zinc oxide nanoparticles as nanoantibiotics against multi-drug resistant clinical bacterial isolates," *Journal of Colloid and Interface Science*, vol. 472, pp. 145–156, 2016.
- [13] G. Pal, P. Rai, and A. Pandey, "Green synthesis of nanoparticles: a greener approach for a cleaner future," *Green Synthesis, Characterization and Applications of Nanoparticles*, vol. 548, pp. 1–26, 2019.
- [14] S. Sarkar and R. Sarkar, "Synthesis, characterization and tribological study of zinc oxide nanoparticles," *Materials Today: Proceedings*, vol. 44, pp. 3606–3612, 2021.
- [15] R. Verma, S. Pathak, A. K. Srivastava, S. Praver, and S. Tomljenovic-Hanic, "ZnO nanomaterials: green synthesis, toxicity evaluation and new insights in biomedical applications," *Journal of Alloys and Compounds*, vol. 876, article 160175, 2021.
- [16] S. C. Ezike, C. N. Hyelnasinyi, M. A. Salawu, J. F. Wansah, A. N. Ossai, and N. N. Agu, "Synergistic effect of chlorophyll and anthocyanin co-sensitizers in TiO<sub>2</sub>-based dye-sensitized solar cells," *Surfaces and Interfaces*, vol. 22, article 100882, 2021.
- [17] B. Sahin, S. Soylu, M. Kara, M. Turkmen, R. Aydin, and H. Cetin, "Superior antibacterial activity against seed-borne plant bacterial disease agents and enhanced physical properties of novel green synthesized nanostructured ZnO using Thymra spicata plant extract," *Ceramics International*, vol. 47, no. 1, pp. 341–350, 2021.
- [18] M. Amde, Z. Q. Tan, R. Liu, and J. F. Liu, "Nanofluid of zinc oxide nanoparticles in ionic liquid for single drop liquid microextraction of fungicides in environmental waters prior to high performance liquid chromatographic analysis," *Journal of Chromatography A*, vol. 1395, pp. 7–15, 2015.
- [19] S. Alamdari, M. Sasani Ghamsari, C. Lee et al., "Preparation and characterization of zinc oxide nanoparticles using leaf extract of Sambucus ebulus," *Applied Sciences*, vol. 10, no. 10, article 3620, 2020.
- [20] A. T. Babu and R. Antony, "Green synthesis of silver doped nano metal oxides of zinc & copper for antibacterial properties, adsorption, catalytic hydrogenation & photodegradation of aromatics," *Journal of Environmental Chemical Engineering*, vol. 7, no. 1, article 102840, 2019.
- [21] A. Ali, S. Ambreen, Q. Maqbool et al., "Zinc impregnated cellulose nanocomposites: synthesis, characterization and



- applications,” *Journal of Physics and Chemistry of Solids*, vol. 98, pp. 174–182, 2016.
- [22] D. Ayodhya and G. Veerabhadram, “One-pot green synthesis, characterization, photocatalytic, sensing and antimicrobial studies of *Calotropis gigantea* leaf extract capped CdS NPs,” *Materials Science and Engineering: B*, vol. 225, pp. 33–44, 2017.
- [23] M. A. Ansari and S. M. M. Asiri, “Green synthesis, antimicrobial, antibiofilm and antitumor activities of superparamagnetic  $\gamma$ -Fe<sub>2</sub>O<sub>3</sub> NPs and their molecular docking study with cell wall mannoproteins and peptidoglycan,” *International Journal of Biological Macromolecules*, vol. 171, pp. 44–58, 2021.
- [24] M. Faizan, J. A. Bhat, C. Chen et al., “Zinc oxide nanoparticles (ZnO-NPs) induce salt tolerance by improving the antioxidant system and photosynthetic machinery in tomato,” *Plant Physiology and Biochemistry*, vol. 161, pp. 122–130, 2021.
- [25] L. Tesfaye Jule, K. Ramaswamy, N. Nagaprasad, V. Shanmugam, and V. Vignesh, “Design and analysis of serial drilled hole in composite material,” *Materials Today: Proceedings*, vol. 45, pp. 5759–5763, 2021.
- [26] T. Amuthan, N. Nagaprasad, R. Krishnaraj, V. Narasimharaj, B. Stalin, and V. Vignesh, “Experimental study of mechanical properties of AA6061 and AA7075 alloy joints using friction stir welding,” *Materials Today: Proceedings*, 2021.
- [27] S. Abel, L. Tesfaye, B. Bekele, N. Nagaprasad, and R. Krishnaraj, “Studying the effect of metallic precursor concentration on the structural, optical, and morphological properties of zinc sulfide thin films in photovoltaic cell applications,” *Advances in Materials Science and Engineering*, vol. 2021, Article ID 7443664, 6 pages, 2021.
- [28] L. Tesfaye, B. Bekele, A. Saka, N. Nagaprasad, K. Sivaramasundaram, and R. Krishnaraj, “Investigating spectroscopic and structural properties of Cr doped TiO<sub>2</sub> NPs synthesized through sol gel deposition technique,” *Tierärztliche Praxis*, vol. 41, pp. 860–872, 2021.
- [29] E. K. Subramaniam, M. Sakthivel, K. Kanthavel, R. Krishnaraj, M. G. Deepan Marudachalam, and R. Palani, “Overall resource effectiveness, cycle time reduction & capacity improvements,” *International Journal of Scientific and Engineering Research*, vol. 2, no. 8, pp. 1–5, 2011.
- [30] R. Sathiyamoorthy and R. Krishnaraj, “Optimization of cellular layout under dynamic demand environment by simulated annealing,” *International Journal of Scientific and Engineering Research*, vol. 3, no. 10, pp. 1–7, 2012.
- [31] V. M. M. Thilak, R. Krishnaraj, M. Sakthivel, K. Kanthavel, M. Marudachalam, and R. Palani, “Transient thermal and structural analysis of the rotor disc of disc brake,” *International Journal of Scientific and Engineering Research*, vol. 2, no. 8, pp. 2–5, 2011.
- [32] S. Varatharajan, R. Krishnaraj, M. Sakthivel, K. Kanthavel, M. G. Deepan Marudachalam, and R. Palani, “Design and analysis of single disc machine top and bottom cover,” *International Journal of Scientific and Engineering Research*, vol. 2, no. 8, pp. 1–6, 2011.
- [33] C. M. Balamurugan, R. Krishnaraj, M. Sakthivel, K. Kanthavel, D. Marudachalam, and R. Palani, “Computer aided modeling and optimization of crankshaft,” *International Journal of Scientific & Engineering Research*, vol. 2, no. 8, pp. 2–7, 2011.
- [34] T. Zahra, K. S. Ahmad, C. Zequine et al., “Electro-catalyst [ZrO<sub>2</sub>/ZnO/PdO]-NPs green functionalization: fabrication, characterization and water splitting potential assessment,” *International Journal of Hydrogen Energy*, vol. 46, no. 37, pp. 19347–19362, 2021.
- [35] M. Vyshakh, R. K. Raj, A. P. Sayooj, and M. Afzal, “Experimental investigation on aluminium gravity die casting,” *International Journal of Applied Environmental Sciences*, vol. 9, no. 2, pp. 213–222, 2014.
- [36] M. Deepu, R. K. Raj, D. Karthik, and N. M. Binoj, “Cycle time optimization of rubber floor mat die,” *International Journal of Applied Environmental Sciences*, vol. 9, no. 2, pp. 229–237, 2014.
- [37] V. S. Arun, R. Krishnaraj, M. N. Rohit, and V. Mohan, “Optimising rejection rate of laser diamond sawing using Taguchi method,” *International Journal of Applied Environmental Sciences*, vol. 9, no. 2, pp. 223–228, 2014.
- [38] R. Krishnaraj, “Investigation on the effect of thermo physical properties on heat and mass transfer—review,” *International Journal of Applied Environmental Sciences*, vol. 9, no. 4, pp. 1893–1900, 2014.
- [39] C. N. Anil Kumar, R. Krishnaraj, M. Sakthivel, and M. Arularasu, “Implementation of safety education program for material handling equipment in construction sites and its effectiveness analysis using T-test,” *International Journal of Applied Environmental Sciences*, vol. 8, no. 15, pp. 1961–1969, 2013.
- [40] L. T. Jule, R. Krishnaraj, N. Nagaprasad, B. Stalin, V. Vignesh, and T. Amuthan, “Evaluate the structural and thermal analysis of solid and cross drilled rotor by using finite element analysis,” *Materials Today: Proceedings*, 2021.
- [41] B. Kassa, J. Leta Tesfaye, B. Bulcha et al., “Effect of Manganese Ions on Spectroscopic and Insulating Properties of Aluminophosphate Glasses,” *Advances in Materials Science and Engineering*, vol. 2021, Article ID 6253069, 11 pages, 2021.
- [42] N. Nagaprasad, B. Stalin, V. Vignesh, M. Ravichandran, N. Rajini, and O. Ismail, “Effect of cellulosic filler loading on mechanical and thermal properties of date palm seed/vinyl ester composites,” *International Journal of Biological Macromolecules*, vol. 147, pp. 53–66, 2020.
- [43] N. Nagaprasad, B. Stalin, V. Vignesh, M. Ravichandran, N. Rajini, and O. Ismail, “Applicability of cellulosic-based Polyalthia longigolia seed filler reinforced vinyl ester biocomposites on tribological performance,” *Polymer Composites*, vol. 42, no. 2, pp. 791–804, 2020.
- [44] B. Stalin, N. Nagaprasad, V. Vignesh, and M. Ravichandran, “Evaluation of mechanical and thermal properties of tamarind seed filler reinforced vinyl ester composites,” *Journal of Vinyl and Additive Technology*, vol. 25, s2, pp. E114–E128, 2019.
- [45] Z. Moradi Alvand, H. R. Rajabi, A. Mirzaei, A. Masoumiasl, and H. Sadatfaraji, “Rapid and green synthesis of cadmium telluride quantum dots with low toxicity based on a plant-mediated approach after microwave and ultrasonic assisted extraction: synthesis, characterization, biological potentials and comparison study,” *Materials Science and Engineering: C*, vol. 98, pp. 535–544, 2019.

## Research Article

# Green Synthesis and Characterizations of Zinc Oxide (ZnO) Nanoparticles Using Aqueous Leaf Extracts of Coffee (*Coffea arabica*) and Its Application in Environmental Toxicity Reduction

Saka Abel,<sup>1</sup> Jule Leta Tesfaye,<sup>1,2</sup> R. Shanmugam,<sup>3</sup> L. Priyanka Dwarampudi,<sup>4</sup> Gudeta Lamessa,<sup>1</sup> N. Nagaprasad ,<sup>5</sup> Mekonen Benti,<sup>6</sup> and Ramaswamy Krishnaraj <sup>2,7</sup>

<sup>1</sup>Department of Physics, College of Natural and Computational Science, Dambi Dollo University, Ethiopia

<sup>2</sup>Centre for Excellence-Indigenous Knowledge, Innovative Technology Transfer and Entrepreneurship, Dambi Dollo University, Ethiopia

<sup>3</sup>TIFAC CORE HD, Department of Pharmacognosy, JSS Academy of Higher Education and Research, JSS College of Pharmacy Ooty, Tamil Nadu, India

<sup>4</sup>Department of Pharmacognosy, JSS Academy of Higher Education and Research, JSS College of Pharmacy Ooty, Tamil Nadu, India

<sup>5</sup>Department of Mechanical Engineering, ULTRA College of Engineering and Technology, Madurai, 625104 Tamil Nadu, India

<sup>6</sup>Department of Civics and Ethical Studies, College of Social Science and Humanities, Dambi Dollo University, Ethiopia

<sup>7</sup>Department of Mechanical Engineering, College of Engineering and Technology, Dambi Dollo University, Ethiopia

Correspondence should be addressed to Ramaswamy Krishnaraj; [prof.dr.krishnaraj@dadu.edu.et](mailto:prof.dr.krishnaraj@dadu.edu.et)

Received 3 July 2021; Accepted 22 July 2021; Published 18 August 2021

Academic Editor: Shanmugam Rajeshkumar

Copyright © 2021 Saka Abel et al. This is an open access article distributed under the Creative Commons Attribution License, which permits unrestricted use, distribution, and reproduction in any medium, provided the original work is properly cited.

A green deposition method of zinc oxide nanoparticles using coffee leaf extraction was successfully prepared. The use of these preparation techniques is accepted by many researchers because it is nonexpensive and simple and has no environmental impact during the operation. The determination and reduction of Zn ions to ZnO NPs were characterized by using a UV-visible spectroscope. The UV-visible spectroscopy result reveals that the large band gap energy is observed in the visible region at the wavelength of 300 nm. X-ray diffraction and SEM analysis confirm that the deposited nanoparticle is highly crystalline with (111), (222), and (100) planes and cubic shape structure. The coffee leaf extraction serves as a reducing agent for stability of the particle length, where its medicinal value outcome showed an important antibacteria of the pathogenic type which appeared on the wound. The present research deals with the green synthesis of ZnO NPs as well as its application in toxicity reduction.

## 1. Introduction

Nanotechnology is the greatest innovative research part in today's condensed material science which basically includes nanoparticles [1, 2]. Nanoparticles are types of materials with a 3D structure, changing in magnitude from 1 to 100 nanometers. This material contains lots or 100s of atoms (molecules) that comprise different forms such as crystal structure, spherical, tubes, and amorphous [3]. Nanoparticles of metals like zinc have exceptional optical properties and electrical and magnetic material goods that make them

broadly used in study and manufacturing events. Amongst the numerous behaviors of metal nanoparticles, the optical studies are more protuberant. The properties of metallic nanoparticles are because of occurrences called surface-plasmonic resonance. The applications of metal nanoparticles includes the following: their contribution in the area of electricity as well as thermal conductors, sensors, optical and electrochemical detectors, antibacterial materials, super paramagnetic materials [4, 5]. Mineral nanoparticles have numerous likely applications for medicinal imaging and illness cure, and they are used extensively for their diverse

features, such as in elevation availability, good ecofriendliness, their skill in drug transmission, and governor of medication statement [6]. A massive list of properties used in the biological synthesis of metal nanoparticles exists. Plant parts, algae, fungus, bacteria, and viruses are used in the biological synthesis of nanoparticles [7]. Herbal cuttings arranged from leaf, stalks, origins, floras, and pips of plants, because of differences in composites, have unlikely possessions on the quantity and physiognomies of created nanoparticles [8, 9]. Shrubberies have a great deal of ordinary reformative and steadying materials. Plants are broadly dispersed and simply available, and they are sources of various metabolites [10]. Actual phytochemicals in the manufacture of nanoparticles contain terpenes, flavonoids, ketones, aldehydes, and carboxylic acid [11].

Additionally, reducing agents like protein, enzymes, and others have a vital role in metallic nanoparticle creation by green plants [12]. The biosynthesis techniques grow nanoparticles of good surface morphology and clear size as related to some of other physicochemical synthesization techniques [13]. The biological growth of nanoparticles depends on the existence of enzymes as well as proteins included in their depositions. Nanoscience has numerous advantages in smart medicinal providing systems. In these schemes, the medicine is endangered and preserved from the location of the entrance to the nerve [14]. The coffee plant is a climber of one to seven meters long, and it has opposite-sided leaves with bulbous moods on both edges. The parts that are commercially used are the leaves, seeds, and stems. In Oromia, Ethiopia, the leaf of coffee is not functional and no studies were conducted, and they simply drop to the ground and lead to environmental toxicity. Using this leaf regardless of its seed incorporation reduces toxicity of the water, air, and environment [15].

Deposition of green nanoparticles from the leaf extract is simpler to use. It is nontoxic, and there is no contagion exposed to the surroundings. Additionally, it is better to be substituted with other techniques of synthesization of nanoparticles. Due to the above declared evidences about the medicinal ideals of the coffee plant, the present study brought a biomimetic approach for the green synthesis of ecofriendly zinc oxide nanoparticles from coffee leaves through UV-visible spectroscopic, scanning electron microscope, X-ray diffraction characterization, and photoluminescence spectral studies.

## 2. Materials and Methods

For the synthesization of nanoparticles cut from the coffee leaf, zinc-nitrate hexahydrate and triple distilled water were arranged. All important materials are cleaned by using nitric acid and additionally by deionized water, then dehydrated by keeping it in a rotisserie before the preparation of nanoparticles. The leaves of the coffee plant were gathered from Dambi Dollo town, Ethiopia.

## 3. Preparation of Extraction from Coffee Plant Leaves

The leaves of the coffee plant (Figure 1) are collected and washed by using warm water to eradicate dirt adverts. The



FIGURE 1: Coffee plant originally taken from Dambi Dollo town, Kellem Wollega, Oromia, Ethiopia.

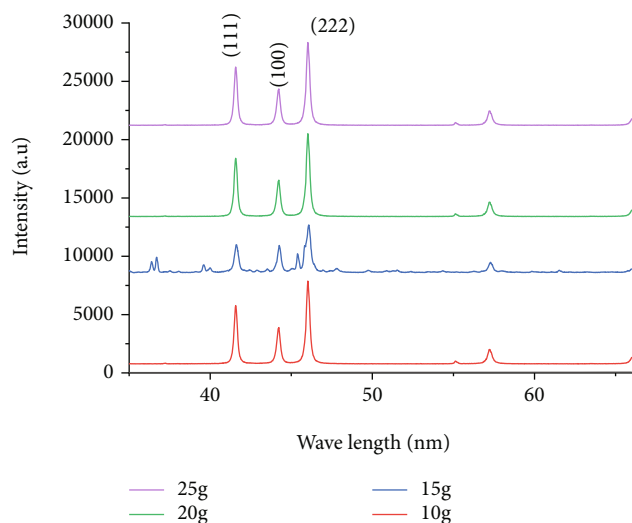


FIGURE 2: XRD patterns of ZnO nanoparticles from extract of coffee leaves.

leaves become dried in air after three weeks, since the season at which the present research was conducted was summer; after drying, the leaves were powdered by using a metal mortar and wood pestle till the ground very well. The extraction of coffee leaves was organized by alternatively changing the masses of prepared ZnO nanoparticles as 10 g, 15 g, 20 g, and 25 g of powder of coffee leaves which was put into 95 milliliters of distilled water at an adjusted temperature of 100°C for 30 min, and the pH value of the solution was measured to be 5. The solution was finally filtered and kept in a freezer at 7°C for further work.

## 4. Deposition of ZnO Nanoparticles from Coffee Leaf Extraction

The precursor basis for the zinc ion used in this study was zinc-nitrite hydroxide which was taken from shops from Finfinnee, Ethiopia. The elucidation of zinc-nitrite hydroxide was set in deionized water. For synthesization of ZnO

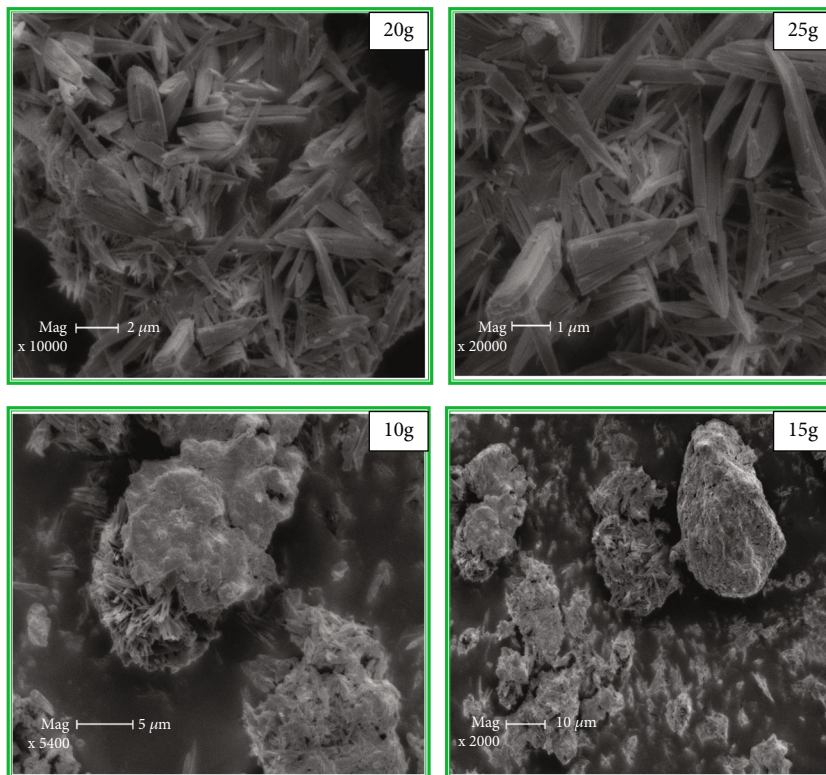


FIGURE 3: Scanning electron microscope analysis of ZnO nanoparticles at different masses of 10 g, 15 g, 20 g, and 25 g.

nanoparticles, the flask volume of 250 mL and the source of zinc (0.1 M) was mixed with 20 mL of the leaf extract of the coffee leaf and stimulated on a magnetic stirrer heated at 80° C, and the stirring was nonstop until a uniform solution was accomplished. The homogenous solution was dehydrated in a hot air oven at the temperature of 120-150°C for 120 min. Currently, the color of prepared nanoparticles is yellow and is crumpled in a metallic mortar-pestle to get a green preparation of ZnO nanoparticles.

## 5. Characterization Techniques

XRD (Shimadzu, 50 kilovolts and 20 milliamperes with Cu-K $\alpha$  radiation with wavelength or  $\lambda = 1.541 \text{ \AA}$ ) was cast off for crystal-structure examination. A Shimadzu ultraviolet-visible spectrophotometer was employed to assess the optical behaviors, and photoluminescence (PL) spectroscopy was also used to analyze the optical properties of the sample. Surface morphological study of the deposited nanoparticle was accompanied using scanning electron microscope (SEM) [15–17].

## 6. Analysis of Crystal Structure of ZnO Nanoparticle Extracts of Coffee Leaves

X-ray diffraction patterns of deposited ZnO NPs show that peaks observed agree with the ordinary data. The existing peaks of XRD (Figure 2) finely agreed with the cubic crystal structure [18]. The fitted sharp as well as peaks involving intensity in Figure 3 reveals that the nanoparticles are enor-

TABLE 1: Evaluation of calculated crystal size  $D$  (nm) from XRD results.

No.	2 theta (degree)	FWHM (radians)	$D$ (nm)
1	25.61	0.195	85.51
2	26.32	9.85	2.50
3	32.70	0.255	56.01
4	34.09	8.06	1.88

mously crystalline. The phase can be indexed for diffractions from the (222), (111), and (100) planes.

From the XRD graphing data, the peaks produced are extensive; the portentous crystallites have sizes in the nanometer range and the diameter was calculated using Scherrer's theories, given by

$$D = \frac{K\lambda}{\beta \cos \theta}, \quad (1)$$

whereas  $K$  is the Debye-Scherrer constant number,  $\lambda$  is the X-ray wavelength,  $\beta$  is the width of the peak of half maximum, and  $\theta$  is the diffraction position [19]. The calculated crystalline size of green synthesized is dignified by XRD obtained around 40 nanometers. The crystal size calculation of the ZnO nanoparticle is shortly discussed in Table 1.

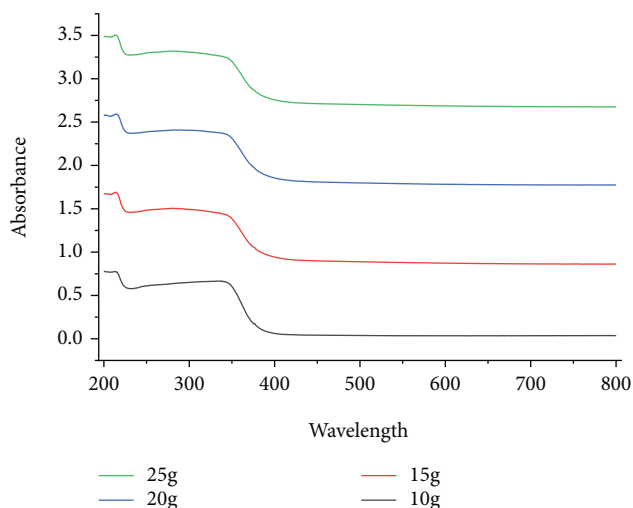


FIGURE 4: UV-visible of ZnO nanoparticles at different masses of 10 g, 15 g, 20 g, and 25 g.

## 7. Scanning-Electron Microscope (SEM) Analysis of ZnO Nanoparticles from Coffee Leaf Extract

Subsequently, the validation of X-ray diffraction outputs was further regulated for the surface morphology of scanning-electron-microscope characterization. The shape as well as crystal size and surface morphology of the ZnO nanoparticle are evidently shown by micrograph of a scanning electron microscope as shown in Figure 3.

Comprehensive structural analyses prove that the produced outputs are cubic shaped and crystal in a nice arrangement. The measured diameters were about 40 nm. Nanoparticles at 10 g and 15 g have an astounding shape and those at 20 g and 25 g are like fixing wood. Generally, the micrograph observed has no void and cracks, and this shows high crystallinity of the sample prepared. These results agree with what has been reported [20].

## 8. Ultraviolet (UV-Vis) Analysis of ZnO NPs from Coffee Leaf Extract

As demonstrated in Figure 4, the immersion spectrum of the equipped ZnO nanoparticles with the absorption peak is nearly 360 nm. It shows the ZnO nanoparticles' exposition, excitation, and absorption (at 360 nm) because of their big excitation binding energy at room temperature. The bands of zinc colloids were alleged at 360 nm, which reveals that the zinc ion is capably minimized by coffee leaf extraction. The appearance of the blue-shifted absorption spectrum with deference to the large value (300 nm) of the ZnO nanoparticles appropriate for the wavelength of the 300-nanometer fascination peak, due to the quantum captivity effect, which is in good agreement with the previously reported [21–23].

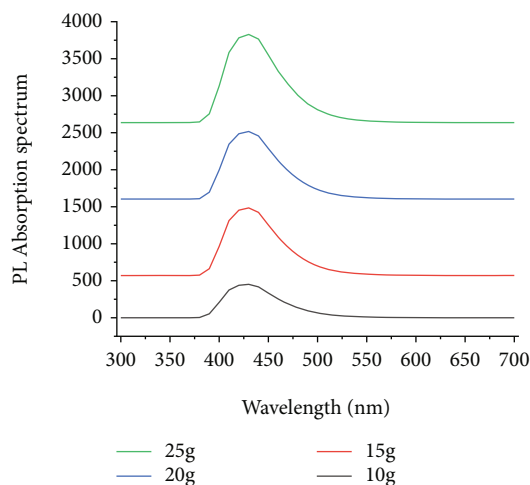


FIGURE 5: Photoluminescence spectra of ZnO NPs with different masses of 10 g, 15 g, 20 g, and 25 g.

## 9. Photoluminescence (PL) Spectral Analysis

Photoluminescent nanoparticles progress as dissimilarity or theranostic proxy assurances to make conceivable the inspection of a precise biological phenomenon as well as the action of diseases with a maximum degree of discernment. Consequently, novel nanoscale ingredients on condition of having higher finding limits, multimodal imaging modalities, and improved therapeutic effects are currently under study. This characterization technique is also used to analyze the optical emission properties of ZnO nanoparticles [24–32].

The PL behaviors of the deposited nanoparticles are shown in Figure 4. Based on the peaks of photoluminescence radiations, it was perceived that with addition of volume of nanoparticles of ZnO NPs, the intensity of photoluminescence peak was increasing with large area to volume rate for small-sized crystalline. This could be predictable to number of icons in the nanoparticles superficial fustily increases as crystal sizes decreases. Hence, the nanoparticles with a small crystal size can characterize the highest luminescence intensity related to the biggest crystal solid [24–29]. This could be predictable to number of ions in the nanoparticles superficial fustily increases as crystal size declines. Moreover, as shown in Figure 5, the trailer recombination rate rises as the size declines due to the increase in intersection between the electron (e<sup>-</sup>) and hole (P<sup>+</sup>) with increasing volume of ZnO NPs of 10 g, 15 g, 20 g, and 25 g [33–47].

## 10. Conclusion

The green synthesis method of ZnO NPs was efficaciously formed using the leaf of the coffee plant. The biological synthesis method used is meek, easily biodegradable, and prepared in a short period of time. The existing yellow color shows the deposition of zinc oxide nanoparticles, which has

supplementarily long established the minimization of zinc ions in zinc oxide nanoparticles by using UV-Vis spectroscopy. The ultraviolet spectroscopic absorption records the highest peak at 300 nm, and PL analysis also confirmed this statement. X-ray diffraction and scanning electron microscope analysis show that the particle-prepared behavior was polycrystalline with no void cubic-shaped zinc oxide nanoparticles. Finally, very high-quality green-synthesized ZnO nanoparticles are obtained for medical application and toxicity reduction.

## Data Availability

The data used to support the findings of this study are included within the article.

## Disclosure

This study was performed as a part of the employment of the authors.

## Conflicts of Interest

The authors declare that there are no conflicts of interest.

## References

- [1] S. Faisal, H. Jan, S. Shah et al., “Green synthesis of zinc oxide (ZnO) nanoparticles using aqueous fruit extracts of *Myristica fragrans*: their characterizations and biological and environmental applications,” *ACS Omega*, vol. 6, no. 14, pp. 9709–9722, 2021.
- [2] A. Jayachandran, A. TR, and A. S. Nair, “Green synthesis and characterization of zinc oxide nanoparticles using *Cayratia pedata* leaf extract,” *Biochemistry and Biophysics Reports*, vol. 26, article 100995, 2021.
- [3] R. A. Gonçalves, R. P. Toledo, N. Joshi, and O. M. Berengue, “Green synthesis and applications of ZnO and TiO<sub>2</sub> nanostructures,” *Molecules*, vol. 26, no. 8, p. 2236, 2021.
- [4] M. C. Patino-Portela, P. A. Arciniegas-Grijalba, L. P. Mosquera-Sanchez et al., “Effect of method of synthesis on antifungal ability of ZnO nanoparticles: chemical route vs green route,” *Advances in nano research*, vol. 10, no. 2, pp. 191–210, 2021.
- [5] S. Awan, K. Shahzadi, S. Javad, A. Tariq, A. Ahmad, and S. Ilyas, “A preliminary study of influence of zinc oxide nanoparticles on growth parameters of *Brassica oleracea var italica*,” *Journal of the Saudi Society of Agricultural Sciences*, vol. 20, no. 1, pp. 18–24, 2021.
- [6] M. S. E. D. Salem, A. Y. Mahfouz, and R. M. Fathy, “The antibacterial and antihemolytic activities assessment of zinc oxide nanoparticles synthesized using plant extracts and gamma irradiation against the uro-pathogenic multidrug resistant *Proteus vulgaris*,” *Biometals*, vol. 34, no. 1, pp. 175–196, 2021.
- [7] R. Hamouda and M. Elshamy, “Using biosynthesized zinc oxide nanoparticles to alleviate the toxicity on banana parasitic-nematode,” *Research*, vol. 67, article 271, 2021.
- [8] M. Raafat, A. S. A. el-Sayed, and M. T. el-Sayed, “Biosynthesis and anti-mycotoxigenic activity of *Zingiber officinale* roscoe-derived metal nanoparticles,” *Molecules*, vol. 26, no. 8, p. 2290, 2021.
- [9] A. Naseer, A. Ali, S. Ali et al., “Biogenic and eco-benign synthesis of platinum nanoparticles (Pt NPs) using plants aqueous extracts and biological derivatives: environmental, biological and catalytic applications,” *Journal of Materials Research and Technology*, vol. 9, no. 4, pp. 9093–9107, 2020.
- [10] M. Asemami and N. Anarjan, “Green synthesis of copper oxide nanoparticles using *Juglans regia* leaf extract and assessment of their physico-chemical and biological properties,” *Green Processing and Synthesis*, vol. 8, no. 1, pp. 557–567, 2019.
- [11] S. Ahmad, S. Munir, N. Zeb et al., “Green nanotechnology: a review on green synthesis of silver nanoparticles — an eco-friendly approach,” *International Journal of Nanomedicine*, vol. 14, pp. 5087–5107, 2019.
- [12] R. Abbasian and H. Jafarizadeh-Malmiri, “Green approach in gold, silver and selenium nanoparticles using coffee bean extract,” *Open Agriculture*, vol. 5, no. 1, pp. 761–767, 2020.
- [13] S. Sarli, M. R. Kalani, and A. Moradi, “A Potent and Safer Anti-cancer and Antibacterial *Taxus*-Based Green Synthesized Silver Nanoparticle,” *International Journal of Nanomedicine*, vol. 15, pp. 3791–3801, 2020.
- [14] M. S. Jameel, A. A. Aziz, and M. A. Dheyab, “Green synthesis: proposed mechanism and factors influencing the synthesis of platinum nanoparticles,” *Green Processing and Synthesis*, vol. 9, no. 1, pp. 386–398, 2020.
- [15] A. Banerjee, A. Sarkar, K. Acharya, and N. Chakraborty, “Nanotechnology: an emerging hope in crop improvement,” *Letters in Applied NanoBioScience*, vol. 10, no. 4, pp. 2784–2803, 2021.
- [16] S. Painuli, P. Semwal, A. Bachheti, R. K. Bachheti, and A. Husen, “Nanomaterials from non-wood forest products and their applications,” *Nanomaterials for Agriculture and Forestry Applications*, vol. 33, pp. 15–40, 2020.
- [17] J. Devasia, B. Muniswamy, and M. K. Mishra, “Investigation of ZnO nanoparticles on in vitro cultures of coffee (*Coffea Arabica* L.),” *International Journal of Nanoscience and Nanotechnology*, vol. 16, no. 4, pp. 271–277, 2020.
- [18] W. J. Keijok, R. H. A. Pereira, L. A. C. Alvarez et al., “Controlled biosynthesis of gold nanoparticles with *Coffea arabica* using factorial design,” *Scientific Reports*, vol. 9, no. 1, article 52496, pp. 16019–16110, 2019.
- [19] L. Rossi, L. N. Fedenia, H. Sharifan, X. Ma, and L. Lombardini, “Effects of foliar application of zinc sulfate and zinc nanoparticles in coffee (*Coffea arabica* L.) plants,” *Plant Physiology and Biochemistry*, vol. 135, pp. 160–166, 2019.
- [20] J. I. García-López, G. Niño-Medina, E. Olivares-Sáenz et al., “Foliar application of zinc oxide nanoparticles and zinc sulfate boosts the content of bioactive compounds in habanero peppers,” *Plants*, vol. 8, no. 8, p. 254, 2019.
- [21] L. P. Mosquera-Sánchez, P. A. Arciniegas-Grijalba, M. C. Patiño-Portela, B. E. Guerra-Sierra, J. E. Muñoz-Florez, and J. E. Rodríguez-Páez, “Antifungal effect of zinc oxide nanoparticles (ZnO-NPs) on *Colletotrichum* sp., causal agent of anthracnose in coffee crops,” *Biocatalysis and Agricultural Biotechnology*, vol. 25, article 101579, 2020.
- [22] A. Bakir, S. Hamimed, A. Landoulsi, and A. Chatti, “Biogenic Zinc Oxide Nano-Structures Differentiation under Musical Sounds,” 2021.
- [23] S. Nurman, R. Yulia, I. Irmayanti, E. Noor, and T. Candra Sunarti, “Optimizing anti-inflammatory activities of Arabica coffee ground (*Coffea arabica* L.) nanoparticle Gel,” *Journal of Natural Pharmaceutical Products*, vol. 16, no. 2, pp. 1–9, 2021.

- [24] R. Pavelkova, P. Matouskova, J. Hoova, J. Porizka, and I. Marova, "Preparation and characterisation of organic UV filters based on combined PHB/liposomes with natural phenolic compounds," *Journal of Biotechnology*, vol. 324, article 100021, 2020.
- [25] T. Desalegn, C. R. Ravikumar, and H. C. A. Murthy, "Eco-friendly synthesis of silver nanostructures using medicinal plant *Vernonia amygdalina* Del. leaf extract for multifunctional applications," *Applied Nanoscience*, vol. 11, no. 2, pp. 535–551, 2021.
- [26] C. Song, M. Huang, J. C. White et al., "Metabolic profile and physiological response of cucumber foliar exposed to engineered MoS<sub>2</sub> and TiO<sub>2</sub> nanoparticles," *NanoImpact*, vol. 20, article 100271, 2020.
- [27] M. Baghaienezhad, M. Boroghani, and R. Anabestani, "Silver nanoparticles synthesis by coffee residues extract and their antibacterial activity," *Nanomedicine Research Journal*, vol. 5, pp. 29–34, 2020.
- [28] M. M. Cohen, "Tulsi - *Ocimum sanctum*: a herb for all reasons," *Journal of Ayurveda and integrative medicine*, vol. 5, no. 4, article 146554, pp. 251–259, 2014.
- [29] S. Abel, J. Leta Tesfaye, R. Kiran et al., "Studying the effect of metallic precursor concentration on the structural, optical, and morphological properties of zinc sulfide thin films in photovoltaic cell applications," *Advances in Materials Science and Engineering*, vol. 2021, Article ID 7443664, 6 pages, 2021.
- [30] L. Tesfaye, B. Bekele, A. Saka, N. Nagaprasad, and K. Sivaramasundaram, "Investigating spectroscopic and structural properties of Cr doped TiO<sub>2</sub> NPs synthesized through sol gel deposition technique," *Tierarztliche Prax.*, vol. 41, pp. 860–872, 2021.
- [31] L. Tesfaye Jule, K. Ramaswamy, N. Nagaprasad, V. Shanmugam, and V. Vignesh, "Design and analysis of serial drilled hole in composite material," *Materials Today: Proceedings*, vol. 45, pp. 5759–5763, 2021.
- [32] L. Tesfaye Jule, K. Ramaswamy, B. Bekele, A. Saka, and N. Nagaprasad, "Experimental investigation on the impacts of annealing temperatures on titanium dioxide nanoparticles structure, size and optical properties synthesized through sol-gel methods," *Materials Today: Proceedings*, vol. 45, pp. 5752–5758, 2021.
- [33] T. Amuthan, N. Nagaprasad, R. Krishnaraj, V. Narasimharaj, B. Stalin, and V. Vignesh, "Experimental study of mechanical properties of AA6061 and AA7075 alloy joints using friction stir welding," *Materials Today: Proceedings*, vol. 46, 2021.
- [34] E. K. Subramaniam, M. Sakthivel, K. Kanthavel, R. Krishnaraj, and R. Palani, "Overall resource effectiveness, cycle time reduction & capacity improvements," *International Journal of Scientific and Engineering Research*, vol. 2, no. 8, pp. 1–5, 2011.
- [35] P. Dharmalingam, K. Kanthavel, R. Sathiyamoorthy, M. Sakthivel, R. Krishnaraj, and C. Elango, "Optimization of cellular layout under dynamic demand environment by simulated annealing," *International Journal of Scientific and Engineering Research*, vol. 3, no. 10, pp. 1–7, 2012.
- [36] V. M. M. Thilak, R. Krishnaraj, M. Sakthivel, K. Kanthavel, M. Marudachalam, and R. Palani, "Transient thermal and structural analysis of the rotor disc of disc brake," *International Journal of Scientific and Engineering Research*, vol. 2, no. 8, pp. 2–5, 2011.
- [37] S. Varatharajan, R. Krishnaraj, M. Sakthivel, K. Kanthavel, and R. Palani, "Design and analysis of single disc machine top and bottom cover," *International Journal of Scientific and Engineering Research*, vol. 2, no. 8, pp. 1–6, 2011.
- [38] C. M. Balamurugan, R. Krishnaraj, M. Sakthivel, K. Kanthavel, D. Marudachalam, and R. Palani, "Computer aided modeling and optimization of crankshaft," *International Journal of Scientific and Engineering Research*, vol. 2, no. 8, pp. 2–7, 2011.
- [39] M. Vyshakh, R. K. Raj, A. P. Sayooj, and M. Afzal, "Experimental investigation on aluminium gravity die casting," *International Journal of Applied Environmental Sciences*, vol. 9, no. 2, pp. 213–222, 2014.
- [40] M. Deepu, R. K. Raj, D. Karthik, and N. M. Binoj, "Cycle time optimization of rubber floor mat die," *International Journal of Applied Environmental Sciences*, vol. 9, no. 2, pp. 229–237, 2014.
- [41] V. S. Arun, R. Krishnaraj, M. N. Rohit, and V. Mohan, "Optimising rejection rate of laser diamond sawing using Taguchi method," *International Journal of Applied Environmental Sciences*, vol. 9, no. 2, pp. 223–228, 2014.
- [42] M. Dakshinamoorthy, M. B. K. Moorthy, M. Sakthivel, R. Krishnaraj, and N. Rajkumar, "Investigation on the effect of thermo physical properties on heat and mass transfer – review," *International Journal of Applied Environmental Sciences*, vol. 9, no. 4, pp. 1893–1900, 2014.
- [43] C. N. A. Kumar, R. Krishnaraj, M. Sakthivel, and M. Arularasu, "Implementation of safety education program for material handling equipment in construction sites and its effectiveness analysis using T-test," *International Journal of Applied Environmental Sciences*, vol. 8, no. 15, pp. 1961–1969, 2013.
- [44] L. T. Jule, R. Krishnaraj, N. Nagaprasad, B. Stalin, V. Vignesh, and T. Amuthan, "Evaluate the structural and thermal analysis of solid and cross drilled rotor by using finite element analysis," *Materials Today: Proceedings*, vol. 47, 2021.
- [45] N. Nagaraj, S. Balasubramaniam, V. Venkataraman, R. Manickam, R. Nagarajan, and I. Sikiru Oluwarotimi, "Effect of cellulosic filler loading on mechanical and thermal properties of date palm seed/vinyl ester composites," *International Journal of Biological Macromolecules*, vol. 147, pp. 53–66, 2020.
- [46] N. Nagaprasad, B. Stalin, V. Vignesh, M. Ravichandran, N. Rajini, and O. Ismail, "Applicability of cellulosic-based *Polyalthia longigolia* seed filler reinforced vinyl ester biocomposites on tribological performance," *Polymer Composites*, vol. 42, no. 2, pp. 791–804, 2021.
- [47] B. Kassa, J. Leta Tesfaye, B. Bulcha et al., "Effect of Manganese Ions on Spectroscopic and Insulating Properties of Alumino-phosphate Glasses," *Advances in Materials Science and Engineering*, vol. 2021, Article ID 6253069, 11 pages, 2021.

## Research Article

# Anticariogenic Effect of Selenium Nanoparticles Synthesized Using *Brassica oleracea*

Ganapathy Dhanraj<sup>1</sup> and Shanmugam Rajeshkumar<sup>2</sup>

<sup>1</sup>Department of Prosthodontics, Saveetha Dental College, Saveetha Institute of Medical and Technical Sciences, Chennai 600 077, India

<sup>2</sup>Department of Pharmacology, Saveetha Dental College, Saveetha Institute of Medical and Technical Sciences, Chennai 600 077, India

Correspondence should be addressed to Shanmugam Rajeshkumar; [ssrajeshkumar@hotmail.com](mailto:ssrajeshkumar@hotmail.com)

Received 20 April 2021; Revised 16 June 2021; Accepted 24 June 2021; Published 10 July 2021

Academic Editor: Abdelwahab Omri

Copyright © 2021 Dhanraj Ganapathy and Rajeshkumar Shanmugam. This is an open access article distributed under the Creative Commons Attribution License, which permits unrestricted use, distribution, and reproduction in any medium, provided the original work is properly cited.

Selenium is a trace element in the human body present in various enzymes with antioxidant activities and several functional proteins. This study is aimed at synthesizing selenium nanoparticles using *Brassica oleracea* (broccoli) and characterizing and assessing the antioxidant and antimicrobial effectiveness against cariogenic microorganisms. UV-visible spectrum displayed a peak at 370 nm which confirms the formation of SeNPs. TEM images of synthesized selenium nanoparticles showed polydisperse nanoparticles, spherical. The size of the particles ranged from 10 to 25 nm, and the average particle size obtained was  $15.2 \pm 1.9$  nm. SEM images of nanoparticles were spherical and ranged in size from 10 to 28 nm. The SeNPs showed effective antimicrobial activity against cariogenic pathogens. The SeNPs synthesized with *Brassica oleracea* extract can be incorporated in toothpaste, gums, and mouthwashes that are cost-effective and biocompatible and used for the prevention of dental caries.

## 1. Introduction

Owing to their characteristic attributes, nanoparticles find extensive implementation in several scientific, medicinal, and industrial domains [1, 2]. Among the various kinds of nanoparticles, selenium has attracted appreciable interest due to its greater bioactivity, protein interactions, strong absorption capability, and reduced toxicity, together with interdisciplinary applications in medicine, therapeutic sciences, nanobioinformatics, and nanobiotechnology [3].

Selenium corresponds to Group VI in the periodic table as an integral trace element. Numerous antioxidant enzymes and functional protein molecules contain selenium and maneuver a crucial role in mitigating oxidative stress, thus minimizing the damage in cardiovascular diseases, cancer, diabetes, and hypercholesterolemia. On the other hand, the intake of selenium is necessary for different metabolic processes and indiscriminate intake beyond acceptable concentration leads to selenium toxicity [4–6].

Selenium is found in nature as ionic forms of selenite ( $\text{Na}_2\text{SeO}_3$ ), selenate ( $\text{Na}_2\text{SeO}_4$ ), and selenium oxide ( $\text{SeO}$ ) among the other forms. Elemental selenium nanoparticles manifest lesser cytotoxicity compared with selenite ( $\text{SeO}_3$ ) and selenate compounds ( $\text{SeO}_4$ ) and show anticancer and several therapeutic properties that enable them to be utilized in versatile medicinal applications [7, 8]. Researchers have reported on the antioxidant function of SeNPs. SeNPs can unswervingly scavenge the free radicals in a size-dependent manner within the size ranging from 5 to 200 nm [9].

Traditional physiochemical methods of SeNP synthesizing are cumbersome, nonecological, and require prerequisites such as high temperatures, toxic substances, reagents, precursors, and complicated procedures. Besides, in the conventional process, the form, size, and instability of the synthesized particle are the main limitations [10]. This creates a great desire to synthesize nanoparticles with harnessed size and nanometer morphology in an eco-friendly mode [11]. The size and the shape of nanoparticles are permanently



related to the unique characteristics, work, and application of nanomaterials [12, 13]. Because of its eco-friendliness, low toxicity along with increased stability, small size, and shape distribution, emerging advances in nanoparticle generation using green syntheses are attracting much attention today [14, 15].

*Brassica oleracea* (broccoli) has all the nutrients that prove its exceptional health benefits, including vitamins, minerals, secondary metabolites, and fiber. The active principles for demonstrating medicinal properties are the breakdown products of sulfur-containing glucosinolates, phenolic isothiocyanates, antioxidants, vitamins, and dietary minerals. These bioactive compounds most likely mediate the medicinal properties of broccoli consumption by the inducement of a range of functions such as antioxidant behavior, enzyme regulation, and the control of apoptosis [16].

Organic chemicals such as S-methyl cysteine sulfoxide and glucosinolates present in *Brassica oleracea* in conjunction with other ingredients inclusive of vitamins C, K, and E and minerals like selenium, iron, and zinc and polyphenols such as kaempferol, glucosides of quercetin, and isorhamnetin are likely to be accountable for the various health benefits of broccoli [17, 18].

Concerning dental problems, caries is one of the most common human diseases characterized by susceptibility to enamel and dentin tissue damage due to acidic by-products generated from dietary carbohydrates owing to bacterial fermentation [19]. This problem is initiated by the acid production from bacteria that ferment carbohydrates resulting in demineralization of dental enamel and the development of caries. Supplementation of calcium and phosphate can aid in the rarefy demineralization of teeth to avoid dental caries. Such ions are also present in the saliva, and their concentration determines remineralization and demineralization [20, 21].

Nanocarriers are presently being reasoned for their application in dentistry, and their particular characteristics identify possible use in the delivery of antimicrobial agents in the prevention and management of oral diseases caused by microbial invasion. Implementation of nanomaterials in dentistry may be divided into two major categories: dental preventive and restorative care [22]. According to caries research, novel approaches to prevent and manage dental caries have been implemented through nanotechnology, in particular through plaque-related biofilm regulation and remineralization of carious lesions [23].

In this area, nanotechnological advances have also provided advantages as novel drivers of innovation. It has been shown that natural biomineralization, which is an integral repair mechanism, is induced by the use of nanotechnology. For enhancing oral health through the prevention of dental caries, the use of nanomaterials in toothpaste and other mouth rinsing solutions can be recommended. Caries is often arrested by nanomaterials used in polishing agents and dental restorative materials. Per se, antimicrobial nanoparticles can inhibit the growth of bacteria inducing dental caries [24].

Dental caries can be addressed by nanotechnology in two primary methods. In the first method, fluoride- and calcium-releasing nanomaterials such as calcium fluoride, calcium

phosphate, hydroxyapatite, and fluorohydroxyapatite are used in a process called remineralization. The second method is to imbibe antimicrobial nanomaterials such as selenium, platinum, quaternary ammonium compounds, and zinc oxide nanoparticles [25, 26]. To present better results, a blend of these two methods can also be used. The anticariogenic effects of selenium nanoparticles through inhibition of cariogenic microbes were not studied extensively and thus need to be explored further. Hence, this study was formulated with the aim to green synthesize selenium nanoparticles using *Brassica oleracea* and study its characterization and antioxidant and antimicrobial effectiveness against cariogenic microorganisms.

## 2. Material and Methods

**2.1. Preparation of Broccoli Extract.** *Brassica oleracea* was procured from organic farms in Poonamallee. Broccoli was washed thoroughly under tap water and made into small pieces to shade dry it for 3-4 days. After that, the shade-dried broccoli pieces were ground into a fine powder. From that, finely grounded broccoli powder 0.7 g was taken and added to 70 mL distilled water. The mixture was kept in a heating mantle at 60-80°C for 10 minutes. Then, the boiled mixture was filtered using Whatman No. 1 filter paper. The filtered broccoli extract was stored in the refrigerator for selenium nanoparticle synthesis.

**2.2. Preparation of Selenium Nanoparticle.** 30 mM of sodium selenite was prepared in 70 mL distilled water. To that 30 mL filtered broccoli, the extract was added and kept in a magnetic stirrer for 2-3 days at 650-800 rpm to obtain uniform dispersion, a mandatory condition in nanoparticle synthesis. The color changes in the reaction mixture were noted continuously using a double-beam UV-visible spectrophotometer at the different wavelength range from 250 to 650 nm. The synthesized broccoli extract-mediated selenium nanoparticles were centrifuged at 8000 rpm for 10 minutes. The obtained selenium nanoparticle pellet was powdered using a hot air oven at 70°C for 2 hours and preserved in airtight vials for further use.

**2.3. Characterization of Selenium Nanoparticles.** The maximum absorbance of broccoli-mediated selenium nanoparticles was measured by using a double-beam UV-vis spectrophotometer (UV-2450, Shimadzu) in the wavelength range of 250-650 nm. The morphological features such as size and shape were analyzed by TEM. The functional groups present in the synthesized selenium nanoparticles were identified by using FT-IR analysis and also subjected to test the elemental analysis using an energy-dispersive X-ray detector (EDX) attached to the SEM machine.

**2.3.1. Antioxidant Activity.** The DPPH assay was used to test the antioxidant activity of biogenic synthesized selenium nanoparticles. Diverse concentrations (2-10  $\mu\text{g/mL}$ ) of broccoli extract-interceded selenium nanoparticle were mixed with 1 mL of 0.1 mM DPPH in methanol and 450  $\mu\text{L}$  of 50 mM Tris HCl buffer (pH 7.4) and incubated for 30 minutes. Later, the reduction in the quantity of DPPH free

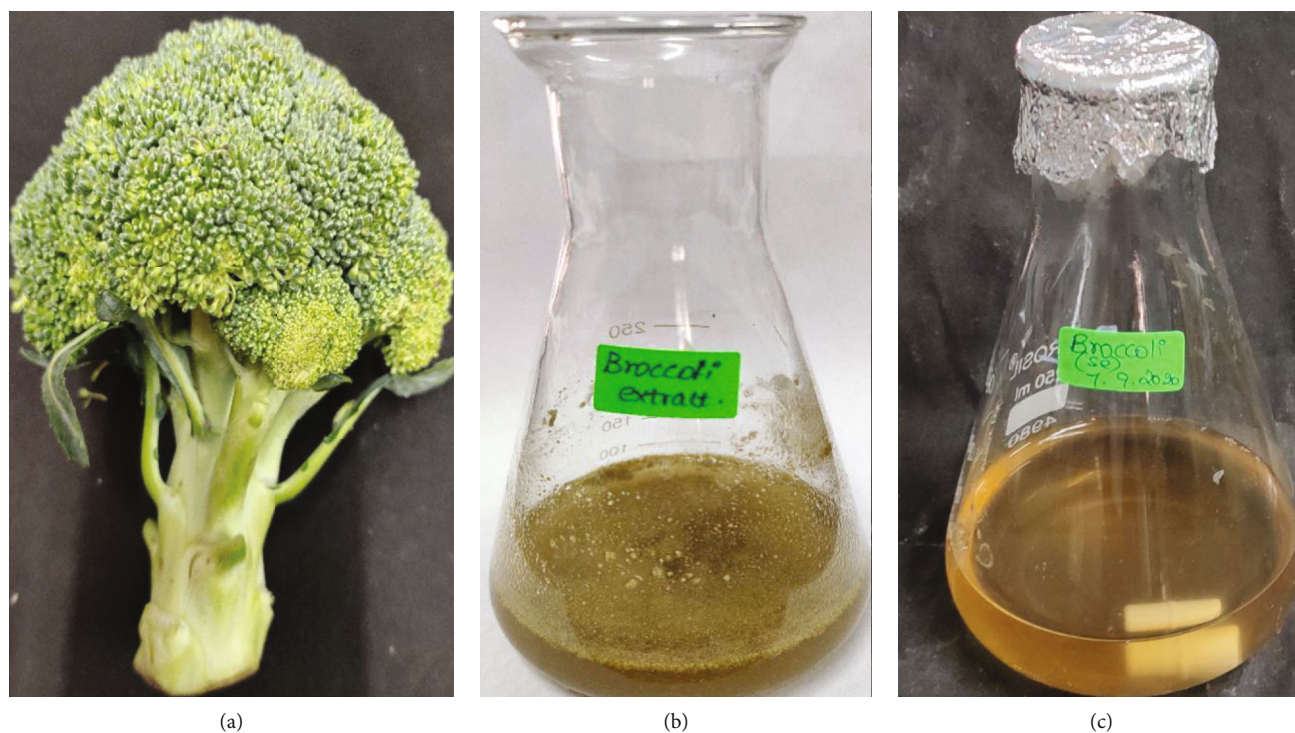


FIGURE 1: Color changes on selenium nanoparticles synthesis: (a) broccoli; (b) plant extract; (c) selenium nanoparticles.

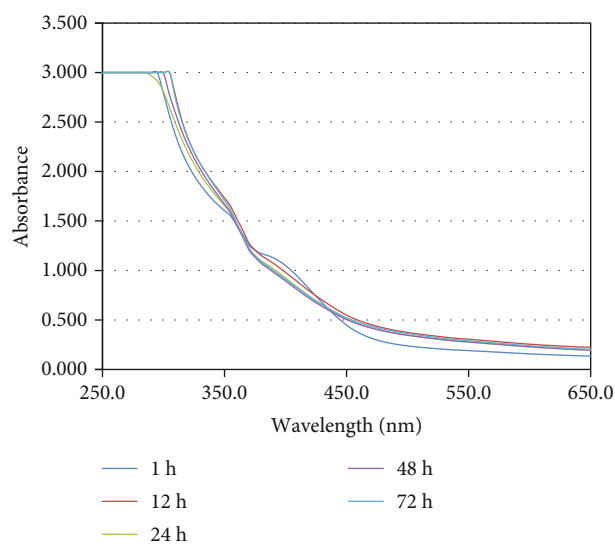


FIGURE 2: UV-vis spectroscopic analysis of broccoli-mediated selenium nanoparticles at different time intervals and wavelength is from 250 nm to 650 nm.

radicals was assessed depending on the absorbance at 517 nm. BHT was employed as control. The percentage of inhibition was determined from the following equation:

$$\% \text{inhibition} = \frac{\text{Absorbance of control} - \text{Absorbance of test sample}}{\text{Absorbance of control}} \times 100. \quad (1)$$

**2.3.2. Anticariogenic Activity.** The anticariogenic activity of broccoli-mediated selenium nanoparticles was tested against

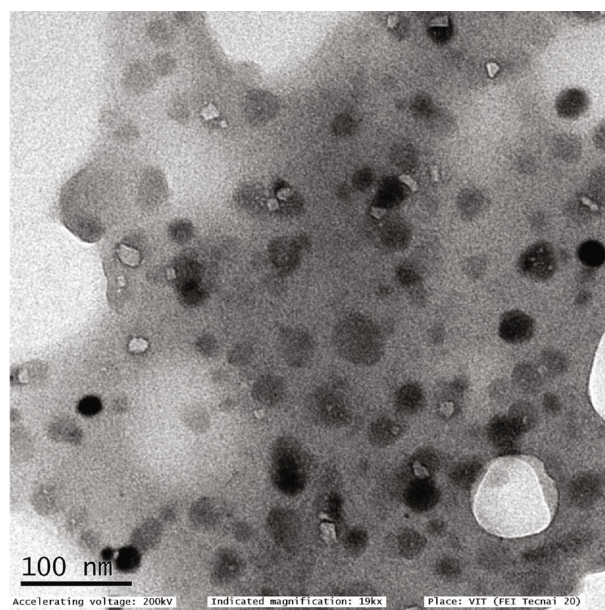


FIGURE 3: Transmission electron microscopic image of selenium nanoparticles synthesized using broccoli extract and scale measures at 100 nm.

oral pathogens such as *S. mutans*, *S. aureus*, *E. faecalis*, *Lactobacillus*, and *C. albicans*. Mueller Hinton agar was utilized for this activity to determine the zone of inhibition. Mueller Hinton agar was prepared and sterilized for 45 minutes at 120 lbs. Media were poured into the sterilized plates and let it stabilize for solidification. The wells were cut using the good cutter, and the test organisms were swabbed. The selenium

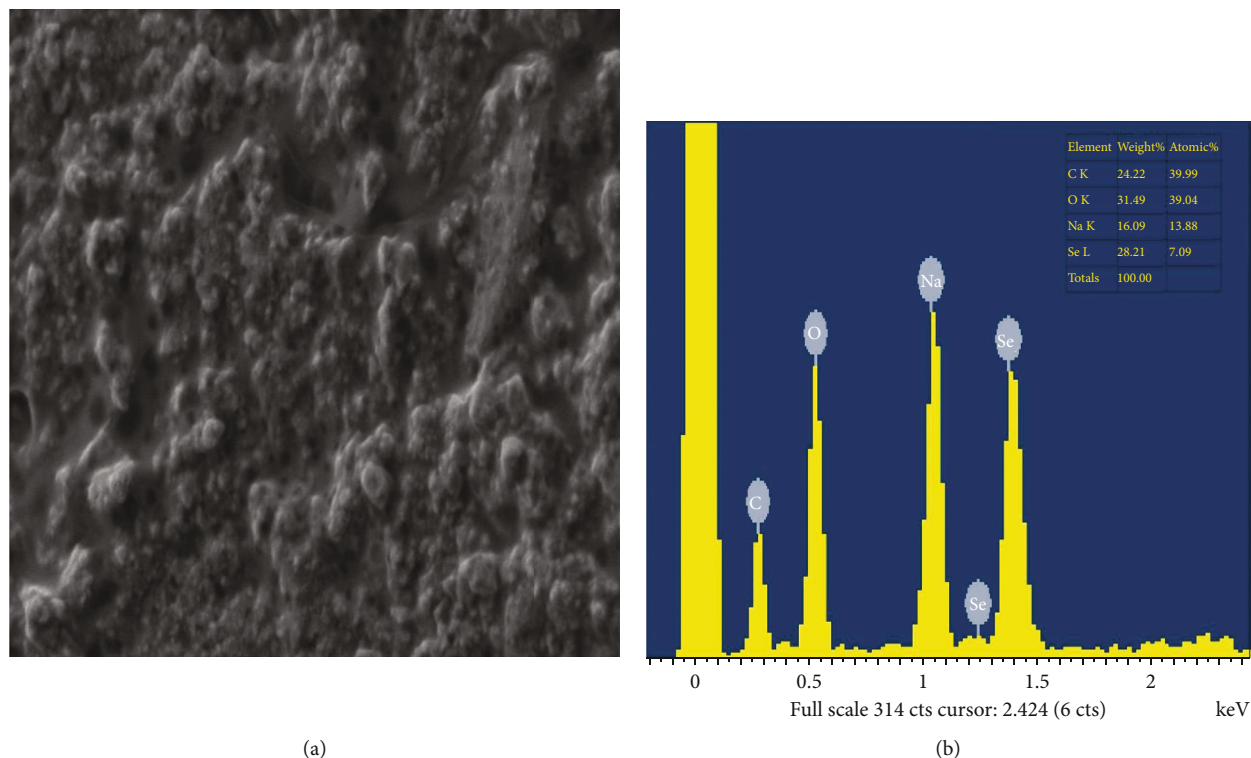


FIGURE 4: Selenium nanoparticles: (a) scanning electron microscopy image; (b) elemental X-ray diffraction spectrum.

nanoparticles with different concentrations were loaded, and the plates were incubated at 37°C for 24 hours. After the incubation time, the zone of inhibition was measured.

### 3. Results and Discussion

Compared to physical or chemical approaches of nanoparticle synthesis, one of the effective methods is the generation of nanoparticles utilizing green sources such as plant phyto-compounds, proteins, and enzymes as reducing agents in the case of microbes. The benefits are that they are nontoxic materials, requiring relatively less complicated and affordable equipment, biodegradable material processing, improved selectivity, and high yields.

Visual coloring is the first stage in the moulding of nanoparticles. It was observed following the incubation period that the color changed to brown. The reaction mixture with *Brassica oleracea* and sodium selenite during incubation showed a time-dependent color shift of 48 h at 30°C, as shown in Figure 1. At the primary reaction stage, the color of the concoction was yellow, which progressively changed to brown over time. After 48 hours of incubation, no further alteration in color was observed. This brown color may be attributed to the arousal of the surface plasmon vibrations by the selenium nanoparticles and thus render beneficial spectroscopic evidence of their formation.

UV-visible spectra have shown a large peak at 370 nm, supporting the formation of SeNPs [27]. The peak intensity increased over time. No further significant elevation in peak intensity was observed after 48 hours of the reaction. The

peak amplitude has increased over time because of the reduction of  $\text{SeO}_3^{2-}$  to  $\text{Se}^0$ . No further peak increase was observed after 48 h, suggesting a maximum conversion of  $\text{SeO}_3^{2-}$  to  $\text{Se}^0$  (Figure 2). Transmission electron microscopy (TEM) images of selenium nanoparticles synthesized in nutrient broth supplementation with 1.0 mM selenite at 72 hours of incubation are shown in Figure 3. The generated nanoparticles were polydisperse, shaped spherically; the particle size ranged from 10 to 25 nm, and the mean particle size that prevailed from the distribution of the corresponding diameter was approximately  $15.2 \pm 1.9$  nm (Figure 3).

Synthesized plant extracts, such as hydrogen bond and the electrostatic interaction, were present in the SEM image of SeNPs and were mounted on the surface because of the interaction with the bioorganic capping molecules attached to the SeNPs. Synthesized SeNPs with sizes ranging from 10.32 nm to 25.88 nm were observed (Figure 4(a)). SEM study of the synthesized SeNPs was easily distinguishable due to their size variation. The SEM picture showed the majority of nanoparticles are spherical in size, ranging from 10 to 25 nm, and uniformly distributed. SEM analysis of SeNPs was readily distinguishable due to the size difference of synthesized SeNPs. Elemental X-ray diffraction assay was used to assess the elemental percentage and presence; selenium nanoparticles synthesized with broccoli extract had an elemental presence of selenium with a 28.02 percent weight percentage and a 7.09 percent atomic percentage (Figure 4(b)).

FT-IR estimation was performed to determine the possible bands present in the biomolecules accountable for near capping peaks and effective stabilization of the metal NPs

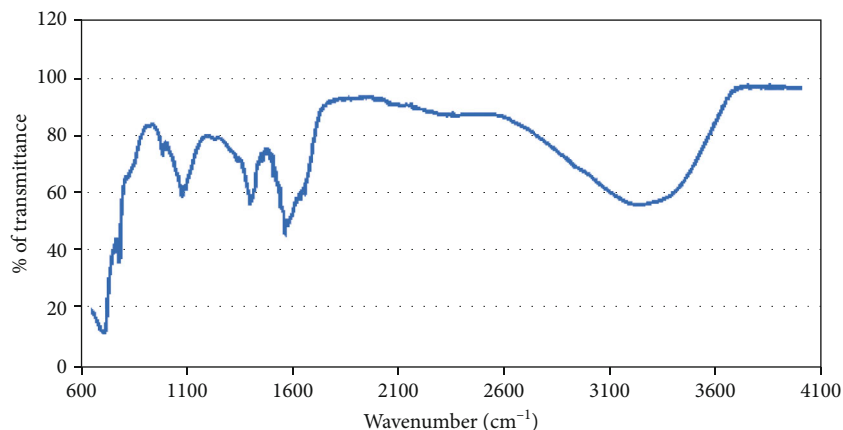


FIGURE 5: Fourier-transform infrared spectroscopy of selenium nanoparticles synthesized using broccoli aqueous extract.

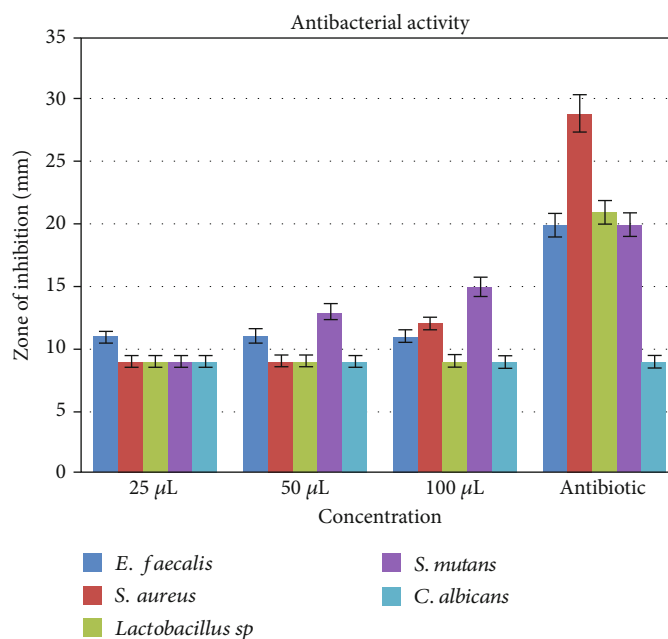


FIGURE 6: Anticariogenic activity against caries-causing microbes (*S. mutans*, *Lactobacillus sp.*, *E. faecalis*, *S. aureus*, and *C. albicans*) at different concentrations and zone of inhibition was measured in millimeter.

synthesized by broccoli extract. FT-IR estimation revealed a weak broad peak at  $3235.32\text{ cm}^{-1}$  indicating the presence of alcohol functional group with O-H stretching, strong to medium peaks at  $1595.30\text{ cm}^{-1}$  indicating amine group with N-H bending,  $1407.07\text{ cm}^{-1}$  indicative of fluoro compounds with C-F stretching, and  $1099.56\text{ cm}^{-1}$  indicating aliphatic ether with C-O stretching (Figure 5).

Selenium nanoparticles displayed potent antimicrobial activity against caries-causing microorganisms at all concentrations closely comparable to the antibiotic controls. The maximum antimicrobial activity against *S. mutans* was observed (Figures 6 and 7). Figure 8 shows the antioxidant activity by DPPH was also important and displayed more efficacy than the controls at concentrations of  $10\text{ }\mu\text{L}$  and  $20\text{ }\mu\text{L}$  selenium nanoparticles. Selenium has a major biological role in species health and is an important component of

the composition of glutathione peroxidases, thioredoxin reductases, and other selenoenzymes [4]. Glutathione peroxidase is an enzyme that prevents tissue oxidative stress and can thus inhibit the activity of harmful free radicals.

UV-vis spectroscopy is one of the most commonly used methods for the structural characterization of SeNPs. The size and shape of the tracked aqueous suspension NPs can usually be analyzed by UV-vis spectroscopy. Our outcome indicates that C leaf extract synthesizes SeNPs. Measurements based on data and spectrophotometers range from 200 to 700 nm with a 420 nm peak indicating SeNP performance.

Energy-dispersive microanalysis spectroscopy was carried out using EDX techniques to gain further perception of the SeNPs' functionality. Our results suggest that selenium binding energies have EDaX peaks of approximately 72.64. The outcome indicates the presence in the pure form of SeNPs of

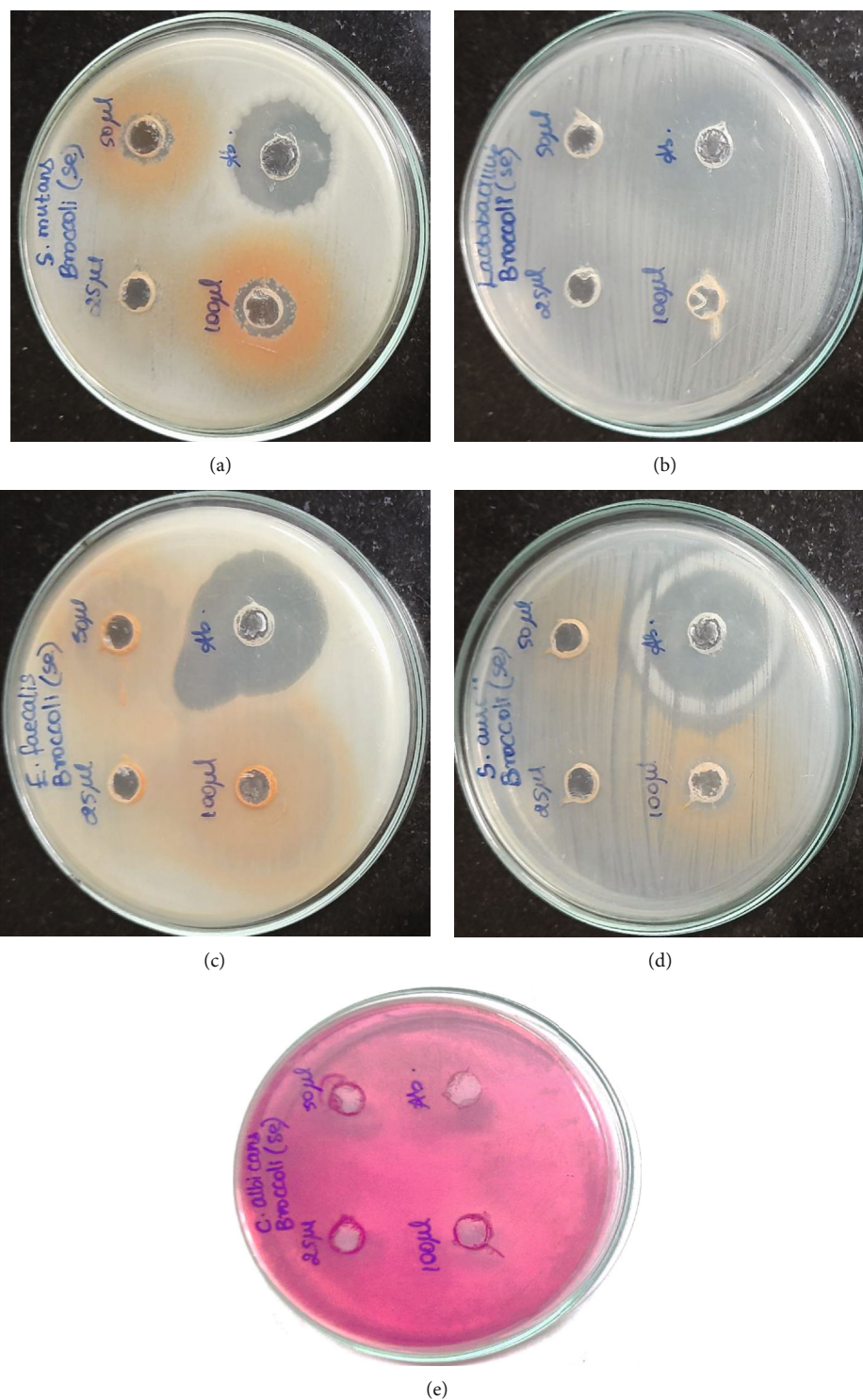


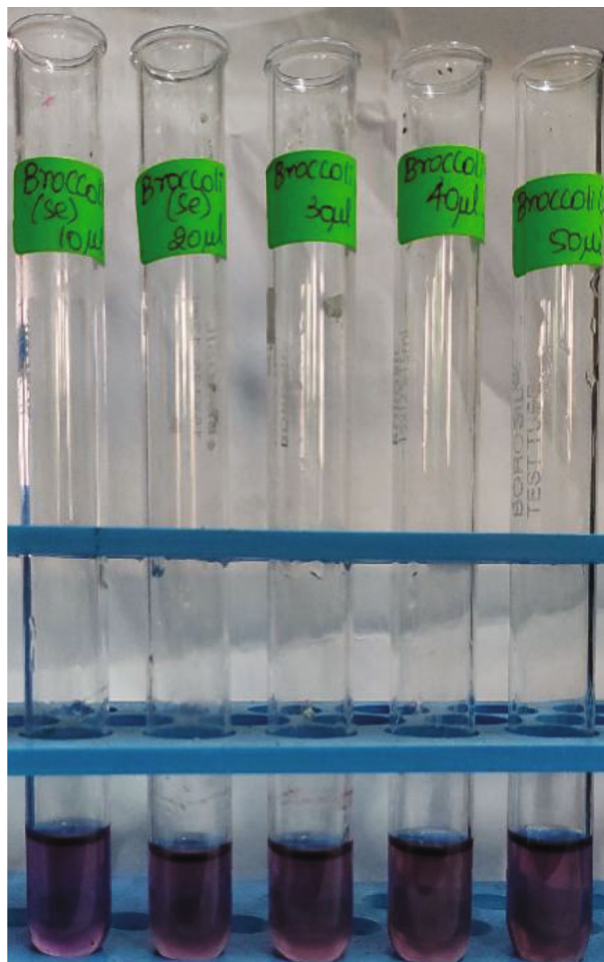
FIGURE 7: Anticariogenic activity of selenium nanoparticles: (a) *S. mutans*; (b) *Lactobacillus* sp.; (c) *E. faecalis*; (d) *S. aureus*; (e) *C. albicans*.

the reaction product. For synthesized extracts of SeNPs, the recorded EDaX showed a strong signal of 3 keV selenium.

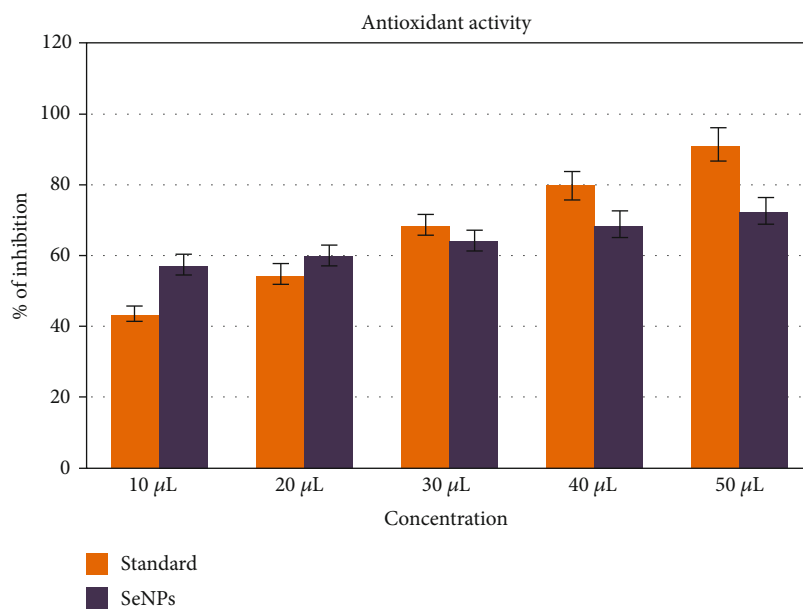
In our study, the bacterial growth was affected by the addition of various sodium selenite concentrations under aerobic conditions to the growth medium. Elevated concentrations of sodium selenite induce a lot of impairment to the genetic configuration in microbes. Thus, significant numbers of bacte-

ria perish because of the stress caused by the existence of toxic inorganic compounds in the atmosphere, thereby reducing the production of selenium nanoparticles [8].

It has also been shown that selenium dioxide ( $\text{SeO}_2$ ) as  $\text{Na}_2\text{SeO}_3$  causes noxious effects on microbial plasmid DNA under stress conditions of  $\text{H}_2\text{O}_2$ , but with greater intensity, whereas other selenium-containing compounds such as



(a)



(b)

FIGURE 8: Antioxidant activity of selenium nanoparticles: (a) color changes; (b) graph representing the antioxidant activity at percentage of inhibition.

$\text{Na}_2\text{SeO}_4$  and  $\text{Na}_2\text{Se}$  have some inhibitory effects on *Escherichia coli* plasmid DNA. Previous studies support our study of the antibacterial activity of selenium on *Staphylococcus* and suggest that selenium is capable of preventing the development of biofilms by bacteria and cytotoxic effect has been demonstrated by SeNPs [28]. In live aureus assays, it was demonstrated that SeNPs inhibited pneumonia in cell lines [29]. In this analysis, the antimicrobial impact of SeNPs on microbes was observed.

The mechanism attributed may be owed to the interruption of the cell wall, indicating that the selenium nanoparticles were able to penetrate the cell wall. The antibacterial role of these selenium nanoparticles can be distinguished by morphological alterations in bacterial strains both intracellular and extracellular. The antimicrobial behavior of selenium nanoparticles is mainly due to the formation of reactive oxygen species, which contributes to the disruption of bilayer phospholipids where intracellular proteins are associated with and inactivated by SeNPs or where the sulfhydryl and the thiol groups existing in membrane proteins can react with and eventually denature them. By altering the cycle of protein synthesis, interfering with the mechanism of respiratory or food metabolism, or impairing the replication of DNA, oxidative stress caused by reactive oxygen induces cell death [30].

Toxicological examinations have demonstrated that small selenium nanoparticles possess a higher surface area and those particle numbers per unit mass can induce harmful respiratory damage and inflammation. The larger particles about 100 nm are more easily engulfed by macrophages. Their aggregation can, thus, decrease the toxicity of the nanoparticles [31, 32].

Selenium nanoparticles can be used in various applications in the prevention of caries in dental tissues. Incorporating selenium nanoparticles in toothpaste, chewing gums, and mouthwashes can potentially help control the growth of caries causing microbes. Similarly, selenium nanoparticles can be incorporated in luting cement, endodontic sealers, pit and fissure sealants, and restorative cement to control secondary dental caries. Further extensive research in these domains will enhance our understanding of the therapeutic effectiveness of selenium nanoparticles in the prevention of dental caries.

#### 4. Conclusion

Nanomaterials have emerged as promising therapeutic agents in the prevention and treatment of dental caries. In this study, SeNPs were synthesized using *Brassica oleracea* extract, characterized using UV-vis spectroscopy which confirmed the SeNP formation and electron microscopic images from TEM and SEM which showed nanoparticles less than 50 nm, and evaluated for the antibacterial activity against dental caries-causing pathogens, and it was found that SeNPs showed effective antimicrobial activity against cariogenic pathogens. The SeNPs synthesized with *Brassica oleracea* extract can be incorporated in toothpastes, gums, and mouthwashes that are cost-effective and also biocompatible and effective for the prevention of dental caries.

#### Data Availability

The data used to support the findings of this study are included within the article.

#### Conflicts of Interest

The authors declare that there is no conflict of interest.

#### Authors' Contributions

DG and SR designed, carried out research, and wrote the manuscript.

#### References

- [1] S. al-Musawi, S. Albukhaty, H. al-Karagoly et al., "Antibacterial activity of honey/chitosan nanofibers loaded with capsaicin and gold nanoparticles for wound dressing," *Molecules*, vol. 25, no. 20, article 4770, 2020.
- [2] M. Jabir, U. I. Sahib, Z. Taqi et al., "Linalool-loaded glutathione-modified gold nanoparticles conjugated with CALNN peptide as apoptosis inducer and NF- $\kappa$ B translocation inhibitor in SKOV-3 cell line," *International Journal of Nanomedicine*, vol. Volume 15, pp. 9025–9047, 2020.
- [3] Z. Qiao, Y. Xie, Y. Qian, and Y. Zhu, " $\gamma$ -Irradiation preparation and characterization of nanocrystalline ZnS," *Materials Chemistry and Physics*, vol. 62, no. 1, pp. 88–90, 2000.
- [4] S. Menon, H. Agarwal, S. Rajeshkumar, P. Jacqueline Rosy, and V. K. Shanmugam, "Investigating the antimicrobial activities of the biosynthesized selenium nanoparticles and its statistical analysis," *Bionanoscience*, vol. 10, no. 1, pp. 122–135, 2020.
- [5] P. Narasingarao and M. M. Häggblom, "Identification of anaerobic selenate-respiring bacteria from aquatic sediments," *Applied and Environmental Microbiology*, vol. 73, no. 11, pp. 3519–3527, 2007.
- [6] J. Zhang, S.-Y. Zhang, J.-J. Xu, and H.-Y. Chen, "A new method for the synthesis of selenium nanoparticles and the application to construction of  $\text{H}_2\text{O}_2$  biosensor," *Chinese Chemical Letters*, vol. 15, no. 11, pp. 1345–1348, 2004.
- [7] P. A. Tran and T. J. Webster, "Antimicrobial selenium nanoparticle coatings on polymeric medical devices," *Nanotechnology*, vol. 24, no. 15, article 155101, 2013.
- [8] N. Srivastava and M. Mukhopadhyay, "Biosynthesis and structural characterization of selenium nanoparticles mediated by *Zooglea ramigera*," *Powder Technology*, vol. 244, pp. 26–29, 2013.
- [9] H. Wang, J. Zhang, and H. Yu, "Elemental selenium at nano size possesses lower toxicity without compromising the fundamental effect on selenoenzymes: comparison with selenomethionine in mice," *Free Radical Biology & Medicine*, vol. 42, no. 10, pp. 1524–1533, 2007.
- [10] A. G. al-Dulimi, A. Z. al-Saffar, G. M. Sulaiman et al., "Immobilization of l-asparaginase on gold nanoparticles for novel drug delivery approach as anti-cancer agent against human breast carcinoma cells," *Journal of Materials Research and Technology*, vol. 9, no. 6, pp. 15394–15411, 2020.
- [11] M. S. Jabir, Y. M. Saleh, G. M. Sulaiman et al., "Green synthesis of silver nanoparticles using *Annona muricata* extract as an inducer of apoptosis in cancer cells and inhibitor for NLRP3 inflammasome via enhanced autophagy," *Nanomaterials*, vol. 11, no. 2, p. 384, 2021.

- [12] O. al Rugaie, M. Jabir, R. Kadhim et al., "Gold nanoparticles and graphene oxide flakes synergistic partaking in cytosolic bactericidal augmentation: role of ROS and NOX2 activity," *Microorganisms*, vol. 9, no. 1, p. 101, 2021.
- [13] G. M. Sulaiman, E. H. Ali, I. I. Jabbar, and A. H. Saleem, "Synthesis, characterization, antibacterial and cytotoxic effects of silver nanoparticles," *Digest Journal of Nanomaterials and Biostructures*, vol. 9, no. 2, pp. 787–796, 2014.
- [14] W. J. al-Kaabi, S. Albukhaty, A. J. M. al-Fartosy et al., "Development of *Inula graveolens* (L.) plant extract electrospun/polycaprolactone nanofibers: a novel material for biomedical application," *Applied Sciences*, vol. 11, no. 2, p. 828, 2021.
- [15] W. Zhang, Z. Chen, H. Liu, L. Zhang, P. Gao, and D. Li, "Biosynthesis and structural characteristics of selenium nanoparticles by *Pseudomonas alcaliphila*," *Colloids and Surfaces B, Biointerfaces*, vol. 88, no. 1, pp. 196–201, 2011.
- [16] C. I. R. Gill, "The effect of cruciferous and leguminous sprouts on genotoxicity, in vitro and in vivo," *Cancer Epidemiology, Biomarkers & Prevention*, vol. 13, no. 7, pp. 1199–1205, 2004.
- [17] G. Brandi, G. F. Schiavano, N. Zaffaroni et al., "Mechanisms of action and antiproliferative properties of *Brassica oleracea* juice in human breast cancer cell lines," *The Journal of Nutrition*, vol. 135, no. 6, pp. 1503–1509, 2005.
- [18] E. H. Jeffery, A. F. Brown, A. C. Kurilich et al., "Variation in content of bioactive components in broccoli," *Journal of Food Composition and Analysis*, vol. 16, no. 3, pp. 323–330, 2003.
- [19] R. A. Bagramian, F. Garcia-Godoy, and A. R. Volpe, "The global increase in dental caries. A pending public health crisis," *American Journal of Dentistry*, vol. 22, no. 1, pp. 3–8, 2009.
- [20] R. H. Selwitz, A. I. Ismail, and N. B. Pitts, "Dental caries," *The Lancet*, vol. 369, no. 9555, pp. 51–59, 2007.
- [21] T. Walsh, H. V. Worthington, A. M. Glenney et al., "Fluoride toothpastes of different concentrations for preventing dental caries in children and adolescents," *Cochrane Database of Systematic Reviews*, vol. 1, 2010.
- [22] K. J. Toumba and M. E. J. Curzon, "A clinical trial of a slow-releasing fluoride device in children," *Caries Research*, vol. 39, no. 3, pp. 195–200, 2005.
- [23] S. Maleki Dizaj, F. Lotfipour, M. Barzegar-Jalali, M.-H. Zarrintan, and K. Adibkia, "Application of Box-Behnken design to prepare gentamicin-loaded calcium carbonate nanoparticles," *Artificial Cells, Nanomedicine, and Biotechnology*, vol. 44, no. 6, pp. 1475–1481, 2016.
- [24] M. Hannig and C. Hannig, "Nanotechnology and its role in caries therapy," *Advances in Dental Research*, vol. 24, no. 2, pp. 53–57, 2012.
- [25] L. Cheng, K. Zhang, M. D. Weir, M. A. S. Melo, X. Zhou, and H. H. K. Xu, "Nanotechnology strategies for antibacterial and remineralizing composites and adhesives to tackle dental caries," *Nanomedicine*, vol. 10, no. 4, pp. 627–641, 2015.
- [26] M. A. S. Melo, S. F. F. Guedes, H. H. K. Xu, and L. K. A. Rodrigues, "Nanotechnology-based restorative materials for dental caries management," *Trends in Biotechnology*, vol. 31, no. 8, pp. 459–467, 2013.
- [27] C. M. Debieux, E. J. Dridge, C. M. Mueller et al., "A bacterial process for selenium nanosphere assembly," *Proceedings of the National Academy of Sciences of the United States of America*, vol. 108, no. 33, pp. 13480–13485, 2011.
- [28] S. Boroumand, M. Safari, E. Shaabani, M. Shirzad, and R. Faridi-Majidi, "Selenium nanoparticles: synthesis, characterization and study of their cytotoxicity, antioxidant and antibacterial activity," *Materials Research Express*, vol. 6, no. 8, article 0850d8, 2019.
- [29] S. Shoeibi and M. Mashreghi, "Biosynthesis of selenium nanoparticles using *Enterococcus faecalis* and evaluation of their antibacterial activities," *Journal of Trace Elements in Medicine and Biology*, vol. 39, pp. 135–139, 2017.
- [30] X. Chen, K. Cai, J. Fang et al., "Fabrication of selenium-deposited and chitosan-coated titania nanotubes with anticancer and antibacterial properties," *Colloids and Surfaces B, Biointerfaces*, vol. 103, pp. 149–157, 2013.
- [31] S. Chaudhary, P. Chauhan, R. Kumar, and K. K. Bhasin, "Toxicological responses of surfactant functionalized selenium nanoparticles: a quantitative multi-assay approach," *Science of The Total Environment*, vol. 643, pp. 1265–1277, 2018.
- [32] R. Tarrahi, A. Khataee, A. Movafeghi, F. Rezanejad, and G. Gohari, "Toxicological implications of selenium nanoparticles with different coatings along with Se<sup>4+</sup> on *Lemna minor*," *Chemosphere*, vol. 181, pp. 655–665, 2017.